

Exploiting the antioxidant and biotechnological potential of marine algae microbiota

Dissertation

With the aim of achieving the degree of
Doctor rerum naturalium (Dr. rer. nat.)

Department of Biology
Subdivision at the Faculty of Mathematics, Informatics and Natural Sciences
University of Hamburg

Submitted by
Jascha Friedemann Helge Macdonald

Hamburg 2025

List of Publications

Publication 1: Community dynamics and metagenomic analyses reveal Bacteroidota's role in widespread enzymatic *Fucus vesiculosus* cell wall degradation – Scientific reports

JFHM contributed significantly to the development of the experiments, in part with the help of the other authors of the publication mentioned. This includes the planning, execution, and evaluation of the following studies: Preparation of *Fucus vesiculosus* enrichment cultures; metabolic studies of bacterial cultures, genomic and metagenomic determination of bacterial communities and their enzymatic potential; preparation of electron microscopy images; cloning and purification of the enzymes FUJM18 and FUJM20; characterisation and activity determination of FUJM18 and FUJM20.

Preparation of the published manuscript in the parts: Introduction, Results, Discussion, Methods.

DOI: <https://doi.org/10.1038/s41598-024-60978-8>

Hamburg, den 13.01.2025



Professor Dr Wolfgang R. Streit

Hamburg, den 13.01.2025



Jascha Macdonald

Publication 2: Exploring *Tetraselmis chui* microbiomes - functional metagenomics for novel catalases and superoxide dismutases

JFHM contributed significantly to the development of the experiments, in part with the help of the other authors of the publication mentioned. This includes the planning, execution, and evaluation of the following investigations: Cultivation of *Tetraselmis chui* cultures; analysis of the *Tetraselmis chui* microbiome metagenome; purification, characterisation, and activity determination of the enzymes TcJM_SOD2, TcIK_SOD3, TcJM_CAT2 and TcIK_CAT3.

Preparation of the published manuscript in the parts: Introduction, Results, Discussion, Methods.

DOI: <https://doi.org/10.1007/s00253-024-13395-w>

Hamburg, den 13.01.2025

Professor Dr Wolfgang R. Streit

Hamburg, den 13.01.2025

Jascha Macdonald

Other contributions and publications

Peters, M. K., Astafyeva, Y., Han, Y., Macdonald, J. F. H., Indenbirken, D., Nakel, J., Viridi, S., Westhoff, G., Streit, W. R., Krohn, I. (2023): *Novel marine metalloprotease—new approaches for inhibition of biofilm formation of Stenotrophomonas maltophilia* – DOI: [10.1007/s00253-023-12781-0](https://doi.org/10.1007/s00253-023-12781-0)

The doctoral student contributed in part to the manuscript in the “Discussion” chapter and to the preparation of Figure 6.

Chapter: Macdonald, J. F. H., Krohn, I., Streit, W. R. (2022): *Chapter 9 - Screening Metagenomes for Algae Cell Wall Carbohydrates Degrading Hydrolases in Enrichment Cultures in Metagenomics, Methods and Protocols* – DOI: [10.1007/978-1-0716-2795-2_9](https://doi.org/10.1007/978-1-0716-2795-2_9)

The doctoral student applied all described methods and wrote the complete chapter. As a book chapter, this publication is not considered peer-reviewed.

Hamburg, den 13.01.2025



Professor Dr Wolfgang R. Streit

Hamburg, den 13.01.2025



Jascha Macdonald

Admission

The following evaluators recommend the admission of the dissertation:

Prof. Dr. Wolfgang R. Streit

Prof. Dr. Elisa Schaum

Day of oral defense: 10.04.2025

Declaration on oath

Affidavit

I hereby declare and affirm that this doctoral dissertation is my own work and that I have not used any aids and sources other than those indicated. If electronic resources based on generative artificial intelligence (gAI) were used in the course of writing this dissertation, I confirm that my own work was the main and value-adding contribution and that complete documentation of all resources used is available in accordance with good scientific practice. I am responsible for any erroneous or distorted content, incorrect references, violations of data protection and copyright law or plagiarism that may have been generated by the gAI.

Eidesstattliche Versicherung

Hiermit versichere ich an Eides statt, die vorliegende Dissertationsschrift selbst verfasst und keine anderen als die angegebenen Hilfsmittel und Quellen benutzt zu haben. Sofern im Zuge der Erstellung der vorliegenden Dissertationsschrift generative Künstliche Intelligenz (gKI) basierte elektronische Hilfsmittel verwendet wurden, versichere ich, dass meine eigene Leistung im Vordergrund stand und dass eine vollständige Dokumentation aller verwendeten Hilfsmittel gemäß der Guten wissenschaftlichen Praxis vorliegt. Ich trage die Verantwortung für eventuell durch die gKI generierte fehlerhafte oder verzerrte Inhalte, fehlerhafte Referenzen, Verstöße gegen das Datenschutz- und Urheberrecht oder Plagiate.

Hamburg, den 15.01.2025



Jascha Friedemann Helge Macdonald

Table of contents

LIST OF PUBLICATIONS	I
ADMISSION	IV
DECLARATION ON OATH	V
TABLE OF CONTENTS	VI
ABSTRACT	VII
ZUSAMMENFASSUNG	IX
INTRODUCTION	1
BIOTECHNOLOGY POTENTIAL OF ALGAE MICROBIOMES	1
PUBLICATION 1: COMMUNITY DYNAMICS AND METAGENOMIC ANALYSES REVEAL BACTEROIDOTA'S ROLE IN WIDESPREAD ENZYMATIC <i>FUCUS VESICULOSUS</i> CELL WALL DEGRADATION	2
PUBLICATION 2: EXPLORING TETRASELMIS CHUI MICROBIOMES - FUNCTIONAL METAGENOMICS FOR NOVEL CATALASES AND SUPEROXIDE DISMUTASES.....	9
DISCUSSION	14
BIOTECHNOLOGY POTENTIAL OF ALGAE MICROBIOMES	14
PUBLICATION 1: COMMUNITY DYNAMICS AND METAGENOMIC ANALYSES REVEAL BACTEROIDOTA'S ROLE IN WIDESPREAD ENZYMATIC <i>FUCUS VESICULOSUS</i> CELL WALL DEGRADATION	15
PUBLICATION 2: EXPLORING TETRASELMIS CHUI MICROBIOMES - FUNCTIONAL METAGENOMICS FOR NOVEL CATALASES AND SUPEROXIDE DISMUTASES.....	24
FURTHER BIOTECHNOLOGICAL POTENTIAL OF ALGAE MICROBIOMES.....	28
PUBLICATION 1: THE BACTERIAL DEGRADATION OF BROWN ALGAE CELL WALL CARBOHYDRATES	30
SUPPLEMENTAL INFORMATION - THE BACTERIAL DEGRADATION OF BROWN ALGAE CELL WALL CARBOHYDRATES.....	48
PUBLICATION 2: THE ANTIOXIDANT POTENTIAL OF <i>T. CHUI</i> MICROBIOMES.	58
SUPPLEMENTAL INFORMATION – THE ANTIOXIDANT POTENTIAL OF <i>T. CHUI</i> MICROBIOMES	74
SCREENING METAGENOMES FOR ALGAE CELL WALL CARBOHYDRATES DEGRADING HYDROLASES IN ENRICHMENT CULTURES	76
FURTHER CONTRIBUTIONS	91
COAUTHORSHIP	91
SUPERVISIONS	92
BACHELOR THESIS.....	92
MASTER THESIS.....	92
REFERENCES	XI
APPENDIX	XXIV
ACKNOWLEDGEMENTS	XXX

Abstract

Algae microbiomes consist of a complex community of Bacteria, Archaea, and Fungi. Metagenomic analyses, molecular tools, modern bioinformatic methods as well as function-based analyses enable the accessibility of these extensive source for valuable biomolecules. In the present dissertation, these methods are used to investigate microbial community dynamics as well as their metabolic capabilities to describe the biotechnological potential. Furthermore, novel proteins were implemented in various industries, targeting future use in sustainable resources and healthcare applications.

Overall, two major studies were carried out.

- i. Publication 1: “Community dynamics and metagenomic analyses reveal Bacteroidota's role in widespread enzymatic *Fucus vesiculosus* cell wall degradation”

The search for alternative, renewable resources is under major investigations. Algae offer valuable biomolecules with applications in the sector of medical research, the food industry, and the energy sector in terms of biofuel. While cultivation of algae is already in large-scale implementations, the processing part of this variable resource still lacks an efficient way. With the focus on brown macroalgae cell wall degradation, I designed enrichment cultures to examine the bacterial community and metabolic dynamics. Additionally, metagenome datasets were screened with Hidden Markov Models (HMM) to investigate the glycosyl-hydrolysing capabilities of the algae surface biome. While 16S rRNA gene amplicon analyses identified Pseudomonadota as the dominating bacterial fraction, the HMM screening reveal Bacteroidota as the phylum with the highest potential for algae cell wall degradation. Further, these observations lay the foundation for the implementation and characterisation of 2 novel, thermostable α -L-fucosidases; FUJM18 and FUJM20.

- ii. Publication 2: “Exploring *Tetraselmis chui* microbiomes - functional metagenomics for novel catalases and superoxide dismutases”
The focus on microalgae for applications in several fields e.g. resources for biofuel, the food industry, cosmetics, nutraceuticals, biotechnology, and healthcare has gained increasing attention over the last decades. In this study,

we investigate the microbiome of the cultured microalga *Tetraselmis chui* (*T. chui*) to highlight their potential for health benefits. In this context, biomolecules like antioxidants play a crucial role in the well-being of living organisms as they metabolise harmful reactive oxygen species (ROS) to reduce oxidative stress. Impaired processing of ROS leads to damaged cells and increases the risk of cancer, inflammatory diseases, and diabetes, among others. Here, we identify, characterise, and test bacterial antioxidants derived from the *T. chui* microbiome metagenome dataset. We identified 258 genes coding for proteins with potential antioxidant activity. Of those, four novel enzymes are expressed and identified as two superoxide dismutases (SOD), TcJM_SOD2 and TcIK_SOD3, and two catalases (CAT), TcJM_CAT2 and TcIK_CAT3. Extensive analyses characterised all implemented enzymes as active even in concentrations down to 25 ng*ml⁻¹ for the SODs and 15 ng*ml⁻¹ for the CATs. Furthermore, sequence-based analyses assign TcJM_SOD2 and TcIK_SOD3 to iron superoxide dismutases (Fe SODs) and TcJM_CAT2 and TcIK_CAT3 to heme-containing catalases. These candidates are phylogenetically classified within the phylum Pseudomonadota. Regarding the biotechnological potential, a toxicity assay did not indicate any harmful effects. The introduced enzymes may benefit medical applications and expand the potential of microalgae microbiomes.

In total, 6 novel proteins are implemented, tested, and characterised (Macdonald et al. (2024): FUJM18; FUJM20. Macdonald et al. (2025): TcJM_SOD2; TcJM_SOD3; TcIK_CAT2; TcIK_CAT3). With increased sensitivities as well as enzyme activity rates and potential thermostability for α -L-fucosidases, all six are interesting candidates for a potential future application.

Zusammenfassung

Das Mikrobiom der Algen besteht aus einer komplexen Gemeinschaft von Bakterien, Archaeen, Pilzen und mikroskopisch kleinen Tieren. Metagenomische Analysen, molekulare Werkzeuge sowie moderne bioinformatische Methoden ermöglichen die Erschließung dieser umfangreichen Quelle für wertvolle Biomoleküle. In der vorliegenden Dissertation werden diese Methoden zur Untersuchung der mikrobiellen Dynamik mikrobieller Gemeinschaften sowie deren Stoffwechsellleistungen zur Beschreibung des biotechnologischen Potenzials zu beschreiben. Darüber hinaus wurden neuartige Proteine für Industriezweigen vorgestellt, mit dem Ziel einer zukünftigen Nutzung nachhaltiger Ressourcen und deren Anwendungen im Gesundheitswesen.

Insgesamt wurden zwei Studien durchgeführt.

- i. Veröffentlichung 1: "Community dynamics and metagenomic analyses reveal Bacteroidota's role in widespread enzymatic *Fucus vesiculosus* cell wall degradation"

Die Suche nach alternativen, erneuerbaren Ressourcen ist Gegenstand umfangreicher Untersuchungen. Algen bieten wertvolle Biomoleküle, die in der medizinischen Forschung, der Lebensmittelindustrie und im Energiesektor in Form von Biokraftstoffen eingesetzt werden können. Während die Kultivierung von Algen bereits in großem Maßstab durchgeführt wird, gibt es für die Verarbeitung dieser wertvollen Ressource noch keine effiziente Methode. Mit dem Fokus auf den Zellwandabbau von braunen Makroalgen habe ich Anreicherungskulturen angelegt, um die bakterielle Gemeinschaft und die Stoffwechsellodynamik zu untersuchen. Zusätzlich wurden Metagenom-Datensätze mit Hidden-Markov-Modellen (HMM) untersucht, um die Glykosyl-Hydrolyse-Fähigkeiten des Algenoberflächen-Bioms zu ermitteln. Während 16S rRNA-Gen-Amplikonanalysen *Pseudomonadota* als die dominierende bakterielle Fraktion identifizierten, zeigte das HMM-Screening *Bacteroidota* als das Phylum mit dem höchsten Potenzial für den Algenzellwandabbau. Darüber hinaus bilden diese Beobachtungen die Grundlage für die Implementierung und Charakterisierung von zwei neuen, thermostabilen α -L-Fucosidasen: FUJM18 und FUJM20.

- ii. Veröffentlichung 2: “Exploring *Tetraselmis chui* microbiomes - functional metagenomics for novel catalases and superoxide dismutases”
Der Fokus auf Mikroalgen für Anwendungen in verschiedenen Bereichen, z.B. Ressourcen für Biokraftstoffe, die Lebensmittelindustrie, Kosmetika, Nutraceuticals, Biotechnologie und Gesundheit, hat in den letzten Jahrzehnten zunehmend an Aufmerksamkeit gewonnen. In dieser Studie untersuchen wir das Mikrobiom der kultivierten Mikroalge *Tetraselmis chui* (*T. chui*), um ihr Potenzial für gesundheitliche Vorteile herauszustellen. In diesem Zusammenhang spielen Biomoleküle wie Antioxidantien eine entscheidende Rolle für das Wohlbefinden lebender Organismen, da sie schädliche reaktive Sauerstoffspezies (ROS) verstoffwechseln, um oxidativen Stress zu reduzieren. Eine gestörte Verarbeitung von ROS führt zu geschädigten Zellen und erhöht das Risiko von Krebs, entzündlichen Erkrankungen und Diabetes, um nur einige zu nennen. Hier identifizieren, charakterisieren und testen wir bakterielle Antioxidantien, die aus dem Metagenom-Datensatz des *T. chui* Mikrobioms stammen. Wir haben 258 Gene identifiziert, die für Proteine mit potenzieller antioxidativer Aktivität kodieren. Davon werden vier neue Enzyme exprimiert und als zwei Superoxid-Dismutasen (SOD), TcJM_SOD2 und TcIK_SOD3, und zwei Katalasen (CAT), TcJM_CAT2 und TcIK_CAT3, identifiziert. Umfangreiche Analysen charakterisierten alle implementierten Enzyme als aktiv, sogar in Konzentrationen bis zu $2,5 \cdot 10^{-5} \text{ mg} \cdot \text{ml}^{-1}$ für die SODs und $1,5 \cdot 10^{-5} \text{ mg} \cdot \text{ml}^{-1}$ für die CATs. Darüber hinaus ordnen sequenzbasierte Analysen TcJM_SOD2 und TcIK_SOD3 den Eisen-Superoxid-Dismutasen (Fe-SODs) und TcJM_CAT2 und TcIK_CAT3 den hämhaltigen Katalasen zu. Diese Kandidaten sind phylogenetisch dem Stamm Pseudomonadota zugeordnet. Was das biotechnologische Potenzial betrifft, so ergab ein Toxizitätstest keine schädlichen Auswirkungen. Die eingeführten Enzyme könnten medizinischen Anwendungen zugutekommen und das Potenzial von Mikroalgen-Mikrobiomen erweitern.

Insgesamt wurden sechs neue Proteine implementiert, getestet und charakterisiert (Macdonald et al. (2024): FUJM18; FUJM20. Macdonald et al. (2025): TcJM_SOD2; TcJM_SOD3; TcIK_CAT2; TcIK_CAT3). Mit erhöhten Empfindlichkeiten sowie Enzymaktivitätsraten und, für die α -L-Fucosidasen, einer Thermostabilität, sind alle sechs interessante Kandidaten für eine mögliche zukünftige Anwendung.

Introduction

Biotechnology potential of algae microbiomes

Aquatic ecosystems cover over 70 % of the earth's surface and harbour the smallest to the biggest forms of life. Additionally, the global marine system acts as a substantial carbon sink, with marine algae playing a crucial role in climate regulation. With over 50,000 identified species in marine and freshwater environments, algae are primary producers of the oxygen essential for terrestrial life (Walker, 1980; Guiry, 2024). The term 'algae' encompasses a variety of taxonomic groups, each contributing to numerous ecosystem services.

Simultaneously, the global climate system is in an unstable and rapidly changing state. The global climate crisis impacts human life, industries, ecosystems, and political decisions. Consequently, this drives the search and investigation of alternative resources and sustainable technologies. Algae and their associated microbiome contain one of those resources. Algae serves multiple purposes as a renewable material with applications in the energy sector and biofuel production (Adeniyi et al., 2018). Furthermore, products of algae origin are used in the food-, nutraceutical, and cosmetic industries, as well as in medical treatments (Wells et al., 2017; Joshi et al., 2018; Krohn et al., 2022).

Algae's surface and surrounding water are inhabited by a diverse community of microorganisms, which are defined as the microbiome, consisting of a variety of pro- and eukaryotes species. The diversity and composition depend on several biotic and abiotic factors like temperature, salinity, season, nutrient concentration, and global location (Martin et al., 2021; Van Der Loos et al., 2021; Stal and Cretoiu, 2022). Additionally, certain algae species and associated biomolecules influence microbial diversity (Steinrücken et al., 2023). Interestingly, mutual interactions occur between the algae and the microorganisms and between the microbial community. These interactions drive metabolic processes and molecular responses to certain conditions and states. The marine microbial community contains a variety of valuable biomolecules like proteins, carbohydrates, and lipids, which have already been harvested (Rotter et al., 2021). Furthermore, algae farms with micro- and macroalgae are well-established (Liu et al., 2023).

In this dissertation, I emphasise the role of the associated microbiomes and point out their potential for various future applications.

This work and its included studies were part of the SuReMetS-project FKZ 031B0944A ("From Sustainable Resources to novel marine nutraceuticals for the management of Metabolic Syndrome"). The project aimed to identify novel biomolecules from marine algae and fish to treat systemic diseases. The University of Hamburg focused to find bacterial enzymes for processing marine organic matter in the form of algae to access valuable enzymes.

For this, enrichment cultures of *Fucus vesiculosus* serve as the experimental setup to characterise an algae cell wall polysaccharide hydrolysing community and establish novel enzymes. This enzyme characterisation was achieved by screening microbiome genomes with Hidden Markov Models (HMM) for genes with hydrolysis capabilities to degrade algae cell walls in an efficient and sustainable way. In the study "Macdonald et al. (2024). Community dynamics and metagenomic analyses reveal Bacteroidota's role in widespread enzymatic *Fucus vesiculosus* cell wall degradation" I published the results in May 2024.

Additionally, genes derived from microalgae microbiomes were identified and tested for their potential antioxidant applications. Antioxidant enzymes are crucial in metabolising reactive oxygen species (ROS). In a second publication, "Macdonald et al., 2025. Exploring *Tetraselmis chui* microbiomes - functional metagenomics for novel catalases and superoxide dismutases ", I investigate the microbiome of a *Tetraselmis chui* culture. Here I screen a metagenome dataset for the antioxidant enzymes Superoxide Dismutase (SOD) and Catalase (CAT). The enzymes should have a beneficial impact for human health applications by metabolising superoxide anions and hydrogen peroxide.

Publication 1: Community dynamics and metagenomic analyses reveal Bacteroidota's role in widespread enzymatic *Fucus vesiculosus* cell wall degradation

Plant cells cover their cells with a dense matrix of polymers. This layer of carbohydrates serves multiple protection and structure-given purposes. The protection against mechanical pressure and tension is crucial in environments driven by water circulation. This mechanical stress and further physical challenges apply especially to macroalgae in tidal areas. These algae are exposed to solar radiation and alternating conditions of

dry and wet phases, as well as changing salinity, temperature, and nutrient conditions. However, specific cell wall compounds create a set of protection characteristics for whole algae groups and species, which are adapted to their habitat. Consequently, the concentration and proportion of single-cell wall polysaccharides and further compounds can differ inter- and intraspecific (Fletcher et al., 2017).

Besides producing breathable oxygen, marine algae play a significant role in the global ecosystem. Phytoplankton and macroalgae serve as food sources for various animals, from microscopic zooplankton to mammals. Furthermore, they are crucial in the world's carbon flux by fixing carbonate during photosynthesis. Dissolved organic matter (DOM) of algae origin is transported in the deep sea and fixes the carbon in the ocean system. The ocean works as a carbon sink through this and additional gas exchanges. About 50 % of the annual carbon fixation is contributed by algae (Field et al., 1998). Furthermore, macroalgae washed ashore are involved in blue carbon cycles (Perkins et al., 2022). Consequently, natural algae systems act against climate change effects.

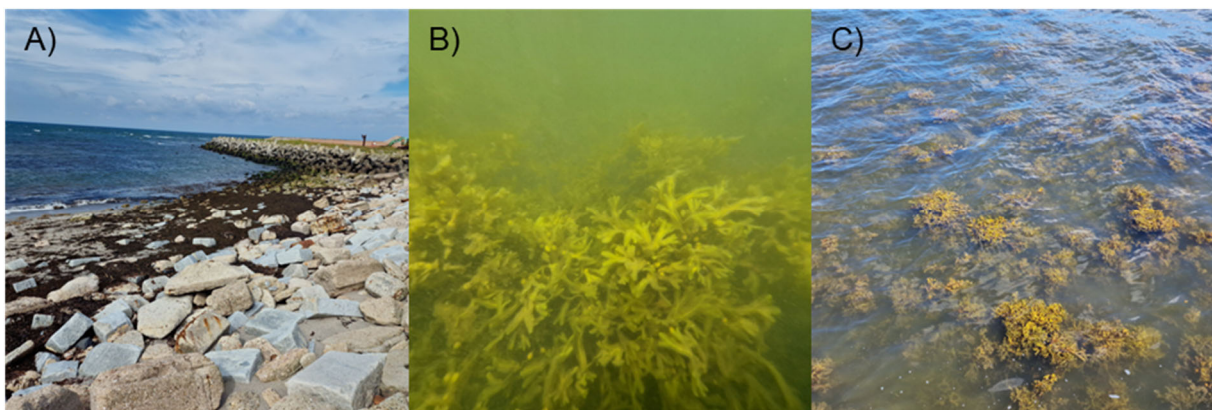


Figure 1: Marine biomass of Brown algae ©Jascha FH Macdonald. **A)** Large quantities of Brown algae washed ashore on the coast of Helgoland (54°17'70" N, 7°88'64" E), North Sea, Germany (July 2024). Degrading biomass consisting of different kelp species, including *Ascophyllum nodosum*, *Laminaria digitata*, *Fucus serratus*, *Fucus spiralis*, *Fucus vesiculosus*, and *Saccorhiza polyschides*. **B) C)** Kelp forests of *Fucus vesiculosus* growing in the Kiel Bight (54°21'56" N, 10°11'43" E), Baltic Sea, Germany (July 2024).

Species of the class Brown algae (Phaeophyceae) are distributed throughout the global marine system. They can be found on the shores of both polar regions as well as all continents in all climate zones. In contrast to green and red algae, including single-cell microalgae species, all Brown algae species are multicellular (Verma et al., 2015). Well-known genera and species are *Sargassum*, name giver to the Sargasso Sea in the North Atlantic report first by Christopher Columbus; *Macrocystis pyrifera* of the order Laminariales known as Kelps, which forms valuable kelp-forest ecosystems in the eastern Pacific with plants up to 60 m in length; and *Fucus*, which is found in

high numbers on the shores of the Northern Pacific and Arctic Sea with a high concentration of the polysaccharide Fucoïdan within the cell wall (Hahn et al., 2012; Cock et al., 2011; Wang et al., 2019).

Fucus vesiculosus is a Brown alga species prominently found washed ashore in large quantities. Gas-filled bladders enable disrupted plants to float on the ocean surface. The plants are deposited through tidal currents on beaches of the North- and Baltic Sea, among others (Fig 1A). For this reason, it is easy to gather and serves as an exemplary representative for all Brown algae, according to the cell wall structure. For these reasons, all investigations in this study were carried out on fresh *F. vesiculosus* samples washed ashore in the Kiel Bight (54°21'56" N, 10°11'43" E) (Fig 1BC).

For many centuries, Brown algae served humans as a resource. First, it is a valuable food with nutraceutical characteristics. While most of seaweed consumption is in East Asia, the global commercial seaweed market was USD 12.04 billion in 2023 and is expected to reach USD 18.66 billion in 2030 (Wells et al., 2017; Commercial Seaweed Market Report, 2024). About 40 % of the annual multicellular algae is produced for direct consumption. In 2012, this equals 24 million tons (Radulovich et al., 2015). Additionally, algae serve as animal nutrition and fertilisers (Christaki (E. Χρηστάκη) et al., 2017). As an increasing consumption of vegan, eco-friendly, and sustainable foods is found, especially in Europe and North America, the demand for novel food products increases. Algae fulfil these requirements, enhancing seaweed food product development (Saari et al., 2021; Li et al., 2021).

Furthermore, the traits of sustainability also apply to the cosmetic industry. Especially in skin care, natural products of algae origin are applied. Various biomolecules affect skin whitening, anti-wrinkling, anti-skin ageing, moistening, skin thickening and sensitising, and work as antioxidants (Joshi et al., 2018). For example, antioxidant molecules like Vitamin E or β -carotene reduce skin ageing and the risk of skin cancer (Schagen et al., 2012; Keen and Hassan, 2016). The Brown alga *F. vesiculosus* is processed for its chlorophyll-c and fucoxanthin, which induces skin-tightening and stimulates skincare metabolic processes (Joshi et al., 2018). Additionally, countless health benefits of algae are already present in the pharmaceutical industry (Schwartz et al., 1990; Gojkovic et al., 2019; Krohn et al., 2022). Recent studies on the main Brown algae cell wall carbohydrate Fucoïdan, which functions as an antioxidant, anti-inflammatory, and anticancer molecule, show beneficial effects for SARS-CoV2

treatment (Rupérez et al., 2002; Hwang et al., 2015; Vishchuk et al., 2016; Díaz-Resendiz et al., 2022).

In addition to that, fossil fuel burning is one of the main drivers of the manmade climate crisis (Soeder, 2021). Consequently, renewable energy sources are needed and are already under investigation. Algae with increased oil content are processed to generate biodiesel and biogas beyond others (Adeniyi et al., 2018). Alginate of Brown algae is processed to produce bioethanol (Lee and Lee, 2016).

The common ground of these products is the involved processing part, which still lacks a universal and efficient method. This degradation includes the hydrolysis of the algae cell wall polysaccharides. These differ not only between taxonomic groups and species but also interspecifically in composition, concentration, and sulfate content beyond other factors, which poses a challenge for enzymatic degradation.

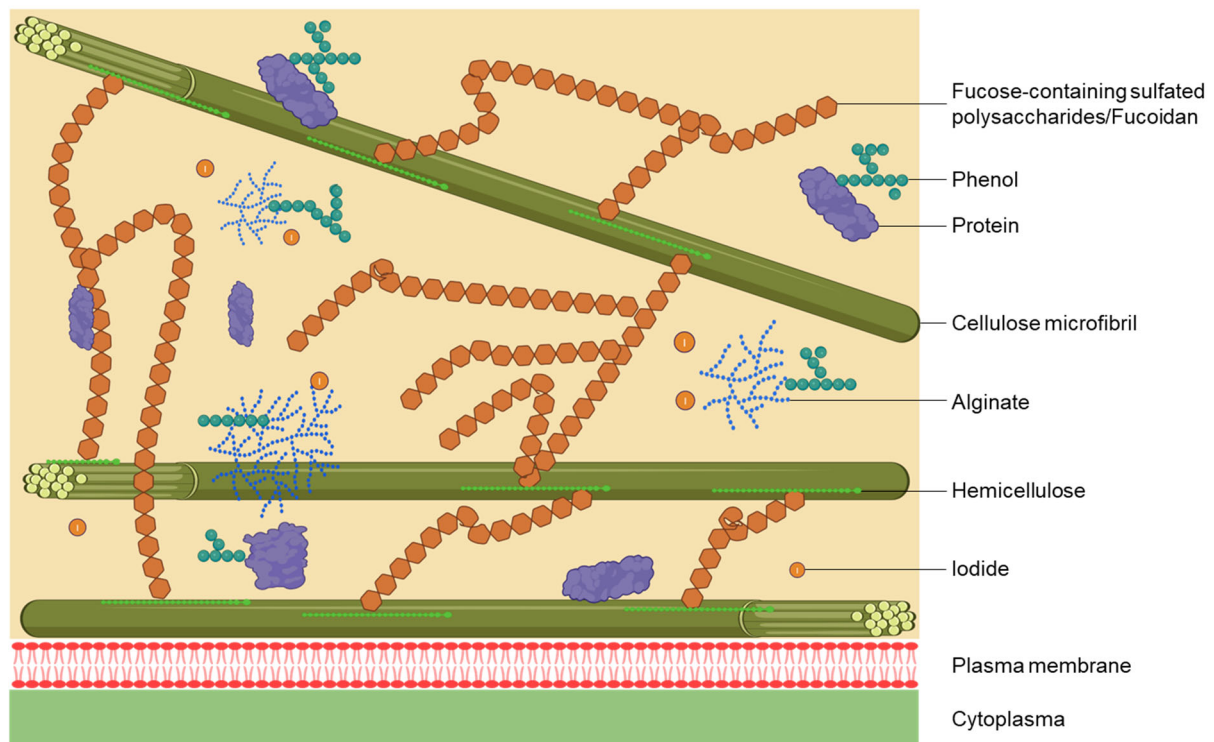


Figure 2: Schematic cross-section structure of Phaeophyceae cell walls. The polysaccharide matrix consists mainly of Cellulose, Fucoidan, and Alginate. The crosslinked structures of Fucoidan form connections between Cellulose microfibrils while presumably interacting with short Hemicellulose chains. Phenols (Phlorotannins) are associated with proteins and Alginate. Adapted from Deniaud-Bouët et al., 2014. Created with BioRender.

In Brown algae, the cell wall polysaccharide matrix consists of the carbohydrates Cellulose, Alginate and Fucoidan, also known as Fucans or Fucose-containing sulfated polysaccharides (Fig 2) (Hahn et al., 2012; Deniaud-Bouët et al., 2014). The structure given Cellulose microfibrils are sparse and interact with Fucoidan chains, which

presumably interact with attached hemicellulose. These interconnections strengthen the cell wall structure. The third carbohydrate, Alginate, crosslinks with phenolic compounds in the form of Phlorotannin. These phenols are secondary metabolites with multiple ecological roles produced by the polymerisation of phloroglucinol (1,3,5-trihydroxybenzene) (Stern et al., 1996). In Brown algae cell walls, the complex molecules that also bind to proteins act similarly to the structure and protection compound Lignin, which is found in plants on land and leads to lignification. Phlorotannins also protect against UV radiation to avoid damage to the DNA, which is especially important to algae in tidal zones like *F. vesiculosus* (Gómez and Huovinen, 2010). Additionally, a soluble form in the cell acts as a storage molecule (Koivikko et al., 2005).

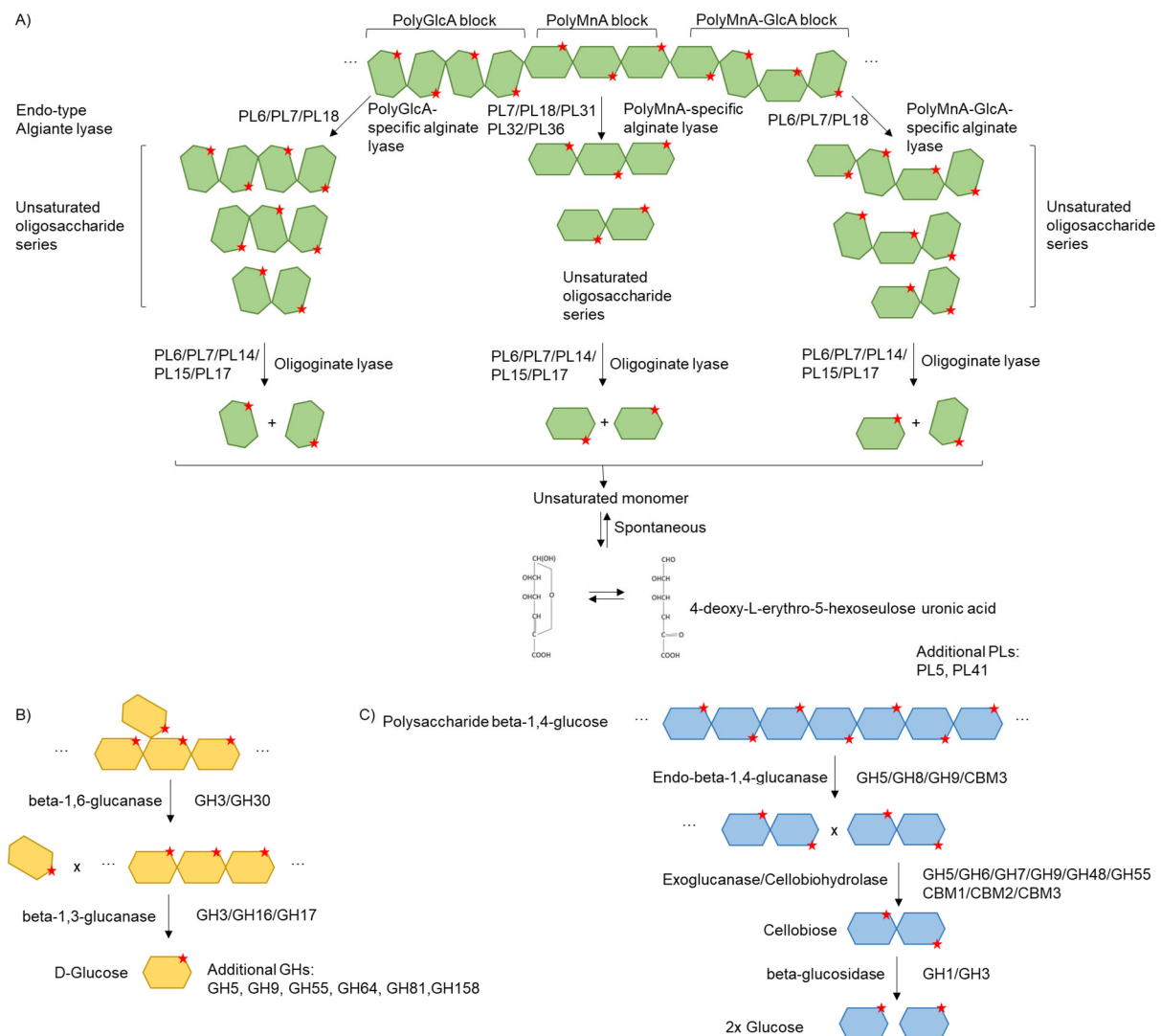


Figure 3: Schematic enzymatic degradation of phaeophycean carbohydrates, with involved enzyme classes and families of glycosyl hydrolases (GH), polysaccharide lyases (PL), and carbohydrate binding modules (CBM). Red stars indicate endocyclic oxygen. Supporting information for Macdonald et al. (2024) Fig 1. Also see Macdonald et al. (2024) Supplementary Table 4. Adapted from Li et al., 2022. **A) Alginate B) Laminarin C) Cellulose.**

The carbohydrate chains comprise varying compositions of saccharides connected with glycosidic bonds. The monosaccharides and their linkage define the carbohydrate group. The best-studied carbohydrate due to its appearance in land plants is Cellulose. Cellulose consists of β -D-glucose linked with β -1,4-glycosidic bonds (Fig 3C). It forms strong fibrils, giving the plant a tear-resistant trait (Li et al., 2022). Additionally, Alginate is made up of a more complex structure, divided into polymeric blocks of α -1,4-L-guluronic acid (PolyGlcA) and β -1,4-D-mannuronic acid (PolyMnA) or mixed PolyMnA-GlcA blocks (Fig 3A) (Dobrinčić et al., 2020). While Alginate becomes detectable in the zygote of *Fucus* shortly after the fertilisation, Cellulose is following within 20 min of development and Fucoidan after 1 h (Brawley et al., 1976; Vreeland et al., 1993). Fucoidan consists of a complex structure with a backbone of alternating α -1,3- and α -1,4-fucose linkages, less frequent also α -1,2-fucose. A fourth Brown algae exclusive carbohydrate is Laminarin. It is a β -1,3-D-glycopyranose with β -1,6-D-glycopyranose branches that acts as a storage molecule and is not found in the cell wall (Fig 3B) (Becker et al., 2017).

It is crucial to degrade those essential carbohydrates to access the cells or the cell wall carbohydrates themselves. With the extension to degrade green and red algae, additional valuable carbohydrates, the complexity of a universal degradation processes increases (e.g. Carrageenan, Mannan, Agar, Porphyran, Ulvan, Pectin) (Khotimchenko et al., 2020; Kaihou et al., 1993; Usov, 2011; Wang et al., 2023; Robic et al., 2009; Eder and Lütz-Meindl, 2010). So far, algae are cultured in large-scale algae farms, which are especially suitable for microalgae. For biofuel, the processing is achieved in different approaches: thermochemical conversion, thermochemical conversion, transesterification and through microbial fuel cells (Koyande et al., 2019). In natural conditions, microbial degradation is achieved by enzyme secretion to hydrolyse the algae cell wall. A more complex and diverse microbial community is assumably more efficient in algae degradation, as the varying cell wall compositions and environmental conditions require an adaptation of the microbiome and the applied enzymes.

Enzymes active on carbohydrates are categorised into enzyme classes and families in the Carbohydrate-Active enZYme database (CAZY, <http://www.cazy.org/>) (Drula et al., 2022). Glycosyl hydrolases (GH) (EC 3.2.1.-) are of enhanced importance for the Brown algae cell wall carbohydrate degradation, as this class includes families like GH29, which comprises several fucosidases. The degradation of the Fucoidan

backbone mainly requires GH29 enzymes α -1,3-L-fucosidase (EC 3.2.1.111), α -1,4-L-fucosidase (EC 3.2.1.-), α -L-fucosidase (EC 3.2.1.51), and α -1,2-fucosidase (EC 3.2.1.63). These enzymes hydrolyse the glycosidic bonds between the saccharides of carbohydrates to cut down polysaccharides into sugar dimers and monomers. In addition, polysaccharide lyases (PL) (EC 4.2.2.-) and carbohydrate esterases (CE) are involved in the Fucoidan degradation as well. Marine Bacteria secrete CAZY-enzymes for external digestion of carbohydrates. Short chains of polysaccharides are then transported into the cell and introduced in their general metabolism.

In the Baltic Sea of the Kiel Bight, the marine bacterial community associated with the Brown algae *F. vesiculosus* is dominated by Pseudomonadota species of the classes α - and γ -proteobacteria (Stratil et al., 2013). However, the phylum Bacteroidota is less abundant but makes one of the significant fractions in natural conditions. Bacteroidota species are well known for their widespread degradation potential associated with natural and synthetic polymers (Huang et al., 2023; Nguyen et al., 2023; Silverio et al., 2024). The investigation of the algae microbiome composition has the potential to offer insights into species interactions and to identify key species of the algae cell wall carbohydrate degradation. This analysis enables an extensive characterisation of the phylum Bacteroidota and its influence in a diverse community. In general, the microalga bacterial community offers a widespread network of Alga-Bacteria interactions as well as Bacteria-Bacteria interactions. This system gets more complex in natural systems, with several other algae species as well as animals like zooplankton grazers entering the biosphere. Alga-Bacteria interactions mainly rely on an exchange of nutrients that benefit both, the microbes as well as the algae (Kouzuma and Watanabe, 2015). Furthermore, the bacterial communities form biofilms on the algae surface (Macdonald et al. (2024) Fig 3). The formation of biofilms is an extracellular matrix of different organisms (mostly Bacteria), lipids, polysaccharides, secreted proteins/enzymes, and extracellular DNA (Appendix Fig 1) (Brading et al., 1995; Lachnit et al., 2011). Biofilms are a form of bacterial interactions driven by quorum sensing. This cell-cell communication benefits the community by increasing the efficiency of energy conversion and nutrient exchange, as well as protection (Jefferson, 2004; Solano et al., 2014).

Furthermore, metagenomic approaches supported with special HMM searches narrow down the enzymatic potential of certain Bacteria species. Due to several

biotechnological catalysts that have been implemented by screening metagenomes of various sources, the conducted method is efficient and already well established for over 20 years (Voget et al., 2003; Fernández-Arrojo et al., 2010). Metagenomes comprise a dataset of all genes in a particular sample. This dataset enables the accessibility to genes of nonculturable Bacteria. The combination with HMMs for function predictions, which work with amino sequence likelihood patterns of empiric data, makes this method a powerful tool for targeted protein searches.

DOM with algae origin results from the degradation processes described by microorganisms of these algae. As DOM is crucial in the global carbon flux, understanding these degradation processes and observing the involved species can help to understand ecosystem compositions and changes. Furthermore, the industrial processing of algae is of significant interest. Novel, efficient enzymes can be applied to increase algae processing in large-scale algae farms. In the published first study, we investigate *F. vesiculosus* enrichment cultures. We observe microbiome composition and general metabolic dynamics and screen metagenome datasets with HMM for 69 enzyme families, with 36 of those involved in the algae cell wall polysaccharide degradation, including glycosyl hydrolases and sulfatases. We use these results to clone, characterise, test, and implement novel α -L-fucosidases for potential industrial applications on Brown algae degradation.

Publication 2: Exploring *Tetraselmis chui* microbiomes - functional metagenomics for novel catalases and superoxide dismutases

In the frame of the SuReMetS-project I implemented novel α -L-fucosidases for the future use of algae for the sustainable extraction of antidiabetic molecules beyond others. However, microalgae microbiomes also offer a rich source of valuable enzymes. Consequently, an extended targeted screening of microalgae microbiomes for antidiabetic, anti-inflammatory, and antioxidant biomolecules seemed profitable.

The SuReMetS-project focuses on the Metabolic Syndrome (MS). This human syndrome is a combination of several life-limiting conditions with potentially fatal consequences. It was found in over 22 % of US citizens, with increasing rates in people with higher weight conditions (Park et al., 2003). The combination of symptoms and definition of MS vary between different health organisations. However, the World Health Organization (WHO) defines it as insulin resistance in combination with at least two symptoms of increased blood pressure, obesity, and impaired lipid metabolism in

the form of an increased rate of triglycerides and/or a decreased rate of high-density lipoproteins (Alberti et al., 2009; Saklayen, 2018). MS leads to an increased risk of developing Type 2 Diabetes and causes lasting damage to the cardiovascular system. Furthermore, this risk factor increases the impact of the development and severity of other illnesses. As a recent example, the COVID-19 pandemic led to a higher infection chance with the Coronavirus for patients with diabetes and/or MS. The infection had an increased deterioration as those patients' immune- and metabolic systems were already stressed (Marhl et al., 2020).

Besides a "healthy" lifestyle, including sporting activities and balanced nutrition, there are pharmaceutical ways to prevent and fight MS. Reactive oxygen species (ROS) can cause severe damage to humans and promote the development of systemic diseases (Liou and Storz, 2010). Simultaneously, increased concentrations of ROS are associated with diabetes. Here, those ROS are not metabolised correctly and cause cell stress. ROS are oxygen radicals, like superoxide (O_2^-) and hydrogen peroxide (H_2O_2), which have a high affinity for reacting with other molecules (Bayr, 2005). Consequently, there is an increased risk of developing and/or promoting cancer, inflammatory diseases, diabetes, and other life-limiting conditions. ROS result from mitochondrial dysfunction, peroxisome, disturbed receptor signalling, and increased activity of enzymes like oxidases, lipoxygenase (EC 1.13.11.-), cyclooxygenases (EC 1.14.99.1), and thymidine phosphorylase (EC 2.4.2.4). Additionally, increased metabolic activity promotes the formation of ROS (Szatrowski and Nathan, 1991; Storz, 2005; Liou and Storz, 2010). Interestingly, those conditions are caused by systemic diseases and promote these (e.g. tumour development) simultaneously. Oxidative stress is promoted by obesity and insulin resistance, while antioxidant activity is disturbed in MS patients (Urakawa et al., 2003; Armutcu et al., 2008).

In a healthy organism, ROS are metabolised by different biomolecules defined as antioxidants. Those molecules are enzymes and different phenolic compounds (e.g. gallic acid) and Vitamin C with antioxidant properties (Francenia Santos-Sánchez et al., 2019). Antioxidants are found in all phylogenetic kingdoms and are crucial for the well-being of organisms. Two well-studied examples of enzymes that use ROS as a substrate are Superoxide Dismutases (EC 1.15.1.1) and Catalases (EC 1.11.1.6). SODs catalyse the decomposition of O_2^- which results in the formation of breathable oxygen (O_2) and H_2O_2 . The H_2O_2 must be processed further, as it resembles another ROS. In the following, CAT reacts with this product of the SOD catalyse, resulting in

the release of O₂ and water (H₂O). These enzymes can be given to affected patients to treat symptoms and causes of the mentioned diseases in different applications like nutraceuticals, medications, injections, or topic applications. The application depends on the type of antioxidant and the condition in which it is treated (Flieger et al., 2021). Therefore, it is beneficial to find a variety of antioxidants with efficient substrate processing rates.

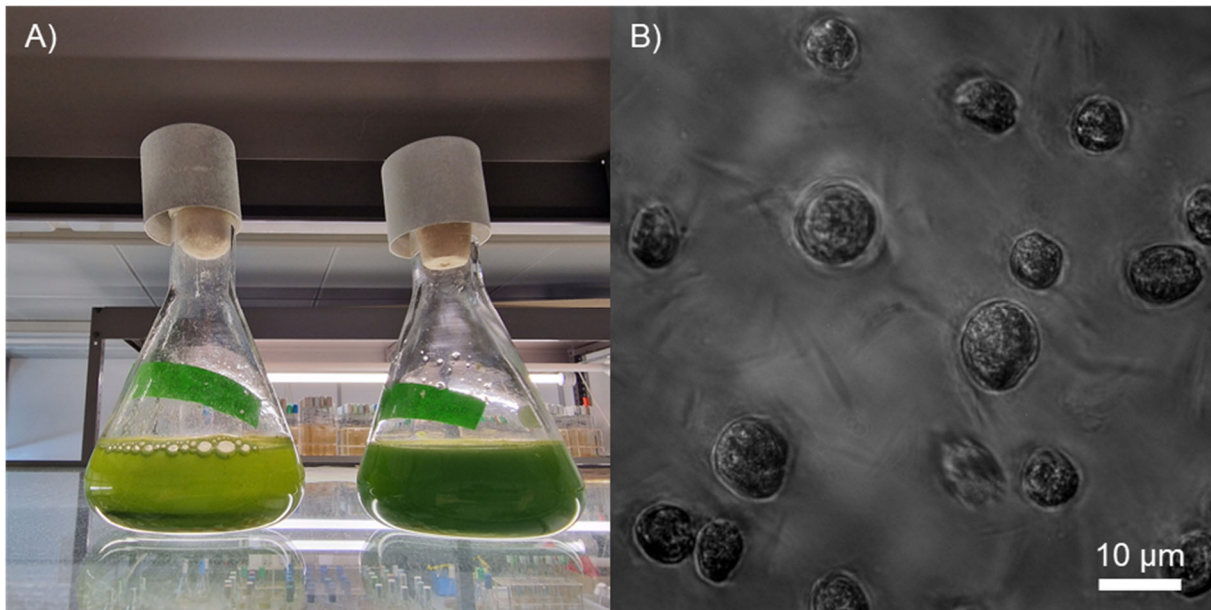


Figure 4: Cultured *Tetraselmis chui* SAG 8-6. **A)** Culture flasks of 2-month old (left) and 4-month old (right) culture. **B)** Optical microscope picture of cultured *T. chui*. Magnification objective 63x with Fluorescence Microscope (AXIO Imager 2, Zeiss, Oberkochen, Germany).

The mechanism and basic structure vary between different groups of SODs or CATs. The SODs groups are defined by a metal co-factor and divided into the following four groups: Fe-SOD, Cu/Zn-SOD, Mn-SOD, and Ni-SOD. SODs can be found in all six kingdoms of life. The evolutionary development of Fe-SOD and Mn-SOD took place in Prokaryotes and Cu/Zn-SOD in Eukaryotes. Following the endosymbiotic theory, Mn-SOD is also found in the mitochondria of Eukaryotes. Ni-SOD is found in Streptomycetota and Cyanobacteria (Steinman, 1978; Smith and Doolittle, 1992; Abreu and Cabelli, 2010). However, CATs are divided into three groups depending on their mechanism. The first two are heme-containing “monofunctional” CATs and heme-containing bi-functional Catalases/Peroxidases. The monofunctional CATs are further divided into three clades. Clade 1 originates from Algae, Plants and Bacteria and contains heme *b*. Clade 2 contains heme *d* and is found in Fungi and Bacteria. Lastly, Clade 3 is the most abundant group found in Bacteria, Archaea, Fungi, Protists, Plants, and Animals (Macdonald et al. (2025) Fig 3). The third CAT group also depends on a metal co-factor and is defined as nonheme Mn-CAT (Zamocky et al., 2008). CAT is the

most efficient enzyme in substrate processing, with a decomposition rate of several million H_2O_2 per Catalase per second (Goodsell, 2004). In Macdonald et al. (2025), microalga microbiomes are suggested as a potential source of those antioxidant enzymes.

Microalgae offer several health benefits (Krohn et al., 2022). One of those is the antioxidant potential. One of the most efficient antioxidants is the keto-carotenoid astaxanthin, which is found in the green alga *Haematococcus pluvialis* and *Tetraselmis suecica* (Holeton et al., 2009; Plaza et al., 2009). Furthermore, in animal studies, feeding experiments with different alga species promoted antioxidant activity (EL-Sabagh et al., 2014; Teimouri et al., 2019; Qiu et al., 2020). As microalgae farming is already well established, harvesting and using those antioxidants is a logical consequence. However, the specific microbiome of microalgae species is crucial for their growth and well-being and, therefore, mandatory for the success of the farming approaches. One industrial cultured microalga species is *Tetraselmis chui* (Fig 4). It is serves as source for fatty acids which find application in the treatment of various diseases (Li et al., 2019; Moser et al., 2022). As for every algae culture system, crucial bacterial microbiomes are attached to the algae and its surroundings, forming a complex network of species interactions by exchanging nutrients (Kouzuma and Watanabe, 2015). An investigation of the microbial community should benefit future farming approaches by increasing the number of bioactive compounds to yield.

Interestingly, microbiomes resemble another potential source for compounds with antioxidant activity. Algae, including their associated microbiome metagenome analyses, hint at elevated numbers of genes coding for antioxidant enzymes like SODs and CATs (Krohn et al., 2022) (see genomes at IMG ID 2507525016). The Bacteria in the microbiome of microalgae express different antioxidants, some of them exclusively found in prokaryotes (Mn-SOD, Fe-SOD, nonheme manganese-containing CAT). So far, numerous antioxidant compounds like carotenoids, exopolysaccharides, CATs, and SODs from marine Bacteria have been described. Those circumstances make the microbiome found in large-scale microalgae farms an additional potential source for those molecules with biotechnological application possibilities.

This assumption led to the experimental design of the publication Macdonald et al. (2025), where *T. chui* enrichment cultures are investigated to examine the antioxidant potential of the associated microalgae. Initial studies of the SuReMetS-project partner

from Marbio, Faculty of Biosciences, Fisheries and Economics, UiT at the Arctic University of Norway, Tromsø, Norway, identified increased antioxidant activity of *T. chui* cultures compared to other microalgae species such as *Nannochloropsis salina*. Metagenome analyses are investigated to reveal novel SODs and CATs, which should be cloned, tested, and characterised. The results will help to promote the extensive use of sustainable algae farming and support future treatment of life-limiting diseases.

Discussion

Biotechnology potential of algae microbiomes

Historically, viable but nonculturable Bacteria pose a challenge to microbial science (Oliver, 1993). Numerous species and genes were unable to be detected. With the implementation of novel molecular tools, these barriers were partially eliminated. Furthermore, improved methods lead to an increase in efficiency, decreasing the costs and time consumption of specific processes. This efficiency is prominently found in genome sequencing and assembly (Mardis, 2011). In addition, the technique of whole metagenome sequencing and bioinformatic approaches like metagenome-assembled genomes (MAGs) and gene prediction with Hidden-Markov Models (HMMs) improved.

With the successful application of those methods, the potential of a powerful pipeline of tools is underlined. Furthermore, the vast potential of algae microbiome for biotechnological applications is pointed out (Fig 5). Six novel enzymes with different functions are implemented (Tab 1). FUJM18 and FUJM20 derive from the *Fucus vesiculosus* microbiome and are α -L-fucosidases and will help in the processing of Brown alga. TcJM_SOD2 and TcIK_SOD3 act as Superoxide Dismutases (SODs). Like the two Catalases (CATs) TcJM_CAT2 and TcIK_CAT3, they originate from the microbiome of the microalga *Tetraselmis chui*. Those antioxidants can be applied in pharmaceutical, cosmetic, and nutraceutical interventions.

Table 1: Novel implemented genes of the present studies.

Gene	Function	Source	Template IMG ID	Length [aa]	NCBI Nucleotide Blast (perc. ident.)
FUJM_18	α -L-fucosidase	<i>F. vesiculosus</i> microbiome	Ga0502370_ 024398_80_ 1447	444	<i>Maribellus</i> <i>comscasis</i> (92.7)
FUJM_20	α -L-fucosidase	<i>F. vesiculosus</i> microbiome	Ga0502371_ 0001890_22 19_3553	426	<i>Butyricimonas</i> <i>faecalis</i> (88.3)
TcJM_SOD2	Fe-superoxide dismutase	<i>T. chui</i> microbiome	Ga0499797_ 000027_110 175_110774	199	<i>Pacificitalea</i> <i>manganoxidans</i> (88.9)
TcIK_SOD3	Fe-superoxide dismutase	<i>T. chui</i> microbiome	Ga0499797_ 000031_370 60_37662	200	<i>Roseitalea</i> <i>porphyridii</i> (88.8)
TcJM_CAT2	Heme-containing "monofunctional" catalase	<i>T. chui</i> microbiome	Ga0499797_ 000030_561 27_57647	506	<i>Pseudosulfitobacter</i> <i>pseudonitzschiae</i> (99.6)
TcIK_CAT3	Heme-containing "monofunctional" catalase	<i>T. chui</i> microbiome	Ga0499797_ 000173_134 86_14940	484	<i>Roseovarius</i> sp. (87.6)

All studies involved different enrichment cultures. These artificial systems are beneficial for implementing stable culture conditions and enabling the observation of culture changes or maintaining single and mixed species environments. These experimental setups can alter the bacterial composition of the microbiome. Consequently, this affects the outcome of the metagenome screening, particularly in comparison to a natural marine microbial community. This influence is known as the bottle effect and gives an advantage to fast-growing Pseudomonadota species (Eilers et al., 2000). Furthermore, the chosen cultivation parameters for temperature and oxygen conditions are influenced by shaking speeds, lid applications, salinity, volume, culture medium, and light conditions, which influence the microbial composition and gene transcription dynamics. Alternation and optimisation of those conditions presumably result in different outcomes, further expanding the potential number of species and genes to find (Sangeetha and Thangadurai, 2024).

Nevertheless, the results of both published studies underline the biotechnological potential of those diverse communities. Besides the implemented novel enzymes, several genes were identified with putative activity on various substrates. In further approaches, those genes can be characterised and tested for additional implementations of biotechnological tools of algae microbiome origin. With this, the industry can maximise the yield of these sustainable farming applications. Those results promote the use of algae farms to find valuable biological compounds for the health sector, the nutraceutical and food industry, and energy and biofuel companies. Furthermore, it is strongly suggested that scientific investigations of algae microbiomes be emphasised.

Publication 1: Community dynamics and metagenomic analyses reveal Bacteroidota's role in widespread enzymatic *Fucus vesiculosus* cell wall degradation

Fucus vesiculosus, as a Brown algae species, synthesises all three phaeophycean-associated cell wall carbohydrates. The content of Fucoidan elevated in this species, as the genes coding for Fucoidan degrading enzymes in our study (Fletcher et al., 2017). In initial studies, we tested several inoculations including soil samples and faeces of herbivore mammals. The marine microbiome attached to the algae was the most successful in enzymatic degradation. Samples from the terrestrial origin of different soils and horse gut microbiota did not lead to significant visual changes in the plants but lack enzymes active on further carbohydrates with marine origin.

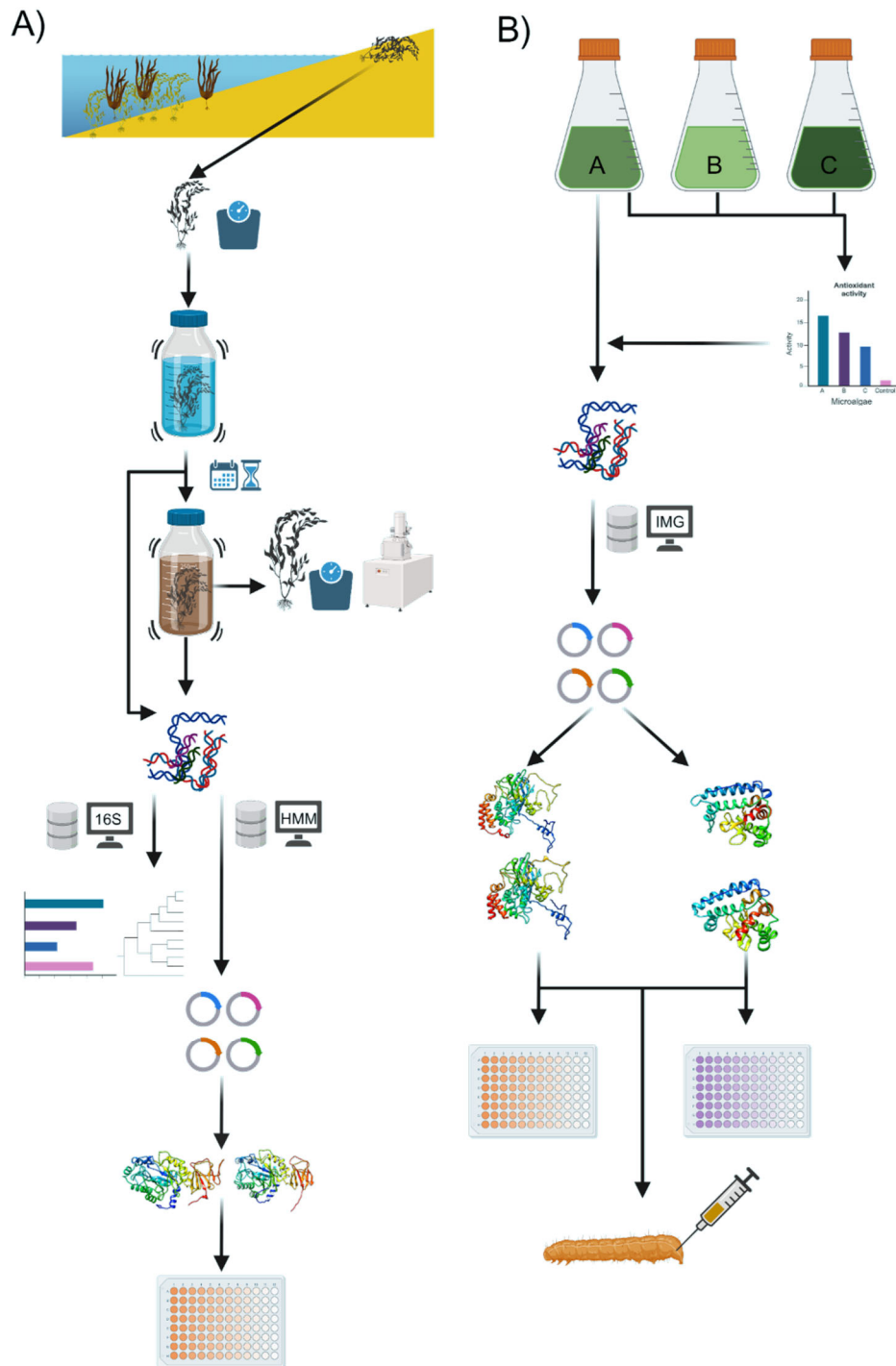


Figure 5: Methodology from the published studies in the thesis: **A)** Macdonald et al. (2024): *Fucus vesiculosus* samples were collected from the shore and transferred into shaking enrichment cultures. Over 25 days, the cultures were monitored regularly for metabolic and phylogenetic changes. Metagenome datasets and Hidden-Markov Models were utilised to identify gene candidates, which were cloned, tested, and characterised. **B)** Macdonald et al. (2025): Initial tests on microalgae cultures highlighted the antioxidant activity of *Tetraselmis chui* cultures. Using a metagenome dataset, putative Superoxide Dismutases and Catalases were identified, cloned, tested, and characterised.

Overall, the conducted 105 HMMs for the 67 GH and 2 Sulfatase families revealed over 17,000 unique genes. The expectation of an increased number of genes in the microbiome coding for enzymes active on Fucoidan is fulfilled in Macdonald et al.

(2024). This conclusion relies on the 1,010 identified genes that belong to GH29, so they resemble putative glycosyl hydrolases that hydrolyse the glycosidic bond of Fucoidan. This equals >8 % of all identified glycosyl hydrolases. The most interesting result is found in the 643 predicted GH29 genes for the phylum Bacteroidota, making it the most crucial phylum for the enzymatic Brown algae cell wall degradation. Furthermore, the highest number of predicted sulfatases was derived from the Bacteroidota phylum too.

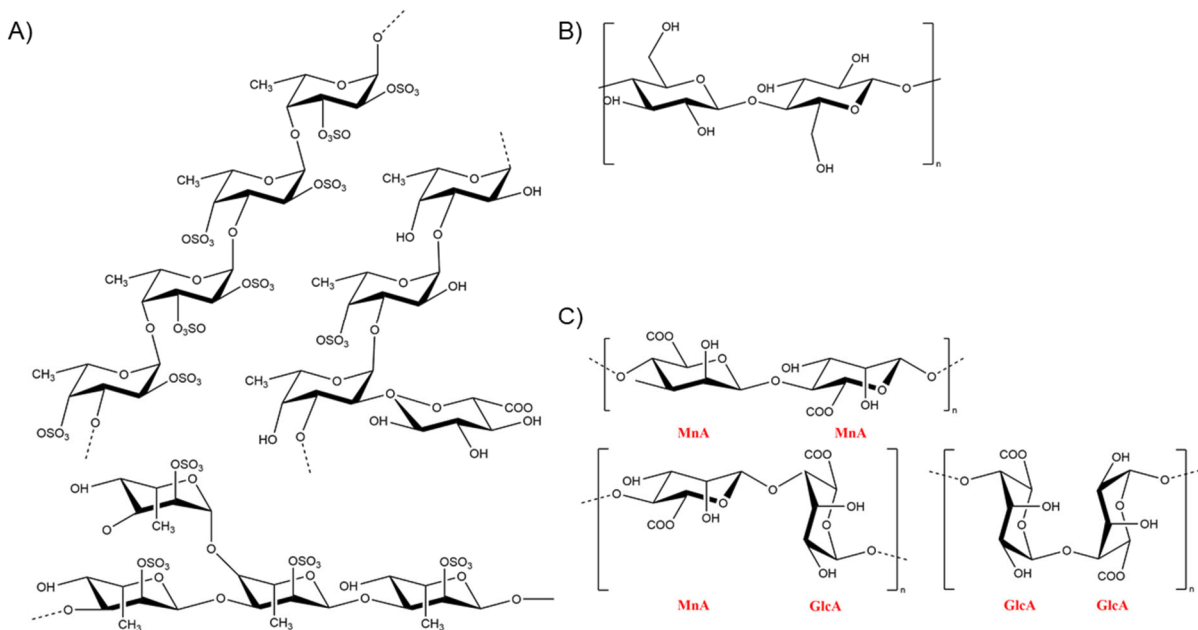


Figure 6: Schematic molecular structures of phaeophyceyan cell wall carbohydrates. Created with ChemDraw v21.0.0. **A)** Fucose-containing sulfated polysaccharide/Fucoidan in Homofucan backbone structure and crosslinked Heterofucan structure. **B)** Cellulose. **C)** Alginate in α -1,4-L-guluronic acid (PolyGlcA), β -1,4-D-mannuronic acid (PolyMnA), and mixed PolyMnA-GlcA blocks.

Fucoidan is degraded in a diverse multistep enzymatic procedure. The backbone of α -L-fucose connected in variable glycosidic bonds contains sulfuric acid groups, that must be detached from the carbohydrate (Fig 6A) (Chevolot et al., 2001; Dobrinčić et al., 2020). Consequently, sulfatases are crucial for the degradation process. In addition, GHs and carbohydrate binding modules (CBMs) are involved in the cascade (Macdonald et al. (2024) Fig 1 and Macdonald et al. (2024) Supplementary Tab 4) (Li et al., 2018; Schultz-Johansen et al., 2018). This study's metagenome approach confirms the capability of the *F. vesiculosus* microbiome to degrade the carbohydrate. However, Fucoidan consists of branches and varying contents of different saccharides besides Fucose, like Galactose and Xylose, beyond others (Makita and Taniguchi, 1985). The second primary Brown algae cell wall carbohydrate is Alginate, which interacts with Phlorotannins. This molecule also has a complex and variable structure of MnA and GlcA blocks (Fig 6C) (Dobrinčić et al., 2020). In contrast to Fucoidan, no

GH families but PLs and CBMs are involved in the degradation of Alginate (Fig 3A, Macdonald et al. (2024) Supplementary Tab 4). A comparable simple structure is found in Cellulose with chains of linked β -D-glucose molecules (Fig 6B). Several GH, CBM and carbohydrate esterase families are involved in the degradation, including more general GH families like GH1, GH3, and GH5 (Fig 3C) (Brumm, 2013; Wang et al., 2020). The most abundant phylum in the enrichment cultures, Pseudomonadota, included relatively low numbers of genes involved in the Fucoidan degradation. However, the observed Pseudomonadota show an increased number of genes for the mentioned general GH families GH1 and GH3 and are presumably active on Cellulose. Nevertheless, the highest number of predicted GH3 genes are synthesised by Bacteroidota. Laminarin, the storage carbohydrate of Brown algae, is degraded by GHs and CBMs (Fig 3B) (Becker et al., 2017; Qin et al., 2017). As for the Cellulose degradation, less predicted associated GH genes were identified compared to the Fucoidan degradation, with Bacteroidota as the most significant phylum, followed by Pseudomonadota.

Studies regarding the expression of Fucoidan degrading glycosyl hydrolases confirm the significant influence of the phylum Bacteroidota due to the elevated expression of the CAZY families GH29 and GH168, especially of the Flavobacteriaceae family (Zhang et al., 2024). Additionally, the high potential for Alginate degradation was confirmed by the expression of several PLs. In the study of Zhang et al., 2024, a similar approach was used to identify Brown algae degrading bacterial communities and genes, including metagenome and HMM approaches. In contrast to the presented first study Macdonald et al., 2024, the observed Brown alga species was *Saccharina japonica* in China, which was not degraded in enrichment cultures but collected and compared directly from the tidal zone of the Bohai Sea at Yantai, China in fresh and decayed form. This approach revealed an increased number of Verrucomicrobiota species, especially from the genus *Lentimonas*, compared to the enrichment culture degradation with high numbers of genes from the GH95 family, which comprises further α -L-fucosidases (EC 3.2.1.51). *Lentimonas* sp. CC10 and *Lentimonas* sp. CC21, isolated from the Baltic Sea, have already been identified as key candidates for extensive fucoidan degradation, our findings further support those results (Sichert et al., 2020). As the presented results unravel hints for the fate of carbon in marine systems and the dynamics of DOM, it is necessary to compare the results to dynamics in natural systems.

The Baltic Sea is a marine habitat with unique characteristics due to its geographic enclosure by the Baltic landmass. Through this, freshwater inflow rates are high, while inflow events of the other marine systems are limited and only appear through Skagerrak and Kattegat. Those conditions lead to a rarely found layering and mixing of different waters, influencing water temperatures, oxygen distribution, and salinity dynamics. Consequently, the marine micro- and macrofauna are interesting to investigate, especially as their composition influences the initial inoculations of the enrichment cultures of the study on *F. vesiculosus* (Snoeijs-Leijonmalm and Andrén, 2017). The HMM search for certain GH and Sulfatase-families assigned 782 genes to species of the genus *Lentimonas*, most of them to one of the two described strains. However, the observed genes of Bacteroidota derive from a more diverse bacterial community. The overall 8442 HMM predicted genes derive from 2619 different species, with 17 of those coding for > 100 predicted genes each. Therefore, Bacteroidota is predicted as a specialised phylum capable of widespread algae cell wall carbohydrate degradation. The Bacteroidota species with the most genes coding for the observed GH and Sulfatase-families are *Mariniflexile fucanivorans* (404 assigned genes) and *Formosa algae* (266 assigned genes). Both Flavobacteriia species were previously described as active on sulfated Fucans (Barbeyron et al., 2008; Silchenko et al., 2016). Furthermore, characteristic polysaccharide utilisation loci (PUL) are previously found in species of Bacteroidota, like *Bacteroides thetaiotaomicron* (Feng et al., 2022; Yu et al., 2024). PUL are specialised gene systems, including genes involved in sensing, degradation, and transporting polysaccharides (Grondin et al., 2017). This genomic characteristic and the metagenome results emphasise the role of Bacteroidota in widespread polysaccharide degradation systems and strengthen our assumption of their crucial role in the Fucoidan and Brown algae degradation.

Furthermore, fouling rates of different *Fucus* species are strongly connected to their surface microbiome. The algae itself produces and secretes biomolecules that, on the one hand, protect the surface and, on the other hand, promote species with beneficial characteristics for the algae (Oppong-Danquah et al., 2023). For example, *Fucus distichus* subsp. *evanescens* was recently found to exclusively release beatine lipids MGTA, ulvaline, and 4-pyridoxic while exhibiting slower rotting compared to *F. vesiculosus* and others. Additionally, Oppong-Danquah et al. observed bacterial and fungal species with antimicrobial and antifouling effects on *F. distichus* subsp. *evanescens*, again missing at the surface of other *Fucus* species. Interestingly, this

study's 16S rRNA gene amplicon results differ from ours despite of the same origin. While the relative abundance of Pseudomonadota was lower and the Bacteroidota significantly elevated in the presented study's initial composition, Oppong-Danquah et al. found Actinomycetota >15 % contrary to their abundance of <1 % in the enrichment culture approach. This variance is possibly caused by the different sampling dates, seasonality, and sampling methods. Other approaches to the *F. vesiculosus* microbiome composition strengthen this assumption, as they are more similar to the presented results of Macdonald et al. (2024) (Parrot et al., 2019). As stated, the initial composition lays the foundation for the degradation process in enrichment cultures, especially caused by the pre- or absence of key species like the described *Lentimonas* sp. CC10 and *Lentimonas* sp. CC21. Another candidate for an efficient, widespread degradation of Brown algae is *Agarivorans albus* B2Z047. This Bacterium was able to perform hydrolysis rates of > 50 % of *Saccharina japonica* and > 30 % of Sargassum. Green and red algae showed limited hydrolysis rates by *A. albus* B2Z047 (Gong et al., 2024). However, the bottle effect influences these initial conditions as well.

The methods used in this study worked out as an efficient pipeline of tools (Fig 5A). Metagenome approaches to screen for Fucoidan active enzymes have already been conducted in previous research (Schultz-Johansen et al., 2018). However, there is room for potential improvements. The *F. vesiculosus* samples were collected through specific time points, e.g. the basis of the metagenome dataset was from samples washed ashore in March 2021. Several time points would unravel the influence of seasonality for a broader identification of the microbiome composition and degradation dynamics (Wietz et al., 2015; Herlemann et al., 2016). Consequently, the number of efficient genes active on algae cell wall carbohydrates should increase. Furthermore, the samples were collected from the tidal zone in semi-dry conditions. It would be interesting to get insights into the degradation success of the microbiome attached to fresh algae that have not yet been exposed to dry conditions. The composition of those microbiomes and those in the surrounding waters is well known and presumably includes algae cell wall carbohydrate active enzymes that are lost during the exposition of the algae to dry conditions and UV radiation (Stratil et al., 2013; Mensch et al., 2016). Multiple observed enrichment cultures lacked in the consistency of the visual degradation processes, presumably caused by those altering inoculation conditions. For the gathering of information on chemical processes in natural conditions, blue

carbon research, and previously described harmful effects of degradation products on sediment systems, it is necessary to combine results on experiments from field studies and laboratory results (He et al., 2024). Furthermore, in extended research, culturing barriers like the bottle effect can be decreased in controlled mesocosm experiments in tidal sites, similar to the studies of Zhang et al., 2024. However, the method used in this study allowed for the improved monitoring of metabolic dynamics solely caused by the microbiome, as the influence of the macrofauna is excluded. The enzymatic influence on the cell wall degradation of Fungi also remains unknown. Nevertheless, Fungi are prominently known as natural degraders and for expressing carbohydrate active enzymes (Zhang et al., 2020). Occasionally, slime mould formation was observed on the surface of the enrichment cultures, indicating at an active fungal community.

For a more detailed knowledge of the cleavage of algae cell wall carbohydrates and the fate of the polysaccharides, molecular enzyme mechanisms and structural transformation of molecules need to be investigated. Current research focuses on the structure of Fucoidan of different origins (Reyes-Weiss et al., 2024). The supply of purified Fucoidan is limited and expensive, as the current extraction methods are time consuming and the yield is low. The methods for *F. vesiculosus* include microwave- and ultrasound-assisted methods as well as enzyme extraction methods, besides extensive pretreatment (Hahn et al., 2012). This research barrier will be partly eliminated, as researchers implemented and improved methods to synthesise Fucoidan oligosaccharides (Crawford et al., 2024). This synthesised carbohydrate can also be applied in health management, as Fucoidan has benefits in several health applications. For example, Fucoidan is indirectly helpful for cancer treatment, as it positively influences the gut microbiota (Li et al., 2024). Furthermore, Fucoidan was proven to prevent, inhibit and cure SARS-CoV-2 infections (Song et al., 2024).

Additionally, α -L-fucose oligosaccharide is part of human milk (Choi et al., 2015). Therefore, a guaranteed supply is crucial for the healthy development of infants and valuable for the baby food industry. Besides their application in health management, these artificial polysaccharides can lead to substantial knowledge about degradation mechanisms and help to establish novel biotechnological tools. The efficiency and implementation of α -L-fucosidases like FUJM18 and FUJM20 will benefit from those techniques in the future.

The enzyme structures of the identified α -L-fucosidases were predicted by AlphaFold2. A structure comparison to α -L-fucosidases of the RCSB Protein Database (PDB) reveals the most structurally similar enzyme entry of the phylum Bacillota (Berman, 2000). This identification is contrary to the nucleotide blast prediction, which assigns the highest sequence similarities of 88.3 % and 92.7 % to Bacteroidota species (Tab 1). However, as a nucleotide sequence similarity resembles evolutionary development, the genes most likely originate from Bacteroidota. As PDB is limited to the entries, enzymes originating from Bacillota might be well-studied and, compared to Bacteroidota, overrepresented. Extensive future protein structure analyses are needed to investigate crystal structures and their relations. The produced bias becomes further apparent as structurally similar, non-bacterial proteins were found to originate from mammals like the wild boar (*Sus scrofa*) and humans (data not shown). Those results strengthen the nucleotide blast assignment for phylogenetic analyses, while the structure prediction and comparison help to identify potential enzyme mechanics.

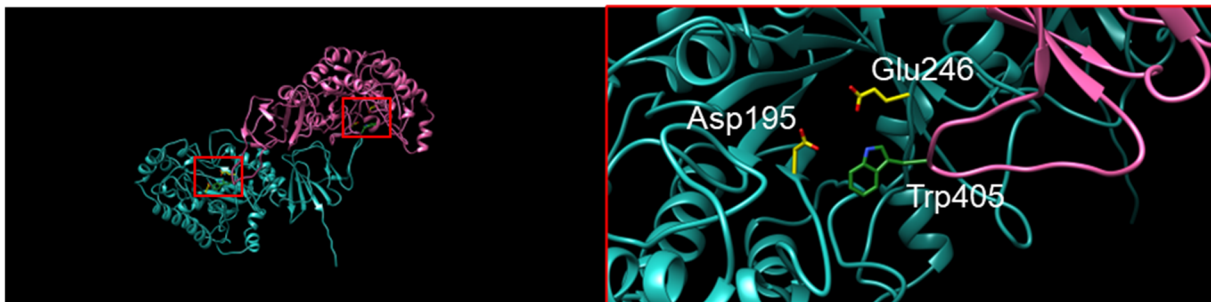


Figure 7: Structure and bonding prediction of a functional FUJM18 dimer. Two active sites are formed by Asp195 and Glu246 residues (yellow) of one enzyme chain, completed by a Trp405 residue (green) of the other enzyme chain. Blue: Nitrogen, Red: Oxygen. Structure and bonding prediction created AlphaFold2, visualisation created with UCSF Chimera v1.177.3 and ChimeraX v1.8 (Pettersen et al., 2004; Jumper et al., 2021).

In detail, for FUJM18 and FUJM20, the most structurally related PDB entry is a GH29 α -L-fucosidase isoenzyme 1 from *Paenibacillus thiaminolyticus* (PDB ID 6GN6) chain described in 2018 (Kovařová et al., 2018). The X-ray diffraction image reveals a polymer of six chains. Each chain consists of an N-terminal domain and a CBM-like C-terminal domain, which is the same structure as in FUJM18 and FUJM20. The larger N-terminal domain includes 13 α -helices and 6 β -strands predicted for FUJM18 and 11 α -helices and 6 β -strands predicted for FUJM20. This domain shares similarities to a $(\beta/\alpha)_8$ barrel. For FUJM18, the active site is located inside the barrel. The prediction for the C-terminal domain shows 1 α -helices and 6 β -strands predicted for FUJM18, while FUJM20 has no α -helices and 7 β -strands. Two chains form dimers as an active subunit. The active site of a 6GN6 chain comprises two residues: a nucleophile Asp186

and an acid/base functioning Glu239 of the N-terminal domain. Interestingly, a Trp392 residue on the C-terminal domain of the second chain of the dimer completes the active site after and the other way around. This orientation results in two active sites per dimer. When the protein sequence of 6GN6 is aligned with FUJM18 and FUJM20, we find all three identical residues in the motive of FUJM18 (Asp195, Glu246, Trp405), for FUJM20 only a corresponding aspartic acid (Asp191) is present (Fig 7). Consequently, FUJM18 is expected to have a highly similar mechanism to 6GN6.

However, bonding predictions do not show a similar structure of FUJM20 dimers, as the C-terminal CBM domains are orientated outwards (Appendix Fig 2). This orientation is contrary to 6GN6 and FUJM18 and further hints at a different molecular mechanism that must be investigated in future studies.

Contrary to GH95, the other α -L-fucosidase family with known mechanism, GH29-fucosidases do not reconfigure the anomeric state of released saccharide residues. The whole reaction happens in 2 steps including a sequential glycosylation and deglycosylation. In the first step, the anomeric compound of the substrate reacts with a residue acting as a nucleophile. Simultaneously, a second residue acts as an acid/base and protonates the glycosidic oxygen. This protonation catalyses the cleave of the aglycone moiety. A glycosyl-enzyme linkage is formed, which is finally cleaved by a water molecule (Koshland, 1953; McCarter and Stephen Withers, 1994; Koval'ová et al., 2018). Through the predicted assignment as well as identified conserved regions of FUJM18 and FUJM20 to GH29, those mechanisms are assumed to be found for those enzyme candidates.

JMFU18 and JMFU20 show significantly higher enzyme activities in elevated temperatures. JMFU18 was exceptionally efficient at 80° C, while JMFU20 showed the highest activity rates at 70° C and 80° C, both in optimal pH conditions of pH 6. In general, JMFU18 was more efficient in substrate processing in the conducted *pnp*-fucopyranose assay compared to JMFU20. The enzyme activity of $61.18 \pm 12.79 \text{ U} \cdot \text{mg}^{-1}$ in optimal conditions was >25 % higher than the activity of JMFU20. This increased enzyme activity supports the calculated HMM prediction, as the score of JMFU18 with 325.3 was higher than that of JMFU20 with 324.4. Highly active α -L-fucosidases are essential for future use in industrial algae processing but are also valuable for treating Fucosidosis, a human disorder on Chromosome 1.

Fucosidosis is a rare disease with <100 known cases that developed life-limiting symptoms caused by the missing enzyme (Johnson, 2015).

All the results helped to implement two novel, thermostable, and highly active α -L-fucosidases for industrial application and gave insights into the global marine biogeochemical processes. The phylogenetic analyses and specialised metagenome screening also give an amazing overview of the microbial algae cell wall degradation potential. With this, the exceptional role of Bacteroidota for carbohydrate processing is emphasised, as well as the adaptation of the microbiome to the Brown algae surface and surroundings. Furthermore, the results of the study serve as proof of concept. Both enzymes FUJM18 and FUJM20 can be used to process Brown macroalgae. This sustainable approach shapes the future of industries that have already started to adapt to novel methods, including renewable resources. A universal, sustainable, and efficient algae cell wall degradation method is still urgently needed. The two implemented enzymes are putative candidates for a future enzyme mixture for a widespread application in algae processing.

Publication 2: Exploring *Tetraselmis chui* microbiomes - functional metagenomics for novel catalases and superoxide dismutases

While Macdonald et al. (2024) focused on the biotechnological potential of algae microbiomes with applications on marine organic matter, this study Macdonald et al. (2025) targets health management approaches and putative applications on humans. Here, microalga cultures were harvested, conducted, and tested for antioxidant activity (Fig 5B). Multiple initial assays (Ferric ion reducing antioxidant power (FRAP), ELISA (anti-inflammatory), Inhibition of dipeptidyl peptidase IV peptidase activity (DPP IV)) from project partners of the University of Norway, Tromsø on microalga cultures of different single species systems revealed *T. chui* and its associated microbiome as an exciting candidate for further investigations.

So far, several studies have shown the antioxidant effects of marine algae extracts. In a corresponding review of Coulombier et al., 2021, 60 individual studies within different *in vitro* and *in vivo* experiments are summarised, comprising various microalgae species and their increased antioxidant potential. Beyond them are commercially interesting microalgae candidates like *Nannochloropsis salina*, *Chlorella vulgaris*, *Scenedesmus quadricauda*, and the conducted *T. chui* (Aremu et al., 2014; Safafar et al., 2015; Rahman et al., 2017; Agregán et al., 2018). However, the antioxidant

influence of the associated microbiome remains less enlightened. This imbalance is presumably due to the higher yield of cultivated microalgae and their exceptional content of antioxidant compounds like carotenoids and exopolysaccharides. Primarily carotenoids are expressed by a variety of organisms and are already established and applied as antioxidant agents (Mapelli-Brahm et al., 2023). However, the published study focuses on marine bacterial enzymes with antioxidant activity. Regardless of the microbiome antioxidant activity results, microalgae remain a highly relevant source of antioxidant compounds. Ranking research results focusing on the extraction and identification of Superoxide Dismutases and Catalases, both microalgae and marine Bacteria are equally crucial as putative sources (Hamidi et al., 2019). Additionally, early research developed methods for antioxidant screenings from 112 isolated marine Bacteria but did not focus on algae microbiomes (Takao et al., 1994).

The general antioxidant activity is mainly described and confirmed for marine Bacteria, similar to the conducted initial tests. Through this, the antioxidant activity of marine Bacteria is confirmed, and their importance for health management is strengthened (Tripathi et al., 2020). In the course of this thesis, the search for novel bioactive compounds is extended. The presented study's results can help emphasise the role of microbiomes and promote another source of commercial bioactive compounds that can be yielded in microalgae farms or produced in biotechnological plants.

Identified and significant enzymes with antioxidant activity are Glutathione Peroxidases (EC 1.11.1.19), Peroxiredoxins, Thioredoxin Reductase, Superoxide Dismutases, and Catalases, Catalase-peroxidase each with several subdivisions (Sáez and Están-Capell, 2014). The screening of the *T. chui* SAG8-6 metagenome focused on SODs and CATs, two linked enzyme classes, as a product of the SOD reaction serves as the substrate for CATs. Moon and Cho, 2023 showed the successful application of *T. chui* as a nutraceutical and identified its antioxidant benefits. However, those results apply to the alga and the associated peptides. The role of the microbiome of this alga regarding the expression of antioxidants is rarely known. In the metagenome analyse, the IMG enzyme classification revealed 258 enzymes with antioxidant activity (number of hits per 50 mb). Besides the group with the most identified genes coding for glutaredoxins (51), genes coding for 9 SODs and 6 CATs were identified.

The four established novel enzymes in Macdonald et al. (2025) have exceptional potential for application in humans, as two conducted assays on invertebrates for toxic

effects did not hint at harmful characteristics. Consequently, it is recommended to test these enzymes in further studies to achieve efficient treatments for inflammatory diseases, cancer, diabetes, and (in general) take care of the metabolic syndrome. Furthermore, the two SODs and two CATs showed activities in low concentrations.

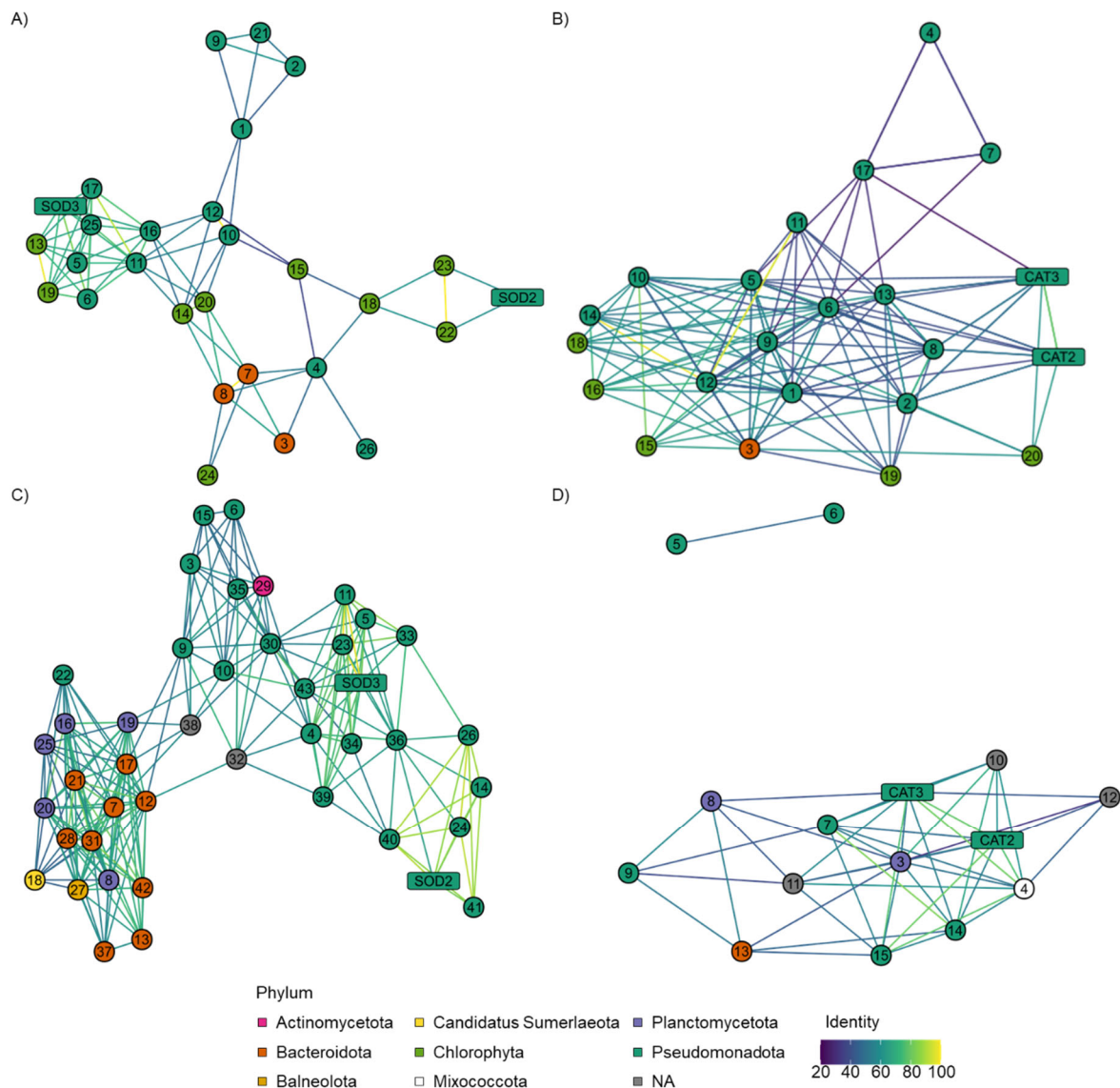


Figure 8: Protein sequence similarity network of different microalgae microbiome metagenome datasets in comparison to TcJM_SOD2 (IMG ID Ga0499797_000027_110175_110774_1), TcIK_SOD3 (IMG ID Ga0499797_000031_37060_37662_1), TcJM_CAT2 (IMG ID Ga0499797_000030_56127_57647_1), and TcIK_CAT3 (IMG ID Ga0499797_000173_13486_14940_1) derived from a *Tetraselmis chui* microbiome metagenome (IMG ID Ga0499797). Supporting data is displayed in Appendix Table 1. Data was processed and provided by the University Medical Centre Hamburg-Eppendorf, Bioinformatics Core, Hamburg, Germany. Supporting data for Macdonald et al. (2025) Fig 1. **A)** Superoxide dismutase sequence network of a *Chlorella vulgaris* microbiome metagenome (IMG ID Ga0483890). **B)** Catalase sequence network of a *Chlorella vulgaris* microbiome metagenome. **C)** Superoxide dismutase sequence network of a *Nannochloropsis salina* microbiome metagenome (IMG ID Ga0500404). **D)** Catalase sequence network of a *Nannochloropsis salina* microbiome metagenome.

Interestingly, all four enzymes most likely derive from α -proteobacteria species, while previous research of algae microbiome-derived antioxidants identified γ -proteobacteria as a bacterial class with increased antioxidant potential (Pawar et al., 2015). Although Macdonald et al. (2025) only included the microbiome of one microalga species, the results are suitable for estimating the potential of other microalgae-associated microbiomes.

An extensive analysis of the novel-identified antioxidant shows the potential of further algae species microbiomes (Fig 8). Over 40 predicted SODs and CATs are found in a *Chlorella vulgaris* culture metagenome dataset (IMG ID Ga0483890) (Fig 8AB). The enzymes TcJM_SOD2, TcIK_SOD3, TcJM_CAT2, and TcIK_CAT3 derived from the *T. chui* microbiome resemble around 80 % sequence similarity to the closest enzyme of the *C. vulgaris* microbiome. Most enzymes derive from the phylum Pseudomonadota. Higher similarities are found for TcJM_SOD2 and TcIK_SOD3 in a SOD network analysis of a *Nannochloropsis salina* culture metagenome (IMG ID GA0500404) (Fig 8CD). Here, 41 SODs were identified. Again, the majority of enzymes derive from Pseudomonadota. This gene distribution also resembles the CATs in the *N. salina* microbiome (Fig 8D). With this, we can further emphasise the antioxidant potential of microalgae microbiomes. These findings lay the foundation for future approaches in the search for novel antioxidants.

Additionally, the structure of the four antioxidants were compared to previously described functional enzymes from PDB and compared in an all-vs-all approach with the Dali Server (Appendix Fig 3, Appendix Fig 4) (Berman, 2000; Holm, 2022). TcJM_SOD2 was structural most similar to a crystal structure of an iron/manganese cambialistic Superoxide Dismutase from *Rhodobacter capsulatus* (7azq, <https://doi.org/10.2210/pdb7AZQ/pdb>, Entry Authors: Ponce-Salvatierra, A., Hermoso, J.A., 2021) (Appendix Fig 3A). Simultaneously, TcIK_SOD3 resembled the most structural similarity to a corresponding iron Superoxide Dismutase from *Acinetobacter* sp. Ver3 (7sbh, <https://doi.org/10.2210/pdb7SBH/pdb>) (Appendix Fig 3B) (Steimbrüch et al., 2022). A closer analysis of the active site of both enzymes revealed a similar orientation of specific residues, assuming an identical reaction mechanism of the enzymes. For both enzymes and the corresponding crystal structures, this includes an iron atom held in place by three Histidine and an Aspartic acid residue. Two close residues of Tyrosine and Glutamine are involved in the cleavage of the superoxide substrate (Abreu et al., 2005). As 7sbh, Fe-SODs form dimers.

In addition, the structural alignment revealed the closest relation of a highdose liganded bacterial Catalase (4b7h, <https://doi.org/10.2210/pdb4b7h/pdb>) to TcJM_CAT2 (Appendix Fig 4A) (Candelaresi et al., 2013). This tetramer-forming enzyme has heme *b* in its active site with a prominent orientated Tyrosine residue, which is involved in the enzyme reaction with Hydrogen peroxide. The similar structure with significant compounds involving a β -barrel next to the active site hints at a similar enzyme mechanism and potential forming of tetramers of TcJM_CAT2 chains. Those findings also apply to TcIK_CAT3 and the structural closest PDB Atomic resolution structure of *Micrococcus lysodeikticus* Catalase (1gwe, <https://doi.org/10.2210/pdb1gwe/pdb>) (Appendix Fig 4B) (Murshudov et al., 2002).

Potential applications of all four enzymes must be investigated in the future. Besides the potential for the cosmetic industry regarding skin rejuvenation, their application in clinical studies is highly interesting. Suppose the initial toxic assays are extended and the enzymes are identified as harmless for human applications. In that case, the enzymes can potentially help thousands of people suffering from several systematic diseases. Affordable medicine for cancer treatments and diabetic patients is urgently needed. Furthermore, the presented research results emphasise the future investigations of microalgae microbiomes. The implementation of novel SODs and CATs by innovative techniques was proven to be efficient and effective.

Further biotechnological potential of algae microbiomes

In an extension study, we tested the metagenomes of the four *F. vesiculosus* enrichment cultures for the putative capability of degrading synthetic polymers based on enzyme function predictions with the metagenome datasets and HMM analyses. This screening will further emphasise the biotechnological potential of marine algae microbiomes in even more fields. For this, HMM screenings based on three models were conducted: an HMM for polyethylene terephthalate (PET) esterases "PETase_UHH_2202" (Fig 9A)), an HMM for Polyurethane (PUR) amidases PU_amidase_UHH_2007, and an HMM for PUR esterases "PU_esterase_UHH_2007" (Fig 9B), available on the Plastics-Active Enzymes Database (PAZy) (Buchholz et al., 2022). Data preparation with the help of Dr Pablo Pérez-García revealed 543 unique (bitscore cut-off 100) genes with putative enzyme activity on PET and PUR (2 PET esterases, 532 PUR amidases, and 9 PUR esterases).

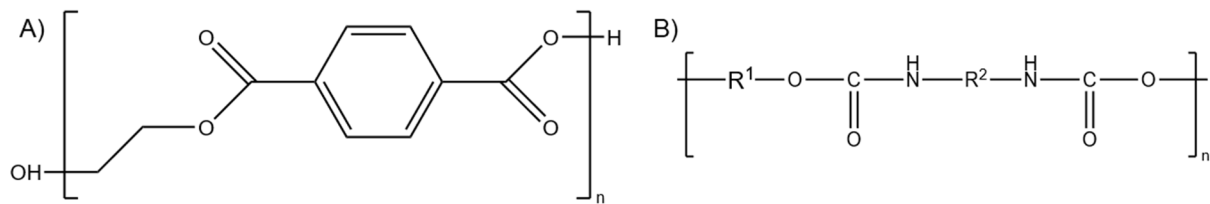


Figure 9: Molecular structure of synthetic polymers which serve as a putative substrate for enzymes of the *F. vesiculosus* microbiome metagenome predicted by HMMs. Created with ChemDraw v21.0.0. **A)** Polyethylene terephthalate. **B)** Schematic structure of Polyurethane with characteristic Urethan-group -NH-CO-O-.

The highest HMM-score for the predicted PET esterases was 105.7 for the gene Ga0502371_0441542_3_347. According to the IMG classification, this gene primarily acts as a triacylglycerol lipase. The gene Ga0502370_001663_2530_4002 is defined as amidase/aspartyl-tRNA(Asn)/glutamyl-tRNA(Gln) amidotransferase subunit A according to IMG. Additionally, it has the highest calculated HMM-score of 330.0 for PUR amidases in the *F. vesiculosus* microbiome metagenome. Finally, the highest HMM-score for PUR esterases was 262.9 for the gene Ga0502373_0181688_3_470, a predicted Ca²⁺-binding RTX toxin-like protein according to IMG. For further confirmation, these enzyme candidates need to be cloned and tested. Those approaches help extend recycling processes to minimise the environmental pollution caused by synthetic polymers, as multimillion tons of plastics have been distributed over the last seven decades (Brandon et al., 2019). The successful identification of several enzyme candidates underlines the enzymatic polymer-degrading potential of algae microbiomes. With this, it is highly recommended to investigate and extend studies approaching algae research and marine microbiomes.

Publication 1: The bacterial degradation of Brown algae cell wall carbohydrates

Full title: Community dynamics and metagenomic analyses reveal Bacteroidota's role in widespread enzymatic *Fucus vesiculosus* cell wall degradation

First author: Jascha F. H. Macdonald

Corresponding author: Dr Ines Krohn

Co-authors: Dr Pablo Pérez-García
Dr Yannik K.-H. Schneider
Dr Patrick Blümke
Dr Daniela Indenbirken
Professor Dr Jeanette H. Andersen
Professor Dr Wolfgang R. Streit

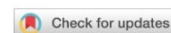
Journal: Scientific reports

Accepted: 29th April 2024

Published: 3rd May 2024

DOI: <https://doi.org/10.1038/s41598-024-60978-8>

scientific reports

**OPEN** **Community dynamics and metagenomic analyses reveal *Bacteroidota*'s role in widespread enzymatic *Fucus vesiculosus* cell wall degradation**

Jascha F. H. Macdonald¹, Pablo Pérez-García², Yannik K.-H. Schneider³, Patrick Blümke⁴, Daniela Indenbirken⁴, Jeanette H. Andersen³, Ines Krohn¹✉ & Wolfgang R. Streit¹

Enzymatic degradation of algae cell wall carbohydrates by microorganisms is under increasing investigation as marine organic matter gains more value as a sustainable resource. The fate of carbon in the marine ecosystem is in part driven by these degradation processes. In this study, we observe the microbiome dynamics of the macroalga *Fucus vesiculosus* in 25-day-enrichment cultures resulting in partial degradation of the brown algae. Microbial community analyses revealed the phylum *Pseudomonadota* as the main bacterial fraction dominated by the genera *Marinomonas* and *Vibrio*. More importantly, a metagenome-based Hidden Markov model for specific glycosyl hydrolyses and sulphatases identified *Bacteroidota* as the phylum with the highest potential for cell wall degradation, contrary to their low abundance. For experimental verification, we cloned, expressed, and biochemically characterised two α -L-fucosidases, FUJM18 and FUJM20. While protein structure predictions suggest the highest similarity to a *Bacillota* origin, protein–protein blasts solely showed weak similarities to defined *Bacteroidota* proteins. Both enzymes were remarkably active at elevated temperatures and are the basis for a potential synthetic enzyme cocktail for large-scale algal destruction.

Keywords *Fucus vesiculosus*, Cell wall degradation, *Bacteroidota*, α -L-fucosidases

Enzymatic algae cell wall carbohydrate (ACW) hydrolysis is a complex process with increasing attention in both industrial and ecological spheres. It enables the use of marine and freshwater algae as sustainable resources for valuable biomolecules already cultivated in large-scale algae farms¹. So far, ACW carbohydrates are degraded in digestion tanks by microorganisms with relatively expensive conversion methods. Increasing the efficiency of the degrading communities and enzymes could benefit multiple fields of applications, such as the renewable energy sector in biofuel production and pharma and nutraceutical industries^{2–5}.

Moreover, marine algae play a significant role in global carbon fluxes within natural marine systems. Understanding multitrophic community interactions and the primary drivers of enzymatic activities associated with the fate of carbon could help to elucidate fundamental processes in marine biogeochemistry⁶. Combining ecological and molecular methods results in new knowledge and insights into ecosystem health for conserving natural systems and understanding their response to global climate change.

So far, the cell disruption of ACWs lacks a needed, universal, and efficient industrial standard. Microbial substrate degradation has a high potential for future sustainable uses. The high variability in size, shape, and bioactive substances within the 169,000 species documented in AlgaeBase (<https://www.algaebase.org>) poses a challenge in establishing a standard procedure for efficiently processing different kinds of algae⁷. However, screening for

¹Department of Microbiology and Biotechnology, Biocenter Klein Flottbek, Institute of Plant Science and Microbiology, University of Hamburg, Ohnhorststr.18, 22609 Hamburg, Germany. ²Institute for General Microbiology, Molecular Microbiology, Kiel University, Kiel, Germany. ³Marbio, Faculty of Biosciences, Fisheries and Economics, UiT - The Arctic University of Norway, Tromsø, Norway. ⁴Technology Platform Next Generation Sequencing, Leibniz Institute of Virology, Hamburg, Germany. ✉email: ines.krohn@uni-hamburg.de

novel enzymes for specific uses and substrates is still under significant investigation. This search benefits from new molecular tools such as “omics”-based analyses and improved protein function prediction methods.

The schematic structure of ACWs mainly consists of a matrix and composition of specific polysaccharides and proteins with unique biochemical characteristics in *Phaeophyceae*, *Rhodophyta*, *Chlorophyta*, and *Bacillariophyceae* (Diatoms), which share biochemical similarities to brown algae. The cell wall of the macroalgae species *Fucus vesiculosus* is composed of the 3 *Phaeophyceae* associated polysaccharides fucoidan, alginate, and cellulose. Additionally, laminarin serves as a storage carbohydrate in the cell^{8–11}. The saccharide composition, as well as linkage variation within the polymer structure, differ inter- and intraspecific. It depends on several biotic and abiotic influences such as seasonality, illumination, temperature, nutrient and CO₂-concentration, age, and part of the organism^{12–17}. These influences lead to a high variability of fucoidan in algae, such as species from the genus *Fucus*. The polysaccharide shows differences in, e.g. the molecular weight of 7 to 1600 kDa, the sulphated content between 9 and 40%, and the L-fucose content ranging from 25 up to 93%^{18–20}.

Consequently, a universal degradation by microorganisms presupposes variable and multiple enzyme compositions. Fucoidan-degrading marine bacteria, such as *Lentimonas* spp., have already been described as reflecting a variable degradation capability by providing hundreds of different fucoidan-targeting enzymes of several classes and families²¹. Similar findings were made in kelp forest macroalgae species of the genus *Laminaria* with a major but varying carbohydrate content of laminarin, so findings from the present study can lead to solutions in multiple fields²². Since *F. vesiculosus* is easy to gather in nature in high quantities, it is suitable as a model organism. It is found in shelf regions all over the northern Atlantic. Furthermore, other *Fucus* species are distributed almost globally with high numbers in the northern Atlantic and Pacific. Therefore, brown algae cell wall polymers are under investigation in this study, focusing on fucoidan.

Similar to varying carbohydrate contents and structures in algae, marine microbial community composition is influenced by several biotic and abiotic factors such as seasonality, salinity, temperature, depth, or location, and is directly connected to substrate concentrations^{23–25}. Previous phylogenetic studies have characterized the natural composition of bacterial species on *Fucus* surfaces in the Baltic Sea. The bacterial community mainly consists of *Pseudomonadota* species with a majority of α - and γ -*proteobacteria*^{26–28}. Isolation approaches unveiled species within this phylum that have developed physiological adaptations to macroalgae surface areas and are genetically tailored to this habitat²⁹. *Bacteroidota* comprises only around 1% of the bacterial community on previously investigated natural *Fucus* surface microbiomes^{26,30}. However, these findings depend on the individual sampling dates, as *Bacteroidota* abundancies are influenced by seasonality³¹. In enrichment experiments over several days, *Bacteroidota* abundancies increased to 20–30%^{27,32}. Furthermore, relatively high abundancies of *Cyanobacteria* and *Planctomycetota* have been observed in investigations of natural *Fucus* microbiomes³³.

Microbial degradation of ACW polymers achieves hydrolysis and cleavage of the glycosidic bond within the polysaccharide structure. This process separates crosslinked structures and cuts long polysaccharide chains into shorter fragments, enabling microorganisms to metabolize and transport the resulting sugar dimers or monomers. Additionally, various secreted enzymes modify the carbohydrate molecule structure.

These carbohydrate-cleaving and modifying enzymes are categorised in the Carbohydrate-Active enZYmes database (CAZy, <http://www.cazy.org/>) into enzyme function-defined classes and families like glycosidases (EC 3.2.1.-), esterase (EC 3.1.-), transferases (EC 2.4.-), lyases (EC 4.2.2.-), as well as associated modules³⁴. Furthermore, the database Sulfatlas (<https://sulfatlas.sb-roscoff.fr/>) offers a classification of sulphatases (SU) that are active on sulphated biomolecules, such as the polysaccharide fucoidan in brown algae cell walls^{35–37}.

For our model organism *Fucus vesiculosus* and its main ACW carbohydrate fucoidan, the cascade of degradation reactions involves enzymes from the families GH29, GH95, GH107, GH141, GH151, GH168, as well as sulphatases S1_17 and S1_25 (Fig. 1)^{21,38–40}. Significantly, family GH29 α -L-fucosidases that target four different linkage types (EC 2.3.1.51; EC 3.2.1.111; EC 3.2.63; EC 3.2.1.127) is of major interest and is involved in the hydrolysis steps resulting in L-fucose monomers.

Numerous studies focus on the polysaccharide degradation potential of *Bacteroidota*. The process of expressing corresponding genes, the secretion system and the carbohydrate transport of this phylum is complex⁴¹. *Bacteroidota* species offer hundreds of polysaccharide utilisation loci to regulate access to complex carbohydrates and prove their glycan-degrading capabilities^{42–44}. Furthermore, starch utilisation systems and TonB-transporters are involved in transporting oligomers into the cells^{45,46}.

Our study combines in vitro enrichment culture approaches with metagenomic and in silico approaches to enable insights into the degrading community regardless of isolation obstacles. Therefore, the so-called “viable but nonculturable” bacteria and their genes remain no longer unknown⁴⁷. We want to evaluate the community dynamics and the enzymatic algae degradation potential in enrichment cultures using “omics”-based analyses. Our observations should allow insights into enrichment advantages and challenges for future algae degradation investigations. Furthermore, they facilitate the screening for novel putative fucoidan degrading enzymes to address the lack of established hydrolysing proteins targeting ACW carbohydrates. Additionally, we want to use our approach to identify and confirm new GH29 enzymes for fucoidan degradation.

Results

Initial Fucus-degradation potential of microbial communities

We observe the impact of microbial degradation in enrichment cultures by multiple metabolic approaches. Our initial testing suggested that the naturally attached microbial community of *Fucus vesiculosus* has great potential for degrading algae. Artificial inoculations with microbiomes from different origins, like soils or animal faeces, did not show comparable effects of biological activity (unpublished data). In the final experimental approach, we utilised 500 ml lightly sealed Schott-flasks for enrichment cultures. These cultures included 300 ml synthetic

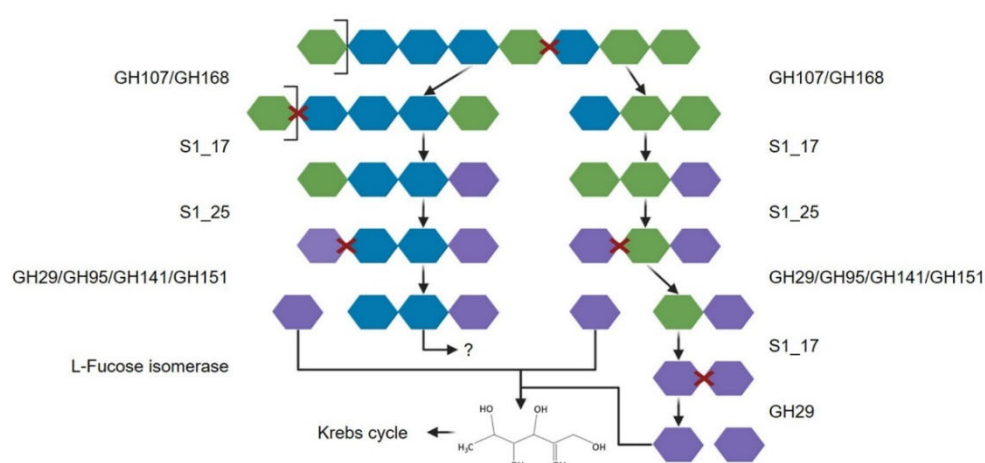


Figure 1. Schematic fucoidan degradation catalysis. Active enzymes from the GH and sulphatase families degrade the schematic structure of homofucan with sulphated α -1,3/1,4-linked L-fucose in multiple steps. Colour key: blue: 2 sulphate groups, green: 1 sulphate group, purple: L-fucose. Adapted from Li et al. (2022)¹. Created with BioRender.com.

seawater (Tropic Marin Classic Meersalz, Hünenberg, Switzerland) and 50 g *F. vesiculosus* collected at Kiel Bight, Germany. We shook the flasks at 60 rpm in a 20 °C environment and adjusted the salinity to 15.

Visual observation of *F. vesiculosus* enrichment culture with a naturally attached microbiome showed a significant change in the plant's structure during the enrichment. A healthy *F. vesiculosus* appearance changed to a mush of plant fractions and cell debris (Fig. 2A). The release of plant cell materials and fractionated alga and the growth of different microorganisms led to a change in the colour of the enrichment medium from clear to greenish to brownish. Furthermore, a smell of sulphur increased, indicating a potential release of thiol groups in organosulphur compounds. After the displayed 25 days (d), the activity in the enrichment cultures comes to a stop with the red-brown colour and less turbidity. The overall weight loss of 50 g *F. vesiculosus* over 20 days in the enrichment set-up was 10.76 ± 0.07 g ($21.52 \pm 0.14\%$, $n = 3$). The *para*-hydroxybenzoic acid hydrazide (phah) assay revealed an increase in the concentration of reducing sugar equivalents starting at 0.04 ± 0.02 mol of fitted values to a L-fucose standard curve and peaks on day 6 (d6) at 4.09 ± 0.47 mol. The concentration decreased and fluctuated from d7 to d16 between 2.61 ± 0.36 mol and 1.15 ± 0.03 mol (Fig. 2B, Supplementary Table 1). The optical density (OD_{600nm}) was monitored as an indicator of the visual change of the medium. The enrichment culture was shaken before sampling to create a heterogeneous distribution of biomass. Microbial density, biofilm formation, and the release of degradation products, such as demolished small algae parts, actively influenced the optical density. Due to the combination of these processes, the OD_{600nm} increased from d0-d7 and fluctuated around a level of 1 in the following.

Ultra High-Performance Liquid Chromatography-Electrospray Ionisation-High Resolution-Mass Spectrometry2 (UHPLC-ESI-HR-MS2) data was recorded to track the composition change throughout the enrichment cultures. Three parallel enrichment culture samples were taken and analysed after 1, 10 and 31 days. Principal component analysis (PCA) of the MS data was used to simplify the datasets (Supplementary Fig. 1). Negative electrospray ionisation (ESI⁻) was chosen beside positive electrospray ionization (ESI⁺), since we expected a high number of carbohydrate metabolites when degrading algae-biomass (Supplementary Fig. 1B). The hydroxyl and carboxyl groups of carbohydrates are not prone to protonation and appear in ESI⁻ commonly as $[M-H]^-$ while in ESI⁺ molecules bearing functional groups prone to protonation such as amines enable the detection of positively charged ions and adducts ($[M+H]^+/[M+Na]^+$). We have chosen the additional metabolomic analysis to encompass a broad range of metabolites in order to track the change in metabolites between the replicates. Three replicates for each time point group together within the two-dimensional PCA for negative and positive ESI. A common change of the chemical composition over time was observed, between 1 and 10 days and 10 and 31 days for all replicates. This change hints at a similar molecular degradation process as indicated by the metabolites in the enrichment cultures. Further, the degradation of *F. vesiculosus* within the first 1–10 days differed from the degradation between 10 and 31 days. These results supported the findings of the pHAH assay and the sugar dynamics (Fig. 2B) and are also represented by the successful degradation process in the enrichment cultures (Fig. 2B).

Bacterial community dynamics

The microbial community in *F. vesiculosus* enrichment cultures consisted of a diverse mix of microorganisms. SEM image analyses revealed insights into algae colonization and attachment processes with different microorganisms. Our image analyses after nine days of enrichment (Fig. 3) revealed noticeable differences in shapes and sizes ranging from $< 1 \mu m$ to $> 15 \mu m$ (Fig. 3Db) of bacteria, possible aggregates, and organic attachments

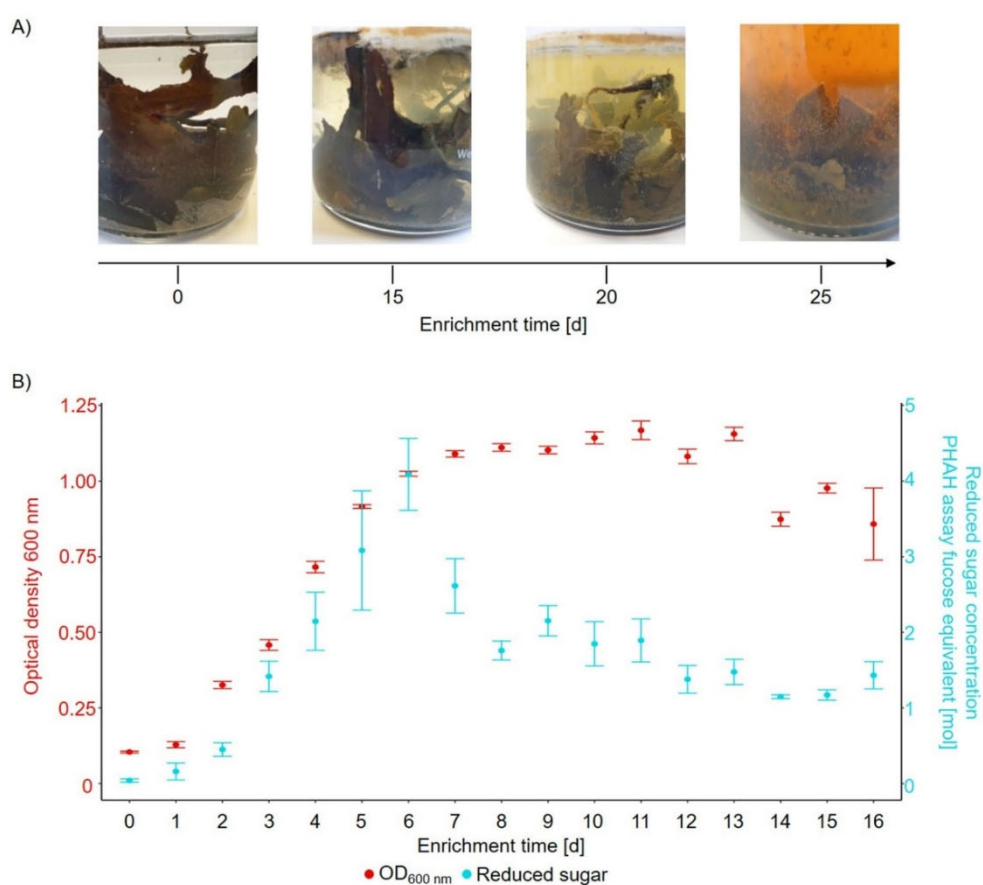


Figure 2. *Fucus vesiculosus* enrichment culture with naturally attached microbiome in synthetic seawater medium. (A) Visual changes in the algae structure medium turbidity and colour, as well as microbial growth and biofilm formation on the surface. (B) Quantification of microbial degradation of *F. vesiculosus* in enrichment culture supernatant over 16 days in triplicates. Colour key: Red dots/left y-axis: optical density of the enrichment culture supernatant at 600 nm. Blue dots/right y-axis: reduced sugar concentration determined with the *para*-hydroxybenzoic acid assay. A standard curve with glucose as an equivalent was used to estimate the sugar concentration in relation.

(Fig. 3Ca, Da) and specific characteristics on the algae surface (Fig. 3A). Interestingly, our images show an increased abundance of bacteria occurred in disrupted parts of the algae surface compared to less degraded areas (Fig. 3C).

We investigated the bacterial community in *F. vesiculosus* enrichment cultures through 16S rRNA gene amplicon analyses. Samples were taken over 15 days (d) (Fig. 4, total combined and filtered reads: 826,738 reads). 16S rRNA gene amplicon results of d0 display the naturally attached bacterial community associated with *F. vesiculosus* on the Baltic Sea shore during November 2022. Above a cut-off of 1% of all bacterial class-associated reads, nine different classes from 5 phyla were identified. In our dataset, *γ-proteobacteria* represented the dominating class with 36.6% of the reads, followed by *Flavobacteriia* with 16.7%. The initial diversity of the bacterial community, measured by Shannon (ShDiv = 4.284) and Simpson (SiDiv = 0.957), decreased as enrichment began. By d3, the diversity further decreased (ShDiv = 2.626, SiDiv = 0.894), resulting in a community with a dominant fraction of *γ-proteobacteria* (61.5%). *Fusobacteriia* abundance increased from initial 0.9% to 16% on d3. Meanwhile, the initially more extensive community of *Flavobacteriia* decreased to 0.2% relative abundance. In the following days of the enrichment, the composition of bacterial classes showed minor fluctuations (d06 ShDiv = 2.924, SiDiv = 0.927; d09 ShDiv = 2.947, SiDiv = 0.922, d12 ShDiv = 2.98, SiDiv = 0.921; d15 ShDiv = 3.13, SiDiv = 0.935).

The change was even more noticeable on the phylum level. Overall, the ratio of *Pseudomonadota* ranged between 58.9% on d0 and 76.0% on d3, making up more than half of the bacterial community over the entire 15-day period. In contrast, members of *Bacteroidota* represented 21.6% of the bacterial composition on d0 but rapidly decreased to 0.8% on d3 while making up 4.7% on d15.

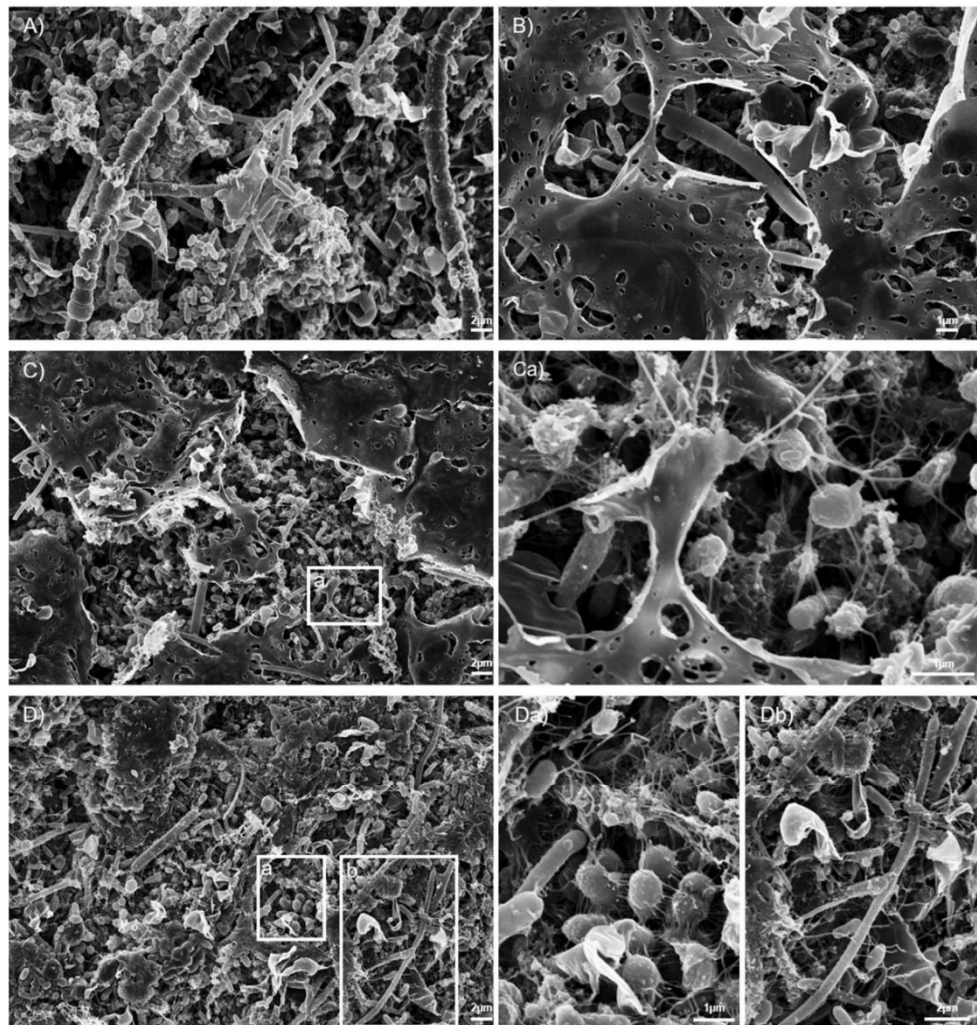


Figure 3. Scanning electron microscopy images of *F. vesiculosus* surfaces and attached microbiome in enrichment cultures after 9 days. (A) Microorganisms on degraded algae parts. Characteristic cell stacks are visible. (B) Degraded algae tissue. (C) Microbial clusters are concentrated in degraded algae parts with (Ca) filamentous attachments of bacteria to the substrate and between individuals. (D) Visual diversity of bacteria, possible aggregates, and organic attachments with variations in shape and sizes in (Da) and (Db) between < 1 and > 15 μm . Scale bars are indicated in the images (Zeiss Leo Gemini 1525 FEG SEM; 5.00 kV).

Furthermore, the number of identified genera decreased from 170 on d0 to 26 on d15. During the ongoing enrichment, five genera above 1% relative abundance dominated the community: γ -proteobacteria species of *Marinomonas*, *Vibrio* and *Psychromonas*, ϵ -proteobacteria species of *Arcobacter* as well as *Fusobacteriota* species of *Propionigenium*. Interestingly, *Psychromonas* were dominant in the initial sampling at d0 with a 21.1% relative abundance ratio. At the beginning of the enrichment process, the ratio of this genus decreased to 1.9% on d3 but ranged between 13.8% and 5.7% in the following 12 days. Besides this, *Marinomonas* species increased in relative abundance from 4.3% on d0 to the highest ratio within the bacterial community of all genera on d3 with 33.5%, followed by fluctuating rates between 15.0 and 20.0%. In contrast, the starting condition of the enrichment culture revealed that the three genera, *Vibrio*, *Arcobacter*, and *Propionigenium*, constituted only minor fractions, ranging from 0.8% to 1.4%, within the bacterial community. However, after 3 days of enrichment, their relative abundances increased (d3: *Arcobacter* 14.2%, *Propionigenium* 16.0%, *Vibrio* 22.8%) and then stayed at similar proportions.

Additionally, *Bacteroidota* were represented mainly by *Algibacter lectus* on d0. This species comprised 5.0% of all individuals of the naturally attached bacterial microbiome at the time the macroalgae were collected. In enrichment conditions, this species was not found after only 3 days. Overall, from 40 genera belonging to

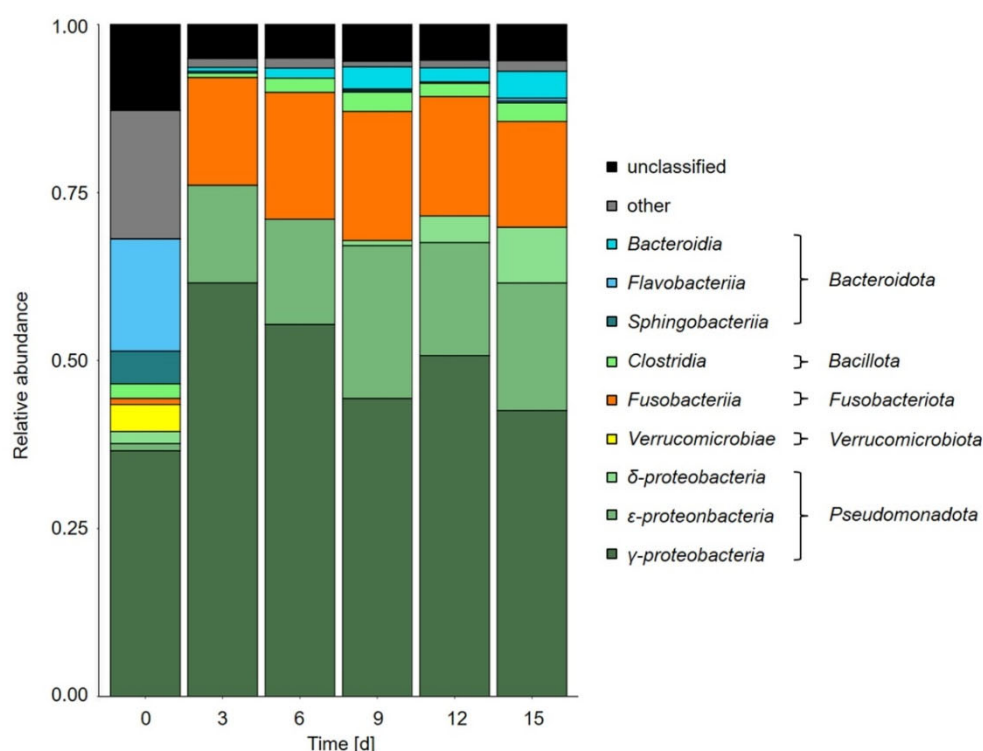


Figure 4. Bacterial community dynamics in *F. vesiculosus* enrichment cultures. 16S rRNA gene amplicon analysis of the microbial community over 15 days on a MiSeq (Illumina) sequencer. Bacterial classes with > 1% of the overall reads are displayed. One-step amplification was utilised to create 16S rRNA gene amplicon libraries. These libraries were subjected to paired-end sequencing using an Illumina MiSeq sequencer (MiSeq Reagent Kit v2, 500 cycles, product number: MS-102-2003), resulting in 2×251 bp reads.

Bacteroidota on d0, only 3 were detected between d3 and d15 in the 16S rRNA gene amplicon dataset (*Dysgonomonas*, *Olivibacter*, *Lutimonas*). The strongest increase was found in the species *Dysgonomonas wimpennyi* of the class *Bacteroidia*, which is only found in a ratio of 0.06% on d0 but then increased up to 3.8% during the enrichment.

Bacteroidota as potential key degrader for *Fucus vesiculosus* cell wall

We sequenced four replicate metagenomes of enrichments after 9 days. Assemblies yielded between 283.16 Mbp to 731.97 Mbp with 399,970 to 1,143,468 assembled contigs, the largest of which ranged from 211.39 Kbp to 350.84 Kbp (Supplementary Table 2).

The phylogenetic classification of 69,146,972 covered gene fragments of the combined metagenome datasets (cut-off > 0.0001 ratio of covered gene fragments) reveals the phylogenetic bacterial composition after 9 days with a Shannon-diversity of 3.998 ± 0.292 and a Simpson-diversity of 0.94 ± 0.016 (Supplementary Fig. 2). Similar to the 16S rRNA gene amplicon data, the dominating fraction of genes originated from *Pseudomonadota* ($91.6 \pm 2.5\%$) followed by *Bacillota* ($2.5 \pm 1.1\%$), *Fusobacteriota* ($2.3 \pm 0.7\%$) and *Spirochaetota* ($1.7 \pm 0.6\%$). In contrast, *Bacteroidota* comprised around $1.6 \pm 0.4\%$ of the bacterial community in the metagenome. Cluster of Orthologous Genes (COG) analyses provided further insights into the gene composition within the dominant phyla (Supplementary Fig. 3). Genes of the category “carbohydrate transport and metabolism (CTM)” included carbohydrate-active enzymes involved in the degrading process of ACW. The general “DNA/RNA metabolism” category turned out as the major gene fraction in all phyla, followed by genes of the category “Translation, ribosomal structure and biogenesis”. Notably, the *Spirochaetota* had the highest proportion of CTM genes at $8.1 \pm 1.1\%$. In contrast, both *Bacteroidota* and *Pseudomonadota* showed similar proportions, at $6.8 \pm 0.9\%$ and $6.7 \pm 0.4\%$, respectively.

How different phyla are involved in the complex degradation process of ACWs is not necessarily represented by the abundance and dominance of specific taxa. Metagenomic analyses indicate the putative degradation potential of specialised bacterial communities, thus emphasizing the importance of understanding their role. With the focus on already-known enzyme families within the glycosyl hydrolases, it is possible to reveal the capability and portion of each phylum on the whole degradation process.

The HMM analysis of coding gene distribution for GHs and SUs families in the metagenome data revealed an elevated number of genes in the *Bacteroidota* compared to all other bacterial phyla (Fig. 5A). A set of 105 different models for GH families led to the identification of 6151 hits with a score above 50 within members of the *Bacteroidota*. All required GH and SU families for the degradation of fucoidan (GH29, GH107, GH168, S1_17, S1_25) were most abundant in this phylum, with SU family S1_17 with the highest quantity of 1467 unique genes. All 8442 unique genes associated with *Bacteroidota* equal 48.8% of the total 17,297 identified GH and SU genes predicted by the HMM analysis of the 10 most abundant phyla.

In total, 1010 GH29 genes (5.84%), 360 GH107 genes (2.08%), 466 GH168 genes (2.69%), 3004 S1_17 genes (17.37%) and 1942 S1_25 genes (11.23%) were predicted. Emphasizing the singular degradation potential of each phylum, normalization was achieved by combining the number of HMM hits per family with the phylogenetic fraction of the corresponding phylum (Fig. 5B). This conversion statistically negates the influence of the phylogenetic abundance and reveals the potential of *Bacteroidota* to degrade ACW even more.

Conversely, *Pseudomonadota*, which is the most abundant phylum based on 16S rRNA gene amplicon analyses and has the highest number of protein-coding genes in the metagenome dataset, exhibited relatively low gene numbers with 2374 hits (13.72%) in the HMM analyses. HMM results assigned most genes to GH1 or GH3 and distributed over 754 species. Both GH families catalyse various substrates compared to specialised families like GH29, GH107, and GH168, which are active exclusively on fucoidan. Interestingly, *Planctomycetota* were represented with a ratio of <0.0001 of covered fragments in the phylogenetic classification but coded for several putative enzymes active on fucoidan (GH29 195 hits; GH107 5 hits; GH168 114 hits; S1_17 432 hits; S1_25 152 hits). The conducted profile HMM searches showed 1281 hits for *Planctomycetota* in 96 species. *Verrucomicrobiota* exhibited apparent specialisation in the degradation of fucoidan, distributing all 1871 HMM hits (10.82%) across 92 different species, with only 4 species having more than 100 hits. For comparison, the 8442 hits of *Bacteroidota* originated from 720 different species, while 17 species of those coded for >100 unique genes of the conducted HMM.

The species *Lentimonas* sp. CC10 (NCBI:txid2676095) harbours the majority of *Verrucomicrobiota*-associated genes, totalling 394 hits (GH29 46 hits; GH107 52 hits; GH168 31 hits; S1_17 158 hits; S1_25 53 hits). *Lentimonas* sp. CC21 (NCBI:txid2676098) contains 270 hits (GH29 54 hits; GH107 16 hits; GH168 26 hits; S1_17 106 hits;

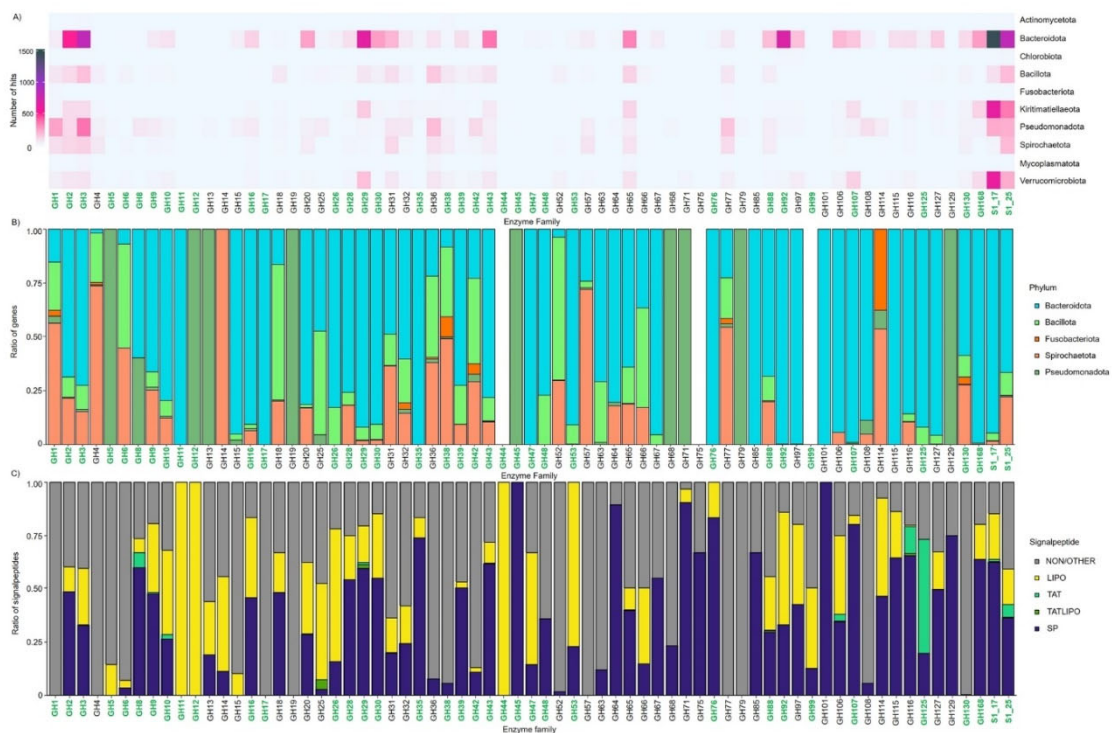


Figure 5. Metagenome analyses of general bacterial gene distributions in GH and sulphatase families based on HMMs. Genes from green highlighted families are involved in algae cell wall polymer degradation. (A) Heatmap with number of genes per enzyme family per phylum. (B) Ratio of unique genes per enzyme family per phylum normalised by the phylogenetic fraction in the metagenome (Supplementary Fig. 3). Bacterial phyla with a ratio of genes above 1% of the whole metagenome are included. (C) Proportions of signal peptides per GH and sulphatase family. Signal peptides were predicted by SignalP v.6.0².

S1_25 23 hits). The *Bacteroidota* species with the most HMM hits was *Mariniflexile fucanivorans* with 404 hits (GH29 49 hits; GH107 5 hits; GH168 26 hits; S1_17 86 hits; S1_25 27 hits) followed by *Formosa algae* with 266 hits. *Reinekea marinisedimentorum* had the highest number of HMM hits among *Pseudomonadota*, totalling 64 putative GH/SU tested genes. Notably, there were no hits for GH29, which is crucial for fucoidan degradation. Likewise, no hits were identified for the 2 SU families. Furthermore, the *Planctomycetota* species *Novipirellula aureliae* codes for 337 putative proteins classified as one of the conducted HMMs (GH29 43 hits; S1_17 86 hits; S1_25 30 hits).

Implementation of novel GH29 fucosidases

By in silico screening, we predicted 1010 unique amino sequences from the combined metagenomes as putative enzymes of the family GH29 (Fig. 5A). This crucial enzyme family in fucoidan degradation includes α -L-fucosidases (EC 3.2.1.51), α -1,3/1,4-L-fucosidases (EC 3.2.1.111), α -1,2-L-fucosidases (EC 3.2.1.63), α -1,6-L-fucosidases (EC 3.2.1.127) and α -L-glucosidases (EC 3.2.1.-) with 106 characterised enzymes in CAZy in January 2024.

We attempted cloning of 20 GH29 genes, for which a HMM score > 320 was calculated (max. 358.2). The putative genes coding for FUJM18 and FUJM20 were successfully cloned in the plasmid pet21a(+) plasmid and overexpressed in *E. coli* BL21 (DE3). The protein blast revealed a similarity to previously predicted but not characterised GH29 fucosidases of 90.6% to *Prolixibacteraceae bacterium* Z1-6 for FUJM18 and 77.3% for *Arenibacter* sp. F26102. The gene sequences of the cloned vector resulted in a HMM score of 321.4 for FUJM18 and 324.4 for FUJM20 (IMG accession origins Ga0502370_024398_80_1447 and Ga0502371_0001890_2219_3553, respectively). The FUJM18 gene coded for a 444 aa protein, and the FUJM20 gene coded for a 426 aa protein. Both amino sequences were identified to include signal peptides. Excluding those signal peptides, the calculated molecular weight of FUJM18 was 51,534.97 kDa, while the molecular weight of FUJM20 was 47,868.3 kDa. The nucleotide homology search for the FUJM18 scaffold (Ga0502370_024398) results in a similarity of 85.71% for *Prolixibacteraceae*. For the FUJM20 scaffold (Ga0502371_0001890) we could analyse a significant BLAST homology for *Flavobacteriaceae*.

Structure prediction and activity assay

In activity assays with pNP- α -L-Fucopyranose (pNP- α -L-Fuc), FUJM18 showed higher activity on the substrate compared to FUJM20. In contrast, FUJM20 showed a more comprehensive range of activity at different pH-values as well as temperatures. FUJM18 and FUJM20 are thermostable α -L-fucosidases with an optimal temperature of 80 °C at pH 6 in 0.1 M sodium citrate buffer (Fig. 6A–C, Supplementary Table 3). FUJM18 was active with a maximum of $61.18 \pm 12.79 \text{ U} \cdot \text{mg}^{-1}$, FUJM20 with $41.77 \pm 1.34 \text{ U} \cdot \text{mg}^{-1}$. The structure prediction of both proteins displayed a beta-sheet comprised of six interleaved beta strands on the C-terminus (Fig. 6D,E). The

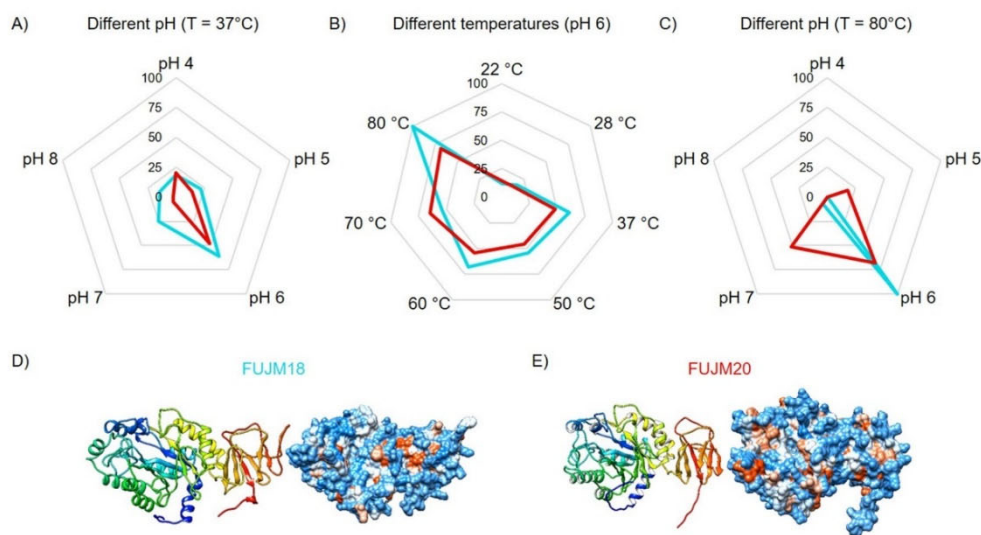


Figure 6. Characterisation of FUJM18 and FUJM20. Relative hydrolysis activity measured with 4-Nitrophenyl- α -L-fucopyranose of the GH29 enzymes FUJM18 and FUJM20 in triplicates. 100% relative activity equals $61.18 \text{ U} \cdot \text{mg}^{-1}$ enzyme activity (Supplementary Table 3). (A) Determining the optimal pH value for the enzyme activity at 37 °C. FUJM18 peaks at pH 6 with $61.12 \pm 27.29\%$ relative activity ($37.39 \pm 16.69 \text{ U} \cdot \text{mg}^{-1}$). (B) Determining the optimal temperature for the enzyme activity at pH 6. FUJM18 peaks at 80 °C with $100 \pm 20.9\%$ relative activity ($61.18 \pm 12.79 \text{ U} \cdot \text{mg}^{-1}$). (C) Determining the optimal pH value for the enzyme activity at the optimal temperature of 80 °C. (D) Predicted structure of FUJM18 by AlphaFold 2. (E) Predicted structure of FUJM20 by AlphaFold 2.

protein database (PDB) structure comparison revealed that both enzyme structure predictions are most similar to the entry α -L-fucosidase isoenzyme 1 from *Paenibacillus thiaminolyticus* chain D (6GN6), with the highest structural similarity of FUJ18JM at a Z-score of 51.6 (Fig. 7, Supplementary movie 1, Supplementary movie 2)⁴⁸. FUJ18 and FUJ20 have a Z-score of 42.9 (Supplementary movie 3). Previous research of crystal structures of the structural most similar enzymes was found to form multimers like the hexamer of α -L-fucosidase isoenzyme 1 from *Paenibacillus thiaminolyticus*.

In summary, the result of our enrichment culture degradation approach shows the outstanding potential of bacterial communities in ACW carbohydrate hydrolysis and the robust pipeline of the “omics”-based gene screening to identify genes/enzymes and species to implement sustainable resources in industrial processes. We identified over 13,000 putative glycosyl hydrolases from 34 enzyme families involved in the degradation process of at least one ACW carbohydrate and over 4900 putative sulphatases of 2 enzyme families. The genomes of *Bacteroidota* species contained an outstanding majority of the identified protein sequences. However, in the microbial community, the fraction of *Bacteroidota* individuals is suppressed by the abundance of *Pseudomonadota*.

As HMM revealed the gene candidates with the highest potential for fucoidan degradation, we could clone, test, and characterise two active, thermostable α -L-fucosidases. These enzyme structures are most similar to an α -L-fucosidase synthesised by a *Bacillota* species. However, protein–protein blast results revealed the highest sequence coverage for *Bacteroidota* species.

Discussion

The intricate, non-consistent structure of ACWs requires an equally complex enzymatic degradation machinery. Considering all ACW carbohydrates, we showed the presence of certain bacteria encoding for certain enzymes from at least five different classes associated with the degradation process: 49 Glycosyl hydrolase families (GH), 24 Polysaccharide lyase families (PL), 4 sulphatase families, 31 Carbohydrate binding module families (CBM) and 7 carbohydrate esterase families (CE) (Supplementary Table 4)^{34,49}.

With diverse structure variations, the backbone of fucoidan is mainly made up of α -1,3/1,4-L-fucose. The carbohydrate structure is divided into homofucan and heterofucan. While homofucan is one chain of α -1,3 or alternating α -1,3/ α -1,4-linked L-fucose with sulphuric acid groups at C2, C3, or C4, the structure of heterofucan is more complex with additional monosaccharides like galactose, xylose, mannose, glucose, rhamnose, and uronic acid that enable crosslinked molecule structures (Supplementary Fig. 4A)^{49,50}. However, laminarin has a less complex structure of β -1,3-D-glucose chains with occasionally β -1,6-D-glucose crosslinks⁵¹. Besides *Phaeophyceae*, to which *Fucus* belongs, laminarin is also a cell compound in *Bacillariophyta*. Another brown alga-associated polysaccharide is cellulose, also found in *Chlorophyta* and as the primary cell wall component in land plants. It consists of non-crosslinked chains of β -1,4-D-glucose⁵². Alginate is the fourth polysaccharide, with brown algae species as the only producers within the kingdom plants. Its complex structure consists of a copolymer with varying configurations of 1,4-linked β -D-mannuronate and α -guluronate residues⁵³.

Further, ACW carbohydrates are carrageenan, agar, and porphyran in red algae; ulvan in green algae; mannan and xylan in red and green algae; and pectin in green algae and *diatoms*⁵⁴. Considering our understanding of crucial enzyme classes and families (Supplementary Table 4) and positive results from HMM analyses,

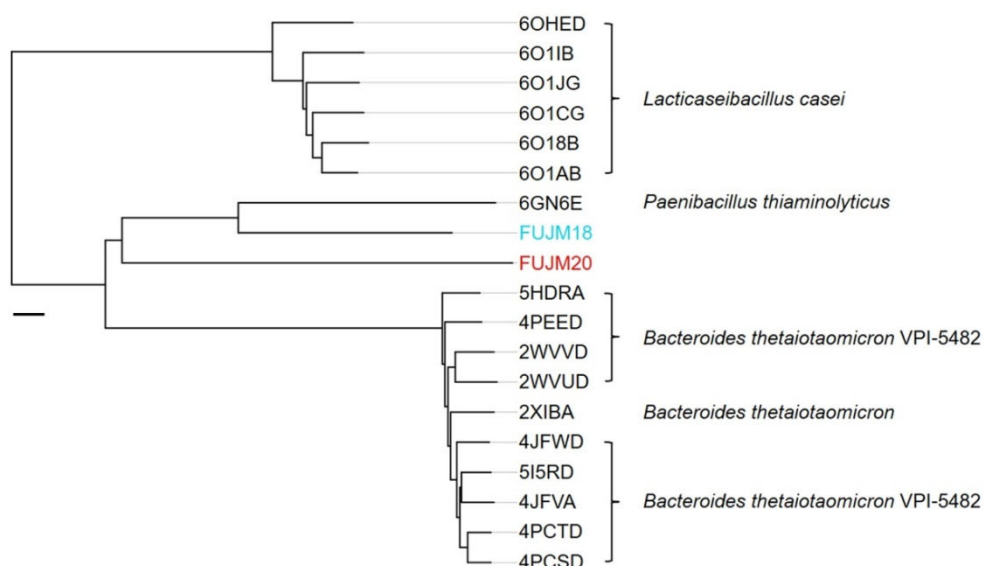


Figure 7. Phylogenetic tree of FUJ18 and FUJ20 based on protein structures in an all against all analyses of the Dali Server and PDB database. Chosen structures have a similarity cut-off of an RMSD value < 2.2. Similarity distance is shown in Z-score; the scale bar indicates a distance of 2.

particularly in GH families associated with laminarin and cellulose degradation (Fig. 5A), it is reasonable to infer that the enriched bacterial community observed is proficient in degrading various carbohydrates. However, the higher number of hits per gene coding for enzyme families active on fucoidan exceeded those for the other mentioned substrates, presumably due to the dominating component of fucoidan in the cell wall carbohydrate composition of *F. vesiculosus*.

The metabolic catalysis of fucoidan is well studied and consists of a cascade of GHs, CBMs and sulphatases (Fig. 1)^{21,38–40}. The sulphated oligosaccharide homofucan is hydrolysed by endo- α -1,3/1,4-fucoidanase from GH families GH107 and GH168, followed by exo-fucose-2/3-sulphate or (fucan)-2/3-O-sulfohydrolase of families S1_17 and S1_25. Additionally, reported active sulphatases are found in families S1_15 and S1_16²¹. Further, α -L-fucosidases classified as GH29, GH95, GH141 and GH151 degrade intermediate oligosaccharides down to the desulphated monosaccharide L-fucose, which is then finally metabolised in the TCA cycle⁴⁹.

During the degradation process of ACWs, we could measure the increase of released and reduced sugars in the supernatant of the enrichment cultures with the pHAH assay over about 7–9 days, followed by a decline to around half of the concentration of the maximum values (Fig. 2B). In a multi-step degradation process, this time point marks a shift in the balance between bacteria breaking down L-fucose and other monomers and the bacteria supplying these monomers along with the exposed carbohydrates. Consequently, the increasing release of ACW compounds led to a deconstruction of the algae in the enrichment culture (Fig. 2A). Regarding industrial usage of algae as an alternative resource, this biomass degradation is only one step of a complex process. Future research needs to address multiple challenges in algae farming and cultivation upscaling. Harmful threats for valuable, farmed algae, like complex zooplanktonic grazer communities that feed on the algae and induce morphologic reactions, are critical for the industrial success of this resource^{55–57}. The degradation process will not occur to the extent of a necessary state, as long cultivation is not productive, and energy and commercial efficiency are lacking. This study does not target or control different zooplankton grazers, but it is anticipated that they will influence both the degradation process and the overall community composition in the mesocosms.

Focusing on bacterial metabolism, energy uptake and conversion are reflected in species abundance. The increasing abundance of *Pseudomonadota* revealed by 16S rRNA gene amplicon analyses hints that this phylum is the most efficient in metabolising at least the sugar monomers into their TCA cycle as well as *Fusobacteriota* and *Bacillota* (Fig. 4). Other influences like temperature, oxygen conditions, medium volume of the enrichment cultures, and the bottle effect are critical for the bacterial community dynamics as well. Initial testing of different temperatures and shaking intensities helped design reproducible degrading conditions, but a bottle effect that favours fast-growing γ -proteobacteria is expected⁵⁸. Especially the initial dominating fraction of γ -proteobacteria shows their association to algae carbohydrate substrates. Furthermore, recent studies of *Psychromonas* underline this association as incubation with pectin and alginate favoured their relative abundance⁵⁹. In contrast, this genus declined in our study's experimental incubation and substrate conditions. However, the impact of γ -proteobacteria in the enzymatic composition of the enrichment culture might not be redeflected as this study solely focuses on the listed GH and SU families. An extended analyses of the metagenome would presumably reline the role of this bacterial class and explain their abundance and their influence to the bottle effect in enrichment cultures. Further experiments of the investigated microbiome in enrichment cultures without the algae as substrate were not carried out, but could help to determine the influence of the bottle effect.

An increasing abundance of δ -proteobacteria and ϵ -proteobacteria indicates the micro-anaerobic conditions and is a disadvantage for aerobic *Bacteroidota*. Furthermore, the putrid smell emerging from the enrichment cultures hints at reducing ϵ -proteobacteria. δ -proteobacteria and ϵ -proteobacteria were previously found in anaerobic environments in the Baltic Sea^{60,61}. The relatively slow shaking and the lightly sealed flask may have caused the low oxygen concentration. Additionally, a biofilm formation on the culture surface could have weakened the mixing effect by altering the surface tension. The activity in the enrichment cultures usually ends after 25 to 30 days (Fig. 2A). As we found a loss of approximately one-fifth of the initial algae wet weight, the microbial degradation is not efficient enough to degrade the major part of the algae. The side effects described above inhibit the degrading community until a turnover event stops the enrichment. Besides anaerobic conditions, these effects could depend on phages that kill the bacteria culture, the release and rising concentration of toxic compounds through cell lysis, inter- and intraspecific competition, nutrient limitations, and general unfavourable medium conditions. Further research must be done to target these challenges to make algae farming possible and lucrative at a high level. With our findings, we contribute to the general understanding of the enrichment culture dynamics and interactions.

Bacteroidota species are prominently known for their degrading capabilities in natural systems with a high potential in several biological hydrolysing applications^{62,63}. The screening approach for metagenomes employed in this study has identified novel putative GH enzymes and other proteins associated with ACW hydrolysis, thereby reinforcing the robustness of these findings. The metagenome approach enables the accessibility of genes of nonculturable bacteria. By using HMM analysis, we were able to underline the exceptional potential of the *Bacteroidota* to degrade sulphated ACW carbohydrates compared to all other phyla. Previous research already described the expression of α -L-fucosidases of GH29 in *Bacteroidota*⁶⁴.

Furthermore, our results support the previously landmark study of Sichert et al., which assigns species belonging to the genus *Lentimonas* from the phylum *Verrucomicrobiota* to express hundreds of genes involved in the fucoidan degradation²¹. In the metagenome of the enrichment culture after 9 days, we can further confirm and strengthen this finding. We found 782 unique genes with HMM analyses originating from *Lentimonas* spp. (mainly *Lentimonas* sp. CC10 NCBI:txid2676095 and *Lentimonas* sp. CC21 NCBI:txid2676098) with putative enzyme functions of the analysed 67 GH families and 2 SU families. Interestingly, the HMMs assign 289 genes of those to the enzyme families GH29, GH107 and GH168 and 386 genes to the enzyme families S1_17 and S1_25. With these results, we can amplify the previously described degrading capabilities of *Verrucomicrobiota*, especially *Lentimonas* spp.²¹. However, putative fucoidan-degrading genes were associated with *Bacteroidota*. Furthermore,

the HMM top scores of the genes from the ACW degrading families originate from this phylum. This leads to an increased variability and possible adaptation to the different conditions and structures of algae cell wall carbohydrates of a *Bacteroidota* community in natural systems. The number of hits throughout multiple GH and SU enzyme families enables the degradation capability of a purified substrate like fucoidan and a composition of multiple natural carbohydrates. Certain specialised *Bacteroidota* species provide multiple potential fucoidan-active enzymes. These species represent important candidates for future approaches to single and mixed-species degradation. So far, previous research investigated the degradation processes of the described *M. fucanivorans*⁵⁵.

These results lead to an imbalance between the abundance of *Pseudomonadota* and *Bacteroidota* and their carbohydrate-degrading activities in *F. vesiculosus* enrichment cultures, especially noticeable by normalising the number of HMM hits (Fig. 5B). We assume this relationship depends on these phyla's L-fucose and general sugar monomer metabolism, which is more efficient in *Pseudomonadota*. The already discussed enrichment culture effects for fast-growing *γ-proteobacteria* also influence this development⁵⁸. The *Bacteroidota* species find a rich source of degradable carbon substrates within the ACW carbohydrates and use energy as a trade-off to synthesise the mandatory enzymes, most of which are then secreted from the cell to the algae cell surface (Fig. 5C). This degradation leads to an increase of different reduced sugar chains on the enrichment culture medium. However, the payoff is for *Pseudomonadota* as they invest less energy on polysaccharide degradation but benefit from an increased energy intake compared to *Bacteroidota*. Influences of selfish uptake also apply to this interaction as this behaviour is found over the whole water column in the bacterioplankton for the *Bacteroidota*, *Pseudomonadota*, and *Verrucomicrobia* beyond others⁶⁶. While our sequence-based analysis shows a cluster of the different GH families and further reveals the dominance of *Bacteroidota* in general, genes of family GH1 are mainly in *Pseudomonadota* genomes (Fig. 8). GH1 itself contains a variety of 27 enzyme activities for a high number of different substrates. It is not as specialised as the GH29 family, which only comprises five enzymatic activities, including four different types of α-L-fucosidases.

In summary, we hypothesise that the key and base findings of this study will provide knowledge to an efficient degradation for algae cell wall carbohydrates. So far, we got a degradation rate of $21.52 \pm 0.14\%$ in wet weight loss of the plant. For similar future degradation approaches, monitoring and adjusting the sugar concentration in the media may increase the degradation efficiency by creating a beneficial environment for *Bacteroidota* while *Pseudomonadota* is inhibited. However, if these adjustments overcome or suppress the discussed enrichment culture, challenges have to be addressed in future studies.

GH29 successfully degrades ACW by catalytically hydrolysing L-fucose dimers and detaching L-fucose monomers from sulphated polymers during the degradation process (Supplementary Fig. 4B). The present approach of metagenome mining by HMMs in combination with enrichment cultures is an efficient way of finding novel, valuable enzymes. In our case, FUJM18 and FUJM20 represent thermostable and functional enzymes that the HMM identified for GH29. As described, the fucoidan is supposed to be pre-treated by enzymes of GH107 and GH168 as well as S1_17 and S1_25. With the pNP-α-L-Fuc assay, it was possible to confirm the enzymes as α-L-fucosidases.

Structural similar entries for α-L-fucosidase isoenzyme 1 from *Paenibacillus thiaminolyticus* (6GN6) and α-L-fucosidase complex from *Lactocaseibacillus casei* (6O1A) in the RCSB PDB Protein data Bank (RCSB.org)

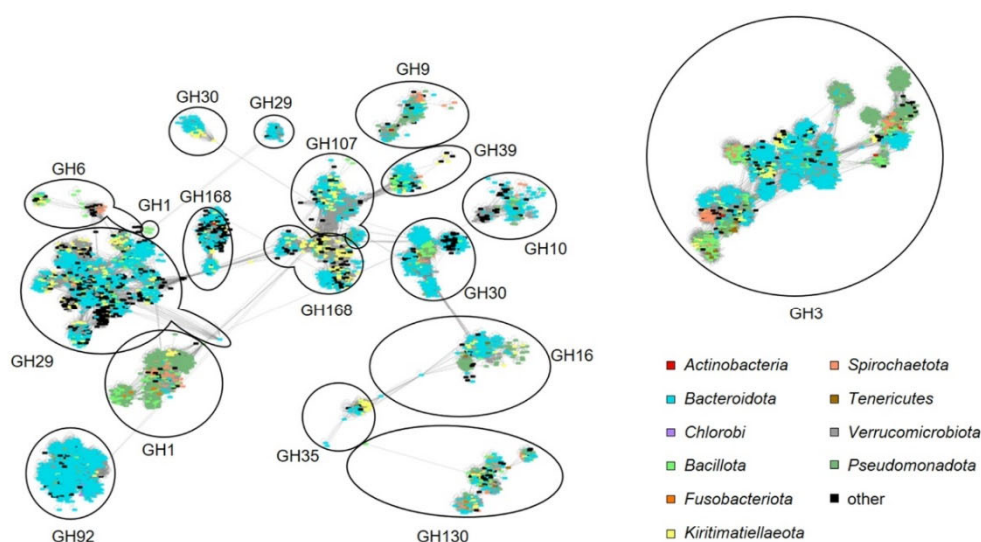


Figure 8. Sequence similarity network of Hidden Markov Model search for glycosyl hydrolases in metagenomic datasets of *Fucus vesiculosus* enrichment culture microbiomes. Filtered GH families are involved in the degradation of *F. vesiculosus* cell wall carbohydrates. Coloured genes indicate the phylum. Data analysed and displayed with Cytoscape v.3.9.1⁴.

www.nature.com/scientificreports/

suggest that the proteins could form multimers with an active site in the centre of the resulting complex (Fig. 7, Supplementary movie 1, Supplementary movie 2)^{48,67,68}.

Overall, we introduced two powerful enzymes with high industrial potential as thermostable candidates for processing marine organic matter.

Conclusion

In summary, our study provides detailed insight into the microbial degrading dynamics in macroalgae enrichment cultures and offers solutions for future high ACW degrading approaches. Our omics analysis shows thousands of putative GH and SU enzymes that could be involved in degrading various carbohydrates and are specialised to fucoidan when attached to *F. vesiculosus* by *Bacteroidota*. As in natural marine surface conditions, we detected a microbial community dominated by *Pseudomonadota* in artificial microcosm experiments but with a declining abundance of *Bacteroidota*⁶⁹. *Pseudomonadota* is likely to be significantly more efficient in metabolising the resulting sugar mono- and dimers, even though their contribution to the initial degradation process is likely minor. The observation of *Bacteroidota* as the potential main driver of fucoidan degradation and *Pseudomonadota* as the dominant phylum sets this assumption. Additionally, HMM scores reveal that the top-scoring genes of enzyme families associated with the fucoidan degradation also originate from *Bacteroidota*.

Future research experiments should establish a universal mixture of ACW degrading proteins found by sequence-based screening of omics-based approaches. This enzyme mixture will enable algae to be a novel resource for industrial, sustainable use. Exemplary, were able to successfully identify and introduce 2 novel, thermostable α -L-fucosidases of GH29 using our conducted screening method.

Methods

Sampling and enrichment

Fresh environmental samples of *F. vesiculosus* were collected at the shore of the Baltic Sea within the tidal zone of the Kiel fjord (54°21'56" N, 10°11'43" E) and transferred to the lab in humid conditions. The samples were stored at 4 °C before processing.

The algae material was rinsed with VE Water, and attached animals like barnacles were removed or excluded, as well as other plant material. For designing the final degradation cultures, initial testing with different enrichment conditions was performed and observed for degradation and microbial activity. These tests included altering temperatures, shaking speeds, oxygen conditions and volumes of medium and algae. Further, artificial inoculations with different soil samples and animal feces (horse, elephant) were tested. For the artificial inoculations, *F. vesiculosus* was autoclaved in advance. In all tested conditions *F. vesiculosus* served as carbon source.

In the final approach applied in this study, 50 g of the algae were transferred into 500 ml Schott flasks containing 300 ml of synthetic seawater (Tropic Marin Classic Meersalz, Hünenberg, Switzerland) with a salinity of 15, mimicking the conditions found in the upper water layer of the Kiel fjord. No additional carbon source was added besides the algae and the minor amounts of sea salts.

The Schott-flasks were lightly sealed to keep micro-anaerobic conditions. The enrichment cultures were kept at 22 °C and slowly shaken on a GFL™ 3015 laboratory shaker at 60 rpm. The enrichment cultures were observed over time up to 30 days. Before aliquot samples were taken for further analyses, the enrichment cultures were manually shaken by hand for a homologous distribution of the components in the supernatant. Fluid samples were transferred and stored at -70 °C until further procedures. After every conduction, the removed volume of supernatant of the enrichment cultures was refilled with fresh medium.

Microbial community analysis

For genomic studies, 1 ml of the supernatant was centrifuged for 5 min at 12,500 g, followed by an isolation of the DNA with the Zymo Research Quick-DNA Fungal/Bacterial Kit (Zymo Research Europe GmbH, Freiburg Germany). 16S rRNA gene amplicon approaches were conducted to investigate the bacterial community dynamics in the enrichment cultures over time using barcode primers 515f. and 806rcbc for 16S rRNA amplicon analyses (1 × PCR ingredients: 2 µl Buffer B(10×) (ThermoFisherScientific, Waltham, MA; USA); 0.4 µl 10 mM dNTPs; 2 µl 25 mM MgCl₂; 0.5 µl, 10 µM FW/RV-Primer (Supplementary Table 5), 0.6 µl DMSO, 0.2 µl DCS-TaQ polymerase (Qiagen, Venlo, Netherlands), 15 µl (2.5 ng µl⁻¹) template DNA, 3.8 µl H₂O)⁷⁰. 16S rRNA gene amplicon libraries were generated by applying a one-step amplification protocol (PCR conditions: 95 °C 5 min, 25 cycles of 95 °C for 45 s, 55 °C for 30 s, 72 °C for 45 s, final extension 72 °C for 2 min). Libraries were paired-end sequenced on a MiSeq (Illumina) sequencer (MiSeq Reagent Kit v2, 500 cycles, product number: MS-102-2003) with 2 × 251 bp (plus 1 × 12 bp Index read)⁷¹. After sequencing, the bioinformatics pipeline performs sequence demultiplexing, adaptor and primer trimming. The 50–300 K sequencing reads per sample were analysed using the 16S Metagenomics Software version 2.6.2.3 (Illumina). This allow us to analyse OTUs (Operational Taxonomic Units) from different time points, comparing taxonomies via a curated database of 16S rRNA gene entries (greengenes.secondgenome.com, based on OTUs and QIIME) (Supplementary Table 5)^{72–76}.

Scanning electron microscopy (SEM) images of *F. vesiculosus* samples after 9 days in enrichment cultures were provided for insights into degrading processes and microbial communities. It was performed as previously published^{77,78}. The samples were fixed in paraformaldehyde (1%) and glutaraldehyde (0.25%) (30,525-89-4 and G4004, Merck, Taufkirchen Deutschland), dehydrated by ascending alcohol series and dried at the critical point with Balzers CPD 030 Critical Point Dryer (BAL-TEC, Schalksmühle, Germany). After coating samples with gold/carbon using a sputter coater SCD 050 (BAL-TEC, Schalksmühle, Germany), scanning electron micrographs were taken with a LEO 1525 (Zeiss, Oberkochen, Germany).

Metabolic dynamics in enrichment cultures

Monitoring the general algae degradation fractionating of the organic matter, bacterial growth, and biological activity, as well as the release of organic compounds was archived by measuring the optical density at 600 nm (OD_{600nm}) in triplicates. An increase or change of turbidity is assumed to correlate with released degradation products and microscale fractions of the algae but also with bacterial growth and can estimate microbial degrading activities. Also, the wet weight loss after 20 days in the enrichment was measured in triplicates. For this, the whole enrichment culture was filtered through a 1×1 mm mesh as every minor plant fraction was considered a degradation product.

The expected hydrolysis of ACW polysaccharides leads to a change in the concentration of sugar monomers and reducing sugar ends. The *para*-hydroxybenzoic acid hydrazide (phah) assay enables the quantification of reducing sugar equivalents and detects open forms as well as hemi-acetal and hemi-ketal of carbohydrates. Therefore, two reagents (A: 0.3 M 4-hydroxybenzhydrazide, 0.6 M HCl; B: 48 mM trisodium citrate, 10 mM $CaCl_2$, 0.5 M NaOH) were mixed 9:1 to a final volume of 1 ml. The mixture was then supplemented with 50 μ l of enrichment culture supernatant and heated at 100 °C with constant mixing. Additionally, L-(-)-Fucose (Sigma-Aldrich, Saint Louis, MO; USA) were used as an equivalent standard and diluted in the synthetic seawater (Tropic Marin Classic Meersalz, Hünenberg, Switzerland) with a salinity of 15. The absorbance determined the concentration at 410 nm. The values were fitted to the L-fucose standard curve prepared in triplicates. This method was conducted in triplicates to the corresponding enrichment culture of the OD measurement.

UHPLC-ESI-HR-MS2 data for metabolomic analysis was recorded using an Acquity I-class UHPLC (Waters, Milford, MA, USA) coupled to a PDA detector and a Vion IMS QToF (Waters). The chromatographic separation was performed using an Acquity C-18 UPLC column (1.7 μ m, 2.1 mm \times 100 mm; Waters). Mobile phases consisted of acetonitrile (HiPerSolv, VWR) for mobile phase A and pH_2O produced by the in-house Milli-Q system as mobile phase B, both containing 0.1% (v/v) formic acid (33,015, Sigma). The gradient was run from 10 to 100% B over 13 min at a flow rate of 0.45 $ml \cdot min^{-1}$. The MS was run in DDA mode, recording a m/z range from 150 to 1000 using a desolvation temperature of 350 °C, a source temperature of 120 °C and a cone voltage of 0.8 kV. Samples were run in ESI+ and ESI- ionisation mode. The collision energy for the generation of product ions in MS2 was set to a mass-dependent ramp from 20 to 60 keV, and N_2 was used as collision gas. The data was processed and analysed using UNIFI 1.9.4 (Waters). Metabolomic analyses, peak picking and principal component analysis were done using Progenesis Q1 (Waters). Freeze-dried samples were dissolved in 80% (v/v) Methanol *aq.* (HiPerSolv, VWR) and 5 μ l of the sample were injected for analysis.

Metagenome sequencing of *F. vesiculosus* enrichment cultures

Metagenomes were prepared of four biological replicates of the enrichment cultures. Interim results of the metabolic data (phah, OD_{600nm} , visual observations) suggested a timepoint of 9 days after the start of the enrichment for the highest degradation activity. This determined the day of sampling the metagenomes. The DNA of 1 ml supernatant from the enrichment cultures was isolated with the Zymo Research Quick-DNA Fungal/Bacterial Kit (Zymo Research Europe GmbH, Freiburg Germany). Library preparation and sequencing were performed at the Leibniz Institute of Virology (LIV, Hamburg). For library preparation, 1 ng total DNA extracted from enrichment cultures at d9 was used as input material by applying the Nextera XT DNA Library Preparation Kit (Illumina, product number: FC-131-1096) according to manufacturer's instructions. Libraries were paired-end sequenced on a NextSeq 500 (Illumina, San Diego, CA; USA) sequencer (NextSeq 500/550 High Output Kit v2.5, 300 Cycles, product number: 20024908) with 2×151 bp (plus 2×8 bp Index reads). Demultiplexing with bcl2fastq (default settings) yielded approximately 112–143 mio reads per sample.

Sequence reads were processed with fastp (v0.21.0) to remove sequences originating from sequencing adapters and sequences of low quality (Phred quality score below 20) from the 3' end of the sequence reads⁷⁹. Processed reads shorter than 40 bp were discarded. The remaining reads were assembled using SPAdes (v3.15.3) in metagenomic mode⁸⁰.

Metagenomic dataset analyses and processing

Profile Hidden Markov Model searches were performed as described previously⁸¹. Shortly, we extracted the curated HMMs related to glycosyl hydrolases (GH*.hmm, Glycohydro*.hmm, Glyco_hydro*.hmm, and Glyc_hyd*.hmm; Supplementary Table 6) from the InterPro/Pfam database in 03/2022⁸² as well as sulphatases S1_17 and S1_25 from the Sulfatlas database in 03/2023^{35,36} and searched all CDS from each metagenome with hmmsearch from the HMMER v.3.3 software package⁸³. Additionally, two HMMs (GH107 and GH168) were designed with the enzymes extracted from the CAZy database³⁴. If a protein-coding region in the metagenome was associated with several enzyme families, the highest HMM score was taken for the final assignment. The reporting cut-off was set at an e-value $< E-10$. N-terminal secretion signal prediction was performed with SignalP v.6.0⁸⁴. The phylogenetic affiliation of each potential hit was inferred from the best BLASTp hit in the NCBI nr-database⁸⁵ using DIAMOND v.2.0.15⁸⁶. "All against all" alignments were performed with DIAMOND BLASTp, reporting only alignments with e-value < 0.01 . In the displayed data of number of genes, the four metagenomic datasets were combined, including only unique gene sequences. Visualisation of the Sequence Similarity Network (SSN) was conducted in Cytoscape v.3.9.1⁸⁷ applying the "Prefuse Force Directed Layout (none)" as described elsewhere⁸⁸. Taxonomic classification was carried out with Kraken2 (v2.12) (KRAKEN) in combination with Bracken (v2.6.2) (BRACKEN)^{89,90}. R v.4.2.3 was conducted for plotting and the visualisation of metabolic, phylogenetic and metagenomic results mainly using the packages ggplot2 v.3.4.4 and ComplexHeatmap v.2.16.0⁹¹⁻⁹³. Additionally, R v.4.2.3 served to perform reported cut-off applications (Kraken analyses 0.0001 ratio of covered fragments). The vegan package v.2.6–4 was used for diversity calculations⁹⁴.

Gene cloning and protein expression

Putative substrate degrading genes were cloned in the pet21a(+)-plasmid and transferred into *Escherichia coli* BL21. The metagenomic DNA was extracted with the Zymo Research Quick-DNA Fungal/Bacterial Kit (Zymo Research Europe GmbH, Freiburg, Germany). Primers were designed for the top-scoring genes of the HMM for enzyme family GH29 involved in the fucoidan degradation cascade and extended with restriction enzyme sites for *ndeI* and *xhoI* and a removed stop codon, which leads to the addition of the His-tag to the insert in the pet21a(+)-plasmid. Potential signal peptides were predicted with SignalP v. 6.0 and excluded from the final insert, as both successfully cloned enzymes were found to include a signal peptide (Sec/SPI)⁸⁴. The resulting primer sequences for the genes coding for the protein FUJM18 are 5'-CAACAAAAAATATGGAACGAAACCG-3' (forward) and 5'-TTTCAGAAATAGCTCAATCACGG-3' (reverse) and for FUJM20 5'-CAGGAATATTCATATCCTATGGATG-3' (forward) and 5'-TTTAATTTTATGTTTAAAGATGGTATC-3' (reverse). After the double digestion with the restriction enzymes for the target genes and the plasmid (2 μ l cutsmart buffer, 1 μ l *ndeI*, 1 μ l *xhoI*, 1000 ng template, ad 20 μ l H₂O), as well as the dephosphorylation of the plasmid (1 μ l FastAp additional to the double digest mixture) for 2 h at 37 °C and the deactivation for 20 min at 65 °C, the Monarch[®] PCR & DNA Cleanup Kit (5 μ g) (New England BioLabs[®] Inc., Ipswich Massachusetts) was used to purify the plasmid. In the following, the ligation product with T4-Ligase was transferred into *E. coli* DH5a by heat shock and sequenced with T7-promoter and T7-terminator primers after growing in LB-medium with 100 μ g⁻¹ ampicillin. Plasmids of successful clones were extracted with the Presto[™] Mini Plasmid Kit (Geneaid, New Taipei City Taiwan R.O.C.) and retransformed by heat shock in the expression strain *E. coli* BL21.

The protein expression was initiated by inoculating auto-induction medium ZYM5052⁹⁵ including 100 μ g⁻¹ ampicillin with the modified *E. coli* BL21 strain at 37 °C until the bacterial growth reached an OD_{600nm} of 0.6 in the media followed by the expression phase at 22 °C overnight. The bacterial cells were disrupted by sonification in the Hielscher Ultrasonics GmbH UP200S (3 \times 1 min, amplitude 70%, cycle 0.5), and the enzymes were purified with the QIAGEN[®] Ni-NTA Fast Start Kit (Venlo, Netherlands). The purified enzyme was rebuffed in 0.1 M potassium phosphate Buffer (PPB, pH 7) until further use.

Sequence and structural alignments of GH29 candidates

Protein structure predictions were calculated with AlphaFold2 and displayed with UCSF Chimera v.1.16, which was also used to generate the supplemental movie files⁹⁶. Furthermore, extended structure comparisons on the protein database (PDB)⁶⁷ were carried out with the Dali server⁹⁷. First, similar protein structures were found through the PDB search tool, followed by an 'All against All' analysis, including the implemented enzymes and protein structures with a cut-off of the RMSD of 2.5 Å.

GH29 α -L-fucosidase activity assay

Two GH29 enzymes (FUJM18, FUJM20) were tested with a 4-Nitrophenyl- α -L-fucopyranoside assay. The enzyme activity was conducted in triplicates at temperatures 22 °C, 28 °C, 37 °C, 50 °C, 60 °C, 70 °C, and 80 °C and from pH values between 4 and 8 (pH 4: sodium acetate; pH 5–6: sodium citrate; pH 7–8: HEPES). For this, 180 μ l 0.1 M reaction buffer was mixed with 10 μ l of 0.15 mg⁻¹ enzyme PBB mixture. After 20 min of incubation at the assay temperature, 10 μ l of 10 mM pNP- α -L-Fuc diluted in Aqua bidest were added and incubated for 15 min. 20 μ l 2 M sodium carbonate was used to adjust the pH to the same level before measuring the absorbance at 405 nm with the plate reader Synergy H1 (BioTek, Winooski). A standard curve using 4-nitrophenol was measured to calculate enzyme activity units (U) in mmol⁻¹min⁻¹ and enzyme activity rates.

Data availability

For the sequences' functional characterisation, the Integrated Microbial Genomes (IMG) pipeline and homology searches were used^{79,98}. Sequence data for the 16S rRNA analyses have been submitted to the European Nucleotide Archive. They are publicly available under accession no. PRJEB65586 and under the IMG ID Ga0502370; Ga0502371; Ga0502372; and Ga0502373.

Received: 13 November 2023; Accepted: 29 April 2024

Published online: 03 May 2024

References

1. Bitog, J. P. *et al.* Application of computational fluid dynamics for modeling and designing photobioreactors for microalgae production: A review. *Comput. Electron. Agric.* **76**, 131–147. <https://doi.org/10.1016/j.compag.2011.01.015> (2011).
2. Ehimen, E. A., Holm-Nielsen, J.-B., Poulsen, M. & Boelsmand, J. E. Influence of different pre-treatment routes on the anaerobic digestion of a filamentous algae. *Renew. Energy* **50**, 476–480. <https://doi.org/10.1016/j.renene.2012.06.064> (2013).
3. Trivedi, J., Aila, M., Bangwal, D. P., Kaul, S. & Garg, M. O. Algae based biorefinery—How to make sense?. *Renew. Sustain. Energy Rev.* **47**, 295–307. <https://doi.org/10.1016/j.rser.2015.03.052> (2015).
4. Salman, J. M. *et al.* Cultivation of blue green algae (*Arthrospira platensis* Gomont, 1892) in wastewater for biodiesel production. *Chemosphere* **335**, 139107. <https://doi.org/10.1016/j.chemosphere.2023.139107> (2023).
5. Adeniyi, O. M., Azimov, U. & Burluka, A. Algae biofuel: Current status and future applications. *Renew. Sustain. Energy Rev.* **90**, 316–335. <https://doi.org/10.1016/j.rser.2018.03.067> (2018).
6. Findlay, S. E. G., Sinsabaugh, R. L., Sobczak, W. V. & Hoostal, M. Metabolic and structural response of hyporheic microbial communities to variations in supply of dissolved organic matter. *Limnol. Oceanogr.* **48**, 1608–1617. <https://doi.org/10.4319/lo.2003.48.4.1608> (2003).
7. Guiry, M. D. & Guiry, G. M. AlgaeBase. World-wide electronic publication. *National University of Ireland, Galway* (2008)
8. Mariani, P., Tolomio, C. & Braghetta, P. An ultrastructural approach to the adaptive role of the cell wall in the intertidal alga *Fucus vesiculosus*. *Protoplasma* **128**, 208–217. <https://doi.org/10.1007/BF01276343> (1985).
9. Rioux, L.-E. & Turgeon, S. L. Seaweed carbohydrates. In *Seaweed Sustainability* (Elsevier: 2015), pp. 141–192.

10. Lahaye, M. & Kaeffer, B. Seaweed dietary fibres: Structure, physico-chemical and biological properties relevant to intestinal physiology. *Sci. Aliments Food Sci. Int. J. Food Sci. Technol.* **17**, 563–584 (1997).
11. Kloareg, B. & Quatrano, R. S. Structure of the cell walls of marine algae and ecophysiological functions of the matrix polysaccharides. *Oceanogr. Mar. Biol.* **26**, 259–315 (1988).
12. Fletcher, H. R., Biller, P., Ross, A. B. & Adams, J. The seasonal variation of fucoidan within three species of brown macroalgae. *Algal. Res.* **22**, 79–86. <https://doi.org/10.1016/j.algal.2016.10.015> (2017).
13. Cheng, Y.-S., Labavitch, J. M. & VanderGheynst, J. S. Elevated CO₂ concentration impacts cell wall polysaccharide composition of green microalgae of the genus *Chlorella*. *Lett. Appl. Microbiol.* **60**, 1–7. <https://doi.org/10.1111/lam.12320> (2015).
14. Black, W. A. The seasonal variation in the combined L-fucose content of the common British Laminariaceae and fucaeeae. *J. J. Sci. Food Agric.* **5**, 445–448 (1954).
15. Honya, M., Mori, H., Anzai, M., Araki, Y. & Nisizawa, K. Monthly changes in the content of fucans, their constituent sugars and sulphate in cultured *Laminaria japonica*. In *Sixteenth International Seaweed Symposium* (eds Kain, J. M. et al.) 411–416 (Springer, 1999).
16. Skriptsova, A. V. Seasonal variations in the fucoidan content of brown algae from Peter the Great Bay, Sea of Japan. *Russ. J. Mar. Biol.* **42**, 351–356. <https://doi.org/10.1134/S1063074016040106> (2016).
17. Fulcher, R. G. & McCully, M. E. Histological studies on the genus *Fucus*. V. An autoradiographic and electron microscopic study of the early stages of regeneration. *J. Botany* **49**(1), 161–165. <https://doi.org/10.1139/b71-027> (1971).
18. Ushakova, N. A. et al. Anticoagulant activity of fucoidans from brown algae. *Biochem. Mosc. Suppl. B Biomed. Chem. B* **3**, 77–83. <https://doi.org/10.1134/S1990750809010119> (2009).
19. Rioux, L.-E., Turgeon, S. L. & Beaulieu, M. Characterization of polysaccharides extracted from brown seaweeds. *Carbohydr. Polym.* **69**, 530–537. <https://doi.org/10.1016/j.carbpol.2007.01.009> (2007).
20. Bilan, M. I. et al. A highly regular fraction of a fucoidan from the brown seaweed *Fucus distichus* L. *Carbohydr. Res.* **339**, 511–517. <https://doi.org/10.1016/j.carres.2003.10.028> (2004).
21. Sichert, A. et al. Verrucomicrobia use hundreds of enzymes to digest the algal polysaccharide fucoidan. *Nat. Microbiol.* **5**, 1026–1039. <https://doi.org/10.1038/s41564-020-0720-2> (2020).
22. Holdt, S. L. & Kraan, S. Bioactive compounds in seaweed: Functional food applications and legislation. *J. Appl. Phycol.* **23**, 543–597. <https://doi.org/10.1007/s10811-010-9632-5> (2011).
23. Wietz, M. et al. Bacterial community dynamics during polysaccharide degradation at contrasting sites in the Southern and Atlantic Oceans. *Environ. Microbiol.* **17**, 3822–3831. <https://doi.org/10.1111/1462-2920.12842> (2015).
24. Vieira, R. P. et al. Relationships between bacterial diversity and environmental variables in a tropical marine environment, Rio de Janeiro. *Environ. Microbiol.* **10**, 189–199. <https://doi.org/10.1111/j.1462-2920.2007.01443.x> (2008).
25. Herlemann, D. P. R., Lundin, D., Andersson, A. F., Labrenz, M. & Jürgens, K. Phylogenetic signals of salinity and season in bacterial community composition across the salinity gradient of the Baltic Sea. *Front. Microbiol.* **7**, 1883. <https://doi.org/10.3389/fmicb.2016.01883> (2016).
26. Mensch, B. et al. Restructuring of epibacterial communities on *Fucus vesiculosus* forma mytili in response to elevated pCO₂ and increased temperature levels. *Front. Microbiol.* **7**, 434. <https://doi.org/10.3389/fmicb.2016.00434> (2016).
27. Stratil, S. B., Neuling, S. C., Knecht, H., Friedrichs, A. K. & Wahl, M. Temperature-driven shifts in the epibiotic bacterial community composition of the brown macroalga *Fucus vesiculosus*. *MicrobiologyOpen* **2**, 338–349. <https://doi.org/10.1002/mbio.379> (2013).
28. Mancuso, F. P., D'Hondt, S., Willems, A., Airoldi, L. & de Clerck, O. Diversity and temporal dynamics of the epiphytic bacterial communities associated with the canopy-forming seaweed *Cystoseira compressa* (Esper) Gerloff and Nizamuddin. *Front. Microbiol.* **7**, 476. <https://doi.org/10.3389/fmicb.2016.00476> (2016).
29. Wolter, L. A. et al. *Pseudooceanicola* algae sp. Nov., isolated from the marine macroalga *Fucus spiralis*, shows genomic and physiological adaptations for an algae-associated lifestyle. *Syst. Appl. Microbiol.* **44**, 126166. <https://doi.org/10.1016/j.syapm.2020.126166> (2021).
30. Oppong-Danquah, E., Blümle, M. & Tasdemir, D. Metabolomics and microbiomics insights into differential surface fouling of three macroalgal species of fucus (*Fucales*, *Phaeophyceae*) that co-exist in the German Baltic Sea. *Mar Drugs* <https://doi.org/10.3390/md21110595> (2023).
31. Díez-Vives, C., Gasol, J. M. & Acinas, S. G. Spatial and temporal variability among marine Bacteroidetes populations in the NW Mediterranean Sea. *Syst. Appl. Microbiol.* **37**, 68–78. <https://doi.org/10.1016/j.syapm.2013.08.006> (2014).
32. Stratil, S. B., Neuling, S. C., Knecht, H., Friedrichs, A. K. & Wahl, M. Salinity affects compositional traits of epibacterial communities on the brown macroalga *Fucus vesiculosus*. *FEMS Microbiol. Ecol.* **88**, 272–279. <https://doi.org/10.1111/1574-6941.12292> (2014).
33. Parrot, D. et al. Mapping the surface microbiome and metabolome of brown seaweed *Fucus vesiculosus* by amplicon sequencing, integrated metabolomics and imaging techniques. *Sci. Rep.* **9**, 1061. <https://doi.org/10.1038/s41598-018-37914-8> (2019).
34. Drula, E. et al. The carbohydrate-active enzyme database: functions and literature. *Nucleic Acids Res.* **50**, D571–D577. <https://doi.org/10.1093/nar/gkab1045> (2022).
35. Barbeyron, T. et al. Matching the diversity of sulfated biomolecules: creation of a classification database for sulfatases reflecting their substrate specificity. *PLoS One* **11**, e0164846. <https://doi.org/10.1371/journal.pone.0164846> (2016).
36. Stam, M. et al. SulfAtlas, the sulfatase database: State of the art and new developments. *Nucleic Acids Res.* **51**, D647–D653. <https://doi.org/10.1093/nar/gkac977> (2023).
37. Hettle, A. G., Vickers, C. J. & Boraston, A. B. Sulfatases: Critical enzymes for algal polysaccharide processing. *Front. Plant. Sci.* **13**, 837636. <https://doi.org/10.3389/fpls.2022.837636> (2022).
38. Schultz-Johansen, M. et al. Discovery and screening of novel metagenome-derived GH107 enzymes targeting sulfated fucans from brown algae. *FEBS J.* **285**, 4281–4295. <https://doi.org/10.1111/febs.14662> (2018).
39. Silchenko, A. S. et al. Fucoidan sulfatases from marine bacterium *Wenyingshuangia fucanilytica* CZ1127T. *Biomolecules* <https://doi.org/10.3390/biom8040098> (2018).
40. Vickers, C. et al. Endo-fucoidan hydrolases from glycoside hydrolase family 107 (GH107) display structural and mechanistic similarities to α-L-fucosidases from GH29. *J. Biol. Chem.* **293**, 18296–18308. <https://doi.org/10.1074/jbc.RA118.005134> (2018).
41. McBride, M. J. & Zhu, Y. Gliding motility and Por secretion system genes are widespread among members of the phylum Bacteroidetes. *J. Bacteriol.* **195**, 270–278. <https://doi.org/10.1128/JB.01962-12> (2013).
42. Bjursell, M. K., Martens, E. C. & Gordon, J. I. Functional genomic and metabolic studies of the adaptations of a prominent adult human gut symbiont, *Bacteroides thetaiotaomicron*, to the suckling period. *J. Biol. Chem.* **281**, 36269–36279. <https://doi.org/10.1074/jbc.M606509200> (2006).
43. Martens, E. C. et al. Recognition and degradation of plant cell wall polysaccharides by two human gut symbionts. *PLoS Biol.* **9**, e1001221. <https://doi.org/10.1371/journal.pbio.1001221> (2011).
44. Martens, E. C., Roth, R., Heuser, J. E. & Gordon, J. I. Coordinate regulation of glycan degradation and polysaccharide capsule biosynthesis by a prominent human gut symbiont. *J. Biol. Chem.* **284**, 18445–18457. <https://doi.org/10.1074/jbc.M109.008094> (2009).

45. Shipman, J. A., Berleman, J. E. & Salyers, A. A. Characterization of four outer membrane proteins involved in binding starch to the cell surface of *Bacteroides thetaiotaomicron*. *J. Bacteriol.* **182**, 5365–5372. <https://doi.org/10.1128/jb.182.19.5365-5372.2000> (2000).
46. Foley, M. H., Cockburn, D. W. & Koropatkin, N. M. The Sus operon: A model system for starch uptake by the human gut Bacteroidetes. *Cell Mol. Life Sci.* **73**, 2603–2617. <https://doi.org/10.1007/s00018-016-2242-x> (2016).
47. Oliver, J. D. The viable but nonculturable state in bacteria. *J. Microbiol.* **43**, 93 (2005).
48. Kovalová, T. *et al.* Active site complementation and hexameric arrangement in the GH family 29; a structure–function study of α -L-fucosidase isoenzyme 1 from *Paenibacillus thiaminolyticus*. *Glycobiology* **29**, 59–73. <https://doi.org/10.1093/glycob/cwy078> (2019).
49. Li, J., He, Z., Liang, Y., Peng, T. & Hu, Z. Insights into algal polysaccharides: A review of their structure, depolymerases, and metabolic pathways. *J. Agric. Food Chem.* **70**, 1749–1765. <https://doi.org/10.1021/acs.jafc.1c05365> (2022).
50. Li, B., Lu, F., Wei, X. & Zhao, R. Fucoidan: Structure and bioactivity. *Molecules (Basel, Switzerland)* **13**, 1671–1695. <https://doi.org/10.3390/molecules13081671> (2008).
51. Kadam, S. U., Tiwari, B. K. & O'Donnell, C. P. Extraction, structure and biofunctional activities of laminarin from brown algae. *Int. J. Food Sci. Technol.* **50**, 24–31. <https://doi.org/10.1111/ijfs.12692> (2015).
52. Duchesne, L. C. & Larson, D. W. Cellulose and the evolution of plant life. *BioScience* **39**, 238–241. <https://doi.org/10.2307/1311160> (1989).
53. Wong, T. Y., Preston, L. A. & Schiller, N. L. ALGINATE LYASE: Review of major sources and enzyme characteristics, structure–function analysis, biological roles, and applications. *Ann. Rev. Microbiol.* **54**, 289–340. <https://doi.org/10.1146/annurev.micro.54.1.289> (2000).
54. Colusse, G. A., Carneiro, J., Duarte, M. E. R., de Carvalho, J. C. & Noseda, M. D. Advances in microalgal cell wall polysaccharides: A review focused on structure, production, and biological application. *Crit. Rev. Biotechnol.* **42**, 562–577. <https://doi.org/10.1080/07388551.2021.1941750> (2022).
55. Zhang, X. & Watanabe, M. M. grazing and growth of the mixotrophic chrysoomonad poterioochromonas malhamensis (Chryso-phyceae) feeding on algae. *J. Phycol.* **37**, 738–743. <https://doi.org/10.1046/j.1529-8817.2001.00127.x> (2001).
56. Lüring, M. & Beekman, W. Grazer-induced defenses in *Scenedesmus* (Chlorococcales; Chlorophyceae): coenobium and spine formation. *Phycologia* **38**, 368–376. <https://doi.org/10.2216/10031-8884-38-5-368.1> (1999).
57. Mayeli, S. M., Nandini, S. & Sarma, S. The efficacy of *Scenedesmus* morphology as a defense mechanism against grazing by selected species of rotifers and cladocerans. *Aquat. Ecol.* **38**, 515–524. <https://doi.org/10.1007/s10452-005-0329-9> (2005).
58. Eilers, H., Pernthaler, J. & Amann, R. Succession of pelagic marine bacteria during enrichment: A close look at cultivation-induced shifts. *Appl. Environ. Microbiol.* **66**, 4634–4640. <https://doi.org/10.1128/AEM.66.11.4634-4640.2000> (2000).
59. Bunse, C., Koch, H., Breider, S., Simon, M. & Wietz, M. Sweet spheres: Succession and CAZyme expression of marine bacterial communities colonizing a mix of alginate and pectin particles. *Environ. Microbiol.* **23**, 3130–3148. <https://doi.org/10.1111/1462-2920.15536> (2021).
60. Grote, J., Jost, G., Labrenz, M., Herndl, G. J. & Jürgens, K. Epsilonproteobacteria represent the major portion of chemoautotrophic bacteria in sulfidic waters of pelagic redoxclines of the Baltic and Black Seas. *Appl. Environ. Microbiol. Appl. Environ. Microbiol.* **74**, 7546–7551. <https://doi.org/10.1128/AEM.01186-08> (2008).
61. Capo, E. *et al.* Deltaproteobacteria and spirochaetes-like bacteria are abundant putative mercury methylators in oxygen-deficient water and marine particles in the Baltic Sea. *Front. Microbiol.* **11**, 574080. <https://doi.org/10.3389/fmicb.2020.574080> (2020).
62. Macfarlane, G. T. & Gibson, G. R. Formation of glycoprotein degrading enzymes by *Bacteroides fragilis*. *FEMS Microbiol. Lett.* **77**, 289–294. <https://doi.org/10.1111/j.1574-6968.1991.tb04363.x> (1991).
63. McKee, L. S. *et al.* Polysaccharide degradation by the Bacteroidetes: mechanisms and nomenclature. *Environ. Microbiol. Rep.* **13**, 559–581. <https://doi.org/10.1111/1758-2229.12980> (2021).
64. Astafyeva, Y. *et al.* Microalgae and bacteria interaction—evidence for division of diligence in the alga microbiota. *Microbiol. Spectr.* **10**, e0063322. <https://doi.org/10.1128/spectrum.00633-22> (2022).
65. Barbeyron, T., L'Haridon, S., Michel, G. & Czjzek, M. *Mariniflexile fucanivorans* sp. nov., a marine member of the Flavobacteriaceae that degrades sulphated fucans from brown algae. *Int. J. Syst. Evol. Microbiol.* **58**, 2107–2113. <https://doi.org/10.1099/ijs.0.65674-0> (2008).
66. Giljan, G. *et al.* Selfish bacteria are active throughout the water column of the ocean. *ISME Commun.* **3**, 11. <https://doi.org/10.1038/s43705-023-00219-7> (2023).
67. Berman, H. M. *et al.* The protein data bank. *Nucleic Acids Res.* **28**, 235–242. <https://doi.org/10.1093/nar/28.1.235> (2000).
68. Wu, H.-J. *et al.* Structural basis of alpha-fucosidase inhibition by iminocyclitols with K(i) values in the micro- to picomolar range. *Angew. Chem. Int. Ed Engl.* **49**, 337–340. <https://doi.org/10.1002/anie.200905597> (2010).
69. Riemann, L. *et al.* The native bacterioplankton community in the central baltic sea is influenced by freshwater bacterial species. *Appl. Environ. Microbiol.* **74**, 503–515. <https://doi.org/10.1128/AEM.01983-07> (2008).
70. Walters, W. *et al.* Improved bacterial 16S rRNA Gene (V4 and V4–5) and fungal internal transcribed spacer marker gene primers for microbial community surveys. *mSystems* <https://doi.org/10.1128/mSystems.00009-15> (2016).
71. Wang, Q., Garrity, G. M., Tiedje, J. M. & Cole, J. R. Naive Bayesian classifier for rapid assignment of rRNA sequences into the new bacterial taxonomy. *Appl. Environ. Microbiol.* **73**, 5261–5267. <https://doi.org/10.1128/AEM.00062-076> (2007).
72. Wang, Y. & Qian, P.-Y. Conservative fragments in bacterial 16S rRNA genes and primer design for 16S ribosomal DNA amplicons in metagenomic studies. *PLoS One* **4**, e7401. <https://doi.org/10.1371/journal.pone.0007401> (2009).
73. Caporaso, J. G. *et al.* Global patterns of 16S rRNA diversity at a depth of millions of sequences per sample. *Proc. Natl. Acad. Sci. USA* **108**(Suppl 1), 4516–4522. <https://doi.org/10.1073/pnas.100080107> (2011).
74. Takahashi, S., Tomita, J., Nishioka, K., Hisada, T. & Nishijima, M. Development of a prokaryotic universal primer for simultaneous analysis of Bacteria and Archaea using next-generation sequencing. *PLoS One* **9**, e105592. <https://doi.org/10.1371/journal.pone.0105592> (2014).
75. Christoff, A. P., Sereia, A. F. R., Boberg, D. R., Moraes, R. L. & Oliveira, L. F. Bacterial identification through accurate library preparation and high-throughput sequencing. *Neoprosp. Microbiome Technol.* **25**, 1–5 (2017).
76. Caporaso, J. G. *et al.* QIIME allows analysis of high-throughput community sequencing data. *Nat. Methods* **7**, 335–336. <https://doi.org/10.1038/nmeth.f.303> (2010).
77. Krohn-Molt, I. *et al.* Insights into microalga and bacteria interactions of selected phycosphere biofilms using metagenomic, transcriptomic, and proteomic approaches. *Front. Microbiol.* **8**, 1941. <https://doi.org/10.3389/fmicb.2017.01941> (2017).
78. Krohn-Molt, I. *et al.* Metagenome survey of a multispecies and alga-associated biofilm revealed key elements of bacterial–algal interactions in photobioreactors. *Appl. Environ. Microbiol.* **79**, 6196–6206. <https://doi.org/10.1128/aem.01641-13> (2013).
79. Chen, S., Zhou, Y., Chen, Y. & Gu, J. fastp: An ultra-fast all-in-one FASTQ preprocessor. *Bioinformatics* **34**, i884–i890. <https://doi.org/10.1093/bioinformatics/bty560> (2018).
80. Bankevich, A. *et al.* SPAdes: A new genome assembly algorithm and its applications to single-cell sequencing. *J. Comput. Biol.* **19**, 455–477. <https://doi.org/10.1089/cmb.2012.0021> (2012).
81. Pérez-García, P., Danso, D., Zhang, H., Chow, J. & Streit, W. R. Exploring the global metagenome for plastic-degrading enzymes. *Methods Enzymol.* **648**, 137–157. <https://doi.org/10.1016/bs.mie.2020.12.022> (2021).
82. Paysan-Lafosse, T. *et al.* InterPro in 2022. *Nucleic Acids Res.* **51**, D418–D427. <https://doi.org/10.1093/nar/gkac993> (2023).

www.nature.com/scientificreports/

83. Mistry, J., Finn, R. D., Eddy, S. R., Bateman, A. & Punta, M. Challenges in homology search: HMMER3 and convergent evolution of coiled-coil regions. *Nucleic Acids Res.* **41**, e121. <https://doi.org/10.1093/nar/gkt263> (2013).
84. Teufel, F. *et al.* SignalP 6.0 predicts all five types of signal peptides using protein language models. *Nat. Biotechnol.* **40**, 1023–1025. <https://doi.org/10.1038/s41587-021-01156-3> (2022).
85. Sayers, E. W. *et al.* Database resources of the national center for biotechnology information in 2023. *Nucleic Acids Res.* **51**, D29–D38. <https://doi.org/10.1093/nar/gkac1032> (2023).
86. Buchfink, B., Reuter, K. & Drost, H.-G. Sensitive protein alignments at tree-of-life scale using DIAMOND. *Nat. Methods* **18**, 366–368. <https://doi.org/10.1038/s41592-021-01101-x> (2021).
87. Shannon, P. *et al.* Cytoscape: A software environment for integrated models of biomolecular interaction networks. *Genome Res.* **13**, 2498–2504. <https://doi.org/10.1101/gr.1239303> (2003).
88. Copp, J. N., Akiva, E., Babbitt, P. C. & Tokuriki, N. Revealing unexplored sequence-function space using sequence similarity networks. *Biochemistry* **57**, 4651–4662. <https://doi.org/10.1021/acs.biochem.8b00473> (2018).
89. Wood, D. E. & Salzberg, S. L. Kraken: Ultrafast metagenomic sequence classification using exact alignments. *Genome Biol.* **15**, R46. <https://doi.org/10.1186/gb-2014-15-3-r46> (2014).
90. Lu, J., Breitwieser, F. P., Thielen, P. & Salzberg, S. L. Bracken: Estimating species abundance in metagenomics data. *PeerJ Comput. Sci.* **3**, e104. <https://doi.org/10.7717/peerj-cs.104> (2017).
91. R Core Team. *R: A Language and Environment for Statistical Computing*. Available at <https://www.R-project.org/> (Vienna, Austria, 2023).
92. Wickham, H. *ggplot2. Elegant Graphics for Data Analysis* 2nd edn. (Springer International Publishing, 2016).
93. Gu, Z., *ComplexHeatmap*; <https://doi.org/10.18129/B9.bioc.ComplexHeatmap> (2017).
94. Oksanen, J., *et al.* *vegan: Community Ecology Package*. Available at <https://CRAN.R-project.org/package=vegan> (2022).
95. Studier, F. W. Protein production by auto-induction in high density shaking cultures. *Protein Expr. Purif.* **41**, 207–234. <https://doi.org/10.1016/j.pep.2005.01.016> (2005).
96. Jumper, J. *et al.* Highly accurate protein structure prediction with AlphaFold. *Nature* **596**, 583–589. <https://doi.org/10.1038/s41586-021-03819-2> (2021).
97. Holm, L. Dali server: Structural unification of protein families. *Nucleic Acids Res.* **50**, W210–W215. <https://doi.org/10.1093/nar/gkac387> (2022).
98. Mukherjee, S. *et al.* Genomes OnLine database (GOLD) vol 7: Updates and new features. *Nucleic Acids Res.* **47**, D649–D659. <https://doi.org/10.1093/nar/gky977> (2019).

Acknowledgements

The authors thank Dr Malik Alawi and Minyue Qi of the Bioinformatics Core of the University Medical Center Hamburg-Eppendorf for performing the sequencing assembly. This work was in part supported by the Aqua-Health FKZ 031B0945C, SuReMetS FKZ 031B0944A, PlastiSea FKZ 031B0867F. We would also like to thank Elke Woelken for providing and preparing the SEM.

Author contributions

J.F.H.M., I.K. and W.R.S. contributed to the experimental design and writing of this article. J.F.H.M. executed the lab work of enrichment cultures, metagenomics, enzyme purification and characterisation. PPG worked on the bioinformatics of metagenomics, P.P.G. and J.F.H.M. on sequence-based screenings and enzyme characterisation. Y.K.H.S. provided and processed MS-datasets. D.I. and P.B. contributed to the sequencing of the metagenomic and amplicon datasets. W.R.S., J.H.A. and I.K. were involved in general project supervision and acquisition of funding. All authors contributed to the manuscript revision and read and approved the submitted version.

Funding

Open Access funding enabled and organized by Projekt DEAL.

Competing interests

The authors declare no competing interests.

Additional information

Supplementary Information The online version contains supplementary material available at <https://doi.org/10.1038/s41598-024-60978-8>.

Correspondence and requests for materials should be addressed to I.K.

Reprints and permissions information is available at www.nature.com/reprints.

Publisher's note Springer Nature remains neutral with regard to jurisdictional claims in published maps and institutional affiliations.

 **Open Access** This article is licensed under a Creative Commons Attribution 4.0 International License, which permits use, sharing, adaptation, distribution and reproduction in any medium or format, as long as you give appropriate credit to the original author(s) and the source, provide a link to the Creative Commons licence, and indicate if changes were made. The images or other third party material in this article are included in the article's Creative Commons licence, unless indicated otherwise in a credit line to the material. If material is not included in the article's Creative Commons licence and your intended use is not permitted by statutory regulation or exceeds the permitted use, you will need to obtain permission directly from the copyright holder. To view a copy of this licence, visit <http://creativecommons.org/licenses/by/4.0/>.

© The Author(s) 2024

Supplemental Information - The bacterial degradation of Brown algae cell wall carbohydrates

Supplementary Table 1

Numerical data referring to Figure 2. R1-R3: replicate, OD_{600 nm}: OD_{600 nm} optical density of the enrichment culture. PHAH OD_{410 nm}: determined absorbance at 410 nm of para-hydroxybenzoic acid hydrazide assay. PHAHFuc: converted PHAH OD_{410 nm} resemble L-fucose concentration calculated on a standard curve of $y = 0.0448x + 0.0052$ (n=21) determined by 7 concentrations of L-(-)-fucose in technical triplicates

DAY	OD _{600 nm} R1	OD _{600 nm} R2	OD _{600 nm} R3	PHAH OD _{410 nm} R1	PHAH OD _{410 nm} R2	PHAH OD _{410 nm} R3	PHAHFUC [MOL] R1	PHAHFUC [MOL] R2	PHAHFUC [MOL] R3
d0	0,102	0,1025	0,1077	0,006	0,008	0,007	0,017857143	0,0625	0,040178571
d1	0,1242	0,1206	0,1399	0,007	0,013	0,017	0,040178571	0,174107143	0,263392857
d2	0,331	0,3344	0,312	0,026	0,021	0,029	0,464285714	0,352678571	0,53125
d3	0,4432	0,4775	0,4529	0,063	0,064	0,079	1,290178571	1,3125	1,647321429
d4	0,6983	0,7132	0,7362	0,089	0,094	0,121	1,870535714	1,982142857	2,584821429
d5	0,915	0,9105	0,9227	0,103	0,158	0,169	2,183035714	3,410714286	3,65625
d6	1,0334	1,0234	1,017	0,164	0,203	0,198	3,544642857	4,415178571	4,303571429
d7	1,0784	1,0998	1,0899	0,141	0,113	0,113	3,03125	2,40625	2,40625
d8	1,0962	1,1203	1,1151	0,089	0,078	0,085	1,870535714	1,625	1,78125
d9	1,0879	1,1123	1,1057	0,093	0,101	0,111	1,959821429	2,138392857	2,361607143
d10	1,1563	1,1511	1,1195	0,076	0,086	0,102	1,580357143	1,803571429	2,160714286
d11	1,203	1,1498	1,1494	0,079	0,087	0,104	1,647321429	1,825892857	2,205357143
d12	1,066	1,1087	1,0685	0,074	0,058	0,069	1,535714286	1,178571429	1,424107143
d13	1,1751	1,1314	1,1592	0,064	0,071	0,079	1,3125	1,46875	1,647321429
d14	0,8487	0,8945	0,879	0,056	0,056	0,058	1,133928571	1,133928571	1,178571429
d15	0,9871	0,9581	0,9855	0,055	0,057	0,061	1,111607143	1,15625	1,245535714
d16	0,9925	0,8165	0,7656	0,074	0,06	0,074	1,535714286	1,223214286	1,535714286

Supplementary Table 2

IMG-accession of provided metagenomes of *F. vesiculosus* microbiomes

IMG/MER ACCESSION NUMBER	NUMBER OF CONTIGS	GC CONTENT	LONGEST CONTIG	MEAN CONTIG	TOTAL CONTIG LENGTH
Ga0502370	399,970	45.29%	211.39 Kbp	707.96 bp	283.16 Mbp
Ga0502371	1,143,468	45.45%	216.74 Kbp	640.13 bp	731.97 Mbp
Ga0502372	715,725	45.23%	350.84 Kbp	695.60 bp	497.86 Mbp
Ga0502373	1,073,390	44.22%	283.36 Kbp	578.47 bp	620.93 Mbp

Supplementary Table 3

Numerical data referring to Figure 6. Enzyme unit (U) in mmol*min⁻¹. Enzyme activities were measured in triplicates and calculated on a standard curve $y = 2.6702x + 0.0529$ (n= 18) determined by 6 concentrations of 4-nitrophenol in triplicates.

GEN	PH	TEMPERATURE	ENZYME ACTIVITY [U/MG]	STANDART DEVIATION
FUJM18	pH 6	22 °C	7.419	0.765
FUJM18	pH 6	28 °C	10.565	7.759
FUJM18	pH 4	37 °C	11.497	1.655
FUJM18	pH 5	37 °C	13.289	4.860
FUJM18	pH 6	37 °C	37.391	16.692
FUJM18	pH 7	37 °C	15.281	6.285
FUJM18	pH 8	37 °C	8.784	4.641
FUJM18	pH 6	50 °C	33.379	4.438
FUJM18	pH 6	60 °C	41.702	7.018
FUJM18	pH 6	70 °C	32.736	11.205
FUJM18	pH 4	80 °C	0	0
FUJM18	pH 5	80 °C	0	0
FUJM18	pH 6	80 °C	61.176	12.790
FUJM18	pH 7	80 °C	4.113	1.237
FUJM18	pH 8	80 °C	0	0

FUJM20	pH 6	22 °C	8.806	0.838
FUJM20	pH 6	28 °C	8.773	4.434
FUJM20	pH 4	37 °C	12.485	0.953
FUJM20	pH 5	37 °C	8.568	1.265
FUJM20	pH 6	37 °C	29.385	15.242
FUJM20	pH 7	37 °C	2.709	0.510
FUJM20	pH 8	37 °C	1.512	2.036
FUJM20	pH 6	50 °C	28.053	8.299
FUJM20	pH 6	60 °C	33.490	5.430
FUJM20	pH 6	70 °C	39.427	5.309
FUJM20	pH 4	80 °C	0	0
FUJM20	pH 5	80 °C	11.020	6.731
FUJM20	pH 6	80 °C	41.768	1.346
FUJM20	pH 7	80 °C	31.338	2.282
FUJM20	pH 8	80 °C	0	0
CONTROL	pH 6	22 °C	0	0
CONTROL	pH 6	28 °C	0	0
CONTROL	pH 4	37 °C	0	0
CONTROL	pH 5	37 °C	0	0
CONTROL	pH 6	37 °C	0	0
CONTROL	pH 7	37 °C	0	0
CONTROL	pH 8	37 °C	0	0
CONTROL	pH 6	50 °C	0	0
CONTROL	pH 6	60 °C	0	0
CONTROL	pH 6	70 °C	0	0
CONTROL	pH 4	80 °C	0	0
CONTROL	pH 5	80 °C	0	0
CONTROL	pH 6	80 °C	0	0
CONTROL	pH 7	80 °C	0	0
CONTROL	pH 8	80 °C	0	0

Supplementary Table 4

Enzyme classes and families involved in algae carbohydrate degradation

ALGAE CELL WALL POLYMER	ALGAE	GH FAMILIES	PL FAMILIES	SULFATASE FAMILIES	CBM FAMILIES	CE FAMILIES
FUCOIDAN	Phaeophyceae	1, 29, 30, 35, 92, 95, 107, 139, 141, 149, 151, 168	-	1_15, 1_16, 1_17, 1_25	35, 47, 51	-
LAMINARIN	Phaeophyceae/ Bacillariophyta	3, 16, 17, 30, 55, 81	-	-	4, 6, 32, 54, 56	-
ALGINATE	Phaeophyceae	-	5, 6, 7, 14, 15, 17, 18, 31, 32, 34, 36, 38, 41	-	2, 13, 16, 32, 35	-
CELLULOSE	Phaeophyceae/ Chlorophyta	1, 3, 5, 6, 7, 8, 9, 10, 12, 16, 26, 39, 44, 45, 48, 51, 55, 74	-	-	1, 2, 3, 4, 5, 6, 9, 10, 17, 22, 28, 32, 37, 46, 60, 63, 65, 72, 76, 78, 80, 81	4
CARRAGEENAN	Rhodophyta	16, 82, 150, 164	-	-	16, 92	-
MANNAN	Chlorophyta/ Rhodophyta	1, 2, 5, 26, 38, 44, 45, 47, 76, 92, 99, 113, 125, 130, 134	-	-	1, 2, 3, 5, 6, 10, 16, 23, 27, 32, 35, 59	-
XYLAN	Chlorophyta/ Rhodophyta	3, 5, 8, 10, 11, 26, 30, 43, 44, 62, 141	-	-	1, 2, 3, 4, 5, 6, 9, 10, 13, 15, 22, 31, 35, 36, 37, 48, 59, 60, 64, 72, 86	1, 3, 4, 20
AGAR	Rhodophyta	16, 50, 86, 96, 117, 118	-	-	6, 13	-
PORPHYRAN	Rhodophyta	16, 86	-	-	13, 92	-

PECTIN	Chlorophyta/	1, 2, 5, 16, 28,	1, 2, 3, 4, 9, 11,	-	1, 13	1, 8, 12
	Bacillariophyta	30, 35, 42, 43, 51, 53, 54, 62	26			
ULVAN	Chlorophyta	2, 3, 39, 43, 78, 88, 92, 105	24, 25, 28, 40	-	-	90

Supplementary Table 5
16S-Amplicon Primer for library preparation

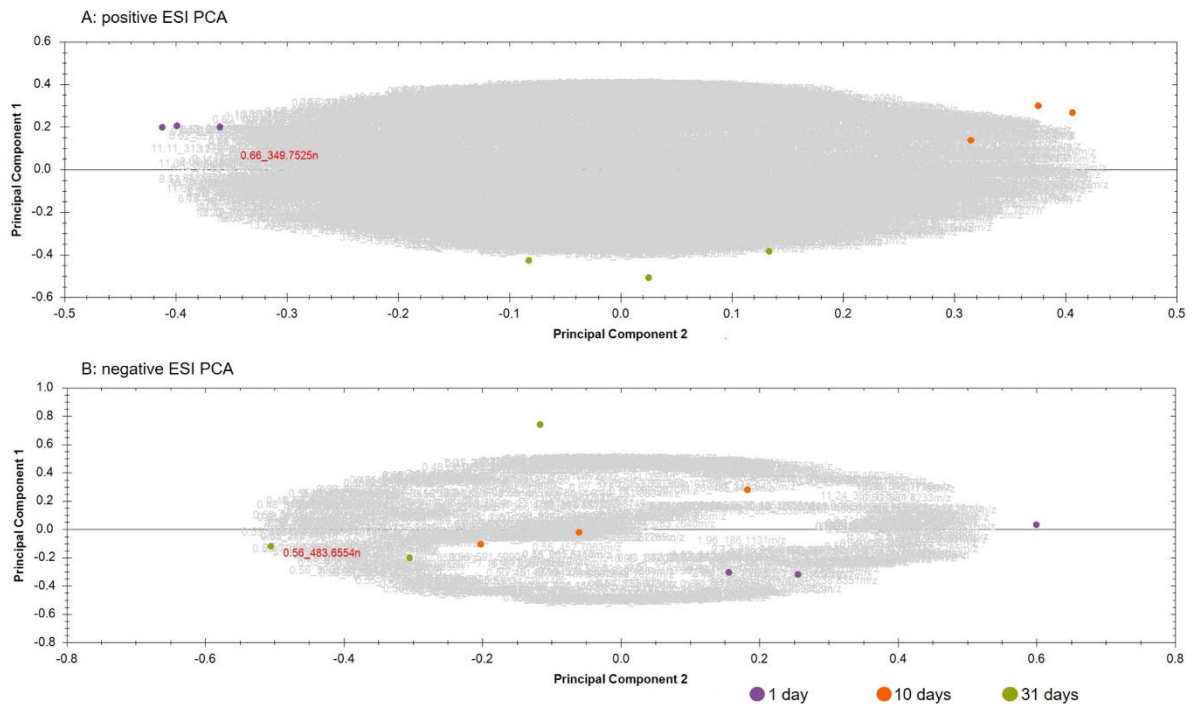
SAMPLE	NAME	FUNCTION	SEQUENCE	NO OF READS
	515f	16S-Amplicon forward	AATGATACGGCGACCACCGAGATCTACACTATGGTA ATTGTGTGCCAGCMGCCGCGGTAA	
d0	806rcbc11	16S-Amplicon reverse	CAAGCAGAAGACGGGCATACGAGATAATTGTGTGTCGGA AGTCAGTCAGCCGGACTACHVGGGTWTCTAAT	318,500
d3	806rcbc12	16S-Amplicon reverse	CAAGCAGAAGACGGGCATACGAGATTGCATACACTGG AGTCAGTCAGCCGGACTACHVGGGTWTCTAAT	96,165
d6	806rcbc13	16S-Amplicon reverse	CAAGCAGAAGACGGGCATACGAGATAGTCGAACGAG GAGTCAGTCAGCCGGACTACHVGGGTWTCTAAT	87,960
d9	806rcbc14	16S-Amplicon reverse	CAAGCAGAAGACGGGCATACGAGATACCAGTGACTCA AGTCAGTCAGCCGGACTACHVGGGTWTCTAAT	207,850
d12	806rcbc15	16S-Amplicon reverse	CAAGCAGAAGACGGGCATACGAGATGAATACCAAGTC AGTCAGTCAGCCGGACTACHVGGGTWTCTAAT	50,994
d15	806rcbc16	16S-Amplicon reverse	CAAGCAGAAGACGGGCATACGAGATGTAGATCGTGTA AGTCAGTCAGCCGGACTACHVGGGTWTCTAAT	65,269

Supplementary Table 6
Hidden Markov Models for Glycosyl Hydrolase (GH) and Sulfatases (S1)

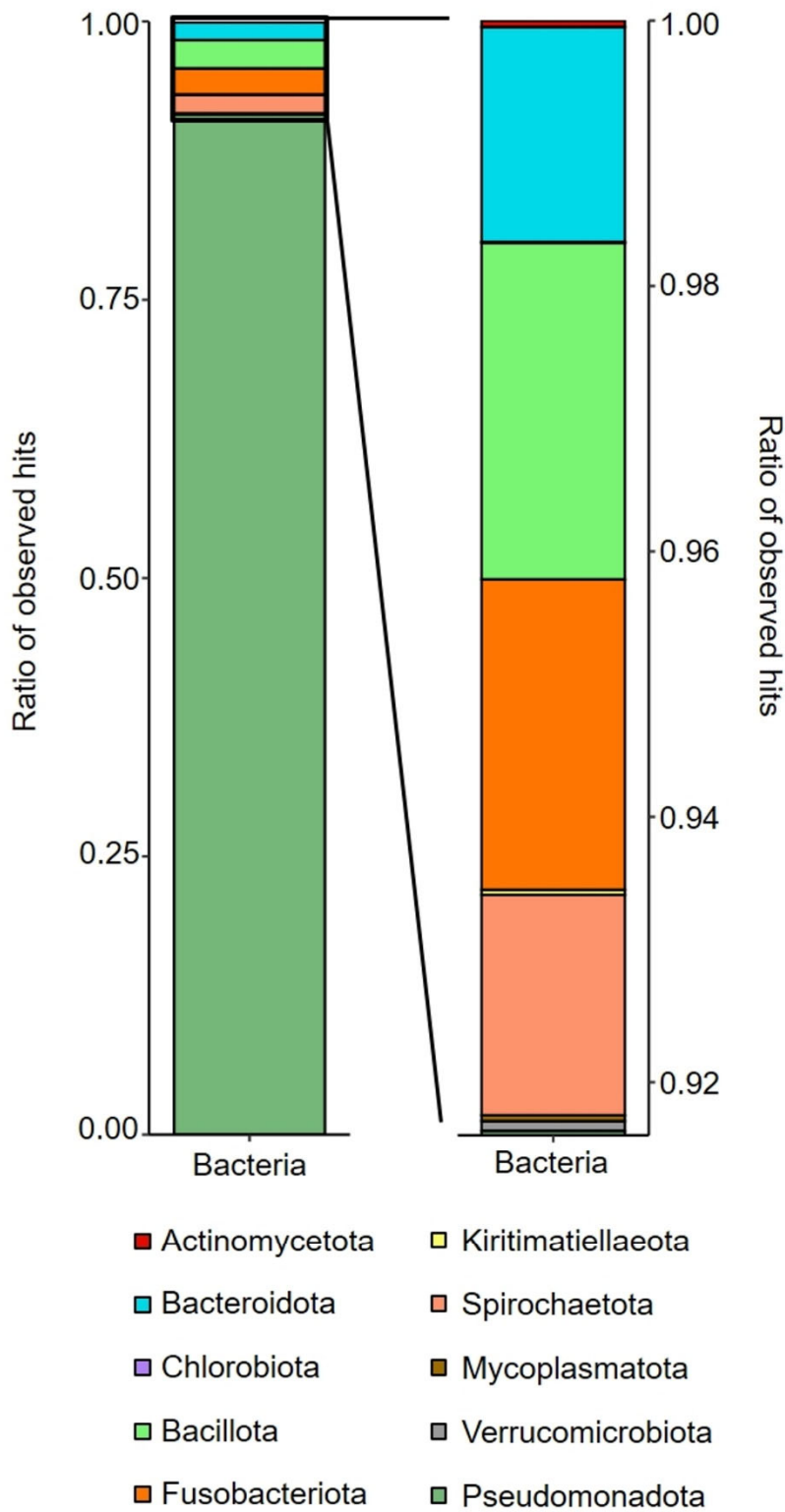
CATEGORY	FAMILY	ACCESSION	TYPE	DESCRIPTION	SOURCE
GH	1	PF00232	Domain	Glycosyl hydrolase family 1	Pfam
GH	2	PF00703	Domain	Glycosyl hydrolases family 2	Pfam
GH	2_C	PF02836	Domain	Glycosyl hydrolases family 2, TIM barrel domain	Pfam
GH	2_N	PF02837	Domain	Glycosyl hydrolases family 2, sugar binding domain	Pfam
GH	3	PF00933	Domain	Glycosyl hydrolase family 3 N terminal domain	Pfam
GH	3_C	PF01915	Domain	Glycosyl hydrolase family 3 C-terminal domain	Pfam
GH	4	PF02056	Family	Family 4 glycosyl hydrolase	Pfam
GH	4C	PF11975	Domain	Family 4 glycosyl hydrolase C-terminal domain	Pfam
GH	5	PF14872	Family	Hypothetical glycoside hydrolase 5	Pfam
GH	5_C	PF18564	Domain	Glycoside hydrolase family 5 C-terminal domain	Pfam
GH	6	PF01341	Domain	Glycosyl hydrolases family 6	Pfam
GH	6_2	PF14871	Family	Hypothetical glycosyl hydrolase 6	Pfam
GH	7	PF00840	Domain	Glycosyl hydrolase family 7	Pfam
GH	8	PF01270	Repeat	Glycosyl hydrolases family 8	Pfam
GH	9	PF00759	Repeat	Glycosyl hydrolase family 9	Pfam
GH	10	PF00331	Domain	Glycosyl hydrolase family 10	Pfam
GH	11	PF00457	Domain	Glycosyl hydrolases family 11	Pfam
GH	12	PF01670	Domain	Glycosyl hydrolase family 12	Pfam
GH	13	PF14883	Family	Hypothetical glycosyl hydrolase family 13	Pfam
GH	14	PF01373	Domain	Glycosyl hydrolase family 14	Pfam
GH	15	PF00723	Repeat	Glycosyl hydrolases family 15	Pfam
GH	16	PF00722	Domain	Glycosyl hydrolases family 16	Pfam
GH	17	PF00332	Domain	Glycosyl hydrolases family 17	Pfam
GH	18	PF00704	Domain	Glycosyl hydrolases family 18	Pfam
GH	19	PF00182	Domain	Chitinase class I	Pfam
GH	20	PF00728	Domain	Glycosyl hydrolase family 20, catalytic domain	Pfam

GH	20b	PF02838	Domain	Glycosyl hydrolase family 20, domain 2	Pfam
GH	25	PF01183	Domain	Glycosyl hydrolases family 25	Pfam
GH	26	PF02156	Domain	Glycosyl hydrolase family 26	Pfam
GH	28	PF00295	Repeat	Glycosyl hydrolases family 28	Pfam
GH	29	PF01120	Family	Alpha-L-fucosidase	Pfam
GH	30	PF02055	Domain	Glycosyl hydrolase family 30 TIM-barrel domain	Pfam
GH	30_2	PF14587	Domain	O-Glycosyl hydrolase family 30 Glycosyl hydrolase family 30 beta sandwich domain	Pfam
GH	30C	PF17189	Domain	domain	Pfam
GH	31	PF01055	Family	Glycosyl hydrolases family 31	Pfam
GH	32C	PF08244	Domain	Glycosyl hydrolases family 32 C terminal	Pfam
GH	32N	PF00251	Domain	Glycosyl hydrolases family 32 N-terminal domain	Pfam
GH	35	PF01301	Domain	Glycosyl hydrolases family 35 Glycosyl hydrolase 36 superfamily, catalytic domain	Pfam
GH	36	PF17167	Repeat	domain	Pfam
GH	36C	PF16874	Domain	Glycosyl hydrolase family 36 C-terminal domain	Pfam
GH	36N	PF16875	Domain	Glycosyl hydrolase family 36 N-terminal domain Glycosyl hydrolases family 38 C-terminal domain	Pfam
GH	38	PF18438	Domain	1	Pfam
GH	38C	PF07748	Domain	Glycosyl hydrolases family 38 C-terminal domain	Pfam
GH	38N	PF01074	Domain	Glycosyl hydrolases family 38 N-terminal domain	Pfam
GH	39	PF01229	Family	Glycosyl hydrolases family 39	Pfam
GH	42	PF02449	Domain	Beta-galactosidase	Pfam
GH	42C	PF08533	Domain	Beta-galactosidase C-terminal domain	Pfam
GH	42M	PF08532	Domain	Beta-galactosidase trimerisation domain	Pfam
GH	43	PF04616	Family	Glycosyl hydrolases family 43	Pfam
GH	44	PF12891	Domain	Glycoside hydrolase family 44	Pfam
GH	45	PF02015	Domain	Glycosyl hydrolase family 45	Pfam
GH	46	PF01374	Domain	Glycosyl hydrolase family 46	Pfam
GH	47	PF01532	Repeat	Glycosyl hydrolase family 47	Pfam
GH	48	PF02011	Repeat	Glycosyl hydrolase family 48	Pfam
GH	49	PF03718	Repeat	Glycosyl hydrolase family 49 Glycosyl hydrolase family 49 N-terminal Ig-like domain	Pfam
GH	49N	PF17433	Domain	domain	Pfam
GH	52	PF03512	Family	Glycosyl hydrolase family 52	Pfam
GH	53	PF07745	Domain	Glycosyl hydrolase family 53	Pfam
GH	56	PF01630	Domain	Hyaluronidase	Pfam
GH	57	PF03065	Domain	Glycosyl hydrolase family 57	Pfam
GH	59	PF02057	Family	Glycosyl hydrolase family 59	Pfam
GH	59M	PF17387	Domain	Glycosyl hydrolase family 59 central domain	Pfam
GH	62	PF03664	Family	Glycosyl hydrolase family 62	Pfam
GH	63	PF03200	Repeat	Glycosyl hydrolase family 63 C-terminal domain	Pfam
GH	63N	PF16923	Domain	Glycosyl hydrolase family 63 N-terminal domain	Pfam
GH	64	PF16483	Domain	Beta-1,3-glucanase	Pfam
GH	65C	PF03633	Family	Glycosyl hydrolase family 65, C-terminal domain Glycosyl hydrolase family 65 central catalytic domain	Pfam
GH	65m	PF03632	Repeat	domain	Pfam
GH	65N	PF03636	Family	Glycosyl hydrolase family 65, N-terminal domain	Pfam
GH	65N_2	PF14498	Domain	Glycosyl hydrolase family 65, N-terminal domain	Pfam
GH	66	PF13199	Domain	Glycosyl hydrolase family 66	Pfam
GH	67C	PF07477	Domain	Glycosyl hydrolase family 67 C-terminus	Pfam
GH	67M	PF07488	Domain	Glycosyl hydrolase family 67 middle domain	Pfam
GH	67N	PF03648	Domain	Glycosyl hydrolase family 67 N-terminus	Pfam
GH	68	PF02435	Family	Levansucrase/Invertase	Pfam
GH	70	PF02324	Family	Glycosyl hydrolase family 70	Pfam
GH	71	PF03659	Family	Glycosyl hydrolase family 71	Pfam
GH	72	PF03198	Domain	Glucanosyltransferase Fungal chitosanase of glycosyl hydrolase group	Pfam
GH	75	PF07335	Family	75	Pfam
GH	76	PF03663	Repeat	Glycosyl hydrolase family 76	Pfam

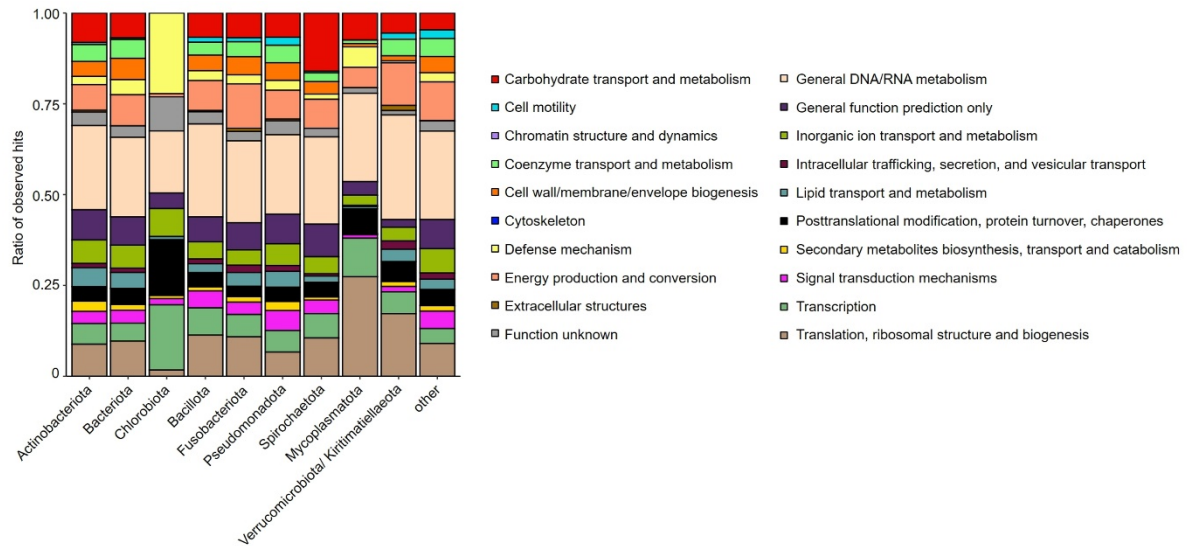
GH	77	PF02446	Domain	4-alpha-glucanotransferase Glycosyl hydrolase family 79 C-terminal beta domain	Pfam
GH	79C	PF16862	Domain	Glycosyl hydrolase family 79, N-terminal domain	Pfam
GH	79n	PF03662	Domain	Glycosyl hydrolase family 79, N-terminal domain	Pfam
GH	80	PF13647	Domain	Glycosyl hydrolase family 80 of chitinase A	Pfam
GH	81	PF03639	Domain	Glycosyl hydrolase family 81 N-terminal domain	Pfam
GH	85	PF03644	Family	Glycosyl hydrolase family 85	Pfam
GH	88	PF07470	Repeat	Glycosyl Hydrolase Family 88	Pfam
GH	92	PF07971	Repeat	Glycosyl hydrolase family 92	Pfam
GH	92N	PF17678	Domain	Glycosyl hydrolase family 92 N-terminal domain	Pfam
GH	97	PF10566	Domain	Glycoside hydrolase 97	Pfam
GH	98C	PF08307	Domain	Glycosyl hydrolase family 98 C-terminal domain	Pfam
GH	98M	PF08306	Domain	Glycosyl hydrolase family 98	Pfam
GH	99	PF16317	Domain	Glycosyl hydrolase family 99	Pfam
GH	100	PF12899	Repeat	Alkaline and neutral invertase	Pfam
GH	101	PF12905	Domain	Endo-alpha-N-acetylgalactosaminidase	Pfam
GH	101C	PF17451	Domain	Glycosyl hydrolase 101 beta sandwich domain	Pfam
GH	106	PF17132	Family	alpha-L-rhamnosidase	Pfam
GH	107	-	Family	Glycosyl hydrolase family 107	caZy/This study
GH	108	PF05838	Domain	Glycosyl hydrolase 108	Pfam
GH	114	PF03537	Domain	Glycoside-hydrolase family GH114	Pfam
GH	115	PF15979	Family	Glycosyl hydrolase family 115 beta-glucosidase 2, glycosyl-hydrolase family 116 N-term	Pfam
GH	116N	PF12215	Family	N-term	Pfam
GH	125	PF06824	Repeat	Metal-independent alpha-mannosidase (GH125)	Pfam
GH	127	PF07944	Repeat	Beta-L-arabinofuranosidase, GH127 Glycosyl hydrolases related to GH101 family, GH129	Pfam
GH	129	PF11308	Family	GH129	Pfam
GH	130	PF04041	Family	beta-1,4-mannooligosaccharide phosphorylase	Pfam
GH	168	-	Family	Glycosyl hydrolase family 168	caZy/This study
Sulfatase	S1_17	-	Family	subfamily S1_17	SulfAtlas
Sulfatase	S1_25	-	Family	subfamily S1_25	SulfAtlas



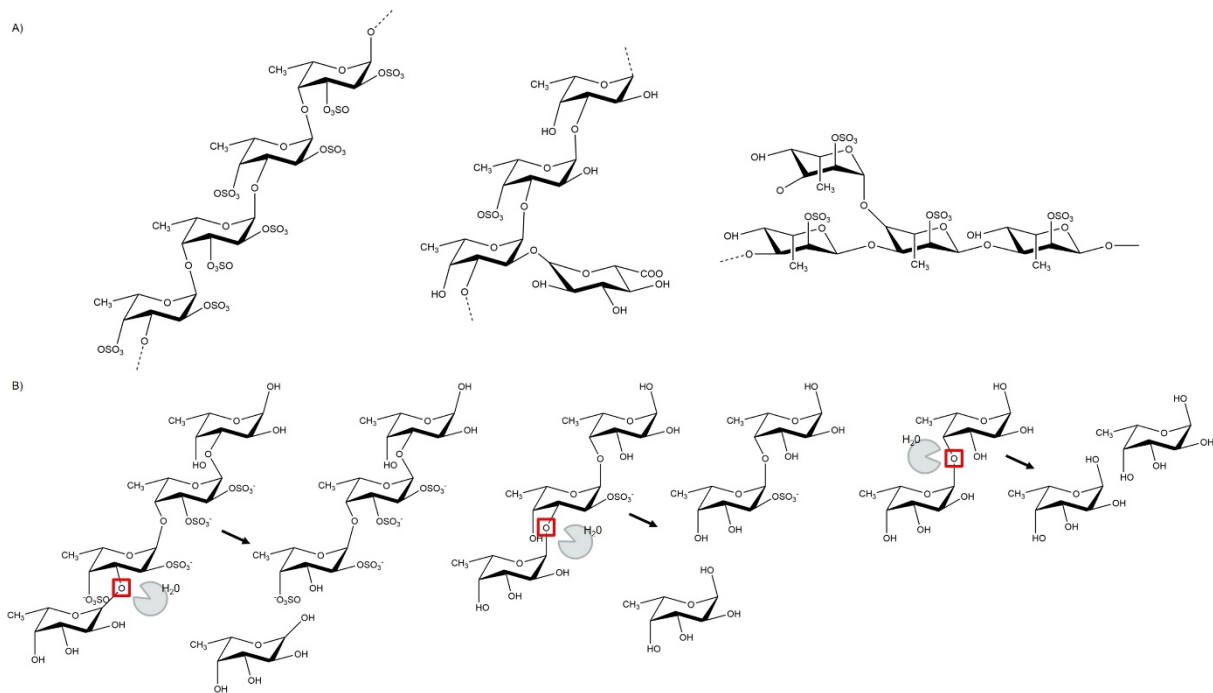
Supplemental Figure 1: Principal component analysis (PCA) of the features for MS-datasets recorded using A: positive Electrospray (ESI); and B: negative ESI. For each time point (1, 10 and 31 days) three replicates were incubated and analysed.



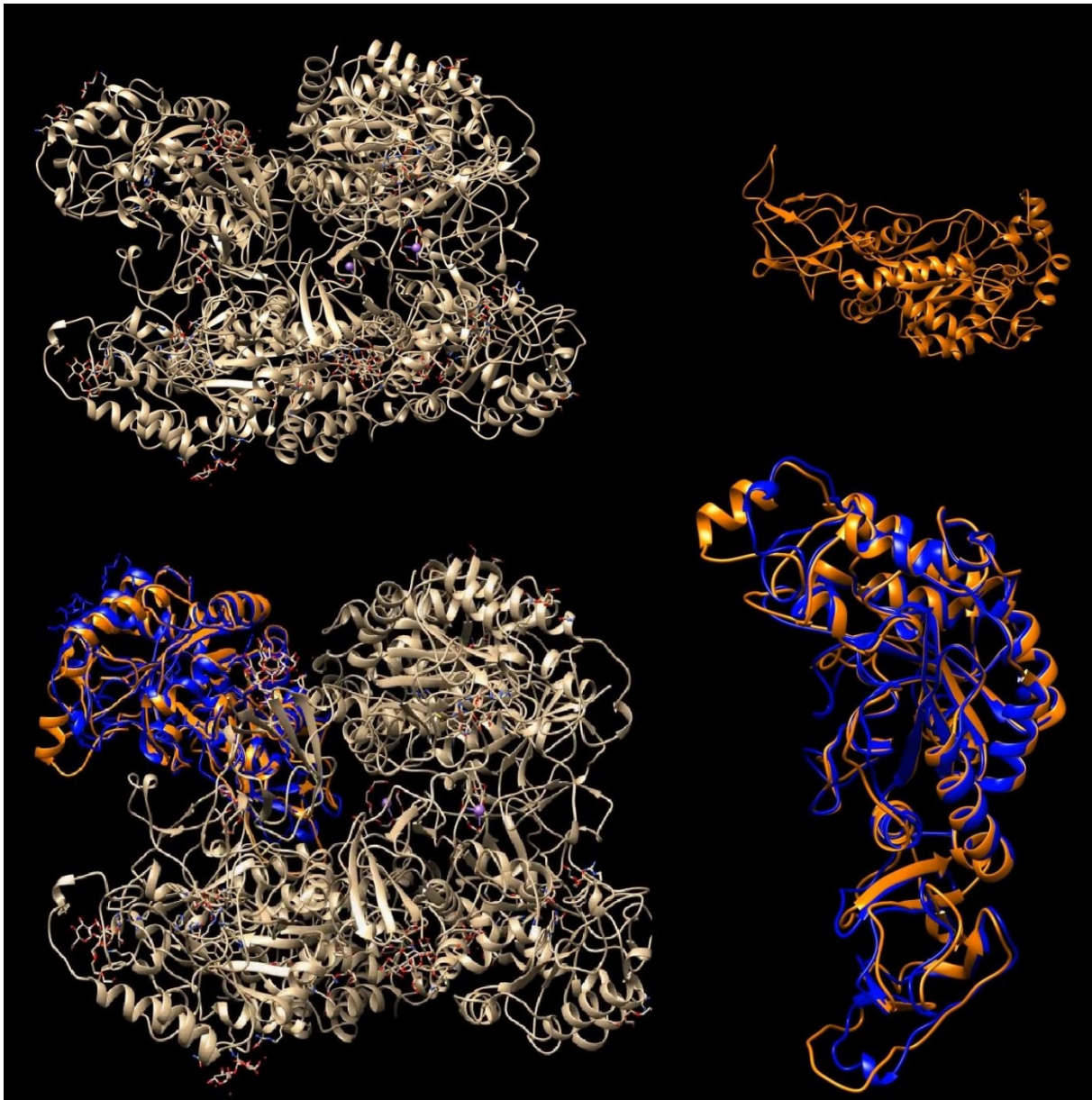
Supplementary Figure 2: Diversity and phylogeny of *F. vesiculosus* microbiome in enrichment cultures after 9 days. Mean metagenome bacterial phylogeny of 4 enrichment cultures representing phyla with a ratio of all covered genes higher than 0.0001% within the whole metagenome. Standard deviation is equal to or below 0.01 for every phyla besides Proteobacteria with ± 0.025 .



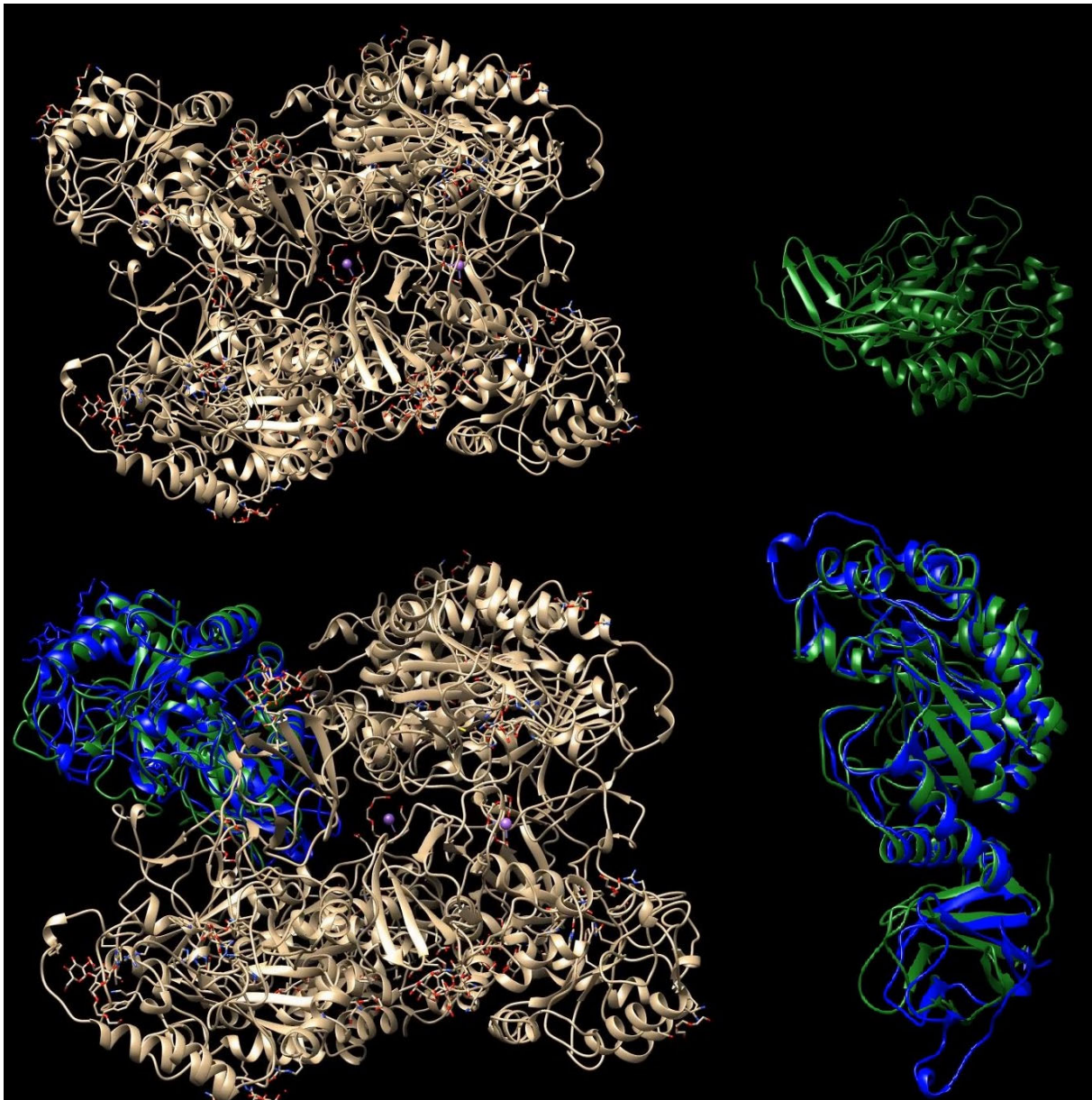
Supplementary Figure 3: Clusters of orthologous groups of proteins of bacteria with a ratio of all covered genes higher than 0.0001% within the whole metagenome in *Fucus vesiculosus* enrichment cultures after 9 days.



Supplementary Figure 4: Detailed schematic structure and function of GH29 enzymes. A) Examples of sulfated fucoidan structures. Homofucan as backbone structure and heterofucan with crosslinks. B) Fucoidan degradation catalyse with GH29. The structure of homofucan with sulphated α 1,3/1,4 linked L-fucose is degraded in multiple steps. Presented are enzymatic reactions with GH29 α L-fucosidase. Structures generated with ChemDraw v.21.0.0. Adapted from Li et al. (2022) 49.



Supplemental Movie 1: Structure comparison of predicted FUJM18 protein structure and α -L-fucosidase isoenzyme 1 from *Paenibacillus thiaminolyticus* (6GN6) from the PDB database. Grey: α -L-fucosidase isoenzyme 1 from *Paenibacillus thiaminolyticus*. Orange: JUFM18 structure prediction by AlphaFold2. BLUE: α -L-fucosidase isoenzyme 1 from *Paenibacillus thiaminolyticus* Chain D. Picture adaptation of original movie.



Supplemental Movie 2: Structure comparison of predicted FUJM20 protein structure and α -L-fucosidase isoenzyme 1 from *Paenibacillus thiaminolyticus* (6GN6) from the PDB database. Grey: α -L-fucosidase isoenzyme 1 from *Paenibacillus thiaminolyticus*. Green: JUFM20 structure prediction by Alphafold2. BLUE: α -L-fucosidase isoenzyme 1 from *Paenibacillus thiaminolyticus* Chain D. Picture adaptation of original movie.



Supplemental Movie 3: Structure comparison of predicted FUJM18 and predicted FUJM20. Orange: JUFM18 structure prediction by Alphafold2. Green: JUFM20 structure prediction by Alphafold2. Picture adaptation of original movie.

Publication 2: The antioxidant potential of *T. chui* microbiomes

Full title: Exploring *Tetraselmis chui* microbiomes - functional metagenomics for novel catalases and superoxide dismutases

First author: Jascha F. H. Macdonald

Corresponding author: Dr Ines Krohn

Co-authors: Dr Yuchen Han
Dr Yekaterina Astafyeva
Lutgardis Bergmann
Marno Gurschke
Dr Philipp Dirksen
Dr Patrick Blümke
Dr Yannik K.-H. Schneider
Dr Malik Alawi
Dr Sebastian Lippemeier
Professor Dr Jeanette H. Andersen

Journal: Applied Microbiology and Biotechnology

Accepted: 26th of December 2024

Published: 13th of January 2025

DOI: <https://doi.org/10.1007/s00253-024-13395-w>

Applied Microbiology and Biotechnology (2025) 109:6
https://doi.org/10.1007/s00253-024-13395-w

BIOTECHNOLOGICALLY RELEVANT ENZYMES AND PROTEINS



Exploring *Tetraselmis chui* microbiomes—functional metagenomics for novel catalases and superoxide dismutases

Jascha F. H. Macdonald¹ · Yuchen Han¹ · Yekaterina Astafyeva¹ · Lutgardis Bergmann¹ · Marno Gurschke¹ · Philipp Dirksen² · Patrick Blümke³ · Yannik K. H. Schneider⁴ · Malik Alawi² · Sebastian Lippemeier⁵ · Jeanette H. Andersen⁴ · Ines Krohn¹

Received: 10 August 2024 / Revised: 26 November 2024 / Accepted: 26 December 2024
© The Author(s) 2025

Abstract

The focus on microalgae for applications in several fields, e.g. resources for biofuel, the food industry, cosmetics, nutraceuticals, biotechnology, and healthcare, has gained increasing attention over the last decades. In this study, we investigate the microbiome of the cultured microalga *Tetraselmis chui* (*T. chui*) to highlight their potential for health benefits. In this context, biomolecules like antioxidants play a crucial role in the well-being of living organisms as they metabolise harmful reactive oxygen species (ROS) to reduce oxidative stress. Impaired processing of ROS leads to damaged cells and increases the risk of cancer, inflammatory diseases, and diabetes, among others. Here, we identify, characterise, and test bacterial antioxidants derived from the *T. chui* microbiome metagenome dataset. We identified 258 genes coding for proteins with potential antioxidant activity. Of those, four novel enzymes are expressed and identified as two superoxide dismutases (SOD), TcJM_SOD2 and TcIK_SOD3, and two catalases (CAT), TcJM_CAT2 and TcIK_CAT3. Extensive analyses characterised all implemented enzymes as active even in concentrations down to 25 ng*ml⁻¹ for the SODs and 15 ng*ml⁻¹ for the CATs. Furthermore, sequence-based analyses assign TcJM_SOD2 and TcIK_SOD3 to iron superoxide dismutases (Fe SODs) and TcJM_CAT2 and TcIK_CAT3 to heme-containing catalases. These candidates are phylogenetically classified within the phylum Pseudomonadota. Regarding the biotechnological potential, a toxicity assay did not indicate any harmful effects. The introduced enzymes may benefit medical applications and expand the potential of microalgae microbiomes.

Key points

- Omics-based discoveries of antioxidant enzymes from *Tetraselmis chui* microbiome
- Two superoxide dismutases and two catalases are identified and tested for activity
- Enzyme sensitivity highlights biotechnological potential of microalgae microbiomes

Keywords Antioxidants · Healthcare · Microalgae microbiome · *Tetraselmis chui* · Catalase · Superoxide dismutase · Metagenome

Introduction

Microalgae like *Tetraselmis chui* have garnered significant attention due to their potential applications in various fields, including biotechnology, biofuel production, food as well as nutraceutical additives, and environmental remediation (Grierson et al. 2011; Cerezuela et al. 2012; Moser et al. 2022; Segovia-Campos et al. 2024). Large-scale farming of *T. chui* is already underway and being optimised through ongoing investigations (Khatoon et al. 2018; Coleman et al. 2023; Yusuf et al. 2023). *T. chui* is prominently used in food as protein enrichment and replacement product with nutritional benefits (Qazi et al. 2021). Most interestingly, *T.*

✉ Ines Krohn
incs.krohn@uni-hamburg.de

¹ Department of Microbiology and Biotechnology, Institute of Plant Science and Microbiology, University of Hamburg, Ohnhorststr.18, 22609 Hamburg, Germany

² Bioinformatics Core, University Medical Center Hamburg-Eppendorf, Hamburg, Germany

³ Leibniz Institute of Virology, Hamburg, Germany

⁴ Marbio, Faculty of Biosciences, Fisheries and Economics, UiT—The Arctic University of Norway, Tromsø, Norway

⁵ BlueBioTech GmbH, Büsum, Germany

chui cultures can be also applied to benefit environmental health by cleaning wastewater of fish farms (Villar-Navarro et al. 2022). Current research focusses on the processing and application of the algae in cosmetics and as animal feed, e.g. in fish farms (Sørensen et al. 2023; Garcia et al. 2024; Simon et al. 2024;).

Overall, *T. chui* is a species of green microalgae belonging to a genus of primary producers in marine and brackish water environments. One area of interest regarding *T. chui* and other microalgae is their interaction with the environmental microbiome, particularly in aquatic ecosystems. The microbiome refers to the complex community of microorganisms, including bacteria, fungi, and protists, that inhabit a specific environment. These microorganisms form symbiotic relationships that play a crucial role in nutrient cycling, carbon fixation, and the overall dynamics of the ecosystem (Cirri and Pohnert 2019).

Molecular tools like functional metagenomic analyses enable us to screen microbiomes to investigate those interactions and screen for novel, valuable biomolecules. For example, antioxidants play a crucial role in mitigating oxidative stress, which can result from various environmental factors such as exposure to pollutants, UV radiation, or fluctuations in temperature (Pizzino et al. 2017). Protection against free radicals like reactive oxygen species (ROS) is crucial for all living species, from single-cell organisms to mammals. Until today, several molecules acting as antioxidants are known, with superoxide dismutase (SOD) and catalase (CAT) among them.

Superoxide dismutases (E.C. 1.15.1.1) are divided into four groups according to their involved metal cofactors. They are indicated by the designation of Ni-SOD, Cu/Zn-SOD, Mn-SOD, and Fe-SOD, with Nickel, Copper/Zinc, Manganese, or Iron as cofactor, respectively. While Mn-SOD and Fe-SOD developed in prokaryotes, Cu/Zn-SOD occurred in eukaryotes (Steinman 1978; Smith and Doolittle 1992). Interestingly, Mn-SOD is found in eukaryote mitochondria, and Cu/Zn-SOD is found in pathogenic bacteria, contrary to their evolution in eukaryotes. Lastly, Ni-SOD is found in Streptomycetota and Cyanobacteria. Overall, SODs are found in all phylogenetic kingdoms (Abreu and Cabelli 2010).

Catalases are enzymes that catalyse the decomposition of hydrogen peroxide into water and oxygen, thereby protecting cells from oxidative damage (Chelikani et al. 2004). CATs belong to an abundant group of heme-containing enzymes. These enzymes found in bacteria, Eukarya and Archaea are highly active. The heme-containing CATs can be classified into two major groups: monofunctional CATs and bifunctional catalase-peroxidases (Zamocky et al. 2008). The monofunctional CATs (EC 1.11.1.6) are divided into three clades, which evolved early in the development of the gene family through gene duplication events (Klotz 2003;

Zamocky et al. 2008). They belong to the hydrogen peroxide reductases. The bifunctional catalase-peroxidase (EC 1.11.1.7) is a donor oxidoreductase that also exhibits peroxidase activity. Additionally, Mn-CATs belong to a third group and form the nonheme manganese-containing CATs (EC 1.11.1.6). This minor group is only found in bacteria (Zamocky et al. 2008; Savelli et al. 2019).

Recent studies on *T. chui* and the associated microbiome have shown that these microalgae can produce antioxidant enzymes like SODs and CATs as part of their defence mechanisms against oxidative stress (Widowati et al. 2017). Additionally, interactions between microalgae and bacteria within the microbiome can influence the production and activity of antioxidants. For example, certain bacterial species may produce compounds that stimulate the production of antioxidants in microalgae or provide protection against oxidative stress through other mechanisms (Krohn et al. 2022). The potential of *Tetraselmis* species in health applications has already been described in former studies (Sansone et al. 2017; Moser et al. 2022; Lopes et al. 2024). Additionally, as this genus and its species *T. chui* have already been applied in culturing approaches (Day and Fenwick 1993; Lu et al. 2017; Patrino et al. 2022), we choose the microbiome of this algae as the foundation for the metagenome analyses.

Understanding the relationship between *T. chui*, the microbiome, and antioxidants has implications for various applications, including aquaculture, bioremediation, and the development of novel antioxidant products. By elucidating the mechanisms underlying these interactions, researchers can harness the beneficial properties of microalgae and their associated microbiota for environmental and biotechnological purposes. This study investigates *T. chui* culture and their associated microbiome to implement novel and efficient antioxidant enzymes.

Material and methods

Culture conditions of the microalgae *T. chui* including associated microorganisms

Single microalgae cultures of *T. chui* SAG 8–6 were cultivated at 21 °C with natural light intensity (14 h light period per day, 10 h dark period per day) in liquid F-medium, simulating its native environmental habitat to support optimal growth and metabolic activity (Guillard and Ryther 1962). Cultures were renewed in 2-month intervals by the inoculation of fresh medium.

Metagenome and total DNA isolation

Cells of a *T. chui* SAG 8–6 culture, including the associated microbial community, were used to prepare the metagenome

dataset. For this, 30 ml of the culture was centrifuged for 30 min at 5000 × g. The resulting pellet was resuspended in the Elution Buffer provided by NucleoBond High Molecular Weight Genomic DNA-Kit (MACHEREY-NAGEL, Düren, Germany). The microalgae suspension was shock-frozen in liquid nitrogen and, after thawing, pipetted on bashing beads. Forty-microlitre Buffer MG, 0.5 mg proteinase K, and 5 mg of lysozyme were added before it was bead-bashed on Vortex-Genie®2 (Scientific Industries, New York, NY, USA) four times for 1 min with breaks on ice for 30 s. After the addition of 600 ml Buffer MG, the suspension was incubated at 55 °C for 30 min in static conditions. DNA elution was performed according to the manufacturer’s instructions. Finally, DNA was eluted in 30 µl of deionised water. DNA concentration and purity were analysed using a NanoPhotometer® NP80 (IMPLEN, Westlake Village, CA, USA).

Sequencing and assembly

Library preparation and sequencing were performed at the Leibniz Institute of Virology (LIV, Hamburg). One nanogram of DNA was subjected to library preparation with the Nextera XT DNA Library Preparation Kit (Illumina, product number: FC-131–1096) according to the manufacturer’s instructions. Illumina short-read sequencing was done on a NextSeq 500 (Illumina, San Diego, CA; USA) sequencer (NextSeq 500/550 High Output Kit v2.5, 300 Cycles, product number: 20022408) with 2 × 151 bp (plus 2 × 8 bp Index reads). Demultiplexing with bcl2fastq (default settings) yielded 86.6 mio reads of the *T. chui* metagenome sample.

Sequence reads were processed with fastp (v0.21.0) to remove sequences originating from sequencing adapters (Chen et al. 2018). Processed reads shorter than 40 bp were discarded. The remaining reads were assembled using IBDA-UD (v1.1.3) (Peng et al. 2012).

Metagenomic dataset analyses and identification of novel antioxidants from *T. chui* microbiome

Critical features of antioxidant activity of *T. chui* microbiome were investigated using IMG function search. Data is shown in the total number of hits for possible antioxidant activity (Nordberg et al. 2014; Chen et al. 2019; Krohn et al. 2022). Genes were selected based on previous literature that investigated antioxidants such as SODs, rhodanese-related sulfurtransferase, CATs, peroxidase I, ferritin, glutaredoxin, glutathione peroxidase, cytochrome c peroxidase, alkylhydroperoxidase, deferrochelataase/peroxidase, and peroxiredoxin (Fones and Preston 2012; Buonvino et al. 2022; Ferdous and Yusof 2021; Matamoros et al. 2010; Lauritano et al. 2023).

Primers were designed from the reference gene in the metagenome for further cloning (Table 1). SignalP v.6.0

Table 1 Cloned antioxidant enzymes including function, length, primer design, IMG accession no., and phylogenetic assignment

Enzyme	Function	Length (aa)	Primer fw (restriction site)	Primer rv (restriction site)	Source	IMG accession no. (Ga0499797_)	NCBI nucleotide-blast (perc. identity)
TcJM_SOD2	Superoxide dismutase	199	CGCGGATCCATGGCT TTTGAACCTTCCCGAT (BamHI)	CCGCTCGAGCATGCG CGACGGACG (XhoI)	<i>T. chui</i> microbiome	000027_110175_110774	<i>Pacificitalea manganoxidans</i> (88.9)
TcIK_SOD3	Superoxide dismutase	200	CGCGGATCCATGGCT TTTGAACCTTCCCGAT (BamHI)	CCCAAGCTTGCT TGTCCAGCCTCAT (HindIII)	<i>T. chui</i> microbiome	000031_37060_37662	<i>Roseitalea porphyridii</i> (88.8)
TcJM_CAT2	Catalase	506	CGCGGATCCATGACA CGTCGCAAAGACAC (BamHI)	CCCAAGCTTGATTCC ACTGATACTCTCGGCT (HindIII)	<i>T. chui</i> microbiome	000030_56127_57647	<i>Pseudosulfobacter pseudodonzschiae</i> (99.6)
TcIK_CAT3	Catalase	484	CGCGGATCCATGACC AAGGACTCAGGA AAACC (BamHI)	CCGCTCGAGGCCTTC CCTGACGCC (XhoI)	<i>T. chui</i> microbiome	000173_13486_14940	<i>Roseovarius</i> sp. (87.6)

(Teufel et al. 2022) for N-terminal secretion signal prediction was conducted on the resulting amino sequence to exclude signal peptides from the final enzyme. In our study, we focus on intracellular antioxidant enzymes. Our sequenced-based analyses did not show any predicted signal peptide for all four characterised enzymes. Sequence-based protein structure predictions were performed using AlphaFold2 and visualised with UCSF Chimera v.1.17.3 (Pettersen et al. 2004; Jumper et al. 2021). The sequences of SODs were compared with the non-redundant protein database of NCBI by using BLASTP. The sequences of bacterial catalases and peroxidases were extracted from RedoxiBase (Savelli et al. 2019, <https://peroxibase.toulouse.inra.fr/>). The phylogenetic tree was constructed with MEGA11 (Tamura et al. 2021) based on the Neighbor-joining method and JTT matrix-based model (Jones et al. 1992) with 1000 bootstrap replications after multiple alignments with T-Coffee (Notredame et al. 2000).

Protein similarity network construction

ORFs in the metagenome of *T. chui* were annotated with Prodigal 2.6.3 in anonymous mode (Hyatt et al. 2010). The identified proteins were screened with hmmsearch 3.3.2 (hmmer.org) for the PFAM motifs PF00199 and PF06628 (Catalase), or PF00081 and PF02777 (Superoxide dismutase) using each motif's trusted cutoff as threshold. Domain-containing proteins were aligned to the NCBI nr database (as of May 2024) with diamond v2.1.9.163 in BLASTP mode for taxonomic classification (Buchfink et al. 2021). Finally, pairwise similarities of these proteins were derived from an all-vs-all alignment and used for network visualisation. Structure comparisons were performed using the Dali server with entries of the RCBS protein database (PDB) (Berman 2000; Holm 2020).

Cloning and purification of antioxidants

In order to express SOD candidates (TcJM_SOD2 and TcIK_SOD3) and CAT candidates (TcJM_CAT2 and TcIK_CAT) identified from the *T. chui* microbiome, gene fragments were amplified from the metagenomic DNA by PCR with the designed primers (Table 1). Two restriction sites at both ends of each PCR product were introduced by primers (Table 1, marked in bold). The restricted PCR fragment was ligated to the appropriate restricted and linearised vector pET21a(+) upstream of the His-tag sequence. After verification via sequencing, the final construct was heat-shock transformed into a chemically competent *Escherichia coli* Rosetta-gami 2(DE3) expression host. Overexpression was archived in autoinduction medium ZYM5052 (Studier 2005), including 100 $\mu\text{g}\cdot\text{ml}^{-1}$ ampicillin at 37 °C until an OD_{600 nm} of 0.6 was reached, followed by an overnight

cultivation at 22 °C. The enzymes were purified using Protono® Ni-NTA columns (Macherey–Nagel, Düren, Germany) following the protocol of polyhistidine-tagged proteins. Finally, the concentrated enzymes were rebuffed in 0.1 M Potassium-Phosphate Buffer (PPB) at pH 7 using Sartorius Vivaspin columns (Sartorius, Göttingen, Germany) and stored at 4 °C.

Superoxide dismutase activity assay

The SOD Determination Kit (19160; Sigma-Aldrich, St. Louis, MO, USA) was used to determine the activity of the cloned, expressed, and purified superoxide dismutases (Huang et al. 2000). The assay uses the reaction of tetrazolium salt, which is reduced by superoxide anions to form a water-soluble formazan dye. This reaction is controlled by a xanthine oxidase and inhibited by the tested SODs. A higher activity of a putative SOD results in a higher inhibition of the described reaction. The reaction took place at 37 °C for 20 min. The inhibition rate was quantified according to the absorption of the tetrazolium salt at 440 nm.

Initial assays were performed to detect suitable enzyme concentrations for activity measurements by conducting the assay with decreasing enzyme concentrations until reaching results within the prescribed OD limits according to the manufacture's protocol. Finally, 3000 $\text{ng}\cdot\text{ml}^{-1}$ of the enzyme stock in 0.1 M PPB pH 7 was tested in triplicates following the assay protocol. Simultaneously, tenfold higher and lower concentrations were tested as well. Assays with PPB served as control. The final assay volume was 240 μl with 20 μl of the enzyme stock. This resulted in the final tested enzyme assay concentrations of 2500 $\text{ng}\cdot\text{ml}^{-1}$, 250 $\text{ng}\cdot\text{ml}^{-1}$, and 25 $\text{ng}\cdot\text{ml}^{-1}$.

The results were tested for normal distribution using the Shapiro–Wilk test to ensure the data met the assumptions of parametric analysis (Shapiro and Wilk 1965). Subsequently, datasets following a normal distribution were compared using a two-tailed unpaired *t* test to evaluate differences between groups. Statistical significance was set at $p < 0.05$, and results are reported as mean \pm standard deviation (SD). Analyses were performed using software R, ensuring robust statistical evaluation (R Core Team 2020).

Catalase activity assay

Catalase activity was measured with the Catalase Colorimetric Activity Kit (EIACATC; Invitrogen, Carlsbad, CA, USA) (Croft et al. 2023). In this assay, horseradish peroxidase reacts with a provided substrate in the presence of H₂O₂, which creates a measurable colour shift of the colourimetry detection reagent. The reaction of the H₂O₂ with the tested catalases inhibits this colour shift and can be determined with absorption at 560 nm.

Inhibition increases proportionally with the enzyme activity of the tested catalase. The substrate processing step lasted for 15 min at 20 °C. The enzyme Unit (U) is given in $\mu\text{mol}\cdot\text{min}^{-1}$. The enzyme activity $\text{U}\cdot\text{ml}^{-1}$ defines the quantity of substrate which is degraded per volume of the tested enzyme per min. This assay provided a $100\text{ U}\cdot\text{ml}^{-1}$ bovine standard catalase to adjust the measured absorbance values at 560 nm to a resulting standard curve of $y = -0.0625x + 0.3963$ ($n = 18$).

First, preliminary tests with decreasing enzyme concentrations were conducted to identify appropriate enzyme concentrations for activity assessments to match the manufacture's specifications according to the protocol. Subsequently, triplicate experiments were performed using an enzyme stock concentration of $600\text{ ng}\cdot\text{ml}^{-1}$ in 0.1 M PPB at pH 7, following the established assay protocol. Additionally, concentrations ten times higher and lower were tested concurrently. Control assays were conducted using PPB. Twenty-five-microlitre enzyme stock was used in the final assay volume of 100 μl . Therefore, the final enzyme concentrations in the assay were $1500\text{ ng}\cdot\text{ml}^{-1}$, $150\text{ ng}\cdot\text{ml}^{-1}$, and $15\text{ ng}\cdot\text{ml}^{-1}$.

The resulting datasets were analysed and tested for normal distribution using R and compared with a two-tailed unpaired t test. The results are reported as mean \pm SD; statistical significance was set at $p < 0.05$.

Toxicology assays

All enzymes were tested on their general toxicology. The assay relies on injecting *Galleria mellonella* larvae with the enzyme (Maguire et al. 2016). Three different concentrations of the enzymes in 0.1 M PPB pH 7 were tested matching the same enzyme stock concentrations conducted and confirmed as being active in the enzyme activity assays in initial tests (TcJM_SOD2/TcIK_SOD3: $30,000\text{ ng}\cdot\text{ml}^{-1}$, $3,000\text{ ng}\cdot\text{ml}^{-1}$, $300\text{ ng}\cdot\text{ml}^{-1}$; TcJM_CAT2/TcIK_CAT3: $6,000\text{ ng}\cdot\text{ml}^{-1}$, $600\text{ ng}\cdot\text{ml}^{-1}$, $60\text{ ng}\cdot\text{ml}^{-1}$).

G. mellonella larvae were stored at 4 °C prior to the assay. For each enzyme and concentration, $3\cdot 10$ larvae received a 5 μl injection in the last pro-leg to apply the enzyme into the organism's haemocoel. Larvae with an injection with 0.1 M PPB pH 7 served as a control and were treated in the same way. Following the injection, ten larvae of each treatment were stored in a petri dish at 22 °C. Larvae were monitored and counted in 24-h intervals over 72 h. Linear models were calculated to determine the statistical significance of the influence of the enzyme on survival rates compared to the control group for each individual tested concentration in an F test.

Results

Metagenome screening shows highly interesting enzyme candidates for antioxidant activity

The metagenome of the *T. chui* enrichment culture microbiome (IMG ID Ga0499797) revealed 258 genes coding for proteins with putative antioxidant activity, according to the IMG gene classifications (Table 2). Metagenome analysis revealed the presence of various genes possibly responsible for the antioxidant activity, including SODs, rhodanese-related sulfurtransferase, CATs, peroxidase I, ferritin, glutaredoxin, glutathione peroxidase, cytochrome c peroxidase, alkylhydroperoxidase, deferrochelate/oxidase, and peroxidase. Most of those genes were assigned for peroxidase and glutaredoxin, with 53 and 51 genes, respectively. Further, nine superoxide dismutases and six catalases were identified. Phylogenetically, most of these genes are associated with *Alphaproteobacteria* and unidentified bacteria. A minor fraction of the assembled genes could be assigned to bacterial candidates from *Betaproteobacteria*, *Gammaproteobacteria*, *Actinobacteria*, *Cytophagia*, *Flavobacteria*, *Clostridia*, and eukaryotic genes from *Chlorophyta*. For further confirmation and enzyme implementation, we cloned, tested, and characterised four novel enzymes (Table 1). Two are assigned as superoxide dismutases (TcJM_SOD2; TcIK_SOD3), and two are catalases (TcJM_CAT2; TcIK_CAT3).

Within the *T. chui* microbiome metagenome, a protein sequence similarity network analysis revealed SODs of two different bacterial phyla (*Bacteroidota*, *Pseudomonadota*) (Fig. 1A, Table S1). One identified SOD was assigned to

Table 2 Potential number of hits with antioxidant activity of the *T. chui* microbiome metagenome according to IMG JGI function prediction (Metagenome IMG ID Ga0499797, date: 31.07.2023). Data shown in total number of hits per 50 Mb

Antioxidant activity	Number of hits
Superoxide dismutase	9
Cu/Zn superoxide dismutase	5
Rhodanese-related sulfurtransferase	42
Catalase (peroxidase I)	22
Catalase	6
Ferritin, oxidative damage protectant	7
Glutaredoxin	51
Glutathione peroxidase	18
Cytochrome c peroxidase	16
Alkylhydroperoxidase	28
deferrochelate/oxidase	1
Peroxiredoxin	53

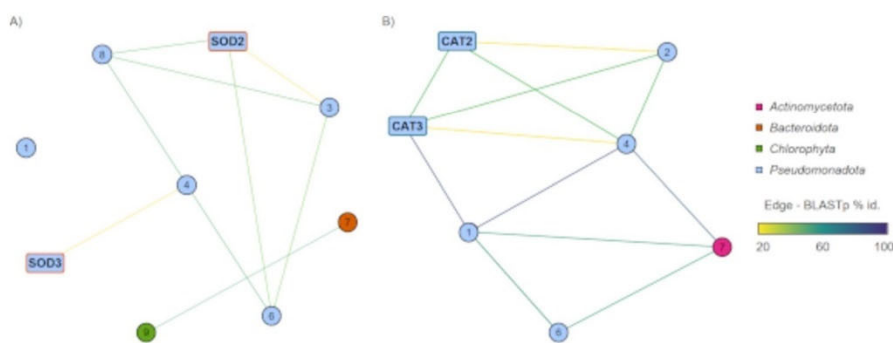


Fig. 1 Protein sequence similarity network of a *T. chui* microbiome metagenome (IMG ID Ga0499797) for antioxidants. Supporting data is displayed in Table S1. **A** Superoxide dismutase sequence network.

Highlighted sequences are characterised in this study (TcJM_SOD2; TcIK_SOD3). **B** Catalase sequence network. Highlighted sequences are characterised in this study (TcJM_CAT2; TcIK_CAT3)

Chlorophyta origin. However, most proteins were potentially synthesised by *Pseudomonadota* species.

The *T. chui* microbiome metagenome protein sequence similarity network for catalases, including the sequences for TcJM_CAT2 and TcIK_CAT3, identified enzymes of two bacterial phyla (Fig. 1B, Table S1). While one CAT originated from *Actinomycetota*, most identified CATs are assigned to *Pseudomonadota*. Two protein sequences from the metagenome acted as templates for the cloned proteins TcJM_CAT2 and TcIK_CAT3 and were identical to the cloned candidates. Interestingly, the network analysis revealed *Sphingorhabdus* sp. 109 to code for one of each enzyme classes of SOD and CAT, originating from the *T. chui* microbiome.

Phylogenetic identification and structural prediction

The phylogenetic identification of the SODs investigated in this study assigned them as Fe-SODs (Fig. 2A). The protein amino-sequences were assigned to *Roseovarius litoreus* (NCBI ID WP_149780105.1) and *Roseitalea* sp. isolate HXMU1422-4 (NCBI ID MBO6637894.1) (Yan et al. 2021) for TcJM_SOD2 and TcIK_SOD3, respectively. Both genes originated from marine α -*proteobacteria*. Further related Fe-SODs described in the phylogenetic analyses originated solely from *Pseudomonadota*, either α -*proteobacteria* or γ -*proteobacteria*. Nucleotide-blast results showed the highest similarity of both genes to the genes of α -*proteobacteria* species, strengthening the classification as *Pseudomonadota* (Table 1).

TcJM_SOD2 has 199 aa, one amino acid less than TcIK_SOD3 (Fig. 2B, Table 1). Fe-SODs commonly form protein homodimers or homotetramers with two chains acting as an active subunit (Alscher 2002). Our predicted structures presumably resembled one of those chains. The protein structure of both SODs is highly similar (root mean square

deviation of atomic positions (rmsd) over the full length: 1.6 Å) (Movie S1).

Our identified CATs from the *T. chui* microbiome metagenome are classed in clade 3 of heme-containing “monofunctional” catalases (Fig. 3A). The purified proteins showed a brown colour, which also indicates that these proteins might contain heme as the prosthetic group. The phylogenetic analyses of the protein showed the highest relation to *Saccharopolyspora erythraea*, an *Actinomycetota*, based on the database Redoxibase (Savelli et al. 2019). Nucleotide-based searches in NCBI (Camacho et al. 2023) revealed the highest similarity to the *Pseudomonadota* species *Pseudosulfobacter pseudonitzschiae* for TcJM_CAT2 and *Roseovarius* sp. for TcIK_CAT3. The rmsd value between both protein structures was 1.6 Å over the full length (Fig. 3B, Movie S2). CAT chains form tetramers but with each chain as an active subunit.

Activity assays for antioxidant candidates

After purifying the proteins, they were diluted in 0.1 M Potassium-Phosphate Buffer (PPB) at pH 7. Relative activity of TcJM_SOD2 and TcIK_SOD3 was determined by the catalyse of superoxide anions and the resulting inhibition of a reduction of a water-soluble tetrazolium salt (SOD Determination Kit (19,160; Sigma-Aldrich, St. Louis, Missouri, USA)).

Catalases react with hydrogen peroxide and decompose the molecule into water and oxygen. The enzyme activity of TcJM_CAT2 and TcIK_CAT3 was determined with a provided bovine catalase standard and is given in U*ml⁻¹; enzyme unit is defined as $\mu\text{mol}\cdot\text{min}^{-1}$ of substrate conversion. The Catalase Colorimetric Activity Kit (EIACATC; Invitrogen, Carlsbad, CA, USA) relies on the principle of inhibiting the reaction of hydrogen peroxide with a horseradish peroxidase and a provided substrate. All measurements were performed in triplicates.

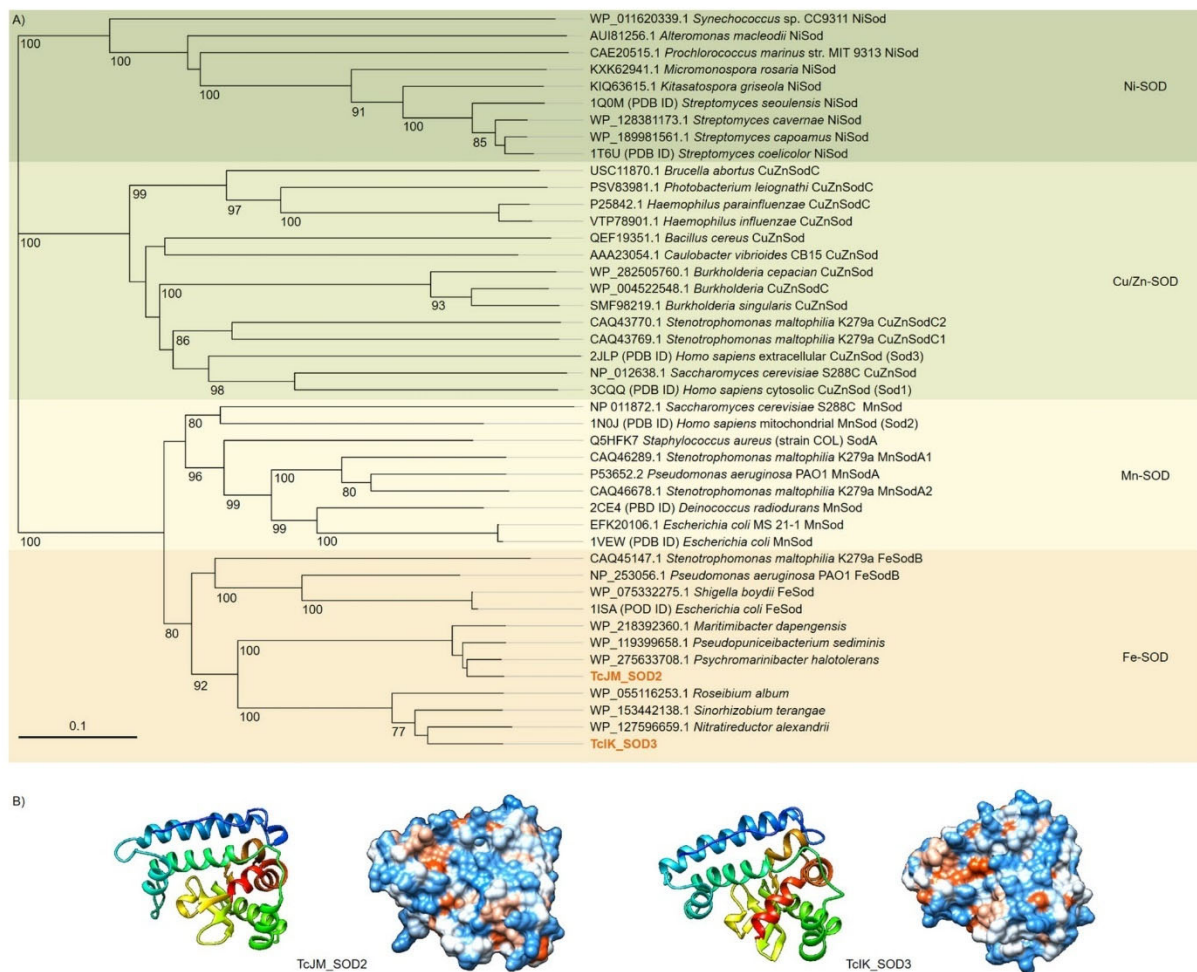


Fig. 2 Characterisation of superoxide dismutases (SODs) TcJM_SOD2 and TcIK_SOD3. **A** Phylogenetic tree of different types of superoxide dismutases (SODs). The sequences of SODs were compared with the non-redundant protein database of NCBI by using BLASTP, and several SOD candidates were chosen from PDB databases. The phylogenetic tree was constructed with MEGA11 based on the Neighbour-joining method and JTT matrix-based model with 1000 bootstrap replications after multiple alignments with T-Coffee (Jones et al. 1992; Notredame et al. 2000; Tamura et al. 2021). The

percentage of bootstrap resamplings ≥ 70 is indicated on the branches. The scale bar represents the expected number of changes per amino acid position. The types of SODs are classified according to Abreu and Cabelli (2010) and Karmakar et al. (2022). Two SODs, identified from our metagenome *T. chui*, are highlighted in orange. **B** Predicted protein structures or potential subunits of the antioxidants in ribbon and hydrophobic surface depiction. Predictions were modelled by AlphaFold2 and visualised in Chimera v1.17.3 (Pettersen et al. 2004; Jumper et al. 2021)

Superoxide dismutases

The conducted assays confirmed TcJM_SOD2 and TcIK_SOD3 as active superoxide dismutases (Fig. 4A). Through initial activity tests, the enzymes with the final assay concentrations of $2500 \text{ ng} \cdot \text{ml}^{-1}$, $250 \text{ ng} \cdot \text{ml}^{-1}$, and $25 \text{ ng} \cdot \text{ml}^{-1}$ were conducted in the assay. The final assay volume of $240 \mu\text{l}$ included $20 \mu\text{l}$ of the enzyme stock. TcJM_SOD2 showed higher activity compared to TcIK_SOD3 in each corresponding concentration and maximum at $2500 \text{ ng} \cdot \text{ml}^{-1}$ of an inhibition rate of $92.92 \pm 1.76\%$, while TcIK_SOD3

at the same concentration had a significant lower inhibition rate of $78.05 \pm 0.52\%$ ($p = 0.004$, $n = 6$). At the enzyme assay concentration of $250 \text{ ng} \cdot \text{ml}^{-1}$, TcIK_SOD3 has a significantly lower inhibition rate of $18.36 \pm 13.38\%$ compared to TcJM_SOD2 with $57.74 \pm 7.63\%$ ($p = 0.033$, $n = 6$). The average inhibition rate of the lowest tested concentrations is $< 10\%$ for both enzymes with no significant difference in activity ($p = 0.581$, $n = 6$). Additionally, the decrease in activity was more remarkable for TcIK_SOD3 than for TcJM_SOD2 with decreasing enzyme concentration. The average of the relative enzyme activity of $2500 \text{ ng} \cdot \text{ml}^{-1}$

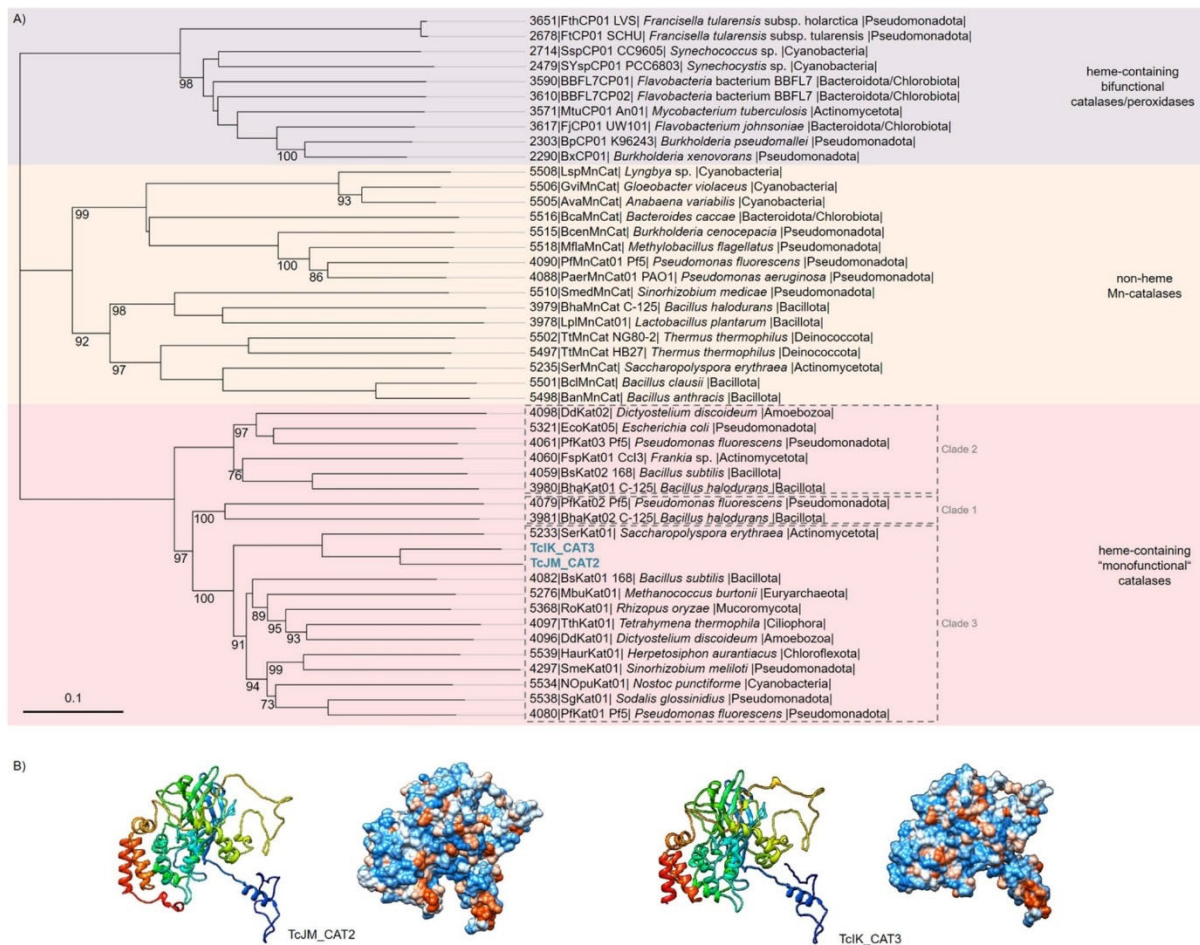


Fig. 3 Characterisation of catalases (CATs) TcJM_CAT2 and TcIK_CAT3. **A** Phylogenetic relationships of bacterial catalases and peroxidases sequences. The sequences of bacterial catalases and peroxidases were extracted from RedoxiBase. The phylogenetic tree was constructed with MEGA11 based on the Neighbour-joining method and JTT matrix-based model with 1000 bootstrap replications after multiple alignments with T-Coffee (Jones et al. 1992; Notredame et al. 2000; Tamura et al. 2021). The percentage of bootstrap resamplings ≥ 70 is indicated on the branches. The scale bar represents the expected number of changes per amino acid position. The types of catalases and peroxidases are classified according to Zamocky et al. (2008) and RedoxiBase (Zamocky et al. 2008;

Savelli et al. 2019). Two catalases (TcJM_CAT2 and TcIK_CAT3) identified from our metagenome *T. chui* are highlighted in blue. The ID numbers correspond to RedoxiBase nomenclature. Clade 1: 55–69 kDa subunit with heme *b*, found in alga, plants, and eubacteria. Clade 2: 75–84 kDa subunit with heme *d*, found in fungi and eubacteria. Clade 3: 43–75 kDa subunit with heme *b* and NADPH as redox-active cofactor, the most abundant subfamily found in bacteria, archaea, fungi, protists, animals, and plants. **B** Predicted protein structures or potential subunits of the antioxidants in ribbon and hydrophobic surface depiction. Predictions were modelled by AlphaFold2 and visualised in Chimera v1.17.3 (Pettersen et al. 2004; Jumper et al. 2021)

enzyme assay concentration of TcJM_SOD2 compared to 250 $\text{ng}\cdot\text{ml}^{-1}$ TcJM_SOD2 decreased significantly by 35.18% ($p=0.018$, $n=6$) and compared to 25 $\text{ng}\cdot\text{ml}^{-1}$ TcJM_SOD2 by 84.3% ($p=0.003$, $n=6$). Similarly, compared to the highest tested assay concentration of TcIK_SOD3, the average of the relative enzyme activity decreased by 59.69% ($p=0.024$, $n=6$) compared to 250 $\text{ng}\cdot\text{ml}^{-1}$ TcIK_SOD3 and 73.23% ($p<0.001$, $n=6$) compared to 25 $\text{ng}\cdot\text{ml}^{-1}$ TcIK_SOD3. Interestingly, the decrease in relative enzyme activity of TcIK_SOD3 between the two

lowest tested enzyme concentrations of 250 $\text{ng}\cdot\text{ml}^{-1}$ and 25 $\text{ng}\cdot\text{ml}^{-1}$ was not significant ($p=0.287$, $n=6$).

Catalases

Both purified enzymes TcJM_CAT2 and TcIK_CAT3 showed catalytic activities determined with the Catalase Colorimetric Activity Kit (EIACATC; Invitrogen, Carlsbad, CA, USA). The final assay volume was 100 μl , including 25 μl of the enzyme dilution. Each enzyme was tested

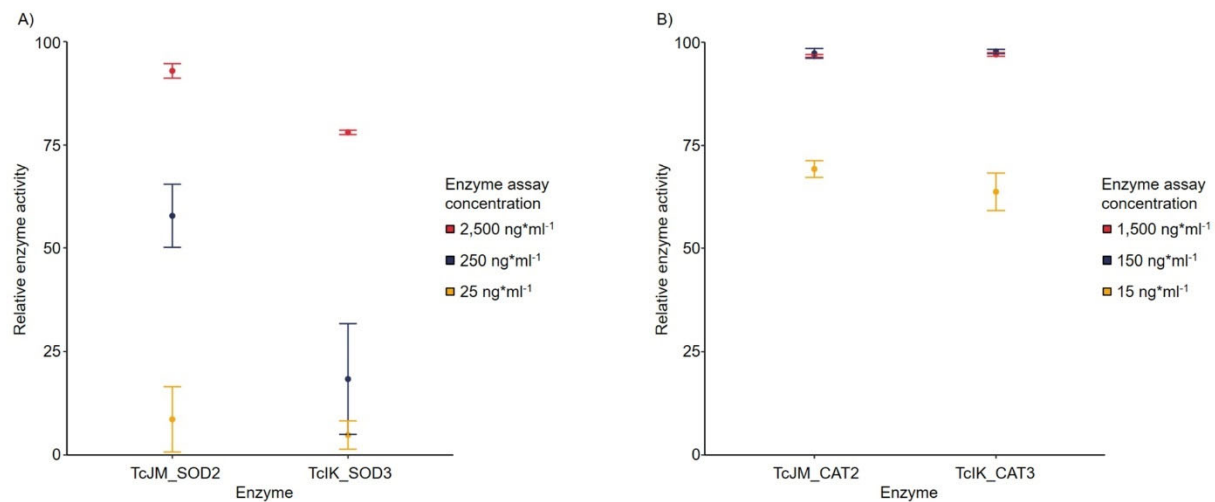


Fig. 4 Enzyme activity of two superoxide dismutases (TcJM_SOD2 and TcIK_SOD3) and two catalases (TcJM_CAT2 and TcIK_CAT3) from the *T. chui* microbiome metagenome. The enzyme activities were determined with enzyme-specific kits. The enzyme con-

centration refers to the concentration in the assay volume. Controls with 0.1 M pH 7 potassium phosphate buffer showed no activity. **A** Superoxide dismutase relative activity. **B** Catalase relative activity (100% = 5.96 U*ml⁻¹)

positive in a final assay concentration of 1500 ng*ml⁻¹, 150 ng*ml⁻¹, and 15 ng*ml⁻¹ in PPB (Fig. 4B). The two highest tested enzyme assay concentrations for both putative catalases showed similar activity values with no significant differences (1500 ng*ml⁻¹: $p=0.426$, $n=6$; 150 ng*ml⁻¹: $p=0.668$, $n=6$). The highest activity of 5.96 ± 0.03 U*ml⁻¹ was determined for TcIK_CAT3 at an assay concentration of 150 ng*ml⁻¹, and TcJM_CAT2 exhibits similar activity of 5.94 ± 0.07 U*ml⁻¹ at the same enzyme concentration level. The enzyme activity was reduced by 28.9–35.9% at the lowest tested concentration for both enzymes, again showing no significant differences between TcJM_CAT2 and TcIK_CAT3 ($p=0.226$, $n=6$). A comparison of the enzyme activity of the different tested enzyme assay concentrations showed similar activities with no significant differences between the two highest tested concentrations of both enzymes (TcJM_CAT2: $p=0.554$, $n=6$; TcIK_CAT3: $p=0.233$, $n=6$). However, the tested enzyme assay concentration of 15 ng*ml⁻¹ was significantly lower as for 1500 ng*ml⁻¹ for both enzymes (TcJM_CAT2: $p=0.002$, $n=6$; TcIK_CAT3: $p=0.009$, $n=6$).

Cell toxicity assay shows no influence on *Galleria mellonella* setup

In order to consider a possible biotechnological application of candidates, e.g. in health management sectors, compatibility with a *Galleria mellonella* setup has to be considered. Harmful effects of the injected enzyme candidates can be confirmed or excluded after a 72-h observation of the larvae (Maguire et al. 2016).

Superoxide dismutases

In the conducted assay, no evidence was found for TcJM_SOD2 and TcIK_SOD3 to significantly improve toxic effects compared to the control (Fig. 5A). All tested setups show a normal death rates compared to the control group of *G. mellonella*.

The highest decrease in the survival rate was found in the *G. mellonella* setup with 5 μ l 30,000 ng*ml⁻¹ TcIK_SOD3 injection, leading to 6.67 ± 0.58 alive individuals after 72 h. The control group decreased to 7.25 ± 1.71 surviving individuals after 72 h. All other tested enzyme concentrations showed higher survival rates. The highest success was in the highest tested concentration of TcJM_SOD2, where after 72 h, 8.67 ± 1.15 individuals were alive. Overall, TcJM_SOD2 had higher survival rates compared to TcIK_SOD3 in the *G. mellonella* assay. The linear models of each tested concentration's survival rates did not differ significantly from the control group (Table S2).

Catalases

The conducted approach found no significant toxic effects for TcJM_CAT2 and TcIK_CAT3 compared to controls (Fig. 5B). The number of living individuals declined in all tested setups over 72 h. However, linear models revealed no significant differences in the mortality between individuals treated with the enzyme in different concentrations and individuals treated with PPB (Table S2).

The highest number of surviving *G. mellonella* after 72 h injected with one of the CATs was found for TcJM_CAT2

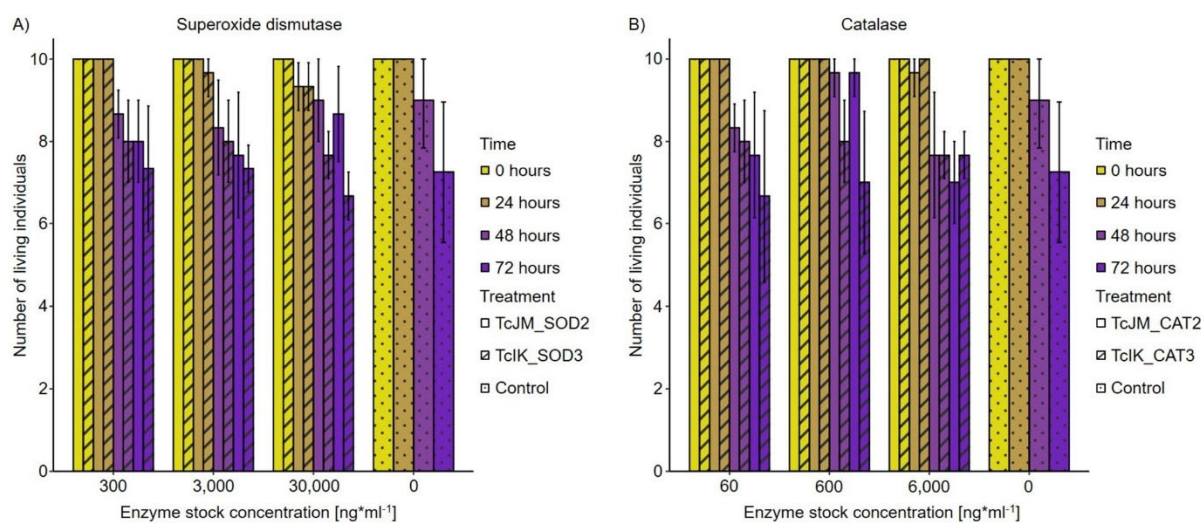


Fig. 5 Toxicologic effects of two catalases and two superoxide dismutases from the *T. chui* microbiome metagenome based on the injection of the enzymes in *Galleria mellonella* larvae. Surviving rates are displayed compared to the control (0.1 M potassium phosphate buffer, pH 7). Calculated linear models showed no significant

differences between the injected samples and the control (Table S2). **A** Toxicologic effects of superoxide dismutases TcJM_SOD2 and TcIK_SOD3. **B** Toxicologic effects of catalases TcJM_CAT2 and TcIK_CAT3

at an enzyme stock concentration of $600 \text{ ng} \cdot \text{ml}^{-1}$ with approximately 9.67 ± 0.58 (maximum 10). In contrast, an injection with $5 \mu\text{l}$ of $60 \text{ ng} \cdot \text{ml}^{-1}$ TcIK_CAT3 led to the highest decrease in surviving larvae after 72 h of 6.67 ± 2.08 . However, the linear model of the control group (7.25 ± 1.71 surviving individuals after 72 h) did not hint at toxic effects caused by the treatments with both CATs in any tested concentration.

Discussion

Microalgae and their associated microbiome offer a variety of valuable biomolecules (Krohn et al. 2022). So far, several studies found their benefits for the health and cosmetic sector and nutraceutical applications (Corinaldesi et al. 2017; Boddu and Divakar 2018). Furthermore, biotechnology tools derived from marine and algae microbiome metagenomes play essential roles in several industries (Kennedy et al. 2010; Kamble and Vavilala 2018). A microbial metagenome derived from *T. chui* cultures lays the foundation of the present study. The functional significance of the identified enzymes, particularly from microalgae and their microbiome, lies in their potential roles in oxidative stress management and their broader applications in biotechnology and medicine. Antioxidant enzymes such as superoxide dismutases and catalases are crucial in protecting cells from reactive oxygen species damage, a function that is conserved across various organisms. This

has implications for applications in therapeutic treatments, industrial biocatalysis, and environmental protection. Our successful implementation of two superoxide dismutases and two catalases underscores the potential of algae microbiomes to benefit the health and cosmetic sector. In our testing methods, all enzymes showed an efficient substrate processing rate even at low enzyme concentrations and are not harmful to the used model organism *G. mellonella*. Precisely, we found two functional Fe-SODs and two functional heme-containing “monofunctional” catalases.

During the aerobic metabolism processes such as cellular respiration, reactive oxygen species (ROS) are formed, which causes oxidative stress (Collin 2019). This stress causes damage to several biomolecules and cells. As a result, these imbalanced conditions lead to an increased potential to develop life-limiting illnesses, especially diabetes, inflammatory diseases, and cancer for humans (Pashkow 2011; Prasad et al. 2018). The treatment with antioxidant medicine is mandatory to target those systemic diseases and stabilise the ROS concentration and human metabolism.

Antioxidants are found in all phylogenetic taxa. However, the proteins in this study are derived from bacteria. Prominent antioxidants are superoxide dismutases and catalases. These enzymes are linked as the product of the SOD reaction is the product of the catalase. In detail, the reaction of SOD with two superoxide ($\text{O}_2^{\cdot -}$) and two hydrons (H^+) results in the release of molecular oxygen (O_2) and hydrogen peroxide (H_2O_2) (Fig. 6A). As H_2O_2 is highly toxic, this reactive

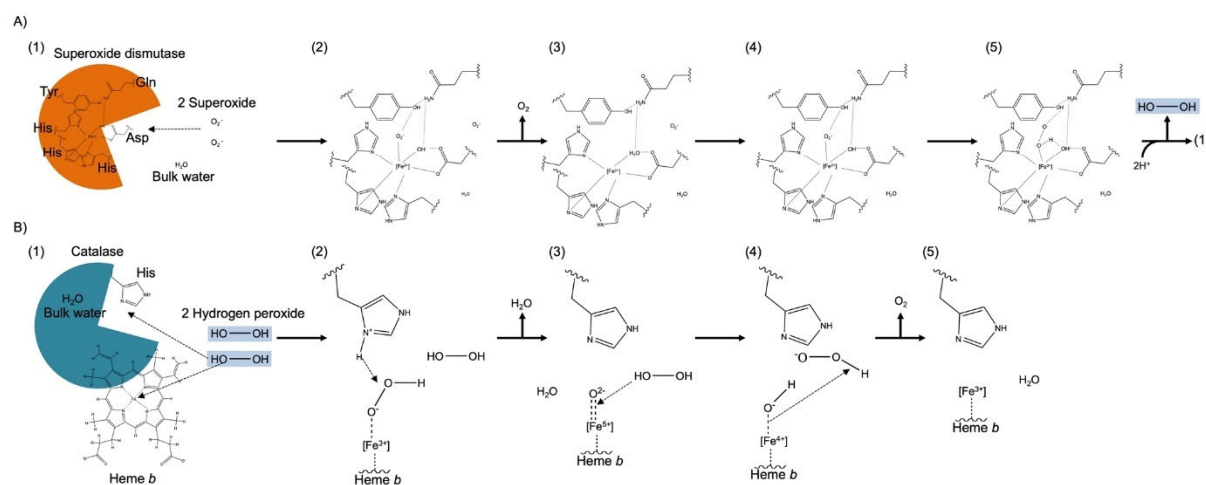


Fig. 6 Schematic mechanism of iron-superoxide dismutases and heme-containing “monofunctional” catalases (Miller 2003; Alfonso-Prieto et al. 2009; Vlasits et al. 2010; Sheng et al. 2014). **A** Fe-Superoxide dismutase reacts with two superoxide molecules, producing O₂ and H₂O₂. (1) Superoxide dismutase with an active site containing Fe³⁺ which is held in place by amino acid residues and water. (2) One O₂⁻ is orientated by the Fe³⁺ molecule and the tyrosine. (3) The O₂⁻ is oxidised to O₂ and released while the iron is now reduced to the Fe²⁺ state. (4) Another O₂⁻ enters the reaction and binds to the hydrogen of tyrosine and the Fe²⁺-water complex. (5) Reorientation of hydrogen results in a positively charged oxygen of the water. Next, the iron changes to the more stable Fe³⁺ state by donating an electron to the oxygen. Finally, the negatively charged oxygen in the water

donates one hydrogen to the O₂⁻ which results in the formation and release of H₂O₂ in the presence of H⁺ ions. The active site is reset to (1). **B** Catalases catalyse the reaction of two hydrogen peroxide molecules to two H₂O and one O₂. (1) Catalase subunit chain of a tetramer with heme *b* and histidine in the active site reacts with two H₂O₂ (products of SOD catalyse). (2) Deprotonation of H₂O₂ by the histidine results in an electrostatic interaction the heme B-Fe³⁺ and the HO₂⁻. In the following, the OH⁻ subtracts the hydrogen of the histidine and forms H₂O as the first product. (3) The split-off oxygen is in a coordinated covalent bond to the heme *b* iron. The second H₂O₂ reacts through a homolytic bond cleavage with the heme *b*-oxygen and forms a chelated HO⁻. (4) A homolytic bond cleavage sets the Fe⁴⁺ to Fe³⁺ which results in the formation of O₂ and H₂O

oxidant has to be processed further. For this, the catalase reacts with 2 H₂O₂ to produce O₂ and 2 H₂O (Fig. 6B).

Biotechnological production of SODs is archived through bacterial enrichment systems (Taniguchi et al. 1989; Benov et al. 1996). In this study, we successfully used an *E. coli* Rosetta-gami 2(DE3) expression host in combination with a pET21a(+) vector to implement 2 Fe-SODs of bacterial origin, e.g. TcJM_SOD2 and TcIK_SOD3 from *Pseudomonadota* species. Both showed detectable substrate activity in enzyme assay concentrations of 25 ng*ml⁻¹ with TcJM_SOD2 showing significantly higher activity rates in higher enzyme concentrations than TcIK_SOD3. This was determined by the inhibition of a reaction of tetrazolium salt with superoxide anions. The conducted method offers results for the relative activity and underlines the potential of SOD activity from algae microbiomes in general. Structural comparisons of both identified SODs to PDB show the closest relation of TcJM_SOD2 to crystal structure of an iron/manganese cambialistic Superoxide Dismutase from *Rhodobacter capsulatus* (7azq, <https://doi.org/https://doi.org/10.2210/pdb7AZQ/pdb>, Entry Authors: Ponce-Salvatierra, A., Hermoso, J.A., 2021) (Berman 2000). Simultaneously, TcIK_SOD3 showed the highest structural similarity to a “Crystal structure of the iron superoxide dismutase from

Acinetobacter sp. Ver3” (7sbh, <https://doi.org/https://doi.org/10.2210/pdb7SBH/pdb>) (Steimbrüch et al. 2022). Both known structures have an active site made up of an iron atom oriented by three histidine and an aspartic acid residue. A tyrosine and a glutamine residue are also involved in the cleavage of the superoxide. TcJM_SOD2 and TcIK_SOD3 exhibit these residues in similar orientations; therefore, the reaction mechanism is assumed to be similar. Future investigations are needed to confirm this mechanism and to investigate differences in activity. Several previous studies investigated potential applications of SODs and CATs, and the general antioxidant activity of various bacteria and environment origin and the influences on expression (Franzon et al. 1990; Wood and Jørgensen 2001; Díaz-Rosales et al. 2006; Gravina et al. 2017).

This study focusses on the general activity of antioxidants derived from microalgae microbiomes and confirms their potential. By the use of metagenomic approaches and datasets, we were able to screen microbiomes for specialised biomolecules and to identify and compare several SODs and CATs (Fig. 1, Table S1).

Catalases are the most efficient proteins in substrate processing (Sepasi Tehrani and Moosavi-Movahedi 2018). In our case, the investigated catalases show measurable

activity rates in picogram scales of $4.22 \pm 0.12 \text{ U} \cdot \text{ml}^{-1}$ for TcJM_CAT2 and $3.88 \pm 0.28 \text{ U} \cdot \text{ml}^{-1}$ for TcIK_CAT3 at the lowest tested assay concentration of $15 \text{ ng} \cdot \text{ml}^{-1}$ (Fig. 4). Structure comparisons of TcJM_CAT2 with previously described CATs revealed a “highdose liganded bacterial Catalase” (PDB entry: 4b7h, <https://doi.org/https://doi.org/10.2210/pdb4b7h/pdb>) (Candelaresi et al. 2013). For TcIK_CAT3, the structural closest PDB entry is a “Atomic resolution structure of *Micrococcus lysodeikticus* Catalase” (PDB entry: 1gwe, <https://doi.org/https://doi.org/10.2210/pdb1gwe/pdb>) (Murshudov et al. 2002). These catalases contain a heme *b* in their active site, along with a significantly placed tyrosine residue. Another characteristic is a α/β -barrel within the structure. These traits as well as the similarity of TcJM_CAT2 and TcIK_CAT3 are presumably the reason for the similar activity rates. To target this assumption, further research has to be conducted in the future, regarding the crystal structure and mechanism of the novel, identified CATs.

The enzyme activity decreased with lower assay concentrations for all identified SODs and CATs in this study. This behaviour can be attributed to the linear relationship between enzyme assay concentration and enzyme activity, as well as the relationship between substrate concentration and enzyme activity (Michaelis et al. 2011). Additionally, the assay’s sensitivity to enzyme concentrations affects the detectability of enzymatic activity, influencing the results for both maximum and minimum activity levels (Bisswanger 2014).

The results of the toxicologic tests of all four antioxidants of this study do not hint at lethal or harmful effects when tested against *G. mellonella* larvae (Fig. 5, Table S2). The tested organisms showed no increased mortality after the treatment with TcJM_SOD2, TcIK_SOD3, TcJM_CAT2, and TcIK_CAT3. Statistically, there are no differences in the survival rates of tested invertebrates treated with the enzymes compared to control organisms. These outcomes suggest extended future studies with the aim of the application of the SODs and CATs on humans and their benefits to human healthcare.

Our results apply to single algae species cultures of *T. chui* in culture bottles, with several culturing characteristics and challenges. Studies have shown that bottle conditions influence the microbiome in species composition gene translate enzymatic activities. This impact on the microbiome is caused by the bottle effect (Hammes et al. 2010). The current advancements in large-scale cultivation of *T. chui* and ongoing research on optimising biomass processing suggest increased future applications and improved yield (Moser et al. 2022; Sørensen et al. 2023; Garcia et al. 2024; Simon et al. 2024). As a result, novel insights into its development and the factors influencing

the microbiome may emerge in the future. Cultivation approaches can also be improved by this study as well as future research focussing on the microbiome of *T. chui*.

The metagenome results and the variations in antioxidants would presumably differ in natural conditions. Nevertheless, our results support the potential of the described microbial community as a source of putative, efficient antioxidants. Furthermore, future and present applications of those algae in large-scale farming approaches also underlie artificial conditions. Directed optimisation for different applications can be archived by altering the culture conditions. Aside from *T. chui*, several microalgae species in large-scale farms are already well established, e.g. *Nannochloropsis salina* and *Chlorella vulgaris* (Cai et al. 2013; Blair et al. 2014). As those cultivation processes are optimised and well-studied, we conclude another benefit of an extended use of microalgae as a source of antioxidants. The conducted techniques of this study can be applied to several microalgae cultures in the future. Moreover, previous studies focussed on the implementation of biotechnological technics to increase the yield and activity of SODs. One method involves conjugating antioxidants with various structures and carriers, such as polyethylene glycol, chondroitin sulfate, or aldehyde dextrans. (Eremin et al. 1996; Veronese et al. 2002; Maksimenko et al. 2010). Those described technics applied to our SODs can lead to an increase in efficiency in substrate processing. By combining these techniques with our conducted applications, additional identified antioxidants can be cloned and tested to incorporate more enzymes with improved substrate efficiency in future studies.

Supplementary Information The online version contains supplementary material available at <https://doi.org/10.1007/s00253-024-13395-w>.

Author contribution JFHM, YH, and IK contributed to the experimental design and writing of this work. LB and SL worked on the algae culturing and metagenome preparation. YKHS and JHA provided data on general antioxidant activity. MA, PD, and MG worked on bioinformatics regarding the metagenome annotation and analysis. YH and YA contributed to the bioinformatics of candidates, as well as JFHM on statistics and data analyses. YH and JFHM executed the lab work of cloning and enzyme purification, characterisation, and activity assays. JHA and IK were involved in general project supervision and acquisition of funding. All authors contributed to manuscript revision, and read and approved the submitted version.

Funding Open Access funding enabled and organized by Projekt DEAL. This work was in part supported by the AquaHealth FKZ 031B0945C and SuReMetS FKZ 031B0944A. In addition, we acknowledge financial support from the Open Access Publication Fund of Universität Hamburg.

Data availability Sequence data have been submitted to the European Nucleotide Archive (ENA). They are publicly available under accession PRJEB77869. Metagenome data is available under IMG ID Ga0499797.

Declarations

Ethical approval The manuscript presents research on *Galleria mellonella* that do not require ethical approval for their study.

Conflict of interest The authors declare no competing interests.

Open Access This article is licensed under a Creative Commons Attribution 4.0 International License, which permits use, sharing, adaptation, distribution and reproduction in any medium or format, as long as you give appropriate credit to the original author(s) and the source, provide a link to the Creative Commons licence, and indicate if changes were made. The images or other third party material in this article are included in the article's Creative Commons licence, unless indicated otherwise in a credit line to the material. If material is not included in the article's Creative Commons licence and your intended use is not permitted by statutory regulation or exceeds the permitted use, you will need to obtain permission directly from the copyright holder. To view a copy of this licence, visit <http://creativecommons.org/licenses/by/4.0/>.

References

- Abreu IA, Cabelli DE (2010) Superoxide dismutases—a review of the metal-associated mechanistic variations. *Biochim Biophys Acta* 1804:263–274. <https://doi.org/10.1016/j.bbapap.2009.11.005>
- Alfonso-Prieto M, Biarnés X, Vidossich P, Rovira C (2009) The molecular mechanism of the catalase reaction. *J Am Chem Soc* 131:11751–11761. <https://doi.org/10.1021/ja9018572>
- Alscher RG (2002) Role of superoxide dismutases (SODs) in controlling oxidative stress in plants. *J Exp Bot* 53:1331–1341. <https://doi.org/10.1093/jxb/53.372.1331>
- Bankevich A, Nurk S, Antipov D, Gurevich AA, Dvorkin M, Kulikov AS, Lesin VM, Nikolenko SI, Pham S, Prjibelski AD, Pyshkin AV, Sirotkin AV, Vyahhi N, Tesler G, Alekseyev MA, Pevzner PA (2012) SPAdes: a new genome assembly algorithm and its applications to single-cell sequencing. *J Comput Biol J Comput Mol Cell Biol* 19:455–477. <https://doi.org/10.1089/cmb.2012.0021>
- Benov LT, Beyer WF, Stevens RD, Fridovich I (1996) Purification and characterization of the Cu, Zn SOD from *Escherichia coli*. *Free Radic Biol Med* 21:117–121. [https://doi.org/10.1016/0891-5849\(95\)02217-1](https://doi.org/10.1016/0891-5849(95)02217-1)
- Berman HM (2000) The Protein Data Bank. *Nucleic Acids Res* 28:235–242. <https://doi.org/10.1093/nar/28.1.235>
- Bisswanger H (2014) Enzyme Assays. *Perspect Sci* 1:41–55. <https://doi.org/10.1016/j.pisc.2014.02.005>
- Blair MF, Kokabian B, Gude VG (2014) Light and growth medium effect on *Chlorella vulgaris* biomass production. *J Environ Chem Eng* 2:665–674. <https://doi.org/10.1016/j.jece.2013.11.005>
- Boddu RS, Divakar K (2018) Metagenomic insights into environmental microbiome and their application in food/pharmaceutical industry. In: Patra JK, Das G, Shin H-S (eds) *Microbial biotechnology*. Springer Singapore, Singapore, pp 23–38
- Buchfink B, Reuter K, Drost H-G (2021) Sensitive protein alignments at tree-of-life scale using DIAMOND. *Nat Methods* 18:366–368. <https://doi.org/10.1038/s41592-021-01101-x>
- Buonvino S, Arciero I, Melino S (2022) Thiosulfate-cyanide sulfur-transferase a mitochondrial essential enzyme: from cell metabolism to the biotechnological applications. *Int J Mol Sci* 23:8452. <https://doi.org/10.3390/ijms23158452>
- Cai T, Park SY, Racharaks R, Li Y (2013) Cultivation of *Nannochloropsis salina* using anaerobic digestion effluent as a nutrient source for biofuel production. *Appl Energy* 108:486–492. <https://doi.org/10.1016/j.apenergy.2013.03.056>
- Camacho C, Boratyn GM, Joukov V, Vera Alvarez R, Madden TL (2023) ElasticBLAST: accelerating sequence search via cloud computing. *BMC Bioinformatics* 24:117. <https://doi.org/10.1186/s12859-023-05245-9>
- Candelaresi M, Gumiero A, Adamczyk K, Robb K, Bellota-Antón C, Sangal V, Munnoch J, Greetham GM, Towrie M, Hoskisson PA, Parker AW, Tucker NP, Walsh MA, Hunt NT (2013) A structural and dynamic investigation of the inhibition of catalase by nitric oxide. *Org Biomol Chem* 11:7778. <https://doi.org/10.1039/c3ob41977k>
- Cerezuela R, Guardiola FA, González P, Meseguer J, Esteban MÁ (2012) Effects of dietary *Bacillus subtilis*, *Tetraselmis chuii*, and *Phaeodactylum tricornutum*, singularly or in combination, on the immune response and disease resistance of sea bream (*Sparus aurata* L.). *Fish Shellfish Immunol* 33:342–349. <https://doi.org/10.1016/j.fsi.2012.05.004>
- Chelikani P, Fita I, Loewen PC (2004) Diversity of structures and properties among catalases. *Cell Mol Life Sci CMLS* 61:192–208. <https://doi.org/10.1007/s00018-003-3206-5>
- Chen I-MA, Chu K, Palaniappan K, Pillay M, Ratner A, Huang J, Huntemann M, Varghese N, White JR, Seshadri R, Smirnova T, Kirton E, Jungbluth SP, Woyke T, Eloë-Fadrosh EA, Ivanova NN, Kyrpidis NC (2019) IMG/M vol 5.0: an integrated data management and comparative analysis system for microbial genomes and microbiomes. *Nucleic Acids Res* 47:D666–D677. <https://doi.org/10.1093/nar/gky901>
- Chen S, Zhou Y, Chen Y, Gu J (2018) fastp: an ultra-fast all-in-one FASTQ preprocessor. *Bioinforma Oxf Engl* 34:i884–i890. <https://doi.org/10.1093/bioinformatics/bty560>
- Cirri E, Pohnert G (2019) Algae-bacteria interactions that balance the planktonic microbiome. *New Phytol* 223:100–106. <https://doi.org/10.1111/nph.15765>
- Coleman B, Van Poucke C, De Witte B, Casciaro V, Moerdijk-Poortvliet T, Muylaert K, Robbens J (2023) Fine-tuning the flavor of *Tetraselmis chuii* by modifying nitrogen supply. *Algal Res* 74:103208. <https://doi.org/10.1016/j.algal.2023.103208>
- Collin F (2019) Chemical basis of reactive oxygen species reactivity and involvement in neurodegenerative diseases. *Int J Mol Sci* 20:2407. <https://doi.org/10.3390/ijms20102407>
- Corinaldesi C, Barone G, Marcellini F, Dell'Anno A, Danovaro R (2017) Marine microbial-derived molecules and their potential use in cosmeceutical and cosmetic products. *Mar Drugs* 15:118. <https://doi.org/10.3390/md15040118>
- Croft AJ, Kelly C, Chen D, Haw TJ, Sverdlov AL, Ngo DTM (2023) Overexpression of mitochondrial catalase within adipose tissue does not confer systemic metabolic protection against diet-induced obesity. *Antioxidants* 12:1137. <https://doi.org/10.3390/antiox12051137>
- Day JG, Fenwick C (1993) Cryopreservation of members of the genus *Tetraselmis* used in aquaculture. *Aquaculture* 118:151–160. [https://doi.org/10.1016/0044-8486\(93\)90288-A](https://doi.org/10.1016/0044-8486(93)90288-A)
- Díaz-Rosales P, Chabrillón M, Arijo S, Martínez-Manzanares E, Moriñigo MA, Balebona MC (2006) Superoxide dismutase and catalase activities in *Photobacterium damsela* ssp. *piscicida*. *J Fish Dis* 29:355–364. <https://doi.org/10.1111/j.1365-2761.2006.00726.x>
- Eremin AN, Litvinchuk AV, Metelitsa DI (1996) Operational stability of catalase and its conjugates with aldehyde dextrans and superoxide dismutase. *Biokhimiia Mosc Russ* 61:664–679
- Ferdous UT, Yusof ZNB (2021) Medicinal prospects of antioxidants from algal sources in cancer therapy. *Front Pharmacol* 12:593116. <https://doi.org/10.3389/fphar.2021.593116>

- Fones H, Preston GM (2012) Reactive oxygen and oxidative stress tolerance in plant pathogenic *Pseudomonas*. *FEMS Microbiol Lett* 327:1–8. <https://doi.org/10.1111/j.1574-6968.2011.02449.x>
- Franzon VL, Arondel J, Sansonetti PJ (1990) Contribution of superoxide dismutase and catalase activities to *Shigella flexneri* pathogenesis. *Infect Immun* 58:529–535. <https://doi.org/10.1128/iai.58.2.529-535.1990>
- Garcia MP, Regueiras A, Lopes G, Matos G, Da Silva LP, Cerqueira MT, Cardoso H, Correia N, Saraiva JA, Silva JL, Martins R, Marques AP (2024) Nonthermal high-pressure microalgae extracts: a new source of natural ingredients for cosmetics. *Algal Res* 81:103591. <https://doi.org/10.1016/j.algal.2024.103591>
- Gravina F, Dobrzanski T, Olchanheski LR, Galvão CW, Reche PM, Pileggi SA, Azevedo RA, Sadowsky MJ, Pileggi M (2017) Metabolic Interference of sod gene mutations on catalase activity in *Escherichia coli* exposed to Gramoxone® (paraquat) herbicide. *Ecotoxicol Environ Saf* 139:89–96. <https://doi.org/10.1016/j.ecoenv.2017.01.027>
- Grierson S, Strezov V, Shah P (2011) Properties of oil and char derived from slow pyrolysis of *Tetraselmis chui*. *Bioresour Technol* 102:8232–8240. <https://doi.org/10.1016/j.biortech.2011.06.010>
- Guillard RR, Ryther JH (1962) Studies of marine planktonic diatoms. I. *Cyclotella nana* Hustedt, and *Detonula confervacea* (Cleve) Grun. *Can J Microbiol* 8:229–239. <https://doi.org/10.1139/m62-029>
- Hammes F, Vital M, Egli T (2010) Critical evaluation of the volumetric “bottle effect” on microbial batch growth. *Appl Environ Microbiol* 76:1278–1281. <https://doi.org/10.1128/AEM.01914-09>
- Holm L (2020) DALI and the persistence of protein shape. *Protein Sci* 29:128–140. <https://doi.org/10.1002/pro.3749>
- Huang P, Feng L, Oldham EA, Keating MJ, Plunkett W (2000) Superoxide dismutase as a target for the selective killing of cancer cells. *Nature* 407:390–395. <https://doi.org/10.1038/35030140>
- Hyatt D, Chen G-L, LoCascio PF, Land ML, Larimer FW, Hauser LJ (2010) Prodigal: prokaryotic gene recognition and translation initiation site identification. *BMC Bioinformatics* 11:119. <https://doi.org/10.1186/1471-2105-11-119>
- Jones DT, Taylor WR, Thornton JM (1992) The rapid generation of mutation data matrices from protein sequences. *Comput Appl Biosci* 8:275–282. <https://doi.org/10.1093/bioinformatics/8.3.275>
- Jumper J, Evans R, Pritzel A, Green T, Figurnov M, Ronneberger O, Tunyasuvunakool K, Bates R, Židek A, Potapenko A, Bridgland A, Meyer C, Kohl SAA, Ballard AJ, Cowie A, Romera-Paredes B, Nikolov S, Jain R, Adler J, Back T, Petersen S, Reiman D, Clancy E, Zielinski M, Steinegger M, Pacholska M, Berghammer T, Bodenstein S, Silver D, Vinyals O, Senior AW, Kavukcuoglu K, Kohli P, Hassabis D (2021) Highly accurate protein structure prediction with AlphaFold. *Nature* 596:583–589. <https://doi.org/10.1038/s41586-021-03819-2>
- Kamble P, Vavilala SL (2018) Discovering novel enzymes from marine ecosystems: a metagenomic approach. *Bot Mar* 61:161–175. <https://doi.org/10.1515/bot-2017-0075>
- Karmakar A, Das AK, Ghosh N, Sil PC (2022) Superoxide dismutase. In: *Antioxidants effects in health*. Elsevier, pp 139–166
- Kennedy J, Flemer B, Jackson SA, Lejon DPH, Morrissey JP, O’Gara F, Dobson ADW (2010) Marine metagenomics: new tools for the study and exploitation of marine microbial metabolism. *Mar Drugs* 8:608–628. <https://doi.org/10.3390/md8030608>
- Khatoun H, Haris H, Rahman NA, Zakaria MN, Begum H, Mian S (2018) Growth, proximate composition and pigment production of *Tetraselmis chui* cultured with aquaculture wastewater. *J Ocean Univ China* 17:641–646. <https://doi.org/10.1007/s11802-018-3428-7>
- Klotz MG (2003) The molecular evolution of catalytic hydroperoxidases: evidence for multiple lateral transfer of genes between prokaryota and from bacteria into eukaryota. *Mol Biol Evol* 20:1098–1112. <https://doi.org/10.1093/molbev/msg129>
- Krohn I, Menanteau-Ledouble S, Hageskal G, Astafyeva Y, Jouannais P, Nielsen JL, Pizzol M, Wentzel A, Streit WR (2022) Health benefits of microalgae and their microbiomes. *Microb Biotechnol* 15:1966–1983. <https://doi.org/10.1111/1751-7915.14082>
- Lauritano C, Montuori E, De Falco G, Carrella S (2023) In silico methodologies to improve antioxidants’ characterization from marine organisms. *Antioxidants* 12:710. <https://doi.org/10.3390/antiox12030710>
- Lopes D, Rey F, Gomes A, Duarte L, Pereira J, Pinho M, Melo T, Domingues R (2024) Tracing the impact of domestic storage conditions on antioxidant activity and lipid profiles in the edible microalgae *Chlorella vulgaris* and *Tetraselmis chui*. *Mar Drugs* 22:254. <https://doi.org/10.3390/md22060254>
- Lu L, Wang J, Yang G, Zhu B, Pan K (2017) Biomass and nutrient productivities of *Tetraselmis chui* under mixotrophic culture conditions with various C: N ratios. *Chin J Oceanol Limnol* 35:303–312. <https://doi.org/10.1007/s00343-016-5299-3>
- Maguire R, Duggan O, Kavanagh K (2016) Evaluation of *Galleria mellonella* larvae as an in vivo model for assessing the relative toxicity of food preservative agents. *Cell Biol Toxicol* 32:209–216. <https://doi.org/10.1007/s10565-016-9329-x>
- Maksimenco AV, Vavaev AV, Bouryachkovskaya LI, Mokh VP, Uchitel IA, Lakomkin VL, Kapelko VI, Tischenko EG (2010) Biopharmacology of enzyme conjugates: vasoprotective activity of supramolecular superoxide dismutase-chondroitin sulfate-catalase derivative. *Acta Naturae* 2:82–94. <https://doi.org/10.32607/20758251-2010-2-4-82-94>
- Matamoros MA, Loscos J, Dietz K-J, Aparicio-Tejo PM, Becana M (2010) Function of antioxidant enzymes and metabolites during maturation of pea fruits. *J Exp Bot* 61:87–97. <https://doi.org/10.1093/jxb/erp285>
- Michaelis L, Menten ML, Johnson KA, Goody RS (2011) The original Michaelis constant: translation of the 1913 Michaelis-Menten paper. *Biochemistry* 50:8264–8269. <https://doi.org/10.1021/bi201284u>
- Miller A-F (2003) Superoxide processing. In: *Comprehensive coordination chemistry II*. Elsevier, pp 479–506
- Moser GAO, Barrera-Alba JJ, Ortega MJ, Alves-de-Souza C, Bartual A (2022) Comparative characterization of three *Tetraselmis chui* (Chlorophyta) strains as sources of nutraceuticals. *J Appl Phycol* 34:821–835. <https://doi.org/10.1007/s10811-021-02675-x>
- Murshudov GN, Grebenko AI, Brannigan JA, Antson AA, Barynin VV, Dodson GG, Dauter Z, Wilson KS, Melik-Adamyants WR (2002) The structures of *Micrococcus lysodeikticus* catalase, its ferryl intermediate (compound II) and NADPH complex. *Acta Crystallogr D Biol Crystallogr* 58:1972–1982. <https://doi.org/10.1107/S0907444902016566>
- Nordberg H, Cantor M, Dusheyko S, Hua S, Poliakov A, Shabalov I, Smirnova T, Grigoriev IV, Dubchak I (2014) The genome portal of the Department of Energy Joint Genome Institute: 2014 updates. *Nucleic Acids Res* 42:D26–31. <https://doi.org/10.1093/nar/gkt1069>
- Notredame C, Higgins DG, Heringa J (2000) T-Coffee: a novel method for fast and accurate multiple sequence alignment. *J Mol Biol* 302:205–217. <https://doi.org/10.1006/jmbi.2000.4042>
- Pashkow FJ (2011) Oxidative stress and inflammation in heart disease: do antioxidants have a role in treatment and/or prevention? *Int J Inflamm* 2011:1–9. <https://doi.org/10.4061/2011/514623>
- Patrinou V, Daskalaki A, Kampantais D, Kanakis DC, Economou CN, Bokas D, Kotzamanis Y, Aggelis G, Vayenas DV, Tekerlekopoulou AG (2022) Optimization of cultivation conditions for *Tetraselmis striata* and biomass quality evaluation for fish feed production. *Water* 14:3162. <https://doi.org/10.3390/w14193162>

- Pettersen EF, Goddard TD, Huang CC, Couch GS, Greenblatt DM, Meng EC, Ferrin TE (2004) UCSF Chimera—a visualization system for exploratory research and analysis. *J Comput Chem* 25:1605–1612. <https://doi.org/10.1002/jcc.20084>
- Pizzino G, Irrera N, Cucinotta M, Pallio G, Mannino F, Arcoraci V, Squadrito F, Altavilla D, Bitto A (2017) Oxidative stress: harms and benefits for human health. *Oxid Med Cell Longev* 2017:8416763. <https://doi.org/10.1155/2017/8416763>
- Prasad N, Ramteke P, Dholia N, Yadav UCS (2018) Therapeutic interventions to block oxidative stress-associated pathologies. In: *Immunity and inflammation in health and disease*. Elsevier, pp 341–362
- Qazi WM, Ballance S, Kousoulaki K, Uhlen AK, Kleinegris DMM, Skjånes K, Rieder A (2021) Protein enrichment of wheat bread with microalgae: *Microchloropsis gaditana*, *Tetraselmis Chui* and *Chlorella Vulgaris* Foods 10:3078. <https://doi.org/10.3390/foods10123078>
- R Core Team (2020) R: a language and environment for statistical computing. R Foundation for Statistical Computing, Vienna, Austria.
- Sansone C, Galasso C, Orefice I, Nuzzo G, Luongo E, Cutignano A, Romano G, Brunet C, Fontana A, Esposito F, Ianora A (2017) The green microalga *Tetraselmis suecica* reduces oxidative stress and induces repairing mechanisms in human cells. *Sci Rep* 7:41215. <https://doi.org/10.1038/srep41215>
- Savelli B, Li Q, Webber M, Jemmat AM, Robitaille A, Zamocky M, Mathé C, Dunand C (2019) RedoxiBase: a database for ROS homeostasis regulated proteins. *Redox Biol* 26:101247. <https://doi.org/10.1016/j.redox.2019.101247>
- Segovia-Campos I, Kanellakopoulos A, Barrozo IJ, Fock-Chin-Ming E, Filella M, Fontaine AB, Pallada S, Triscone G, Perron K, Ariztegui D (2024) Strontium-90 pollution can be bioremediated with the green microalga *Tetraselmis chui*. *Environ Sci Process Impacts* 26:622–631. <https://doi.org/10.1039/D3EM00336A>
- Sepasi Tehrani H, Moosavi-Movahedi AA (2018) Catalase and its mysteries. *Prog Biophys Mol Biol* 140:5–12. <https://doi.org/10.1016/j.pbiomolbio.2018.03.001>
- Shapiro SS, Wilk MB (1965) An analysis of variance test for normality (complete samples). *Biometrika* 52:591–611. <https://doi.org/10.1093/biomet/52.3-4.591>
- Sheng Y, Abreu IA, Cabelli DE, Maroney MJ, Miller A-F, Teixeira M, Valentine JS (2014) Superoxide dismutases and superoxide reductases. *Chem Rev* 114:3854–3918. <https://doi.org/10.1021/cr4005296>
- Simon A, Lippemeier S, Mueller J, Schlachter M, Kaiser F, Schulz C (2024) A question of digestion: how microalgae species affects lipid and fatty acid digestibility in rainbow trout (*Oncorhynchus mykiss*). *Aquaculture* 593:741311. <https://doi.org/10.1016/j.aquaculture.2024.741311>
- Smith Michael W, Doolittle Russell F (1992) A comparison of evolutionary rates of the two major kinds of superoxide dismutase. *J Mol Evol* 34. <https://doi.org/10.1007/BF00182394>
- Sørensen M, Kousoulaki K, Hammerø R, Kokkali M, Kleinegris D, Marti-Quijal FJ, Barba FJ, Palihawadana AM, Egeland ES, Johnsen CA, Romarheim OH, Bisa S, Kiron V (2023) Mechanical processing of *Phaeodactylum tricornutum* and *Tetraselmis chui* biomass affects phenolic and antioxidant compound availability, nutrient digestibility and deposition of carotenoids in Atlantic salmon. *Aquaculture* 569:739395. <https://doi.org/10.1016/j.aquaculture.2023.739395>
- Steimbrüch BA, Sartorio MG, Cortez N, Albanesi D, Lisa M-N, Repizo GD (2022) The distinctive roles played by the superoxide dismutases of the extremophile *Acinetobacter* sp. Ver3. *Sci Rep* 12:4321. <https://doi.org/10.1038/s41598-022-08052-z>
- Steinman HM (1978) The amino acid sequence of manganese superoxide dismutase from *Escherichia coli* B. *J Biol Chem* 253:8708–8720
- Studier FW (2005) Protein production by auto-induction in high-density shaking cultures. *Protein Expr Purif* 41:207–234. <https://doi.org/10.1016/j.pep.2005.01.016>
- Tamura K, Stecher G, Kumar S (2021) MEGA11: molecular evolutionary genetics analysis version 11. *Mol Biol Evol* 38:3022–3027. <https://doi.org/10.1093/molbev/msab120>
- Taniguchi M, Nakagawa I, Hoshino K, Itoh T, Ohno K, Fujii M (1989) Production of superoxide dismutase from *Streptococcus lactis* using a bioreactor with a microfiltration module. *Agric Biol Chem* 53:2447–2453. <https://doi.org/10.1080/00021369.1989.10869690>
- Teufel F, Almagro Armenteros JJ, Johansen AR, Gislason MH, Pihl SI, Tsirigos KD, Winther O, Brunak S, Von Heijne G, Nielsen H (2022) SignalP 6.0 predicts all five types of signal peptides using protein language models. *Nat Biotechnol* 40:1023–1025. <https://doi.org/10.1038/s41587-021-01156-3>
- Veronese FM, Caliceti P, Schiavon O, Sergi M (2002) Polyethylene glycol–superoxide dismutase, a conjugate in search of exploitation. *Adv Drug Deliv Rev* 54:587–606. [https://doi.org/10.1016/S0169-409X\(02\)00029-7](https://doi.org/10.1016/S0169-409X(02)00029-7)
- Villar-Navarro E, Ruiz J, Garrido-Pérez C, Perales JA (2022) Microalgae biotechnology for simultaneous water treatment and feed ingredient production in aquaculture. *J Water Process Eng* 49:103115. <https://doi.org/10.1016/j.jwpe.2022.103115>
- Vlasits J, Jakopitsch C, Bernroither M, Zamocky M, Furtmüller PG, Obinger C (2010) Mechanisms of catalase activity of heme peroxidases. *Arch Biochem Biophys* 500:74–81. <https://doi.org/10.1016/j.abb.2010.04.018>
- Widowati I, Zainuri M, Kusumaningrum HP, Susilowati R, Hardivillier Y, Leignel V, Bourgougnon N, Mouget J-L (2017) Antioxidant activity of three microalgae *Dunaliella salina*, *Tetraselmis chuii* and *Isochrysis galbana* clone Tahiti. *IOP Conf Ser Earth Environ Sci* 55:012067. <https://doi.org/10.1088/1755-1315/55/1/012067>
- Wood NJ, Jørgensen J (2001) Catalase and superoxide dismutase activity in ammonia-oxidising bacteria. *FEMS Microbiol Ecol* 38:53–58. <https://doi.org/10.1111/j.1574-6941.2001.tb00881.x>
- Yan W, Feng X, Zhang W, Nawaz MZ, Luo T, Zhang R, Jiao N (2021) Genomes of diverse isolates of *Prochlorococcus* high-light-adapted clade II in the Western Pacific Ocean. *Front Mar Sci* 7:619826. <https://doi.org/10.3389/fmars.2020.619826>
- Yusuf N, Yusof NS, Jusoh M, Ahmad Zakeri H, Muhamad Zalan N (2023) Growth pigments production and phytochemicals variation in *Tetraselmis chui* under different cultivation parameters. *Int Aquat Res*. <https://doi.org/10.22034/iar.2023.1993193.1481>
- Zamocky M, Furtmüller PG, Obinger C (2008) Evolution of catalases from bacteria to humans. *Antioxid Redox Signal* 10:1527–1548. <https://doi.org/10.1089/ars.2008.2046>

Publisher's Note Springer Nature remains neutral with regard to jurisdictional claims in published maps and institutional affiliations.

Supplemental information – The antioxidant potential of *T. chui* microbiomesTable S1: Profile hidden Markov model (HMM) search for SODs (PF00081 and PF02777) and CATs (PF00199 and PF06628) against the *Tetraselmis chui* metagenome. Taxonomic affiliation was inferred from the best BLASTp hit in NCBI's nr-database.

No.	IMG Query ID (Ga0499797_)	HMM	HMM e-value	HMM score	BlastP subject	BlastP Identity	Species assignment (BlastP subject)
A)							
1	000026_192	Sod_Fe_N	5.8E-24	88.5	WP_159642379.1	100	<i>Sphingorhabdus</i> sp. 109
TcJM_SOD2	000027_110175_110774_1	Sod_Fe_N	3.8E-28	84.1	WP_149780105.1	100	<i>Roseovarius litoreus</i>
3	000027_113	Sod_Fe_N	1.3E-22	84.1	WP_149780105.1	100	<i>Roseovarius litoreus</i>
4	000031_37	Sod_Fe_N	2.4E-25	92.9	WP_109767327.1	98	<i>Oceaniradius stylonematis</i>
TcIK_SOD3	000031_37060_37662_1	Sod_Fe_N	7E-31	92.9	WP_109767327.1	98	<i>Oceaniradius stylonematis</i>
6	000036_74	Sod_Fe_N	2.5E-22	83.2	WP_089419839.1	99.5	Roseobacteraceae bacterium
7	000038_26	Sod_Fe_N	1.2E-30	109.9	TVR83868.1	81.7	Saprospirales bacterium
8	000083_66	Sod_Fe_N	4.5E-25	92	WP_260277506.1	100	<i>Paracoccus maritimus</i>
9	056429_1	Sod_Fe_C	1.8E-10	44.9	KAK3246025.1	90.3	<i>Cymbomonas tetramitiformis</i>
B)							
1	000001_642	Catalase	1.6E-179	601.1	WP_159643319.1	100	<i>Sphingorhabdus</i> sp. 109
2	000030_55	Catalase	1.7E-173	581.3	WP_089419967.1	99.6	Roseobacteraceae bacterium
TcJM_CAT2	000030_56127_57647_1	Catalase	4.9E-179	581.3	WP_089419967.1	99.6	Roseobacteraceae bacterium
TcIK_CAT3	000173_13486_14940_1	Catalase	1.9E-188	612.3	WP_084354968.1	94.2	<i>Primorskyibacter flagellatus</i>
6	000217_8	Catalase	1.4E-180	604.6	PHQ68604.1	98.4	<i>Paracoccus</i> sp.
7	167948_1	Catalase	1.8E-78	268.5	WP_292606672.1	99.4	<i>Nocardioides</i> sp. REDSEA-S30_B4

Table S2: Statistical F-test comparison of linear models for the toxicological effects on *Galleria mellonella* larvae of the tested antioxidant enzymes to a control.

Enzyme	Concentration (mg/ml)	Estimate	Std.error	Statistic	p.value
TcJM_SOD2	0.0003	0.104	0.342	0.304	0.773
TcJM_SOD2	0.003	-0.063	0.353	-0.177	0.866
TcJM_SOD2	0.03	0.187	0.375	0.499	0.638
TcIK_SOD3	0.0003	-0.229	0.381	-0.601	0.573
TcIK_SOD3	0.003	-0.312	0.328	-0.954	0.384
TcIK_SOD3	0.03	-0.645	0.329	-1.964	0.107
TcJM_CAT2	0.00006	0.063	0.353	0.177	0.866
TcJM_CAT2	0.0006	-0.77	0.486	-1.587	0.173
TcJM_CAT2	0.006	0.479	0.364	1.317	0.245
TcIK_CAT3	0.00006	0.396	0.419	0.944	0.388
TcIK_CAT3	0.0006	0.312	0.393	0.795	0.463
TcIK_CAT3	0.006	0.229	0.431	0.532	0.618



Movie S1: Structure comparison of predicted TcJM_SOD2 and predicted TcIK_SOD3. Yellow: TcJM_SOD2 structure prediction by AlphaFold2. Purple: TcIK_SOD3 structure prediction by AlphaFold2. Picture adaptation of original movie.



Movie S2: Structure comparison of predicted TcJM_CAT2 and predicted TcIK_CAT3. Blue: TcJM_SOD2 structure prediction by AlphaFold2. Orange: TcIK_SOD3 structure prediction by AlphaFold2. Picture adaptation of original movie.

Screening Metagenomes for Algae Cell Wall Carbohydrates Degrading Hydrolases in Enrichment Cultures

Book: Streit, W.R., Daniel, R. (eds) Metagenomics. Methods in Molecular Biology. ISBN: 978-1-0716-2794-5

First author: Jascha F. H. Macdonald

Co-authors: Dr Ines Krohn
Professor Dr Wolfgang Streit

Published: 29th October 2022

DOI: https://doi.org/10.1007/978-1-0716-2795-2_9

Note: Not peer-reviewed

Methods in
Molecular Biology 2555

Springer Protocols



Wolfgang R. Streit
Rolf Daniel *Editors*

Metagenomics

Methods and Protocols

Third Edition

 Humana Press



Chapter 9

Screening Metagenomes for Algae Cell Wall Carbohydrates Degrading Hydrolases in Enrichment Cultures

Jascha F. H. Macdonald, Ines Krohn, and Wolfgang R. Streit

Abstract

Sustainable use of natural products is one of the key challenges for the future. An increasing focus is on marine organic matter, mostly algae. New biotechnological tools for processing high amounts of micro- and macroalgae are necessary for efficient industrial degradation of marine matter. Secreted glycosyl hydrolases can be enriched and tested on the specific algae cell wall polymers of all algae groups (Rhodophyta; Phaeophyceae; Chlorophyta/Charophyta). Metagenomic analyses established new possibilities to screen algae-associated microbiomes for novel degrading enzymes in combination with sequence-based function prediction.

Key words Meta-omics, Biotechnology, Algae, Enzymatic degradation, Glycoside hydrolases, Enrichment culture, Sustainability

1 Introduction

The need for sustainable resources and their efficient use is one of the key challenges of the twenty-first century. Facing global climate change, new approaches focus on *novel* and renewable resources from marine origin with one major interest in algae processing. So far, the cell disruption of algae cells lacks an urgently needed, efficient molecular method. These processes benefit from new molecular techniques like “omics”-based analyses, providing a powerful tool for large-scale enzyme screening for efficient algae cell wall-specific glycoside hydrolases.

Especially in the energy sector are shifts from using fossil fuels to renewable energy such as solar power, wind energy, and biofuel [1, 2]. Additionally, the global food market is changing toward alternative, healthy, and sustained food production [3]. The main approach is to rearrange the already existing state, establish new land-use strategies, extend the use of renewable energies, and reform economic systems toward ecological designs to keep a stable

biodiversity and the emission level of greenhouse gases at a low level as well as reduce the environmental pollution. Another promising approach is investigating new resources and techniques. To obtain these novel sources of future energy and food, new high-scale biotechnological molecular processing techniques need to be introduced to many different industries.

One resource of interest are marine and freshwater algae from the single-cell phytoplankton to abundant macroalgae, from the smallest known eukaryote, the picoplankton *Ostreococcus tauri* (diameter $\sim 1 \mu\text{m}$) [4] to the kelp forest-forming order Laminariales (more than 40 m in height) [5]. Algae are a global key organism group in the ecosystem, serving as the basic energy source for the whole life in the ocean's food chain, thereby influencing high trophic levels and having an impact on the whole fishery industry. Furthermore, it plays an important role in the Earth's atmosphere composition by being the major global net primary producer [6, 7]. The immense potential of algae biomass products is found in the fuel and energy sector (e.g., biodiesel, biogas, bioethanol) as well as the food and nonfood products with a wide variety (e.g., pharmaceuticals, cosmetics, animal feeds) [8]. Therefore, a comparable wide variety of efficient processing and culturing techniques are urgently needed.

Metagenomic techniques first appeared in 1991 [9] and led to numerous publications about the novel enzymes for industrial applications [10–13]. Furthermore, a number of reviews show the basics and advantages of this powerful molecular tool [14–18].

An increased level of putative hydrolyses can be obtained in optimized, multispecies enrichment cultures [19]. Since the aim is to degrade different algae, they are used as the main substrate and carbon source in the enrichment culture and therefore give a competing advantage to organisms with the ability to hydrolyze the substrate. For this reason, media in enrichment cultures should be modified to manipulate the microbial community and enhance the growth of the target group. This group is then described and further investigated by metagenomic, metaproteomic, and metatranscriptomic analyses.

Industrial processing of high-scale amounts of algae biomass requires efficient glycosylic hydrolases to degrade the polymer matrix in the cell wall of the algae. This complex net of carbohydrates serves as protection, energy storage, and structure component for the organism and consists of a specific composition of different molecules, depending on the algae taxonomic group (Table 1). While cellulose, mannan, and xylan appear in several groups, there are eight specific carbohydrates only synthesized by special taxa of brown, green, or red algae [20]. Additionally, the orthosilicic acid-based diatoms cell wall consists of pectin and laminarin. Some of these polysaccharides are also found in other organism groups like cellulose (land plants), sulfated fucans

Table 1
Specific cell wall carbohydrates per algae taxa

Phaeophyceae	Chlorophyta/Charophyta	Rhodophyta
Fucoidan	Pectin	Carrageenan
Laminarin	Mannan	Mannan
Alginate	Xylan	Xylan
Cellulose	Cellulose	Agar
	Ulvan	Porphyran



Fig. 1 The brown alga *F. vesiculosus*. The enrichment culture shows different degradation states after 1–25 days

(animals), and alginate (bacteria). Even though the polysaccharides make up the major portion of the algae cell wall, e.g., sulfated fucans in brown algae up to 45% [21], there are also other components such as proteins, phlorotannins (which are equivalent to lignin in land plants), and halide compounds in brown algae [22–25]. Especially the complex phlorotannins in brown algae strengthen the structure of the plant and need to be further investigated for additional degradation success (Fig. 1).

1.1 Algae Cell Wall Polymers: Structure and Enzymatic Degradation

One molecular tool to degrade the algae polymer is glycosyl hydrolase, which is described by the Carbohydrate Active Enzymes database (CAZy) (<http://www.cazy.org/>; 26). So far, they are organized into 18 clans with more than 170 families. The following glycosyl hydrolases are the most important for the degradation of algae cell walls: endo- α -1,4-L-fucanase (EC 3.2.1.212); endo- α -(1,3)-L-fucanase (EC 3.2.1.211); α -1,2/1,3/1,4-L-

fucosidases (EC 3.2.1.51/EC 3.2.1.111/EC 3.2.1.51); laminarinase (EC 3.2.1.39); endo-1,3(4)- β -glucanase (EC 3.2.1.6); β -1,3-glucosidase (EC 3.2.1.-); exo- β -1,3-glucanase (EC 3.2.1.58); β -1,6-glucanase (EC 3.2.1.75); endo- β -1,3-glucanase (EC 3.2.1.39); laminarin-degrading enzyme (EC 3.2.1.-); cellobiohydrolases (EC 3.2.1.91); polygalacturonase (EC 3.2.1.15); endo- β -1,4-glucanase/cellulase (EC 3.2.1.4); β -mannosidase (EC 3.2.1.25); β -mannanase (EC 3.2.1.78); endo- β -1,4-xylanase (EC 3.2.1.8); endo-1,3- β -xylanase (EC 3.2.1.32); exo-1,4- β -xylosidase (EC 3.2.1.-); β -fucosidase (EC 3.2.1.38); κ -carrageenase (EC 3.2.1.83); I-carrageenase (EC 3.2.1.157); β -carrageenase (EC 3.2.1.-); λ -carrageenases (EC 3.2.1.162); β -agarase (EC 3.2.1.81); α -agarase (EC 3.2.1.158); α -neoagarooligosaccharide hydrolase (EC.3.2.1.159); and β -porphyranase (EC 3.2.1.178). These components need to mix a universal algal cell wall degrading cocktail with glycoside hydrolases. For additional degrading effects, enzymes from the polysaccharide lyases (EC 4.-.-) can be investigated, especially for the degradation of alginate (EC 4.2.2.3; EC 4.2.2.11; EC 4.2.2.26) and ulvan [26].

Brown algae are multicellular macroalgae with famous abundant genera like *Fucus*, Laminariales, and Sargassum. Sulfated fucans, also known as fucoidan in brown algae, consist of a polysaccharide mainly made up of L-fucose with α -1,3-bonds and/or α -1,4-bonds of a sulfate group at position 4, depending on the species (Fig. 2b) [27]. They are mainly found in the genus *Fucus* like in the abundant *Fucus vesiculosus* (Fig. 1), which is found in many coastal areas of the northern Atlantic Ocean. In contrast, the genus *Laminaria*, which forms the kelp forests and therefore might be an interesting candidate for cultivation, mainly synthesizes the carbohydrate laminarin, composed of (1,3)- β -D-glucan (Fig. 2a) [28]. Additionally, alginate consist of linear copolymers containing blocks of (1,4)-linked-D-mannuronate and α -L-guluronate residues (Fig. 2c) [29].

The polysaccharide pectin is a family of α -1,4-linked galacturonic acid with covalent links and found in the cell wall of green algae [30]. Furthermore, mannan (β -1,4-linked backbone containing mannose or a combination of glucose and mannose residues), xylan (β -(1,4)-linked β -xylopyranose), and ulvan (α - β -(1,4)-linked monosaccharides of rhamnose, xylose, glucuronic acid, and iduronic with characteristic repeating disaccharide units) make up the cell wall of the green algae [31, 32].

Cellulose hydrolyzation had already been investigated for several years, leading to a high number of described cellulases caused by its common appearance in land plants and as a consequence numerous enzymes developed by organisms from all kingdoms, breaking down the β -1,4-glycosidic bonds of the molecule [33]. It is found in brown and green algae.

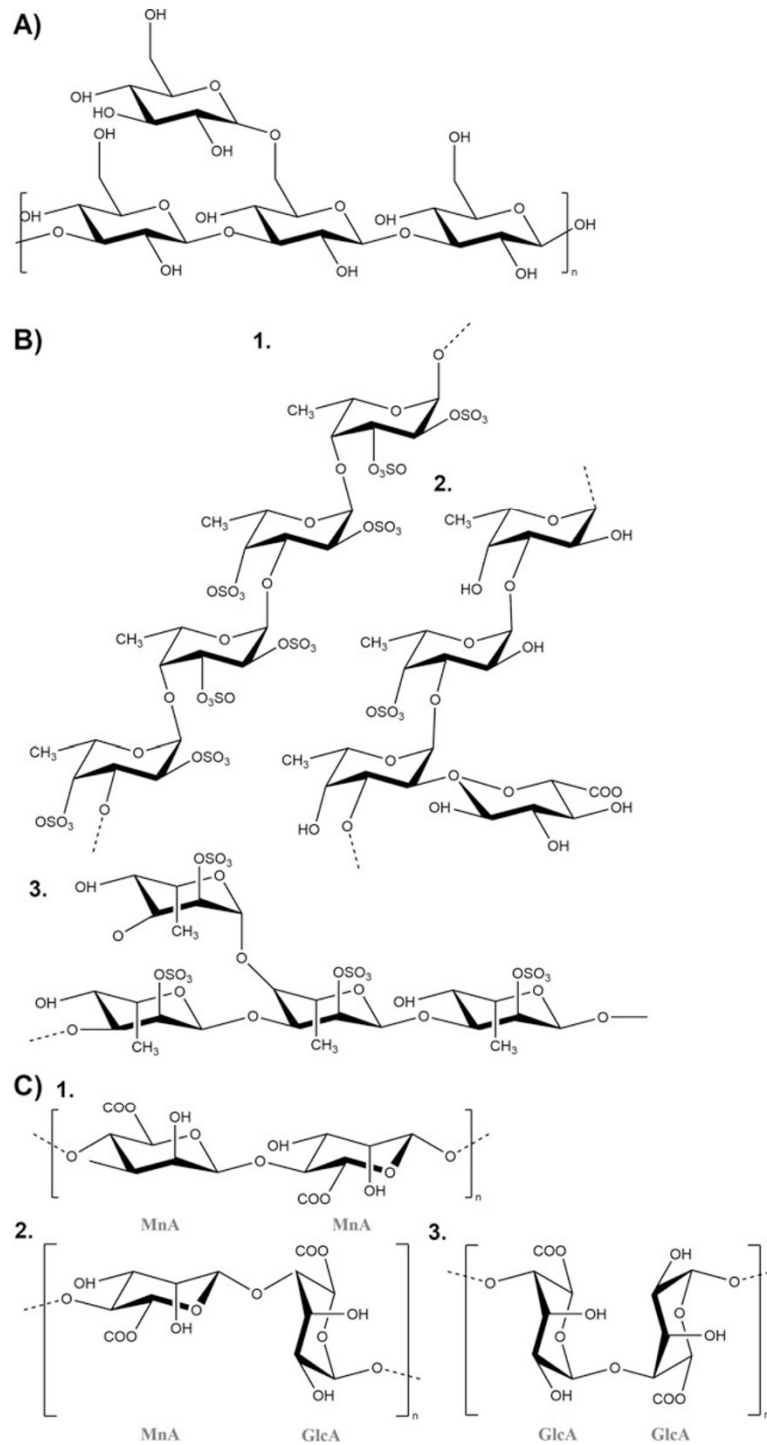


Fig. 2 Molecular chain structure of polysaccharides. **(a)** Laminarin (*Sargassum fusiforme*). **(b)** Fucoidan: (1) Homofucan, (2/3) Heterofucan. **(c)** Alginate: (1) poly mannuronic acid (MnA), (2) poly L-guluronic acid (GlcA), (3) poly mannuronic acid-guluronic acid

The abundant polysaccharides found in red algae seaweed are carrageenan and agar. The gel-forming carrageenan has a wide variety of structures composed of a backbone of α -D-1,3 and β -D-1,4 galactose residues that are sulfated at up to 40% [34], while agar, known for its usage in microbiology, has a structure of alternating 1,3-linked β -D-galactopyranose and 1,4-linked 3,6-anhydro- α -L-galactopyranose or agariose [35]. Porphyrin is related to agarose and highly substituted by 6-O-sulfation of the L-galactose units and 6-O-methylation of the D-galactose units [36].

Screening for enzymes for just one taxonomic group, the parameters can be adjusted to the algae group of interest and the associated cell wall polymers; otherwise for a universal approach, all carbohydrases should be targeted. Metagenomics databases significantly reduce the amount of time and workload to achieve this goal.

2 Materials

2.1 Media and Consumables

1. Synthetic seawater medium: For 35 PSU, 40 g Tropic Marin © Classic Sea Salt (CSS) + 1 L VE-Water; salinity adjustments can be achieved by setting the proportion of salt (e.g., 15 PSU = ~ 17 g CSS + 1 L VE-Water).
2. 500-mL flasks.
3. Centrifuge bottles.
4. TWEEN 20.
5. 0.1 M Tris-HCl.

2.2 Glucose Oxidase Assay Kit

1. Buffer (pH 7): 1 L H₂O, 13.6 g potassium dihydrogen, 0.5 g bovine serum albumin, and 0.2 g sodium azide.
2. POD mixture: 12 mL buffer +0.09% (w/v) p-hydroxybenzoic, 3 g peroxidase +4-aminoantipyrine, and 188 mL H₂O.
3. D-Glucose: 4.5 g D-glucose and 50 mL H₂O.
4. Glucose oxidase standard: 50 mL buffer and 3 g glucose oxidase standard (~2.9 U).

2.3 Thin-Layer Chromatography

1. Solvent solution: Chloroform: methanol (4:1).
2. Mobile phase: 10.73 mL chloroform, 10.73 mL pyridine, 3.08 mL 98% formic acid, and 1.44 mL H₂O.
3. Stationary phase: TLC silica gel 60 F₂₅₄ (10 × 20 cm).
4. Reagent solution: 225 mL 100% ethanol, and 25 mL sulfuric acid (*see Note 1*).

3 Methods

3.1 Enrichment of Highly Cell Wall-Hydrolyzing Microbial Communities

A universal mixture of enzymes for algal cell wall hydrolyses is not yet established and can be obtained by combining the results of multiple single-alga species/substrate approaches. The advantage of single-alga species approaches is the possibility of adjusting the parameters of the enrichment cultures to optimal degrading conditions to gain access to the most efficient hydrolyzing communities. These parameters are especially the temperature, shaking speeds, salinity, pH, and oxygen availability. It is recommended to use model organisms to represent all different phycological taxa of brown, red, and green algae to keep the time required low due to focusing on specific polymer structures. The following protocol is an example of the brown macroalgae *F. vesiculosus*, commonly found in tidal zones of the northern Atlantic Ocean.

1. Collect environmental samples of algae directly on the shore. Optimal condition would be within the tidal zone.
2. Transfer the samples to the lab in humid, cool conditions.
3. Prepare synthetic seawater medium. Adjust the salinity to the condition of the sample location or to 35 PSU if the natural conditions are unknown. Vary the salinity for exceptional natural systems like the Baltic Sea (*see Note 2*).
4. Rinse the collected algae with VE-Water to minimize the amount of attached sand. Remove muscles, barnacles, snails, and all other visible animals.

3.2 Enrichment Cultures

1. Immediately transfer about 50 g algae material in a 500-mL flask and add 300 mL synthetic seawater (*see Note 3*).
2. Set up the enrichment culture at 22 °C (*see Note 4*).
3. Take regular samples for sugar assay analyses (*see Subheading 3.6*).

3.3 Characterize Initial Microbial Community

The development of the microbial community is best analyzed by comparing the composition of species after certain time points to the starting conditions. Assuming that the degrading conditions are optimized, the involved taxa should benefit and dominate the culture. These certain time points can be determined by the substrate customized sugar assays as described in Subheading 3.6.

1. Wash freshly collected algae as described in Subheading 3.1, step 4.
2. Transfer 50 g algae to a centrifuge bottle and add 40 mL TWEEN 20 + 160 mL 0.1 M Tris-HCl.
3. Shake the bottles at 120 rpm for 1 h.
4. Carefully remove the algae from the bottle and replace it with 50 g of a new prepared sample.

132 Jascha F. H. Macdonald et al.

5. Repeat **step 3**.
6. Remove the algae again.
7. Centrifuge at $15,000\times g$ for 20 min.
8. Discard the supernatant and resuspend the pellet in 20 mL Tris-HCl, transfer into a Falcon tube, and centrifuge at $17,000\times g$ for 10 min.

3.4 Meta-Omics Analyses

The highest degradation activity is displayed by the peak of the sugar concentration in the medium. This peak is usually followed by a decline caused by the microbial species that feed on this sugar but are not involved in the cell wall degradation process. The growth of that community gives a disadvantage to the degrading species. To avoid this and optimize the degradation, bioreactor approaches (Fig. 3) with sugar filtering conditions are suitable. However, the metagenomics analyses give access to all genes within the culture and should be screened with the introduction given to CAZY enzyme families. Metatranscriptomes and metaproteomes help

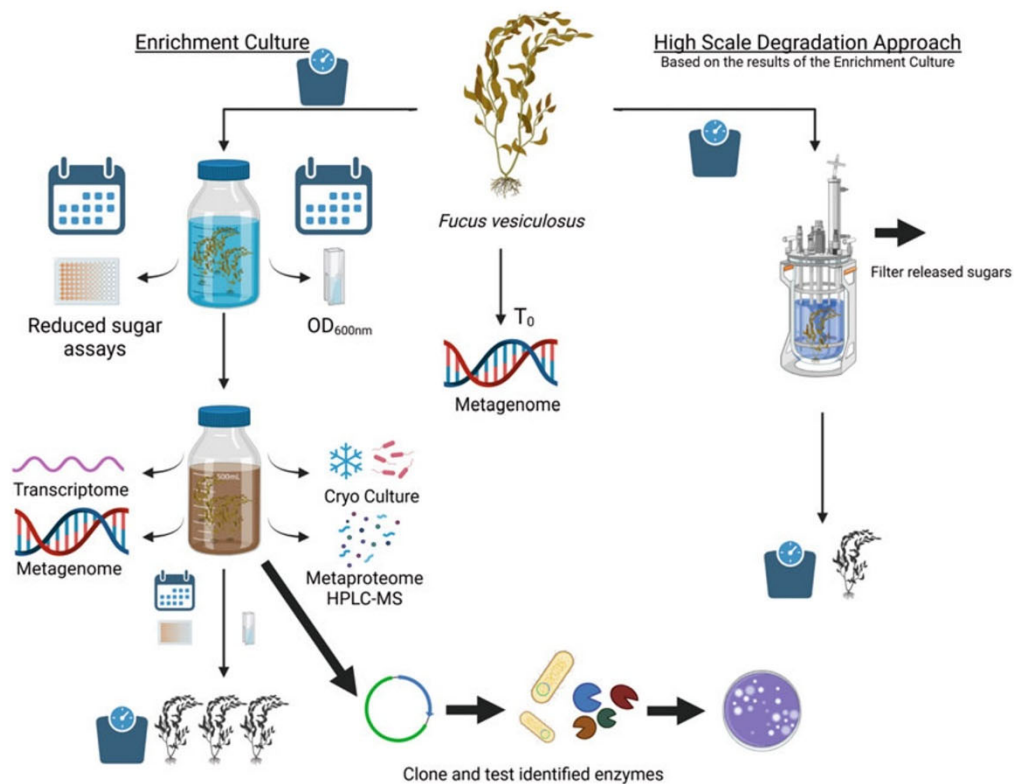


Fig. 3 Workflow for efficient identification, enrichment, screening, and cloning of alga cell wall hydrolases. (Figure created with BioRender.com)

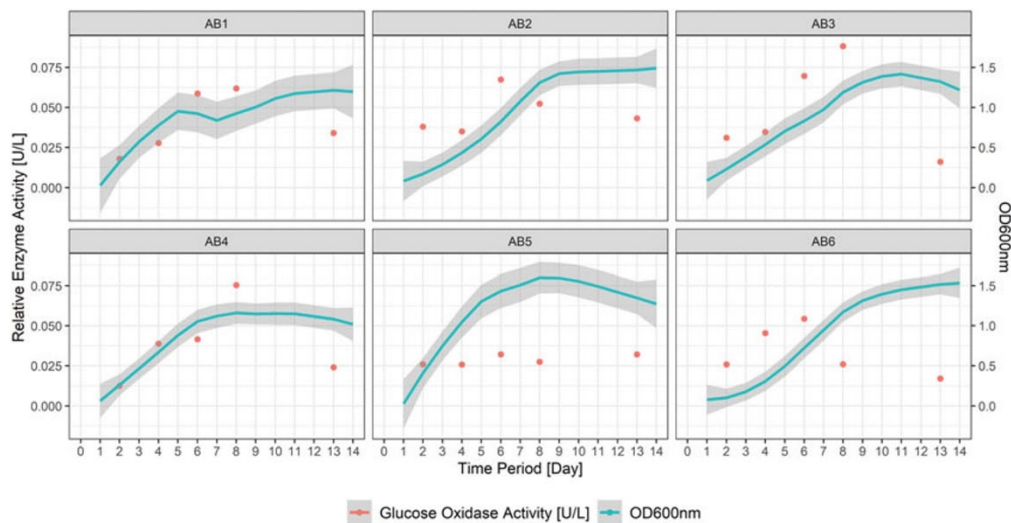


Fig. 4 Degradation quantification of *F. vesiculosus* enrichment culture replicates (AB1-AB6) over time. The optical density (OD_{600nm}) (blue) displays the turbidity of the medium influenced by growing bacteria/fungi and released degradation products and small alga parts. The enzyme activity (red) displays the concentration of the released glucose in the media

narrow down the most active degrading genes as well as comparing phylogeny of the metagenome from the degrading time point to phylogeny of the metagenome at the start of the enrichment culture.

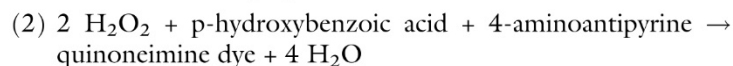
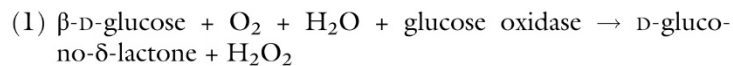
3.5 Degradation Quantification

The degradation of the algae cell wall causes a release of intercellular substances into the media. Especially pigmented chloroplasts as well as small fragments of the disunited plant have a visual influence on the turbidity of the media. Additionally, fungi, bacteria, and other microscopic organisms influence the tint. The combination of these parameters can be used as a degradation scale and measured by the optical density OD_{600nm} (Fig. 4). Furthermore, the difference in wet weight of the alga measured before and after the enrichment process gives the net turnover.

3.6 Glucose Oxidase Assay

Representing general sugar release through polymer degradation, glucose is measured over time within the enrichment culture. Additional sugar assays for different saccharides can be approached, respectively, adjusted to the alga taxa serving as a substrate (*see Note 5*). The glucose content is measured over the units of enzyme activity (U) of glucose oxidase designed with the protocol of the Glucose Oxidase Assay Kit (K-Glox) by Megazyme (Megazyme Bray, Co. Wicklow, Ireland). The principle is the catalyzing effect on the oxidation of β -D-glucose to D-glucono- δ -lactone, releasing

hydrogen peroxide (1). Hydrogen peroxide then reacts with p-hydroxybenzoic acid and 4-aminoantipyrine (2). The formation of a quinoneimine dye complex can be quantified by the absorption at a wavelength of 510 nm. The used sample is the fluid medium phase of the enrichment culture. It is recommended to filter the medium through a 0.2 μm syringe filter if the medium is very turbid due to released pigments of the degradation process.



1. Mix the following separated approaches in a microplate: one “Blank,” one “Standard,” and for every sample “Sample.”
2. Mix 50 μL of D-glucose with 200 μL of POD mixture for each approach.
3. Let the mixture incubate at 25 $^\circ\text{C}$ for 5 min.
4. Read the absorbance at 510 nm (A1).
5. Add to “Blank” 50 μL distilled water, to “Standard” 50 μL glucose oxidase standard, and to “Sample” 50 μL of the corresponding sample. Mix the approaches.
6. Let the mixture incubate at 25 $^\circ\text{C}$ for 20 min.
7. Read the absorption at 510 nm (A2).
8. Calculate the glucose oxidase activity as follows:
Determine the absorbance difference (A2-A1) for blank, samples, and calibration curve standards. Subtract the absorbance difference of the blank from the samples and standards to obtain $\Delta A_{510 \text{ nm}/20 \text{ min}}$. Test sample values are obtained by direct cross-reference to the calibration curve of glucose oxidase activity versus $\Delta A_{510 \text{ nm}/20 \text{ min}}$ (*see Note 6*).

Alternatively:

$$U/L = (\Delta A_{\text{sample}}/\Delta A_{\text{standard}}) \times U/L \text{ standard} \times F$$

If the sample is diluted during preparation, the result must be multiplied by the dilution factor, F.

3.7 Thin-Layer Chromatography (TLC) Analyses for Lipopolysaccharides

For the characterization of the content and degradation products of the algal cell wall in the enrichment cultures, TLC is a beneficial procedure due to its simple and quick implementation that requires relatively less specialist and expensive instruments. TLC relies on the principle of a stationary phase holding a sample and a mobile phase that separates the sample into its components through capillary action. The liquid mobile phase is adjusted to the substances of interest. For lipopolysaccharides (LPS), the following protocol is

suitable and highly depends on their concentration. Therefore, it is recommended to freeze-dry the samples from the liquid supernatant of the enrichment cultures and try different dilution factors when resuspending the product in the solvent solution.

1. Prepare standards as control and comparison.
2. Add the mobile phase into the TLC chamber for pre-equilibration for 1.5 h.
3. Dissolve the freeze-dried samples in the solvent solution. Concentrations and volume of freeze-dried samples depend on LPS concentration.
4. Spot 20 μL of each sample at the stationary phase and mark spots and let it dry (*see Note 7*).
5. Put the stationary phase in the TLC chamber with the mobile phase.
6. Let the mobile phase rise over the stationary phase until it nearly reaches the top, remove it from the chamber, and air-dry the plate.
7. Briefly dip the plate in the reagent solution.
8. Bake the TLC plate at 250 °C, and LPS should appear as brown spots (*see Note 8*).

4 Notes

1. Slowly add sulfuric acid to ethanol.
2. In mesocosms, seawater mediums work as fine as established sea salt additives from aquarist suppliers.
3. Cutting the macroalga simulates mechanical degradation and offers more surface area for the microbiome to interact.
4. Slow shaking at 60 rpm of the enrichment culture is convenient for the oxygen concentration in the media, and the simulation of natural tidal wave movements.
5. L-Fucose is suitable for measuring brown algae degradation and is also offered in established kits.
6. Preparing several standards for a curve is recommended.
7. There are several methods to extract carbohydrates out of the fresh algae to determine the initial content [37]. For *F. vesiculosus*, microwaving is the recommended method.
8. Instead of baking in an oven, it is easier to use a heating plate to have more control over where to apply heat.

136 Jascha F. H. Macdonald et al.

References

1. Bórawski P, Beldycka-Bórawska A, Szymańska EJ et al (2019) Development of renewable energy sources market and biofuels in the European Union. *J Clean Prod* 228:467–484
2. Daroń M, Wilk M (2021) Management of energy sources and the development potential in the energy production sector—a comparison of EU countries. *Energies* 14:685
3. Smith P, Gregory PJ (2013) Climate change and sustainable food production. *Proc Nutr Soc* 72:21–28
4. Pfeuty B, Thommen Q, Corellou F et al (2012) Circadian clocks in changing weather and seasons: lessons from the picoalga *Ostreococcus tauri*. *BioEssays* 34:781–790
5. Bolton JJ (2010) The biogeography of kelps (Laminariales, Phaeophyceae): a global analysis with new insights from recent advances in molecular phylogenetics. *Helgol Mar Res* 64: 263–279
6. Field B, Randerson JT et al (1998) Primary production of the biosphere: integrating terrestrial and oceanic components. *Science* 281: 237–240
7. Arrigo KR (2005) Marine microorganisms and global nutrient cycles. *Nature* 437:349–355
8. Adeniyi OM, Azimov U, Burluka A (2018) Algae biofuel: current status and future applications. *Renew Sust Energ Rev* 90:316–335
9. Schmidt TM, DeLong EF, Pace NR (1991) Analysis of a marine picoplankton community by 16S rRNA gene cloning and sequencing. *J Bacteriol* 1991:4371–4378
10. Ferrer M, Golyshina OV, Chernikova TN et al (2005) Novel hydrolase diversity retrieved from a metagenome library of bovine rumen microflora. *Environ Microbiol* 7:1996–2010
11. Ferrer M, Golyshina OV, Plou FJ et al (2005) A novel alpha-glucosidase from the acidophilic archaeon *Ferroplasma acidiphilum* strain Y with high transglycosylation activity and an unusual catalytic nucleophile. *Biochem J* 391: 269–276
12. Beloqui A, Pita M, Polaina J et al (2006) Novel polyphenol oxidase mined from a metagenome expression library of bovine rumen: biochemical properties, structural analysis, and phylogenetic relationships. *J Biol Chem* 281: 22933–22942
13. Voget S, Leggewie C, Uesbeck A et al (2003) Prospecting for novel biocatalysts in a soil metagenome. *Appl Environ Microbiol* 69: 6235–6242
14. Streit WR, Schmitz RA (2004) Metagenomics - the key to the uncultured microbes. *Curr Opin Microbiol* 7:492–498
15. Schmeisser C, Steele H, Streit WR (2007) Metagenomics, biotechnology with non-culturable microbes. *Appl Microbiol Biotechnol* 75:955–962
16. Daniel R (2004) The soil metagenome – a rich resource for the discovery of novel natural products. *Curr Opin Biotechnol* 15:199–204
17. Krohn I, Bergmann L, Qi M et al (2021) Deep (Meta)genomics and (Meta)transcriptome analyses of fungal and bacteria consortia from aircraft tanks and kerosene identify key genes in fuel and tank corrosion. *Front Microbiol* 12: 722259
18. Krohn-Molt I, Wemheuer B, Alawi M et al (2013) Metagenome survey of a multispecies and alga-associated biofilm revealed key elements of bacterial-algal interactions in photobioreactors. *Appl Environ Microbiol* 79: 6196–6206
19. Bari L, Yeasmin S (2021) Microbes culture methods. In: Chaplan MJ (ed) Reference module in biomedical sciences. Elsevier
20. Bäumgen M, Dutschei T, Bornscheuer UT (2021) Marine polysaccharides: occurrence, enzymatic degradation and utilization. *Chem-biochem* 22:2247–2256
21. Deniaud-Bouët E, Kervarec N, Michel G et al (2014) Chemical and enzymatic fractionation of cell walls from Fucales: insights into the structure of the extracellular matrix of brown algae. *Ann Bot* 114:1203–1216
22. Quatrano RS, Stevens PT (1976) Cell wall assembly in fucus zygotes. *Plant Physiol* 1976: 224–231
23. Vreeland V, Waite JH, Epstein L (1998) Polyphenols and oxidases in substratum adhesion by marine algae and mussels. *J Phycol* 1998: 1–8
24. Wiencke C, Clayton MN, Schoenwaelder M (2004) Sensitivity and acclimation to UV radiation of zoospores from five species of Laminariales from the Arctic. *Mar Biol* 145:31–39
25. Verhaeghe EF, Fraysse A, Guerquin-Kern J-L et al (2008) Microchemical imaging of iodine distribution in the brown alga *Laminaria digitata* suggests a new mechanism for its accumulation. *J Biol Inorg Chem* 13:257–269
26. Drula E, Garron M-L, Dogan S et al (2022) The carbohydrate-active enzyme database: functions and literature. *Nucleic Acids Res* 50: D571–D577

27. Berteau O, Mulloy B (2003) Sulfated fucans, fresh perspectives: structures, functions, and biological properties of sulfated fucans and an overview of enzymes active toward this class of polysaccharide. *Glycobiology* 13:29R–40R
28. Kadam SU, Tiwari BK, O'Donnell CP (2015) Extraction, structure and biofunctional activities of laminarin from brown algae. *Int J Food Sci Technol* 50:24–31
29. Lee KY, Mooney DJ (2012) Alginate: properties and biomedical applications. *Prog Polym Sci* 37:106–126
30. Mohnen D (2008) Pectin structure and biosynthesis. *Curr Opin Plant Biol* 11:266–277
31. Moreira LRS, Filho EXF (2008) An overview of mannan structure and mannan-degrading enzyme systems. *Appl Microbiol Biotechnol* 79:165–178
32. Bastawde KB (1992) Xylan structure, microbial xylanases, and their mode of action. *World J Microbiol Biotechnol* 1992:353–368
33. Béguin P, Aubert J-P (1994) The biological degradation of cellulose. *FEMS Microbiol Rev* 1994:25–58
34. Necas J, Bartosikova L (2013) Carageenan: a review. *Vet Med* 2013:187–205
35. Juanes JA (1991) International workshop on Gelidium: proceedings of the international workshop on Gelidium Held in Santander, Spain, September 3–8 1990, *Developments in Hydrobiology Series*, vol 68. Springer, Dordrecht
36. Morrice LM, McLean MW, Long WF et al (1984) Porphyrin primary structure. In: Bird CJ, Ragan MA (eds) Eleventh international seaweed symposium. Springer, Dordrecht, pp 572–575
37. Jönsson M, Allahgholi L, Sardari RR et al (2020) Extraction and modification of macroalgal polysaccharides for current and Next-Generation applications. *Molecules* 2020:930

Further Contributions

Coauthorship

Title: Novel marine metalloprotease—new approaches for inhibition of biofilm formation of *Stenotrophomonas maltophilia*

First author: Dr Marie Kristin Peters

Corresponding author: Dr Ines Krohn

Co-authors: Dr Yekaterina Astafyeva
Dr Yuchen Han
Jascha F. H. Macdonald
Dr Daniela Indenbirken
Dr Jacqueline Nakel
Dr Sanamjeet Viridi
Dr Guido Westhoff
Professor Dr Wolfgang R. Streit

Journal: Applied Microbiology and Biotechnology

Accepted: 7th September 2023

Published: 27rd September 2023

DOI: <https://doi.org/10.1007/s00253-023-12781-0>

Supervisions

Bachelor Thesis

Author: Johannes Amann
Title: Klonierung und Charakterisierung von potentiellen Polymer-abbauenden Enzymen aus dem Metagenom von *Nannochloropsis salina*
Supervisors: Dr Ines Krohn
Jascha Macdonald
Project: SuReMetS
Date: March 2022

Master Thesis

Author: Mandy Dittmer
Title: Characterisation of the Microbiome from marine and terrestrial Enrichment Cultures based on the Degradation of Polyurea Polymers
Supervisors: Professor Dr Wolfgang Streit
Dr Christel Vollstedt
Jascha Macdonald (Lab supervision)
Project: Bayer CropScience AG (BCS) – Bayer AG
Date: August 2022

References

- Abreu, I. A., and Cabelli, D. E. (2010). Superoxide dismutases—a review of the metal-associated mechanistic variations. *Biochim. Biophys. Acta* 1804, 263–274. doi: 10.1016/j.bbapap.2009.11.005
- Abreu, I. A., Rodriguez, J. A., and Cabelli, D. E. (2005). Theoretical Studies of Manganese and Iron Superoxide Dismutases: Superoxide Binding and Superoxide Oxidation. *J. Phys. Chem. B* 109, 24502–24509. doi: 10.1021/jp052368u
- Adeniyi, O. M., Azimov, U., and Burluka, A. (2018). Algae biofuel: Current status and future applications. *Renew. Sustain. Energy Rev.* 90, 316–335. doi: 10.1016/j.rser.2018.03.067
- Agregán, R., Munekata, P., Franco, D., Carballo, J., Barba, F., and Lorenzo, J. (2018). Antioxidant Potential of Extracts Obtained from Macro- (*Ascophyllum nodosum*, *Fucus vesiculosus* and *Bifurcaria bifurcata*) and Micro-Algae (*Chlorella vulgaris* and *Spirulina platensis*) Assisted by Ultrasound. *Medicines* 5, 33. doi: 10.3390/medicines5020033
- Alberti, K. G. M. M., Eckel, R. H., Grundy, S. M., Zimmet, P. Z., Cleeman, J. I., Donato, K. A., et al. (2009). Harmonizing the metabolic syndrome: a joint interim statement of the International Diabetes Federation Task Force on Epidemiology and Prevention; National Heart, Lung, and Blood Institute; American Heart Association; World Heart Federation; International Atherosclerosis Society; and International Association for the Study of Obesity. *Circulation* 120, 1640–1645. doi: 10.1161/CIRCULATIONAHA.109.192644
- Aremu, A. O., Masondo, N. A., Stirk, W. A., Ördög, V., and Van Staden, J. (2014). Influence of culture age on the phytochemical content and pharmacological activities of five *Scenedesmus* strains. *J. Appl. Phycol.* 26, 407–415. doi: 10.1007/s10811-013-0144-y
- Armutcu, F., Ataymen, M., Atmaca, H., and Gurel, A. (2008). Oxidative stress markers, C-reactive protein and heat shock protein 70 levels in subjects with metabolic syndrome. *Clin. Chem. Lab. Med.* 46, 785–790. doi: 10.1515/CCLM.2008.166
- Barbeyron, T., L'Haridon, S., Michel, G., and Czjzek, M. (2008). *Mariniflexile fucanivorans* sp. nov., a marine member of the Flavobacteriaceae that degrades sulphated fucans from brown algae. *Int. J. Syst. Evol. Microbiol.* 58, 2107–2113. doi: 10.1099/ijs.0.65674-0
- Bayr, H. (2005). Reactive oxygen species: *Crit. Care Med.* 33, S498–S501. doi: 10.1097/01.CCM.0000186787.64500.12
- Becker, S., Scheffel, A., Polz, M. F., and Hehemann, J.-H. (2017). Accurate Quantification of Laminarin in Marine Organic Matter with Enzymes from Marine Microbes. *Appl. Environ. Microbiol.* 83, e03389-16. doi: 10.1128/AEM.03389-16

- Berman, H. M. (2000). The Protein Data Bank. *Nucleic Acids Res.* 28, 235–242. doi: 10.1093/nar/28.1.235
- Brading, M. G., Jass, J., and Lappin-Scott, H. M. (1995). “Dynamics of Bacterial Biofilm Formation,” in *Microbial Biofilms*, eds. H. M. Lappin-Scott and J. W. Costerton (Cambridge University Press), 46–63. doi: 10.1017/CBO9780511525353.004
- Brandon, J. A., Jones, W., and Ohman, M. D. (2019). Multidecadal increase in plastic particles in coastal ocean sediments. *Sci. Adv.* 5, eaax0587. doi: 10.1126/sciadv.aax0587
- Brawley, S. H., Wetherbee, R., and Quatrano, R. S. (1976). Fine-structural studies of the gametes and embryo of *Fucus vesiculosus* L. (Phaeophyta). II. The cytoplasm of the egg and young zygote. *J. Cell Sci.* 20, 255–271. doi: 10.1242/jcs.20.2.255
- Brumm, P. J. (2013). Bacterial genomes: what they teach us about cellulose degradation. *Biofuels* 4, 669–681. doi: 10.4155/bfs.13.44
- Buchholz, P. C. F., Feuerriegel, G., Zhang, H., Perez-Garcia, P., Nover, L., Chow, J., et al. (2022). Plastics degradation by hydrolytic enzymes: The PLASTICS-ACTIVE enzymes database—PAZY. *Proteins Struct. Funct. Bioinforma.* 90, 1443–1456. doi: 10.1002/prot.26325
- Candelaresi, M., Gumiero, A., Adamczyk, K., Robb, K., Bellota-Antón, C., Sangal, V., et al. (2013). A structural and dynamic investigation of the inhibition of catalase by nitric oxide. *Org. Biomol. Chem.* 11, 7778. doi: 10.1039/c3ob41977k
- Chevolot, L., Mulloy, B., Ratiskol, J., Foucault, A., and Collicec-Jouault, S. (2001). A disaccharide repeat unit is the major structure in fucoidans from two species of brown algae. *Carbohydr. Res.* 330, 529–535. doi: 10.1016/S0008-6215(00)00314-1
- Choi, S. S. H., Lynch, B. S., Baldwin, N., Dakoulas, E. W., Roy, S., Moore, C., et al. (2015). Safety evaluation of the human-identical milk monosaccharide, l-fucose. *Regul. Toxicol. Pharmacol.* 72, 39–48. doi: 10.1016/j.yrtph.2015.02.016
- Christaki (E. Χρηστακη), E., Karatzia (M. Καρατζια), M., and Florou-Paneri (Π. Φλωρου-Πανερη), P. (2017). The use of algae in animal nutrition. *J. Hell. Vet. Med. Soc.* 61, 267. doi: 10.12681/jhvms.14894
- Cock, J. M., Peters, A. F., and Coelho, S. M. (2011). Brown algae. *Curr. Biol.* 21, R573–R575. doi: 10.1016/j.cub.2011.05.006
- Commercial Seaweed Market Report (2024). Commercial Seaweed Market by Product (Brown Seaweed, Red Seaweed, and Green Seaweed), by Form (Leaf, Powdered, and Flakes), and by End-User (Agriculture, Food & Beverage, Animal Feed, Cosmetic, and Pharmaceutical) - Global Opportunity Analysis and Industry Forecast, 2024-2030. Available at: <https://www.nextmsc.com/report/commercial-seaweed-market> (Accessed June 25, 2024).

- Coulombier, N., Jauffrais, T., and Lebouvier, N. (2021). Antioxidant Compounds from Microalgae: A Review. *Mar. Drugs* 19, 549. doi: 10.3390/md19100549
- Crawford, C. J., Schultz-Johansen, M., Luong, P., Vidal-Melgosa, S., Hehemann, J.-H., and Seeberger, P. H. (2024). Automated Synthesis of Algal Fucoidan Oligosaccharides. *J. Am. Chem. Soc.* 146, 18320–18330. doi: 10.1021/jacs.4c02348
- Deniaud-Bouët, E., Kervarec, N., Michel, G., Tonon, T., Kloareg, B., and Hervé, C. (2014). Chemical and enzymatic fractionation of cell walls from Fucales: insights into the structure of the extracellular matrix of brown algae. *Ann. Bot.* 114, 1203–1216. doi: 10.1093/aob/mcu096
- Díaz-Resendiz, K. J. G., Covantes-Rosales, C. E., Benítez-Trinidad, A. B., Navidad-Murrieta, M. S., Razura-Carmona, F. F., Carrillo-Cruz, C. D., et al. (2022). Effect of Fucoidan on the Mitochondrial Membrane Potential ($\Delta\Psi_m$) of Leukocytes from Patients with Active COVID-19 and Subjects That Recovered from SARS-CoV-2 Infection. *Mar. Drugs* 20, 99. doi: 10.3390/md20020099
- Dobrinčić, A., Balbino, S., Zorić, Z., Pedisić, S., Bursać Kovačević, D., Elez Garofulić, I., et al. (2020). Advanced Technologies for the Extraction of Marine Brown Algal Polysaccharides. *Mar. Drugs* 18, 168. doi: 10.3390/md18030168
- Drula, E., Garron, M.-L., Dogan, S., Lombard, V., Henrissat, B., and Terrapon, N. (2022). The carbohydrate-active enzyme database: functions and literature. *Nucleic Acids Res.* 50, D571–D577. doi: 10.1093/nar/gkab1045
- Eder, M., and Lütz-Meindl, U. (2010). Analyses and localization of pectin-like carbohydrates in cell wall and mucilage of the green alga *Netrium digitus*. *Protoplasma* 243, 25–38. doi: 10.1007/s00709-009-0040-0
- Eilers, H., Pernthaler, J., and Amann, R. (2000). Succession of Pelagic Marine Bacteria during Enrichment: a Close Look at Cultivation-Induced Shifts. *Appl. Environ. Microbiol.* 66, 4634–4640. doi: 10.1128/AEM.66.11.4634-4640.2000
- EL-Sabagh, M. R., Abd Eldaim, M. A., Mahboub, D. H., and Abdel-Daim, M. (2014). Effects of *Spirulina Platensis* Algae on Growth Performance, Antioxidative Status and Blood Metabolites in Fattening Lambs. *J. Agric. Sci.* 6, p92. doi: 10.5539/jas.v6n3p92
- Feng, J., Qian, Y., Zhou, Z., Ertmer, S., Vivas, E. I., Lan, F., et al. (2022). Polysaccharide utilization loci in *Bacteroides* determine population fitness and community-level interactions. *Cell Host Microbe* 30, 200–215.e12. doi: 10.1016/j.chom.2021.12.006
- Fernández-Arrojo, L., Guazzaroni, M.-E., López-Cortés, N., Beloqui, A., and Ferrer, M. (2010). Metagenomic era for biocatalyst identification. *Curr. Opin. Biotechnol.* 21, 725–733. doi: 10.1016/j.copbio.2010.09.006
- Field, C. B., Behrenfeld, M. J., Randerson, J. T., and Falkowski, P. (1998). Primary Production of the Biosphere: Integrating Terrestrial and Oceanic Components. *Science* 281, 237–240. doi: 10.1126/science.281.5374.237

- Fletcher, H. R., Biller, P., Ross, A. B., and Adams, J. M. M. (2017). The seasonal variation of fucoidan within three species of brown macroalgae. *Algal Res.* 22, 79–86. doi: 10.1016/j.algal.2016.10.015
- Flieger, J., Flieger, W., Baj, J., and Maciejewski, R. (2021). Antioxidants: Classification, Natural Sources, Activity/Capacity Measurements, and Usefulness for the Synthesis of Nanoparticles. *Materials* 14, 4135. doi: 10.3390/ma14154135
- Francenia Santos-Sánchez, N., Salas-Coronado, R., Villanueva-Cañongo, C., and Hernández-Carlos, B. (2019). “Antioxidant Compounds and Their Antioxidant Mechanism,” in *Antioxidants*, ed. E. Shalaby (IntechOpen). doi: 10.5772/intechopen.85270
- Gojkovic, Z., Lindberg, R. H., Tysklind, M., and Funk, C. (2019). Northern green algae have the capacity to remove active pharmaceutical ingredients. *Ecotoxicol. Environ. Saf.* 170, 644–656. doi: 10.1016/j.ecoenv.2018.12.032
- Gómez, I., and Huovinen, P. (2010). Induction of Phlorotannins During UV Exposure Mitigates Inhibition of Photosynthesis and DNA Damage in the Kelp *Lessonia nigrescens*. *Photochem. Photobiol.* 86, 1056–1063. doi: 10.1111/j.1751-1097.2010.00786.x
- Gong, Y., Shang, D.-D., Sun, C.-L., Du, Z.-J., and Chen, G.-J. (2024). Direct Degradation of Fresh and Dried Macroalgae by *Agarivorans albus* B2Z047. *Mar. Drugs* 22, 203. doi: 10.3390/md22050203
- Goodsell, D. S. (2004). Catalase. *RCSB Protein Data Bank*. doi: 10.2210/rcsb_pdb/mom_2004_9
- Grondin, J. M., Tamura, K., Déjean, G., Abbott, D. W., and Brumer, H. (2017). Polysaccharide Utilization Loci: Fueling Microbial Communities. *J. Bacteriol.* 199. doi: 10.1128/JB.00860-16
- Guiry, M. D. (2024). How many species of algae are there? A reprise. Four kingdoms, 14 phyla, 63 classes and still growing. *J. Phycol.* 60, 214–228. doi: 10.1111/jpy.13431
- Hahn, T., Lang, S., Ulber, R., and Muffler, K. (2012). Novel procedures for the extraction of fucoidan from brown algae. *Process Biochem.* 47, 1691–1698. doi: 10.1016/j.procbio.2012.06.016
- Hamidi, M., Kozani, P. S., Kozani, P. S., Pierre, G., Michaud, P., and Delattre, C. (2019). Marine Bacteria versus Microalgae: Who Is the Best for Biotechnological Production of Bioactive Compounds with Antioxidant Properties and Other Biological Applications? *Mar. Drugs* 18, 28. doi: 10.3390/md18010028
- He, X., Yan, W., Chen, X., Li, Q., Li, M., Yan, Y., et al. (2024). Degradation of algae promotes the release of arsenic from sediments under high-sulfate conditions. *Environ. Pollut.* 342, 123154. doi: 10.1016/j.envpol.2023.123154
- Herlemann, D. P. R., Lundin, D., Andersson, A. F., Labrenz, M., and Jürgens, K. (2016). Phylogenetic Signals of Salinity and Season in Bacterial Community

- Composition Across the Salinity Gradient of the Baltic Sea. *Front. Microbiol.* 7. doi: 10.3389/fmicb.2016.01883
- Holeton, C., Lindell, K., Holmborn, T., Hogfors, H., and Gorokhova, E. (2009). Decreased astaxanthin at high feeding rates in the calanoid copepod *Acartia bifilosa*. *J. Plankton Res.* 31, 661–668. doi: 10.1093/plankt/fbp016
- Holm, L. (2022). Dali server: structural unification of protein families. *Nucleic Acids Res.* 50, W210–W215. doi: 10.1093/nar/gkac387
- Huang, J., Gao, K., Yang, L., and Lu, Y. (2023). Successional action of Bacteroidota and Firmicutes in decomposing straw polymers in a paddy soil. *Environ. Microbiome* 18, 76. doi: 10.1186/s40793-023-00533-6
- Hwang, P.-A., Hung, Y.-L., and Chien, S.-Y. (2015). Inhibitory activity of *Sargassum hemiphyllum* sulfated polysaccharide in arachidonic acid-induced animal models of inflammation. *J. Food Drug Anal.* 23, 49–56. doi: 10.1016/j.jfda.2014.05.004
- Jefferson, K. K. (2004). What drives bacteria to produce a biofilm? *FEMS Microbiol. Lett.* 236, 163–173. doi: 10.1111/j.1574-6968.2004.tb09643.x
- Johnson, W. G. (2015). “Disorders of Glycoprotein Degradation,” in *Rosenberg’s Molecular and Genetic Basis of Neurological and Psychiatric Disease*, (Elsevier), 369–383. doi: 10.1016/B978-0-12-410529-4.00033-4
- Joshi, S., Kumari, R., and Upasani, V. N. (2018). Applications of Algae in Cosmetics: An Overview. 7.
- Jumper, J., Evans, R., Pritzel, A., Green, T., Figurnov, M., Ronneberger, O., et al. (2021). Highly accurate protein structure prediction with AlphaFold. *Nature* 596, 583–589. doi: 10.1038/s41586-021-03819-2
- Kaihou, S., Hayashi, T., Otsuru, O., and Maeda, M. (1993). Studies on the cell-wall mannan of the siphonous green algae, *Codium latum*. *Carbohydr. Res.* 240, 207–218. doi: 10.1016/0008-6215(93)84184-8
- Keen, M. A., and Hassan, I. (2016). Vitamin E in dermatology. *Indian Dermatol. Online J.* 7, 311–315. doi: 10.4103/2229-5178.185494
- Khotimchenko, M., Tiasto, V., Kalitnik, A., Begun, M., Khotimchenko, R., Leonteva, E., et al. (2020). Antitumor potential of carrageenans from marine red algae. *Carbohydr. Polym.* 246, 116568. doi: 10.1016/j.carbpol.2020.116568
- Koivikko, R., Loponen, J., Honkanen, T., and Jormalainen, V. (2005). CONTENTS OF SOLUBLE, CELL-WALL-BOUND AND EXUDED PHLOROTANNINS IN THE BROWN ALGA *Fucus vesiculosus*, WITH IMPLICATIONS ON THEIR ECOLOGICAL FUNCTIONS. *J. Chem. Ecol.* 31, 195–212. doi: 10.1007/s10886-005-0984-2
- Koshland, D. E. (1953). STEREOCHEMISTRY AND THE MECHANISM OF ENZYMATIC REACTIONS. *Biol. Rev.* 28, 416–436. doi: 10.1111/j.1469-185X.1953.tb01386.x

- Kouzuma, A., and Watanabe, K. (2015). Exploring the potential of algae/bacteria interactions. *Curr. Opin. Biotechnol.* 33, 125–129. doi: 10.1016/j.copbio.2015.02.007
- Kovaľová, T., Kovaľ, T., Benešová, E., Vodičková, P., Spiwok, V., Lipovová, P., et al. (2018). Active site complementation and hexameric arrangement in the GH family 29; a structure–function study of α -L-fucosidase isoenzyme 1 from *Paenibacillus thiaminolyticus*. *Glycobiology*. doi: 10.1093/glycob/cwy078
- Koyande, A. K., Show, P.-L., Guo, R., Tang, B., Ogino, C., and Chang, J.-S. (2019). Bio-processing of algal bio-refinery: a review on current advances and future perspectives. *Bioengineered* 10, 574–592. doi: 10.1080/21655979.2019.1679697
- Krohn, I., Menanteau-Ledouble, S., Hageskal, G., Astafyeva, Y., Jouannais, P., Nielsen, J. L., et al. (2022). Health benefits of microalgae and their microbiomes. *Microb. Biotechnol.* 15, 1966–1983. doi: 10.1111/1751-7915.14082
- Lachnit, T., Meske, D., Wahl, M., Harder, T., and Schmitz, R. (2011). Epibacterial community patterns on marine macroalgae are host-specific but temporally variable. *Environ. Microbiol.* 13, 655–665. doi: 10.1111/j.1462-2920.2010.02371.x
- Lee, O. K., and Lee, E. Y. (2016). Sustainable production of bioethanol from renewable brown algae biomass. *Biomass Bioenergy* 92, 70–75. doi: 10.1016/j.biombioe.2016.03.038
- Li, H., Dong, T., Tao, M., Zhao, H., Lan, T., Yan, S., et al. (2024). Fucoidan enhances the anti-tumor effect of anti-PD-1 immunotherapy by regulating gut microbiota. *Food Funct.* 15, 3463–3478. doi: 10.1039/d3fo04807a
- Li, J., He, Z., Liang, Y., Peng, T., and Hu, Z. (2022). Insights into Algal Polysaccharides: A Review of Their Structure, Depolymerases, and Metabolic Pathways. *J. Agric. Food Chem.* 70, 1749–1765. doi: 10.1021/acs.jafc.1c05365
- Li, T., Li, M., Hou, L., Guo, Y., Wang, L., Sun, G., et al. (2018). Identification and characterization of a core fucosidase from the bacterium *Elizabethkingia meningoseptica*. *J. Biol. Chem.* 293, 1243–1258. doi: 10.1074/jbc.M117.804252
- Li, X., Bi, X., Wang, S., Zhang, Z., Li, F., and Zhao, A. Z. (2019). Therapeutic Potential of ω -3 Polyunsaturated Fatty Acids in Human Autoimmune Diseases. *Front. Immunol.* 10, 2241. doi: 10.3389/fimmu.2019.02241
- Li, Y., Zheng, Y., Zhang, Y., Yang, Y., Wang, P., Imre, B., et al. (2021). Brown Algae Carbohydrates: Structures, Pharmaceutical Properties, and Research Challenges. *Mar. Drugs* 19, 620. doi: 10.3390/md19110620
- Liou, G.-Y., and Storz, P. (2010). Reactive oxygen species in cancer. *Free Radic. Res.* 44, 479–496. doi: 10.3109/10715761003667554
- Liu, Y., Cao, L., Cheung, W. W. L., and Sumaila, U. R. (2023). Global estimates of suitable areas for marine algae farming. *Environ. Res. Lett.* 18, 064028. doi: 10.1088/1748-9326/acd398

- Macdonald, J. F. H., Han, Y., Astafyeva, Y., Bergmann, L., Gurschke, M., Dirksen, P., et al. (2025). Exploring *Tetraselmis chui* microbiomes—functional metagenomics for novel catalases and superoxide dismutases. *Appl. Microbiol. Biotechnol.* 109, 6. doi: 10.1007/s00253-024-13395-w
- Macdonald, J. F. H., Pérez-García, P., Schneider, Y. K.-H., Blümke, P., Indenbirken, D., Andersen, J. H., et al. (2024). Community dynamics and metagenomic analyses reveal Bacteroidota's role in widespread enzymatic *Fucus vesiculosus* cell wall degradation. *Sci. Rep.* 14, 10237. doi: 10.1038/s41598-024-60978-8
- Makita, A., and Taniguchi, N. (1985). "Glycosphingolipids * *Sialic acid-containing glycosphingolipids (the gangliosides) are discussed in a separate chapter (see Chapter 3).," in *New Comprehensive Biochemistry*, (Elsevier), 1–99. doi: 10.1016/S0167-7306(08)60020-4
- Mapelli-Brahm, P., Gómez-Villegas, P., Gonda, M. L., León-Vaz, A., León, R., Mildenerger, J., et al. (2023). Microalgae, Seaweeds and Aquatic Bacteria, Archaea, and Yeasts: Sources of Carotenoids with Potential Antioxidant and Anti-Inflammatory Health-Promoting Actions in the Sustainability Era. *Mar. Drugs* 21, 340. doi: 10.3390/md21060340
- Mardis, E. R. (2011). A decade's perspective on DNA sequencing technology. *Nature* 470, 198–203. doi: 10.1038/nature09796
- Marhl, M., Grubelnik, V., Magdič, M., and Markovič, R. (2020). Diabetes and metabolic syndrome as risk factors for COVID-19. *Diabetes Metab. Syndr. Clin. Res. Rev.* 14, 671–677. doi: 10.1016/j.dsx.2020.05.013
- Martin, K., Schmidt, K., Toseland, A., Boulton, C. A., Barry, K., Beszteri, B., et al. (2021). The biogeographic differentiation of algal microbiomes in the upper ocean from pole to pole. *Nat. Commun.* 12, 5483. doi: 10.1038/s41467-021-25646-9
- McCarter, J. D., and Stephen Withers, G. (1994). Mechanisms of enzymatic glycoside hydrolysis. *Curr. Opin. Struct. Biol.* 4, 885–892. doi: 10.1016/0959-440X(94)90271-2
- Mensch, B., Neulinger, S. C., Graiff, A., Pansch, A., Künzel, S., Fischer, M. A., et al. (2016). Restructuring of Epibacterial Communities on *Fucus vesiculosus* forma *mytili* in Response to Elevated pCO₂ and Increased Temperature Levels. *Front. Microbiol.* 7. doi: 10.3389/fmicb.2016.00434
- Moon, S.-H., and Cho, S.-J. (2023). Evaluation of the antioxidant activity of *Tetraselmis chuii* after in vitro gastrointestinal digestion and investigation of its antioxidant peptides. *Algal Res.* 76, 103328. doi: 10.1016/j.algal.2023.103328
- Moser, G. A. O., Barrera-Alba, J. J., Ortega, M. J., Alves-de-Souza, C., and Bartual, A. (2022). Comparative characterization of three *Tetraselmis chui* (Chlorophyta) strains as sources of nutraceuticals. *J. Appl. Phycol.* 34, 821–835. doi: 10.1007/s10811-021-02675-x
- Murshudov, G. N., Grebenko, A. I., Brannigan, J. A., Antson, A. A., Barynin, V. V., Dodson, G. G., et al. (2002). The structures of *Micrococcus lysodeikticus*

- catalase, its ferryl intermediate (compound II) and NADPH complex. *Acta Crystallogr. D Biol. Crystallogr.* 58, 1972–1982. doi: 10.1107/S0907444902016566
- Nguyen, T. T. H., Vuong, T. Q., Han, H. L., Li, Z., Lee, Y.-J., Ko, J., et al. (2023). Three marine species of the genus *Fulvivirga*, rich sources of carbohydrate-active enzymes degrading alginate, chitin, laminarin, starch, and xylan. *Sci. Rep.* 13, 6301. doi: 10.1038/s41598-023-33408-4
- Oliver, J. D. (1993). “Formation of Viable but Nonculturable Cells,” in *Starvation in Bacteria*, ed. S. Kjelleberg (Boston, MA: Springer US), 239–272. doi: 10.1007/978-1-4899-2439-1_11
- Oppong-Danquah, E., Blümel, M., and Tasdemir, D. (2023). Metabolomics and Microbiomics Insights into Differential Surface Fouling of Three Macroalgal Species of *Fucus* (Fucales, Phaeophyceae) That Co-Exist in the German Baltic Sea. *Mar. Drugs* 21, 595. doi: 10.3390/md21110595
- Park, Y.-W., Zhu, S., Palaniappan, L., Heshka, S., Carnethon, M. R., and Heymsfield, S. B. (2003). The metabolic syndrome: prevalence and associated risk factor findings in the US population from the Third National Health and Nutrition Examination Survey, 1988-1994. *Arch. Intern. Med.* 163, 427–436. doi: 10.1001/archinte.163.4.427
- Parrot, D., Blümel, M., Utermann, C., Chianese, G., Krause, S., Kovalev, A., et al. (2019). Mapping the Surface Microbiome and Metabolome of Brown Seaweed *Fucus vesiculosus* by Amplicon Sequencing, Integrated Metabolomics and Imaging Techniques. *Sci. Rep.* 9, 1061. doi: 10.1038/s41598-018-37914-8
- Pawar, R., Mohandass, C., Sivaperumal, E., Sabu, E., Rajasabapathy, R., and Jagtap, T. (2015). Epiphytic marine pigmented bacteria: A prospective source of natural antioxidants. *Braz. J. Microbiol.* 46, 29–39. doi: 10.1590/S1517-838246120130353
- Perkins, A. K., Santos, I. R., Rose, A. L., Schulz, K. G., Grossart, H.-P., Eyre, B. D., et al. (2022). Production of dissolved carbon and alkalinity during macroalgal wrack degradation on beaches: a mesocosm experiment with implications for blue carbon. *Biogeochemistry* 160, 159–175. doi: 10.1007/s10533-022-00946-4
- Peters, M. K., Astafyeva, Y., Han, Y., Macdonald, J. F. H., Indenbirken, D., Nakel, J., et al. (2023). Novel marine metalloprotease—new approaches for inhibition of biofilm formation of *Stenotrophomonas maltophilia*. *Appl. Microbiol. Biotechnol.* 107, 7119–7134. doi: 10.1007/s00253-023-12781-0
- Pettersen, E. F., Goddard, T. D., Huang, C. C., Couch, G. S., Greenblatt, D. M., Meng, E. C., et al. (2004). UCSF Chimera—A visualization system for exploratory research and analysis. *J. Comput. Chem.* 25, 1605–1612. doi: 10.1002/jcc.20084
- Plaza, M., Herrero, M., Cifuentes, A., and Ibáñez, E. (2009). Innovative Natural Functional Ingredients from Microalgae. *J. Agric. Food Chem.* 57, 7159–7170. doi: 10.1021/jf901070g

- Qin, H.-M., Miyakawa, T., Inoue, A., Nakamura, A., Nishiyama, R., Ojima, T., et al. (2017). Laminarinase from *Flavobacterium* sp. reveals the structural basis of thermostability and substrate specificity. *Sci. Rep.* 7, 11425. doi: 10.1038/s41598-017-11542-0
- Qiu, S., Shen, Y., Zhang, L., Ma, B., Amadu, A. A., and Ge, S. (2020). Antioxidant assessment of wastewater-cultivated *Chlorella sorokiniana* in *Drosophila melanogaster*. *Algal Res.* 46, 101795. doi: 10.1016/j.algal.2020.101795
- Radulovich, R., Neori, A., Valderrama, D., Reddy, C. R. K., Cronin, H., and Forster, J. (2015). "Farming of seaweeds," in *Seaweed Sustainability*, (Elsevier), 27–59. doi: 10.1016/B978-0-12-418697-2.00003-9
- Rahman, N. A., Khatoon, H., Yusuf, N., Banerjee, S., Haris, N. A., Lananan, F., et al. (2017). *Tetraselmis chuii* biomass as a potential feed additive to improve survival and oxidative stress status of Pacific white-leg shrimp *Litopenaeus vannamei* postlarvae. *Int. Aquat. Res.* 9, 235–247. doi: 10.1007/s40071-017-0173-2
- Reyes-Weiss, D. S., Bligh, M., Rhein-Knudsen, N., Hehemann, J.-H., Liebeke, M., Westereng, B., et al. (2024). Application of MALDI-MS for characterization of fucoidan hydrolysates and screening of endo-fucoidanase activity. *Carbohydr. Polym.* 340, 122317. doi: 10.1016/j.carbpol.2024.122317
- Robic, A., Rondeau-Mouro, C., Sassi, J.-F., Lerat, Y., and Lahaye, M. (2009). Structure and interactions of ulvan in the cell wall of the marine green algae *Ulva rotundata* (Ulvales, Chlorophyceae). *Carbohydr. Polym.* 77, 206–216. doi: 10.1016/j.carbpol.2008.12.023
- Rotter, A., Barbier, M., Bertoni, F., Bones, A. M., Cancela, M. L., Carlsson, J., et al. (2021). The Essentials of Marine Biotechnology. *Front. Mar. Sci.* 8, 629629. doi: 10.3389/fmars.2021.629629
- Rupérez, P., Ahrazem, O., and Leal, J. A. (2002). Potential Antioxidant Capacity of Sulfated Polysaccharides from the Edible Marine Brown Seaweed *Fucus vesiculosus*. *J. Agric. Food Chem.* 50, 840–845. doi: 10.1021/jf010908o
- Saari, U. A., Herstatt, C., Tiwari, R., Dedehayir, O., and Mäkinen, S. J. (2021). The vegan trend and the microfoundations of institutional change: A commentary on food producers' sustainable innovation journeys in Europe. *Trends Food Sci. Technol.* 107, 161–167. doi: 10.1016/j.tifs.2020.10.003
- Sáez, G. T., and Están-Capell, N. (2014). "Antioxidant Enzymes," in *Encyclopedia of Cancer*, ed. M. Schwab (Berlin, Heidelberg: Springer Berlin Heidelberg), 288–294. doi: 10.1007/978-3-662-46875-3_7210
- Safar, H., Van Wagenen, J., Møller, P., and Jacobsen, C. (2015). Carotenoids, Phenolic Compounds and Tocopherols Contribute to the Antioxidative Properties of Some Microalgae Species Grown on Industrial Wastewater. *Mar. Drugs* 13, 7339–7356. doi: 10.3390/md13127069
- Saklayen, M. G. (2018). The Global Epidemic of the Metabolic Syndrome. *Curr. Hypertens. Rep.* 20, 12. doi: 10.1007/s11906-018-0812-z

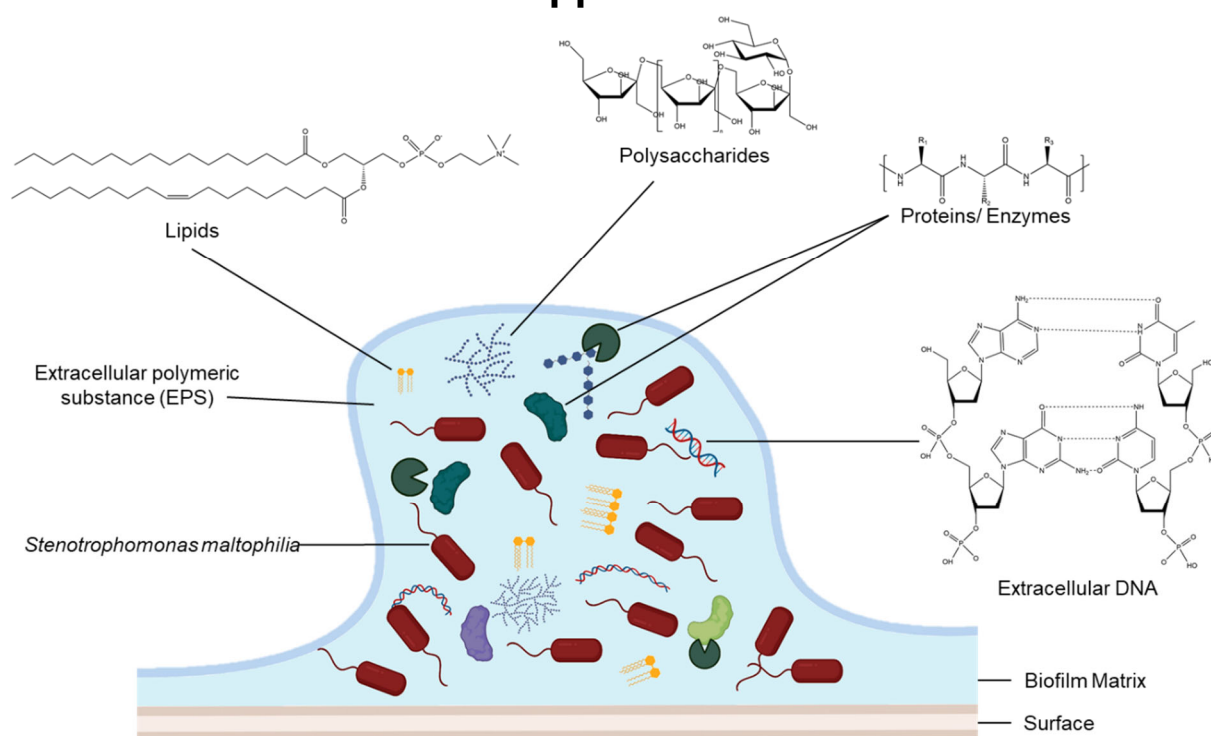
- Sangeetha, J., and Thangadurai, D. eds. (2024). *Algal farming systems: from production to application for a sustainable future.*, First edition. Palm Bay, FL: Apple Academic Press.
- Schagen, S. K., Zampeli, V. A., Makrantonaki, E., and Zouboulis, C. C. (2012). Discovering the link between nutrition and skin aging. *Dermatoendocrinol.* 4, 298–307. doi: 10.4161/derm.22876
- Schultz-Johansen, M., Cueff, M., Hardouin, K., Jam, M., Larocque, R., Glaring, M. A., et al. (2018). Discovery and screening of novel metagenome-derived GH 107 enzymes targeting sulfated fucans from brown algae. *FEBS J.* 285, 4281–4295. doi: 10.1111/febs.14662
- Schwartz, R. E., Hirsch, C. F., Sesin, D. F., Flor, J. E., Chartrain, M., Fromtling, R. E., et al. (1990). Pharmaceuticals from cultured algae. *J. Ind. Microbiol.* 5, 113–123. doi: 10.1007/BF01573860
- Sichert, A., Corzett, C. H., Schechter, M. S., Unfried, F., Markert, S., Becher, D., et al. (2020). Verrucomicrobia use hundreds of enzymes to digest the algal polysaccharide fucoidan. *Nat. Microbiol.* 5, 1026–1039. doi: 10.1038/s41564-020-0720-2
- Silchenko, A. S., Ustyuzhanina, N. E., Kusaykin, M. I., Krylov, V. B., Shashkov, A. S., Dmitrenok, A. S., et al. (2016). Expression and biochemical characterization and substrate specificity of the fucoidanase from *Formosa algae*. *Glycobiology*, glycob; cww138v3. doi: 10.1093/glycob/cww138
- Silverio, M. P., Neumann, T., Schaubruch, K., Heermann, R., Pérez-García, P., Chow, J., et al. (2024). Metagenome-derived SusD-homologs affiliated with Bacteroidota bind to synthetic polymers. *Appl. Environ. Microbiol.*, e00933-24. doi: 10.1128/aem.00933-24
- Smith, Michael W., and Doolittle, Russell F. (1992). A comparison of evolutionary rates of the two major kinds of superoxide dismutase. *J. Mol. Evol.* 34. doi: 10.1007/BF00182394
- Snoeijs-Leijonmalm, P., and Andrén, E. (2017). “Why is the Baltic Sea so special to live in?,” in *Biological Oceanography of the Baltic Sea*, eds. P. Snoeijs-Leijonmalm, H. Schubert, and T. Radziejewska (Dordrecht: Springer Netherlands), 23–84. doi: 10.1007/978-94-007-0668-2_2
- Soeder, D. J. (2021). “Fossil Fuels and Climate Change,” in *Fracking and the Environment*, (Cham: Springer International Publishing), 155–185. doi: 10.1007/978-3-030-59121-2_9
- Solano, C., Echeverz, M., and Lasa, I. (2014). Biofilm dispersion and quorum sensing. *Curr. Opin. Microbiol.* 18, 96–104. doi: 10.1016/j.mib.2014.02.008
- Song, Y., Singh, A., Feroz, M. M., Xu, S., Zhang, F., Jin, W., et al. (2024). Seaweed-derived fucoidans and rhamnan sulfates serve as potent anti-SARS-CoV-2 agents with potential for prophylaxis. *Carbohydr. Polym.* 337, 122156. doi: 10.1016/j.carbpol.2024.122156

- Stal, L. J., and Cretoiu, M. S. eds. (2022). *The Marine Microbiome*. Cham: Springer International Publishing. doi: 10.1007/978-3-030-90383-1
- Steimbrüch, B. A., Sartorio, M. G., Cortez, N., Albanesi, D., Lisa, M.-N., and Repizo, G. D. (2022). The distinctive roles played by the superoxide dismutases of the extremophile *Acinetobacter* sp. Ver3. *Sci. Rep.* 12, 4321. doi: 10.1038/s41598-022-08052-z
- Steinman, H. M. (1978). The amino acid sequence of mangano superoxide dismutase from *Escherichia coli* B. *J. Biol. Chem.* 253, 8708–8720.
- Steinrücken, P., Jackson, S., Müller, O., Puntervoll, P., and Kleinegris, D. M. M. (2023). A closer look into the microbiome of microalgal cultures. *Front. Microbiol.* 14, 1108018. doi: 10.3389/fmicb.2023.1108018
- Stern, J. L., Hagerman, A. E., Steinberg, P. D., and Mason, P. K. (1996). Phlorotannin-protein interactions. *J. Chem. Ecol.* 22, 1877–1899. doi: 10.1007/BF02028510
- Storz, P. (2005). Reactive oxygen species in tumor progression. *Front. Biosci.* 10, 1881. doi: 10.2741/1667
- Stratil, S. B., Neulinger, S. C., Knecht, H., Friedrichs, A. K., and Wahl, M. (2013). Temperature-driven shifts in the epibiotic bacterial community composition of the brown macroalga *Fucus vesiculosus*. *MicrobiologyOpen* 2, 338–349. doi: 10.1002/mbo3.79
- Szatrowski, T. P., and Nathan, C. F. (1991). Production of large amounts of hydrogen peroxide by human tumor cells. *Cancer Res.* 51, 794–798.
- Takao, T., Kitatani, F., Watanabe, N., Yagi, A., and Sakata, K. (1994). A Simple Screening Method for Antioxidants and Isolation of Several Antioxidants Produced by Marine Bacteria from Fish and Shellfish. *Biosci. Biotechnol. Biochem.* 58, 1780–1783. doi: 10.1271/bbb.58.1780
- Teimouri, M., Yeganeh, S., Mianji, G. R., Najafi, M., and Mahjoub, S. (2019). The effect of *Spirulina platensis* meal on antioxidant gene expression, total antioxidant capacity, and lipid peroxidation of rainbow trout (*Oncorhynchus mykiss*). *Fish Physiol. Biochem.* 45, 977–986. doi: 10.1007/s10695-019-0608-3
- Tripathi, V. C., Horam, S., Singh, A., Lata, M., Reddy, T. J., Arockiaraj, J., et al. (2020). The discovery of antioxidants in marine microorganisms and their protective effects on the hepatic cells from chemical-induced oxidative stress. *Free Radic. Res.* 54, 150–161. doi: 10.1080/10715762.2020.1725499
- Urakawa, H., Katsuki, A., Sumida, Y., Gabazza, E. C., Murashima, S., Morioka, K., et al. (2003). Oxidative stress is associated with adiposity and insulin resistance in men. *J. Clin. Endocrinol. Metab.* 88, 4673–4676. doi: 10.1210/jc.2003-030202
- Usov, A. I. (2011). “Polysaccharides of the red algae,” in *Advances in Carbohydrate Chemistry and Biochemistry*, (Elsevier), 115–217. doi: 10.1016/B978-0-12-385520-6.00004-2

- Van Der Loos, L. M., D'hondt, S., Willems, A., and De Clerck, O. (2021). Characterizing algal microbiomes using long-read nanopore sequencing. *Algal Res.* 59, 102456. doi: 10.1016/j.algal.2021.102456
- Verma, P., Arun, A., and Sahoo, D. (2015). "Brown Algae," in *The Algae World*, eds. D. Sahoo and J. Seckbach (Dordrecht: Springer Netherlands), 177–204. doi: 10.1007/978-94-017-7321-8_6
- Vishchuk, O. S., Sun, H., Wang, Z., Ermakova, S. P., Xiao, J., Lu, T., et al. (2016). PDZ-binding kinase/T-LAK cell-originated protein kinase is a target of the fucoidan from brown alga *Fucus evanescens* in the prevention of EGF-induced neoplastic cell transformation and colon cancer growth. *Oncotarget* 7, 18763–18773. doi: 10.18632/oncotarget.7708
- Voget, S., Leggewie, C., Uesbeck, A., Raasch, C., Jaeger, K.-E., and Streit, W. R. (2003). Prospecting for Novel Biocatalysts in a Soil Metagenome. *Appl. Environ. Microbiol.* 69, 6235–6242. doi: 10.1128/AEM.69.10.6235-6242.2003
- Vreeland, V., Grotkopp, E., Espinosa, S., Quiroz, D., Laetsch, W. M., and West, J. (1993). The pattern of cell wall adhesive formation by *Fucus* zygotes. *Hydrobiologia* 260–261, 485–491. doi: 10.1007/BF00049060
- Walker, J. C. G. (1980). "The Oxygen Cycle," in *The Natural Environment and the Biogeochemical Cycles*, (Berlin, Heidelberg: Springer Berlin Heidelberg), 87–104. doi: 10.1007/978-3-662-24940-6_5
- Wang, H., Zhu, B., and Yao, Z. (2023). Porphyran, porphyran oligosaccharides and porphyranase: Source, structure, preparation methods and applications. *Algal Res.* 73, 103167. doi: 10.1016/j.algal.2023.103167
- Wang, M., Hu, C., Barnes, B. B., Mitchum, G., Lapointe, B., and Montoya, J. P. (2019). The great Atlantic *Sargassum* belt. *Science* 365, 83–87. doi: 10.1126/science.aaw7912
- Wang, Z. Y., Wang, R. X., Zhou, J. S., Cheng, J. F., and Li, Y. H. (2020). An assessment of the genomics, comparative genomics and cellulose degradation potential of *Mucilaginites polytrichastri* strain RG4-7. *Bioresour. Technol.* 297, 122389. doi: 10.1016/j.biortech.2019.122389
- Wells, M. L., Potin, P., Craigie, J. S., Raven, J. A., Merchant, S. S., Helliwell, K. E., et al. (2017). Algae as nutritional and functional food sources: revisiting our understanding. *J. Appl. Phycol.* 29, 949–982. doi: 10.1007/s10811-016-0974-5
- Wietz, M., Wemheuer, B., Simon, H., Giebel, H., Seibt, M. A., Daniel, R., et al. (2015). Bacterial community dynamics during polysaccharide degradation at contrasting sites in the Southern and Atlantic Oceans. *Environ. Microbiol.* 17, 3822–3831. doi: 10.1111/1462-2920.12842
- Yu, B., Lu, Z., Zhong, S., and Cheong, K.-L. (2024). Exploring potential polysaccharide utilization loci involved in the degradation of typical marine seaweed polysaccharides by *Bacteroides thetaiotaomicron*. *Front. Microbiol.* 15, 1332105. doi: 10.3389/fmicb.2024.1332105

-
- Zamocky, M., Furtmüller, P. G., and Obinger, C. (2008). Evolution of Catalases from Bacteria to Humans. *Antioxid. Redox Signal.* 10, 1527–1548. doi: 10.1089/ars.2008.2046
- Zhang, T., Liu, H., Lv, B., and Li, C. (2020). Regulating Strategies for Producing Carbohydrate Active Enzymes by Filamentous Fungal Cell Factories. *Front. Bioeng. Biotechnol.* 8, 691. doi: 10.3389/fbioe.2020.00691
- Zhang, Y.-S., Zhang, Y.-Q., Zhao, X.-M., Liu, X.-L., Qin, Q.-L., Liu, N.-H., et al. (2024). Metagenomic insights into the dynamic degradation of brown algal polysaccharides by kelp-associated microbiota. *Appl. Environ. Microbiol.* 90, e02025-23. doi: 10.1128/aem.02025-23

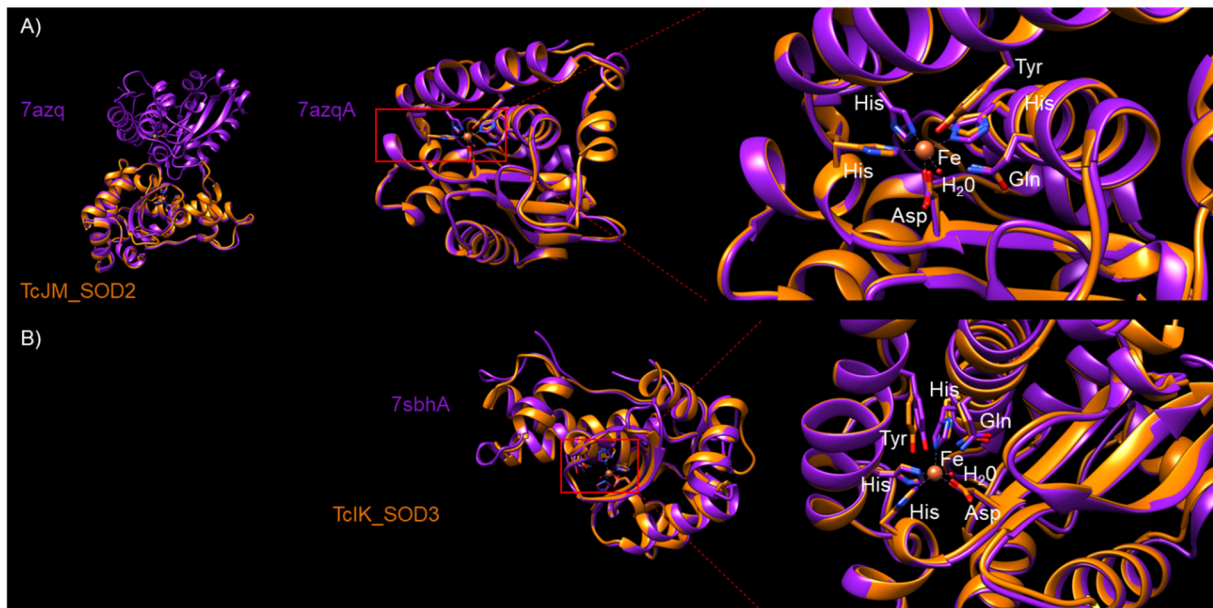
Appendix



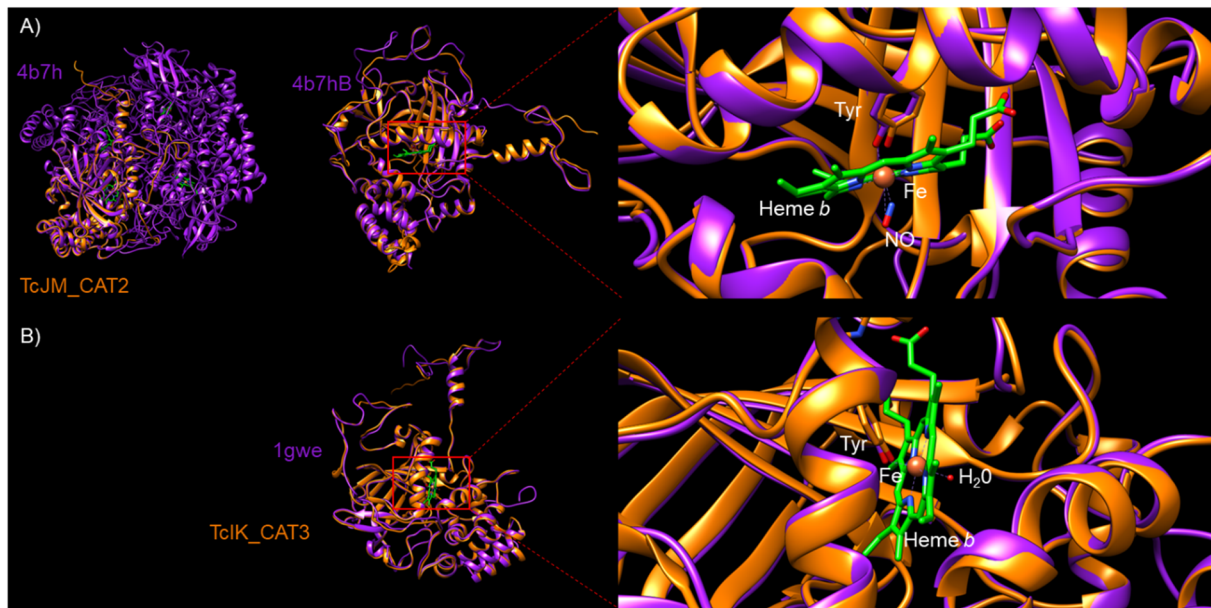
Appendix Figure 1: Model of *S. maltophilia* K279a biofilm structure including selected extrapolymeric substances of lipids (structure: phosphatidylcholin), polysaccharides (structure: levan), proteins/enzymes and extracellular DNA. Created with BioRender.com and ChemDraw 21.0.0.28 (<https://perkinelmerinformatics.com>). Extracted from Figure 6A (authors contribution) in Peters et al., 2023.



Appendix Figure 2: Structure and bonding prediction of a functional FUJM20 dimer. Structure and bonding predicted with AlphaFold2, visualised with UCSF Chimera v1.177.3 and ChimeraX v1.8 (Pettersen et al., 2004; Jumper et al., 2021).



Appendix Figure 3: Predicted structures and comparison of cloned, functional Superoxide Dismutases derived from the *Tetraselmis chui* microbiome. Structures predicted with AlphaFold2, visualised with UCSF Chimera v1.177.3, structure searches and all-vs-all comparison applied with Dali Server against structures derived from the RCSB Protein database (PDB, <https://www.rcsb.org>) (Berman, 2000; Pettersen et al., 2004; Jumper et al., 2021; Holm, 2022). **A)** Structure comparison of TcJM_SOD2 to “Crystal structure of the iron/manganese cambialistic superoxide dismutase from *Rhodobacter capsulatus* complex with Fe” (7azq, <https://doi.org/10.2210/pdb7AZQ/pdb>) (z-value 0.5 Å). Overview displayed by a dimer structure of 7azq and a detailed view of the aligned protein chains. Detailed view of the active site containing the Iron-atom. The active site of 7azq consists of the residues His28, His82, Asp165, His169 that orientate the Iron and Tyr36 as well as Gln78. The assumed corresponding residues of TcJM_SOD2 are His28, Tyr36, Gln78, His82, Asp164 and His168. **B)** Structure comparison of TcIK_SOD3 to “Crystal structure of the iron superoxide dismutase from *Acinetobacter* sp. Ver3” (7sbh, <https://doi.org/10.2210/pdb7SBH/pdb>) (z-value 1.2 Å). Detailed view of the aligned protein chains. Detailed view of the active site containing the Iron-atom. The active site of 7sbh consists of the residues His28, His80, Asp164, His168 that orientate the Iron and Tyr36 as well as Gln76. The assumed corresponding residues of TcJM_SOD2 are His27, Tyr35, Gln73, His77, Asp160 and His164.



Appendix Figure 4: Predicted structures and comparison of cloned, functional Catalases derived from the *Tetraselmis chui* microbiome. Structures predicted with AlphaFold2, visualised with UCSF Chimera v1.177.3, structure searches and all-vs-all comparison applied with Dali Server against structures derived from the RCSB Protein database (PDB, <https://www.rcsb.org>) (Berman, 2000; Pettersen et al., 2004; Jumper et al., 2021; Holm, 2022). **A)** Structure comparison of TcJM_CAT2 to “Structure of a highdose liganded bacterial catalase” (4b7h, <https://doi.org/10.2210/pdb4B7H/pdb>) (z-value 1.2 Å). Overview displayed by a dimer structure of 4b7h and a detailed view of the aligned protein chains. Detailed view of the active site containing the Heme *b*. The active site of 4b7h consists of the Heme *b* and residue Tyr353. The assumed corresponding residue of TcJM_SOD2 is Tyr342. **B)** Structure comparison of TcIK_CAT3 to “Atomic resolution structure of *Micrococcus lysodeikticus* catalase” (1gwe, <https://doi.org/10.2210/pdb1GWE/pdb>) (z-value 1.6 Å). Detailed view of the aligned protein chains. Detailed view of the active site containing the Heme *b*. The active site of 1gwe consists of the Heme *b* and residue Tyr343. The assumed corresponding residue of TcJM_SOD2 is Tyr339.

Appendix Table 1: Supportive data for Figure 7.

No.	IMG Query ID	HMM	HMM score	BlastP subject	BlastP Identity	Species
A)	Ga0483890_					<i>Chlorella vulgaris</i>
1	00007_436	Sod_Fe_N	87	WP_223613760.1	99.6	<i>Phyllobacterium calauticae</i>
2	00008_164	Sod_Fe_N	82.5	WP_181267511.1	100	<i>Sphingomonas ursincola</i>
3	00019_214	Sod_Fe_N	101.6	WP_235148482.1	86.4	<i>Dyadobacter</i> sp. CY345
4	00037_206	Sod_Fe_N	87.3	WP_305572893.1	97.5	<i>Phreatobacter</i> sp.
5	00038_119	Sod_Fe_N	92.7	WP_137932185.1	100	<i>Mesorhizobium comanense</i>
6	00043_100	Sod_Fe_N	94.5	WP_105737248.1	100	<i>Phyllobacterium</i> sp.
7	00048_98	Sod_Fe_N	111.3	WP_295934642.1	97	uncultured <i>Dyadobacter</i> sp.
8	00049_98	Sod_Fe_N	111.3	WP_295934642.1	97	uncultured <i>Dyadobacter</i> sp.
9	00095_64	Sod_Fe_N	92.7	WP_075152223.1	98.5	<i>Sphingomonas koreensis</i>
10	00113_3	Sod_Fe_N	104.3	WP_013544049.1	99.5	<i>Variovorax paradoxus</i>
11	00221_40	Sod_Fe_N	99.4	WP_034463928.1	96.5	<i>Afipia</i> sp. P52-10
12	00354_46	Sod_Fe_N	103.7	WP_013541695.1	99	<i>Variovorax</i> sp.

13	00660_29	Sod_Fe_C	77.7	KAI3433430.1	100	<i>Chlorella vulgaris</i>
14	00660_30	Sod_Fe_N	38.8	KAI3433430.1	100	<i>Chlorella vulgaris</i>
15	00702_18	Sod_Fe_C	63.1	KAI3428127.1	86.7	<i>Chlorella vulgaris</i>
16	01276_2	Sod_Fe_N	103.3	WP_296571591.1	100	<i>Phreatobacter</i> sp.
17	02398_5	Sod_Fe_N	105	WP_265080492.1	98	<i>Rhodopseudomonas</i> sp. P2A-2r
18	02576_12	Sod_Fe_C	59.2	KAI3435487.1	61.5	<i>Chlorella vulgaris</i>
19	02576_6	Sod_Fe_C	74.2	KAI3435486.1	98.5	<i>Chlorella vulgaris</i>
20	02576_8	Sod_Fe_N	41.8	KAI3435486.1	100	<i>Chlorella vulgaris</i>
21	03036_2	Sod_Fe_N	99.2	WP_137871339.1	99.5	<i>Sphingopyxis</i> sp. 2PD
22	03179_10	Sod_Fe_C	46.8	KAI3431838.1	100	<i>Chlorella vulgaris</i>
23	03179_2	Sod_Fe_C	46.8	KAI3431838.1	100	<i>Chlorella vulgaris</i>
24	03179_9	Sod_Fe_C	23	KAI3431838.1	100	<i>Chlorella vulgaris</i>
25	03719_2	Sod_Fe_N	100.8	WP_043351079.1	99.5	<i>Methylobacterium</i> sp.
26	03893_4	Sod_Fe_N	87.2	WP_068734157.1	94.7	<i>Tardiphaga robiniae</i>
B)	Ga0483890_					<i>Chlorella vulgaris</i>
1	00001_522	Catalase	593.1	WP_340035255.1	91.4	<i>Aminobacter</i> sp. Piv2-1
2	00009_431	Catalase	611.8	WP_223611615.1	99.6	<i>Phyllobacterium</i> <i>calauticae</i>
3	00022_178	Catalase	603.7	WP_019943699.1	86.3	<i>Dyadobacter</i> <i>beijingensis</i>
4	00029_176	Catalase	80	WP_305577679.1	93.6	<i>Phreatobacter</i> sp.
5	00063_131	Catalase	586.2	WP_169571150.1	88.5	<i>Sphingobium</i> <i>psychrophilum</i>
6	00085_54	Catalase	598.2	WP_273304227.1	99.6	<i>Sphingomonadaceae</i> sp.
7	00170_21	Catalase	84.9	QNQ11853.1	72.8	<i>Sphingomonas</i> <i>alpina</i>
8	00192_32	Catalase	637.5	WP_034465763.1	94.1	<i>Afipia</i> sp. P52-10
9	00245_22	Catalase	617.3	WP_286517245.1	97.1	<i>Variovorax</i> sp.
10	00331_43	Catalase	611.8	WP_056521151.1	88.2	<i>Variovorax</i> sp. Root411
11	00440_37	Catalase	114.4	WP_091995066.1	100	<i>Methylobacterium</i> sp.
12	00550_31	Catalase	556	WP_179698242.1	99.6	<i>Methylobacterium</i> sp.
13	01108_16	Catalase	545.4	WP_093218129.1	88.2	<i>Variovorax</i> sp.
14	01131_16	Catalase	129.4	WP_274929355.1	100	<i>Methylobacterium</i> sp. 092160098-2
15	02422_1	Catalase	59.3	KAI3425754.1	41.1	<i>Chlorella vulgaris</i>
16	03650_1	Catalase	55.1	XP_005847557.1	97.3	<i>Chlorella variabilis</i>
17	03878_1	Catalase	84.5	WP_043757105.1	100	<i>Methylobacterium</i> sp.
18	06692_1	Catalase	43.7	KAI3425754.1	97.3	<i>Chlorella vulgaris</i>
19	06692_2	Catalase	48	KAI3425754.1	95.7	<i>Chlorella vulgaris</i>
20	06692_3	Catalase	103.3	KAI3425754.1	98.5	<i>Chlorella vulgaris</i>
C)	Ga0500404_					
3	00001_595	Sod_Fe_N	102.7	WP_043949068.1	91.5	<i>Candidatus</i> <i>Phaeomarinobacter</i> <i>ectocarpi</i>
4	00023_243	Sod_Fe_N	101	WP_014129804.1	95	<i>Pelagibacterium</i> <i>halotolerans</i>
5	00119_74	Sod_Fe_N	96.8	WP_306145257.1	84.9	<i>Roseibium</i> sp. MMSF_3412

6	00121_136	Sod_Fe_N	88.6	OAN99667.1	100	<i>Sphingomonadales bacterium EhC05</i>
7	00154_23	Sod_Fe_N	109.4	KJS04440.1	91.5	<i>Flavobacteriales bacterium BRH_c54</i>
8	00167_33	Sod_Fe_N	115.8	WP_207398455.1	76.4	<i>Bremerella alba</i>
9	00194_82	Sod_Fe_N	113.6	WP_061331729.1	100	<i>Marinobacter</i> sp.
10	00201_67	Sod_Fe_N	104	WP_019961498.1	79.4	<i>Woodsholea maritima</i>
11	00279_26	Sod_Fe_N	96.9	WP_306024536.1	100	<i>Oceaniradius stylonematis</i>
12	00281_56	Sod_Fe_N	115.9	RUA34553.1	97	<i>Bacteroidota bacterium</i>
13	00307_2	Sod_Fe_N	109.9	WP_044217179.1	98.1	<i>Phaeodactylibacter xiamenensis</i>
14	00317_14	Sod_Fe_N	84.3	WP_227285974.1	99.5	<i>Boseongicola</i> sp. H5
15	00323_62	Sod_Fe_N	103.3	WP_072674833.1	100	<i>Erythrobacter sanguineus</i>
16	00483_28	Sod_Fe_N	115.2	WP_037249758.1	100	<i>Rhodopirellula</i> sp.
17	00513_26	Sod_Fe_N	109.9	TVR83868.1	81.7	<i>Saprospirales bacterium</i>
18	00607_26	Sod_Fe_N	105	OPZ08953.1	61	candidate division BRC1 bacterium ADurb.BinA292
19	00726_24	Sod_Fe_N	116	RMH28364.1	83.2	<i>Planctomycetota bacterium</i>
20	00818_6	Sod_Fe_N	113	WP_164103444.1	84.1	<i>Candidatus Laterigemmans baculatus</i>
21	00870_7	Sod_Fe_N	105	WP_052599883.1	87.6	<i>Aureispira</i> sp.
22	00943_27	Sod_Fe_N	108.3	GGH03325.1	92.2	<i>Glycocaulis albus</i>
23	01013_27	Sod_Fe_N	92.5	WP_109767327.1	99	<i>Oceaniradius stylonematis</i>
24	01027_44	Sod_Fe_N	83.2	WP_012177740.1	100	<i>Dinoroseobacter</i> sp.
25	01038_9	Sod_Fe_N	104.3	TVS04628.1	62.1	<i>Phycisphaerales bacterium</i>
26	01167_16	Sod_Fe_N	82.7	WP_290560629.1	100	<i>Aestuariivita</i> sp.
27	01453_8	Sod_Fe_N	109	WP_018128400.1	81.7	<i>Balneola vulgaris</i>
28	01529_1	Sod_Fe_N	108.9	WP_120710191.1	95.5	<i>Ulvibacterium marinum</i>
29	01676_13	Sod_Fe_N	115.9	WP_227756481.1	91.7	<i>Dermatobacter hominis</i>
30	02404_1	Sod_Fe_N	99.1	GJM12296.1	80.1	<i>Pseudohongiella</i> sp.
31	03712_1	Sod_Fe_N	105.7	WP_127140257.1	100	<i>Flavobacteriaceae</i> sp.
32	05581_2	Sod_Fe_N	62.6	TFJ80133.1	100	<i>Microchloropsis salina</i>
33	06570_1	Sod_Fe_N	71.8	WP_146299725.1	100	<i>Nitratireductor mangrovi</i>
34	08590_1	Sod_Fe_N	29.8	WP_187970154.1	87.4	<i>Aquibium microcysteis</i>
35	10237_3	Sod_Fe_N	107.3	WP_083559110.1	77.4	<i>Oceanococcus atlanticus</i>
36	11404_2	Sod_Fe_N	97.5	WP_028795535.1	95.4	<i>Thalassobaculum salexigens</i>
37	16615_2	Sod_Fe_N	102	WP_211372123.1	98	<i>Flagellimonas olearia</i>

38	16911_1	Sod_Fe_C	141.6	TFJ80133.1	100	<i>Microchloropsis salina</i>
39	21300_1	Sod_Fe_N	96.1	WP_007196653.1	100	<i>Hoeflea phototrophica</i>
40	24088_1	Sod_Fe_N	85.5	WP_292021230.1	99	<i>Maritimibacter</i> sp. UBA3975
41	24298_1	Sod_Fe_N	52.4	WP_259546105.1	94.1	<i>Roseibacterium beibuensis</i>
42	32366_1	Sod_Fe_C	146.3	WP_152131889.1	98.5	<i>Flagellimonas olearia</i>
43	37763_2	Sod_Fe_N	63.8	WP_294130624.1	100	<i>Pseudohongiella</i> sp.
D)						
3	00039_2	Catalase	633.5	WP_008661361.1	99.2	<i>Rhodopirellula europaea</i>
4	00053_3	Catalase	616.2	RZO57880.1	84.4	<i>Sandaracinaceae bacterium</i>
5	00079_61	Catalase	43.3	WP_290560031.1	100	<i>Aestuariivita</i> sp.
6	00114_114	Catalase	96.5	AWY99835.1	60.2	<i>Rhodobiaceae bacterium</i>
7	00475_13	Catalase	620.6	WP_299750394.1	83.2	<i>Devosia</i> sp.
8	00674_18	Catalase	607.1	WP_146392910.1	81.3	<i>Allorhodopirellula solitaria</i>
9	00988_10	Catalase	583.1	WP_255599329.1	94.2	<i>Hasllibacter</i> sp. MH4015
10	01037_21	Catalase	221.2	TFJ82773.1	98.3	<i>Microchloropsis salina</i>
11	01037_22	Catalase	73.3	TFJ82773.1	98.4	<i>Microchloropsis salina</i>
12	01037_24	Catalase-rel	73.3	TFJ82773.1	99.1	<i>Microchloropsis salina</i>
13	07277_1	Catalase	610.3	WP_283413272.1	99.2	<i>Algoriphagus winogradskyi</i>
14	19074_1	Catalase	496.4	WP_140926851.1	93.2	<i>Sandaracinobacter neustonicus</i>
15	37537_1	Catalase	250.2	WP_245451469.1	92.3	<i>Georhizobium profundum</i>

Acknowledgements

To round off this work, I write this rhyme,
Since in 2020, I am working online.
If there's one thing missing from this PhD's epic:
It's creativity—so far, it's been logic-centric.

To point out people as part of my PhD,
I write this, of course without ChatGPT.
There are no rules in the acknowledgment section,
the following fellows brought this work to perfection.

To start, **Ines Krohn**, who gave me the chance,
Stood by my side with algae, help, and guidance.
In gratitude, I pen these lines for you—
Your support in science helped see me through.

To learn and grow as a microbiologist,
Wolfgang Streit put me on his list.
For this, I'm grateful to this day,
and for bringing Fucus from Kiel Bay.

To unravel the mysteries of the sea,
Elisa Schaum she sent me in the land of the tea,
For setting me up on this PhD track,
I offer my thanks and give a nod back.

To **Eva Spieck**, with knowledge to spare,
She shaped the Tuesday talks with care.
With nitrification, she leads the way,
In marine microbiology, making strides each day.

To find laughter, drinks, and a friendly place,
and **Robert** spreading papers all over my workspace.
A true friend from the start to the end,
Guiding me through, a companion to depend.

To access the world of data science,
Pablo and I formed a strong alliance.
Working with you was always a pleasure,
And our regular beers were time well-treasured.

To share gossip, stories, and laughter with flair,
Just down the hall—**Luise** and **Marcel** were there.
We laughed, played games, and shared a fun diss,
And rocked the Down Under Star Wars pub quiz.

To know the crew and have lots of fun,
With beer, talks, and shenanigans spun,
I joined a room full of people to adore—
The working group team I truly care for.

To call honourable mentions of the Großraumbüro:

Alan, Tim, Lea, Marie, Yekaterina, Marno, Tabea, Sasi, Hongli, Golo, Nico.

Furthermore, the staff I thank more than I can:

Angela, Inka, Nurcan, Lutgardis and Yuchen.

To reach out to partners far in the north,
Yannik and **Jeanette** helped set things forth.
Thanks to all in SuReMetS who shared this quest—
I hope our paths cross again; you're the best.

To move on now to a more personal part,
Listing all my friends would be too hard to start.
But if I miss this special one, it wouldn't be fair—
Thank you, dear **Eva**, for always being there.

Um alle einzuschließen, wechsele ich hier den Stil,
denn auch meiner ganzen Familie verdanke ich viel.
Martina und **Niels**, das ist ja wohl klar,
und auch **Lina**, waren immer für mich da.